NOTICE

The quality of this microform is heavily dependent upon the quality of the original thesis submitted for microfilming. Every effort has been made to ensure the highest quality of reproduction possible.

If pages are missing, contact the university which granted the degree.

Some pages may have indistinct print especially if the original pages were typed with a poor typewriter ribbon or if the university sent us an inferior photocopy.

Reproduction in full or in part of this microform is governed by the Canadian Copyright Act, R.S.C. 1970, c. C-30, and subsequent amendments.

AVIS

La qualité de cette microforme dépend grandement de la qualité de la thèse soumise au microfilmage. Nous avons tout fait pour assurer une qualité supérieure de reproduction.

S'il manque des pages, veuillez communiquer avec l'université qui a conféré le grade.

La qualité d'impression de certaines pages peut laisser à désirer, surtout si les pages originales ont été dactylographiées à l'aide d'un ruban usé ou si l'université nous a fait parvenir une photocopie de qualité inférieure.

La reproduction, même partielle, de cette microforme est soumise à la Loi canadienne sur le droit d'auteur, SRC 1970, c. C-30, et ses amendements subséquents.

ISBN 0-315-55496-7

UNIVERSITY OF ALBERTA

A STUDY OF INTERSECTING CIRCULAR TURBULENT JETS

BY

ABDUL AZIZ KHAN

A THESIS

SUBMITTED TO THE FACULTY OF GRADUATE STUDIES AND RESEARCH

IN PARTIAL FULFILMENT OF THE REQUIREMENTS FOR THE DEGREE

OF MASTER OF SCIENCE

IN

WATER RESOURCES

DEPARTMENT OF CIVIL ENGINEERING

EDMONTON, ALBERTA

FALL, 1989

University of Alberta
Edmonton
Canada T6G 2G7

Department of Civil Engineering
220 Civil/Electrical Engineering Building
Telephone (403) 492-4235
Fax (403) 492-0249

May 24, 1989

Mr. Abdul Khan
Graduate Student
Dept. of Civil Engineering
Univ. of Alberta

Dear Mr. Khan:

I hereby give you permission to reproduce diagrams from my book "Turbulent Jets" published by Elsevier (1976) in your M.Sc. thesis.

Yours sincerely,

N. Rajaratnam, Ph.D., P.Eng.
Professor of Civil Engineering

NR/ds

UNIVERSITY OF ALBERTA

RELEASE FORM

NAME OF AUTHOR ABDUL AZIZ KHAN

TITLE OF THESIS A STUDY OF INTERSECTING CIRCULAR TURBULENT JETS

DEGREE FOR WHICH THESIS WAS PRESENTED MASTER OF SCIENCE

YEAR THIS DEGREE GRANTED FALL, 1989

(SIGNED) A. Aziz Khan .....

PERMANENT ADDRESS:
41-A Zaryab Colony
Peshawar City, N-W.F.P.
PAKISTAN

DATED May 25th 1989

UNIVERSITY OF ALBERTA

FACULTY OF GRADUATE STUDIES AND RESEARCH

The undersigned certify that they have read, and recommend to the Faculty of Graduate Studies and Research for acceptance, a thesis entitled A STUDY OF INTERSECTING CIRCULAR TURBULENT JETS submitted by ABDUL AZIZ KHAN in partial fulfilment of the requirements for the degree of MASTER OF SCIENCE in WAT R RESOURCES.

.....
Supervisor

.....

.....

Date 24 May 89

ABSTRACT

The intersection of two circular turbulent jets, having the same nozzle diameter and velocity, with intersection angles of 30,60,90 and 120 degrees, is studied experimentally. Experiments with intersecting jets show that, when two jets intersect; backflow occurs and the resulting jet behaves more like a three dimensional jet. These features cannot be predicted by vector addition of velocity or momentum fluxes or by using Reichardt's hypothesis.

The intersection of the two jets gives rise to a pressure hill, which affects the flow both upstream and down stream of it. The high positive pressure causes the flow to diverge in a plane normal to the plane of the nozzles. This makes the jet grow more rapidly in the vertical direction. Initially the growth rate of the resulting jet, in the transverse direction is negative and is due to converging flow in the plane of the nozzles. However, the two growth rates become approximately equal in the later part of the resulting jet. The velocity profiles in the transverse direction are found to be Gaussian, while in the vertical direction the velocity profiles show scatter in the outer region. The centreline velocity profiles, for experiments 1 to 4, in the resulting jet have been found to be similar. An effort is made to predict the stagnation pressure, maximum velocity and their locations. The length scales for centreline velocity and pressure profiles are found to vary

linearly with the $\cos(\alpha/2)$, where α is the angle of intersection.

In the region before the intersection, the stagnation pressure causes the incoming flow to diverge, and this results in higher growth rate in vertical direction near the intersection. The centreline velocity, after some initial distance from the nozzle, is less than that of a single jet; where the pressure is higher. The transverse velocity profiles when plotted in a non-dimensional form are similar and found to be Gaussian. The vertical velocity profiles are also similar and essentially Gaussian.

ACKNOWLEDGEMENTS

The author wishes to express his sincere gratitude to Dr. N. Rajaratnam for suggesting this topic and his guidance and advice throughout the course of this study.

The author would like to thank S. Lovell for his assistance in the construction and maintenance of the experimental set up.

Finally, the author would like to thank Government of Islamic Republic of Pakistan for the scholarship given through Ministry of Science and Technology.

Table of Contents

List of Figures

List of Plates

List of symbols

Symbol	Description
A	area of the nozzle
b	length scale in radial or vertical direction
$\overline{b}$	distance along radial direction where u is zero
b_0	half the height of the rectangular nozzle
b_p	length scale, in longitudinal direction of the resultant jet, for pressure in the resultant jet
b_u	length scale, in longitudinal direction of the resultant jet, for velocity in longitudinal direction of the resultant jet
b_Y	length scale, in vertical direction, for velocity in longitudinal direction of the resultant jet
b_{Y1}	length scale, in vertical direction, for velocity in longitudinal direction of the single jet
b_Z	length scale, in transverse direction, for velocity in longitudinal direction of the resultant jet
b_{Z1}	length scale, in transverse direction, for velocity in longitudinal direction of the single jet
D	distance between the centre of the nozzles

d	diameter of the nozzle
f	function
H	distance from the nozzle, along the longitudinal axis of the single jet, to the geometric intersection point
h	height of the rectangular nozzle
L	distance, along the resultant jet, from the transverse plane passing through the centre of the nozzles to the geometric intersection point
M_o	initial momentum of the individual jet
p_i	instantaneous pressure in the jet
p_m	minimum pressure in the forward flow of the resultant jet
p_s	maximum or stagnation pressure in the resultant jet
r	space co-ordinate in radial direction(single circular jet)
S	distance from stagnation point to the geometric intersection point
u	longitudinal velocity
u_i	instantaneous velocity in longitudinal direction
u_m	longitudinal velocity at the centre
u_{max}	maximum velocity in the longitudinal direction of the resultant jet
U_o	longitudinal velocity at the nozzle

v	radial velocity
v_e	entrainment velocity
v_i	instantaneous velocity in radial direction
X	space co-ordinate along longitudinal direction of the resultant jet
X1	space co-ordinate along the longitudinal direction of the single jet
X_p	measured, from the stagnation point, along the longitudinal direction of the resultant jet
X_u	measured, from the maximum velocity point in the resultant jet, along the longitudinal direction
Y	space co-ordinate in vertical direction(resultant jet)
Y1	space co-ordinate in vertical direction(single jet)
Z	space co-ordinate in transverse direction(resultant jet)
Z1	space co-ordinate in transverse direction(single jet)
α	total angle of intersection
α_e	entrainment coefficient
ζ	distance from the maximum velocity point in the resultant jet to the geometric intersection point

	dimensionless space co-ordinate, space co-ordinate divided by the length scale in that direction
ξ	distance measured from the nozzle to the point where the velocity in case of intersection jet is equal to that of single jet
ρ	mass density of the fluid
τ	turbulent shear stress

1. INTRODUCTION

1.1 General

Applications of intersecting turbulent jets can be found in fire chambers of boilers, in mixing vessels and in some energy dissipators. Merging of two streams is another case of intersecting jets.

It is generally believed that intersecting jets can be combined using vector addition of velocities or momentum flux densities or by using Reichardt's hypothesis in which the jet momentum equation is recast in a linear form. However, the study conducted by Maxwell and Snorrason(1979 and 1981), and the present study show that when two jets of equal diameter and nozzle velocity intersect, backflow is observed. This feature cannot be predicted by vector addition of velocities or momentum flux densities or by Reichardt's method.

A model, for two intersecting axisymmetric turbulent jets of same diameter and nozzle velocity, based on Reichardt's hypothesis, in which the pressure inside the jet is ignored, predicted that two jets keep their individual directions after intersection, a solution which did not seem reasonable and disagreed with the preliminary experimental observations. Hence an experimental study was performed on circular turbulent jets intersecting at included angles of

30, 60, 90 and 120 degrees and the results are presented in this thesis.

1.2 Existing work

A search of literature indicated that not much experimental work has been done on intersecting turbulent jets. Maxwell and Snorrason (1979) made a simple model, based on momentum principle, to predict the axis of the resultant flow and verified it with measurements. A second study by the same authors in 1981 was mainly concerned with the backflow and intersection regions of the intersecting jets.

1.3 Scope of present study

This study was conducted to investigate in detail the mean flow properties of intersecting axisymmetric turbulent jets of same diameter and nozzle velocity. Fig. 1.1 shows the plan view of two intersecting axisymmetric turbulent jets. All the measurements were taken with a Prandtl tube. A total of five experiments were done. The first four experiments involved circular turbulent intersecting jets, and the last experiment was conducted on a single circular jet.

2. LITERATURE REVIEW

A free turbulent jet is a jet issuing into a large stagnant mass of same fluid with a large enough Reynolds number and is unaffected by solid boundaries. Examples are, jets of air issuing into a large expanse of air or water jets issuing into a large reservoir. Turbulent free jets issuing from different nozzle shapes have been studied extensively in the last several decades. Abramovich(1963) and Rajaratnam(1976) provide rather extensive treatments of the subject. A brief description of circular, plane and three dimensional free turbulent jets is given below to help in interpreting the behavior of intersecting jets.

2.1 Circular turbulent jet

Consider a circular jet of diameter d issuing from nozzle with a velocity of U_o. Let u and v be the time averaged velocities in the axial(X) and radial(r) directions respectively. Starting with time averaged Reynolds equations and continuity equation in cylindrical co-ordinates, with slender flow approximations and neglecting laminar shear stresses and for constant pressure outside the jet, the Reynolds equations reduce to

$$u\frac{\partial u}{\partial X} + v\frac{\partial u}{\partial r} = \frac{1}{\rho r}\frac{\partial r\tau}{\partial r} \qquad [2.1]$$

where τ is turbulent shear stress and ρ is the mass density of the fluid.

The continuity equation is

$$\frac{\partial ru}{\partial X} + \frac{\partial rv}{\partial r} = 0 \qquad [2.2]$$

Upon integration, Eq. 2.1 reduces to

$$\frac{d}{dX} \int_0^\infty 2\pi r dr \rho u^2 = 0 \qquad [2.3]$$

Eq. 2.3 is the integral momentum equation and states that momentum flux in axial direction is constant.

Integration of Eq. 2.2 gives

$$\frac{d}{dX} \int_0^\infty ru dr = -\bar{b}\, v_e \qquad [2.4]$$

where $\bar{b}$ is the value of r where u is zero

Taylor's entrainment hypothesis (Taylor, 1958) can be written as

$$-v_e = \alpha_e u_m \qquad [2.5]$$

where α_e is the entrainment coefficient.

Experiments have shown (Rajaratnam, 1976) that velocity profiles beyond the potential core are similar and in general can be written as

$$\frac{u}{u_m} = f(\eta) \qquad [2.6]$$

where $\eta = \frac{r}{b}$ and b is the value r where $u = \frac{u_m}{2}$, u_m and b are the velocity and length scales respectively.
The normalized velocity profiles are satisfactorily described by the expression

$$\frac{u}{u_m} = \exp(-0.693\eta^2) \qquad [2.7]$$

Using the integral momentum and continuity equations, it can be shown that

$$u_m \propto \frac{1}{X} \qquad [2.8]$$

$$b \propto X \qquad [2.9]$$

The above equations show that the centreline velocity decays inversely with the axial distance and the growth of the jet is linear. In non-dimensional form, the above equations can be rewritten as

$$\frac{u_m}{u_o} = \frac{C_1}{X/d} \qquad [2.10]$$

$$\frac{b}{d} = C_2 \frac{X}{d} \qquad [2.11]$$

Different investigators have obtained different values for C_1 and C_2. The values of C_1 and C_2 seem to vary somewhat with the nozzle characteristics, nozzle Reynolds number up to some large value and the range of axial tances covered. However, for practical purposes it h. been suggested (Rajaratnam, 1976) that values of 6.1 and 0.1 be used.

2.2 Plane turbulent jet

Theoretically a plane turbulent jet is one with an infinite wide nozzle. The analytical solution follows the same procedure as in the axisymmetric case, except that cartesian co-ordinate system is used.

The normalized velocity profiles can be described by

$$\frac{u}{u_m} = f(\eta) = \exp(-0.693\eta^2) \qquad [2.12]$$

where $\eta = \frac{y}{b}$

In case of plane turbulent jet the velocity and length scale are given as

$$u_m \propto \frac{1}{X^{1/2}} \qquad [2.13]$$

$$b \propto X \qquad [2.14]$$

The above equations can be rewritten as

$$\frac{u_m}{u_o} = \frac{C_1}{(\frac{X}{b_o})^{1/2}} \qquad [2.15]$$

$$b = C_2 X \qquad [2.16]$$

where $2b_o$ is the height of the nozzle. It has been suggested(Rajaratnam, 1976) that for practical purposes, C_1 and C_2 can be given average values of 3.50 and 0.10 respectively.

2.3 Three dimensional jets

A definition sketch of a three dimensional jet is shown in Fig. 2.1. Consider a rectangular nozzle and let U_o be the velocity at the nozzle and let u_m be the velocity at the centreline. Fig. 2.1b shows the variation of u_m/U_o with X/h, where h is the height of nozzle. It has been found from experiments (Rajaratnam, 1976) and as shown in the Fig. 2.1b that three distinct regions exist. In region I, u_m is constant and is equal to U_o and this region gives the extent of the potential core of the three dimensional jet. In region II, u_m decays with X at a rate approximately equal to that of the plane turbulent jet, and is called the characteristic decay region. Region III in which u_m decays inversely with X is called the axisymmetric-type decay region.

For a jet issuing from a square nozzle it has been found experimentally (Rajaratnam, 1976), that the potential core is followed by axisymmetric-type decay region, with a short transition between the two. Three dimensional jets which possess the three distinct regions are called slender jets and those in which the characteristic decay region is absent are called bluff jets.

2.3.1 Slender jets

It is difficult to draw a boundary between slender and bluff jets in terms of the aspect ratio and a rectangular jet is said to behave like a slender jet for aspect ratio greater than 5 (Rajaratnam, 1976).

It has been found experimentally that in the characteristic decay region, the distribution of u(Y) is similar, but the distribution of u(Z) is non-similar and this region displays a saddle shape with maximum velocity occurring away from the centre (Rajaratnam, 1976). If b_Y and b_Z are the length scales in Y and Z direction respectively, the variation of b_Y/h and b_Z/h with X/h is shown in Fig. 2.2. It is clear that b_Z/h varies in a much more complex manner than b_Y/h.

2.3.2 Bluff jets

A rectangular nozzle having a aspect ratio of about unity will produce a bluff jet. A square jet shows similarity of u(Y) and u(Z) profiles (Rajaratnam, 1976), which can be written as

$$\frac{u}{u_m} = f(\eta_Y) \qquad [2.17]$$

$$\frac{u}{u_m} = f(\eta_Z) \qquad [2.18]$$

where $\eta_Y = \frac{Y}{b_Y}$ and $\eta_Z = \frac{Z}{b_Z}$

For a square jet, the variation of b_Y/h and b_Z/h with X/h has been found to be linear (Rajaratnam, 1976) and can be described by the equation

$$\frac{b_Y}{h} = \frac{b_Z}{h} = C_2 \frac{X}{h} \qquad [2.19]$$

where C_2 is approximately equal to 0.097.

As the momentum in a jet is conserved, using dimensional analysis it can be shown that

$$\frac{u_m}{u_o} = \frac{C_1}{X/\sqrt{A}} \qquad [2.20]$$

where A is cross-sectional area of the nozzle and C_1 is approximately equal to 7.0.

The decay of the normalized maximum velocity with the distance from the nozzle for different shapes, such as square, equilateral triangular, rectangular and elliptical nozzles of aspect ratio up to 10, can be described by one general curve by using $\sqrt{A}$ as the characteristic length. It has been found (Rajaratnam, 1976) that b_y follows equation 2.19 for aspect ratio of up to about 10, whereas variation of b_z is complex except for aspect ratio of unity.

2.4 Reichardt's hypothesis

Reichardt showed, both for circular and plane turbulent jets, that the jet momentum equation can be reduced to a linear equation in u^2, thus making it possible to analytically find the mean velocity field of series of parallel circular or plane turbulent jets. A brief description of the derivation of the equation for circular turbulent jet is given below.

Consider a circular turbulent jet of diameter d and nozzle velocity U_o. Neglecting laminar shear stresses, the Navier-Stokes equation can be reduced to

$$u_i\frac{\partial u_i}{\partial x} + v_i\frac{\partial u_i}{\partial r} = -\frac{1}{\rho}\frac{\partial p_i}{\partial x} \qquad [2.21]$$

where u_i and v_i are instantaneous velocities and p_i is instantaneous pressure.

Using the continuity equation , Eq. 2.16 can be reduced to

$$\frac{\partial r u_i^2}{\partial X} + \frac{\partial r u_i v_i}{\partial r} = - \frac{1}{\rho} \frac{\partial p_i}{\partial X} \qquad [2.22]$$

Assume(following Reichardt)

$$u_i v_i = - \lambda \frac{\partial u_i^2}{\partial r} \qquad [2.23]$$

where λ is assumed to be a function of X only.

Eq. 2.17 can be rewritten as

$$\frac{\partial u_i^2}{\partial X} = \frac{\lambda}{r} \left[\frac{\partial}{\partial r}\left(\frac{r \partial u_i^2}{\partial r}\right)\right] - \frac{1}{\rho} \frac{\partial p_i}{\partial X} \qquad [2.24]$$

Time averaging the above equation, neglecting normal turbulent stress and mean pressure in the jet, Eq. 2.24 can be written as

$$\frac{\partial u^2}{\partial X} = \frac{\lambda}{r} \left[\frac{\partial}{\partial r}\left(\frac{r \partial u^2}{\partial r}\right)\right] \qquad [2.25]$$

before

$$\frac{u}{u_m} = f(\eta) \qquad [2.26]$$

$$u_m = \frac{C_1}{X} \qquad [2.27]$$

$$b = C_2 X \qquad [2.28]$$

Let

$$\frac{u^2}{u_m^2} = F \qquad [2.29]$$

and

$$\lambda = C_3 X^s \qquad [2.30]$$

Using the above equations and Eq. 2.19, the exponent s is found to be 1. Eq. 2.19 can be written as

$$\frac{\partial u^2}{\partial X} = \frac{C_3 X}{r} \left[\frac{\partial}{\partial r}\left(\frac{r \partial u^2}{\partial r}\right)\right] \qquad [2.31]$$

The solution of the above equation is

$$u^2 = \frac{B}{X^2} \exp\left(-\frac{r^2}{kX^2}\right) \qquad [2.32]$$

where $k = 2C_3$, and B is a constant to be determined.

Applying the conditions

$$r = b;\ u = \frac{1}{2} u_m$$

$$r = 0;\ u = u_m$$

the constants are

$$B = X^2 u_m^2 \text{ and } k = \frac{b^2}{X^2 2 \ln 2}$$

Using the above equations, Eq. 2.20 can be written as

$$\frac{u^2}{u_m^2} = \exp(-\eta^2 2\ln 2) \qquad [2.33]$$

The above equation is linear in u^2, thus solutions for u^2 can be superimposed.

In case of intersecting circular turbulent jet the pressure inside the jet cannot be ignored. However, with the inclusion of the pressure term, the equations are not linear and have to be solved numerically.

2.5 Earlier work on intersecting jets

Maxwell and Snorrason(1979) developed a mathematical model, based on the momentum principle, to predict the axis of the resultant flow. A brief description of the model is given below.

Consider two nozzles A and B and let U_A and U_B be the velocity of jets A and B respectively at the nozzle (see Fig. 2.3). Assuming that the backflow and the forward flow are in the same line and the flow is two dimensional, writing momentum conservation equation in X and Y directions, the following equation can be derived

$$\beta = \arctan\left(\frac{Q_B U_B \sin\alpha}{Q_A U_A + Q_B U_B \cos\alpha}\right) \qquad [2.34]$$

where α is the intersection angle, β is the angle between X and the axis of the resultant flow, Q is the volumetric flow rate at the nozzle.

If the nozzle areas are the same, Eq. 2.22 is reduced to

$$\beta = \arctan\left(\frac{\sin\alpha}{\cos\alpha+\frac{U_A^2}{U_B^2}}\right) \qquad [2.35]$$

For a water jet(A) and a water jet produced by a bubble screen(B), the Eq. 2.30 can be written as

$$\beta = \arctan\left(\frac{U_B^2\delta A\sin\alpha}{U_A^2\delta A+U_B^2\delta A\cos\alpha}\right) \qquad [2.36]$$

where U_A and U_B are the maximum velocities just before the intersection. An equation for the decay rate of the maximum velocity is also given in the report. However, the equation for the decay rate of the maximum velocity given in the report is for a single jet and does not take into account the effect of intersection on the decay rate. In the above equation it is assumed that the area of the filament of maximum flux is same in both the jets and is equal to δA.

The model was also verified with the experimental measurements. The experiments were performed using air jets having same diameter. The results obtained were partly checked with water jets. The angle of intersection was kept

constant at 90 degrees, while the ratio U_A/U_B was varied from 0.48 to 2.06. For the case of water jet and water jet produced by bubble screen, the angle was kept constant at 90 degrees and the ratio of water to air discharge at the nozzle was varied from 2.866 to 29.412. The data for both set of measurements agree reasonably well with the model.

An experimental study, conducted by Maxwell and Snorrason(1981), with air jets, having same diameter and intersection angle of 90 degrees, was mainly oriented to investigate the mean velocity field, in the plane of the nozzle, in backflow and intersection region. Contours of equal velocity in both forward and backflow region for different X values were also plotted. Some velocity profiles, in Y and Z directions, in backflow and forward flow regions were also obtained. The velocity profiles in the forward flow region, in Y and Z directions, were similar and were found to be approximately Gaussian. In the backflow region, velocity profiles in Z direction, were similar and approximately elliptical or cubic, while in the Y direction the velocity profiles were found to be Gaussian. In the backflow region, the growth rate, in Z direction, was negligible, while in Y direction it was found to be approximately linear.

The above study was mainly confined to the backflow and intersection regions and no attempt was made to find the effect of intersecting jets on the growth and decay rate of

individual jet before intersection, and the properties of the resultant jet.

3. EXPERIMENTAL ARRANGEMENT

3.1 Experiment in water

In the early stages of this study, it was decided to investigate the mean flow properties of circular turbulent submerged water jets,intersecting at 180 degrees. The jets were set-up in a jet tank 4.88 m(16 feet) long, 2.44 m(8 feet) wide and 1.22 m(4 feet) deep. Two identical brass tubes, 25.4 mm(1 inch) long, with 12.7 mm(1/2 inch) internal diameter and having a bellmouth entry, were used as nozzles. Each nozzle was fitted in a copper pipe having 25.4 mm(1 inch) internal diameter. The copper pipes were L-shaped and were attached to the beam, fixed at the top of the tank along its width, with the nozzles 0.6 m(2 feet) under the water surface.

The water level in the jet tank was maintained by means of an overflow tank, connected to the tank through a stand-pipe. Water to the jets was drawn from a constant head overhead tank through 25.4 mm(1 inch) tygon tubing. To control the velocity at the nozzles, a valve was provided in each line. A 1/3 hp pump was used to supply water from the sump to the overhead tank. A 2-D traverse was fixed to a beam, running along the width of the tank. The beam was mounted on rollers to allow the movement along the length of the tank.

To have the same nozzle velocity, two 3 mm(1/8 inch) pitot-static tubes were used and the valve adjusted until the water manometers, inclined at 30 degrees, gave the same reading. The process of adjustment of the velocities at the nozzle was quite time consuming and had to be repeated each time the pump was shut off.

As the measuring system and the jets were about 0.6 m(2 feet) below the surface of water, vibrations in both the copper pipes and pitot tubes were uncontrolable. Further, it was difficult to align the jets perfectly. The total head and especially the static head readings showed high fluctuations and was believed to be due to the above reasons. However, when the same experiment was performed in air, it was found that the intersection point was highly sensitive to an obstruction in the flow, in case of pitot-static tube in the flow, the intersection point was found to move at the back of the tube, thus making any type of measurements with a pitot-static tube impossible.

3.2 Experiment in air

A schematic diagram of the experimental set up in air is shown in Fig. 3.1. The nozzles used were the same as described under submerged water jets. In this case, each nozzle was fitted in a copper pipe of internal diameter of 38 mm(1.5 inches) and 380 mm long. A 19 mm(3/4 inch) pipe

was connected to each of the copper pipe through a smooth expanding joint.

Each copper pipe was clamped to a universal work bench shown in plate 1. The universal work benches were fixed to a level platform, such that issuing jets were in a horizontal plane. The top part of the universal work bench, to which the copper pipe was clamped, could be moved in the longitudinal(X_1) and vertical(Y_1) direction, thus enabling a perfect alignment of the nozzles.

Each of the copper pipes had a 3 mm(1/8 inch) tap just before the nozzle, which was connected to a vertical differential water manometer. When the two differential water manometer gave the same reading, the velocity of the jets at the nozzle should be equal. A 19 mm(3/4 inch) tygon tube was used to connect each of the copper pipe to a pressure regulator, thus giving a better control over the nozzle velocity, which could be adjusted easily to any desired value. The two pressure regulators were connected to the main pipe through a T-joint.

The air for the jets was supplied by the main compressor of University of Alberta. A moisture trap was installed in the main line to remove moisture from the air. To bring the air close to room temperature, a heater was installed in the main line.

A three dimensional traverse used in the study is shown in plate 2. The minimum recordable distances in the X,Y,Z

directions were 0.1 mm, 0.3 mm(0.001 ft) and 1.26 mm(1/20 inch) respectively.

For precision measurements of pressure and total head, micromanometers, shown in plate 3, which can be set to a slope as small as 1:25 were used. Alcohol of specific gravity of 0.81 was used as the manometer fluid. The micromanometer scale was divided into millimeters and can be read up to an accuracy of 0.2 millimeter.

3.3 Velocity and pressure measuring instruments

A brief description of the instruments used is given below.

3.3.1 Pitot cylinder

A pitot cylinder is a cylindrical tube, having three holes 45 degrees apart in a plane perpendicular to its axis. The holes are located at an axial distance of about four diameters from its end. The pitot cylinder was originally designed to measure the total head and angle of flow in a plane perpendicular to the axis of the cylinder. This is done by rotating the cylinder in a flow until the two outer holes give the same readings. Then the direction of the middle hole gives the direction of flow and its reading gives the total head. By measuring the pressure at the same point, velocity can be obtained.

In order to avoid rotating of the pitot cylinder and making two measurements at a point, Beltaos(1972) calibrated the pitot cylinder in a potential core of the wind tunnel and developed calibration curves. Now, if the pitot cylinder is placed in the flow, three readings can be obtained. Using the calibration charts, values of velocity, pressure and the direction of flow relative to the direction of the central hole can be obtained.

As the flow in the intersection region is curved, and the exact direction of flow is not known beforehand, it was decided to use the pitot cylinder, already calibrated by Beltaos(1972). However, from the preliminary measurements with the pitot cylinder, it was found that it always gave positive pressure. The results, obtained in a single jet, from a pitot cylinder and a pitot-static tube, showed that using the calibration charts, the pitot cylinder always gave positive pressure in the jet and an error of about 8% in velocity.

The pitot cylinder was recalibrated in the potential core of a single jet, but the results were the same. A one hole pitot cylinder 1 mm(0.04 inch) in diameter used by Beltaos(1974) was recalibrated but the results obtained were the same. Hence, the use of the pitot cylinder was abandoned and it was decided to work with the pitot-static tube.

3.3.2 Pitot-static tube

All the measurements were taken with a 1.5 mm(1/16 inch) pitot-static tube. It has been found, Chue(1975), that velocity measurements with pitot-static tubes, for Reynolds number greater than 500, can be made up to an accuracy of 1%, while the static pressure measurements are found to be essentially insensitive to Reynolds number in the range of 3000 to 53,000.

The velocity and static pressure can be measured accurately, when the pitot-static tube is aligned perfectly in the direction of flow. However, some correction has to be applied, if the flow is at an angle to the tube. As the error, due to yaw or pitch angle, in the total head and static pressure is of the same sign (Chue, 1975), velocity can be measured without any significant errors for angles up to 5 to 10 degrees. It has been found that static pressure is highly sensitive to the yaw or pitch angle, which may be because of the component of velocity normal to static pressure holes (Chue, 1975). A compensation effect can be achieved by providing five or six evenly spaced static pressure holes around the circumference (Chue, 1975), but some error still exists. The error in velocity and static pressure measurements have been found negligible for yaw or pitch angle less than 5 degrees. In the present study no corrections were applied for angle of attack.

It has been found that the turbulence intensity in the flow also introduces errors in the measurements with a pitot-static tube. To apply any kind of correction for turbulent effect, turbulence intensity has to be measured independently for the flow conditions in question. No corrections for turbulence effects were applied to the measurements made in this study.

3.4 Co-ordinate system

Two types of co-ordinate systems were used, X1,Y1,Z1 and X,Y,Z. As shown in Fig.1.1, X1 is measured, from the nozzle, along the longitudinal axis of single jet, whereas Z1 and Y1 are normal to X1, and are in horizontal and vertical directions respectively. As shown in Fig. 1.1, X is measured, from a transverse plane passing through the centre of the nozzles, along the longitudinal axis of the resultant jet. Y and Z are normal to X, and in the vertical and horizontal directions respectively. The Y-Z plane is called the transverse plane.

3.5 Measurement techniques

Before the intersection region, the pitot-static tube was set in the X1 direction. To take measurements near the intersection region, a fine thread was used to determine the

direction of flow and only those readings for which the flow was in X1 direction were taken.

To determine the maximum velocity u_m at any section, the pitot tube was fixed in the Y1 or Y direction and was traversed in the Z1 or Z direction, thus finding the point of maximum velocity in the Z1 or Z direction. Then the velocity profile in the Y1 or Y direction was obtained. Knowing the point of maximum velocity u_m, the velocity profile in the Z1 or Z direction was obtained.

4. EXPERIMENTAL RESULTS AND ANALYSIS

4.1 Experiments

A total of five experiments were conducted. The first four experiments dealt with intersecting circular turbulent jets and the last experiment was carried out on a single circular turbulent jet. The significant details of the five experiments are given in table 4.1 and the symbols appearing in the table are defined in the definition sketch, Fig. 1.1.

Experiment	Angle α	D (cm)	L (cm)	H (cm)	U_o (m/s)
1	60°	12.64	10.95	12.64	34.46
2	90°	21.93	10.96	15.50	34.57
3	30°	5.87	10.95	11.34	34.55
4	120°	37.95	10.96	21.91	34.57
5*	----	----	----	----	34.55

* Single jet

Table 4.1. Details of experiments

In all the experiments, the nozzle velocity was about 34.5 meter per seconds and for this velocity, compressibility effects are negligible. The nozzle Reynolds

number was about 31,000. In all the experiments, only the time averaged velocity (u) in X1 or X direction was measured. In the first two experiments the velocity and pressure profiles in the transverse(Z1 or Z) and vertical(Y1 or Y) directions, at a number of X1 and X stations, were measured, along with the variation of velocity and pressure in X1 and X directions. In experiments 3 and 4, only the variation of velocity and pressure in X1 and X directions were measured. In all the experiments, involving intersecting jets, the distance(L) from a transverse plane, passing through the centre of the nozzles, to the geometric intersection of the jets was kept constant. In the last experiment with the single circular jet, the centreline velocity and pressure profiles were obtained, to compare with the results of intersecting turbulent jets.

4.2 Results and analysis

This section deals with the experimental results and analysis of the individual experiments.

4.2.1 Experiment 1

In this experiment, velocity and pressure profiles in transverse(Z1 or Z) and vertical(Y1 or Y) directions were measured at different X1 and X stations. Centreline velocity and pressure profiles were also measured.

Fig. 4.1 through 4.8 show the transverse velocity profiles at different X1 stations. The transverse pressure profiles, at the same stations, are shown in Fig. 4.9 through 4.16. At each station, velocity and pressure profiles were measured both in +Z1 and -Z1 direction. Near and in the intersection region, the flow at the edge of the jet in +Z1 direction, due to backflow and intersection of the jets, was not in X1 direction. So the velocity and pressure in +Z1 direction were measured up to the point where the flow was in X1 direction.

From Fig. 4.1 through 4.16 which show pseudo-nondimensional transverse velocity and pressure profiles, it is clear that after X1/d=2.03, transverse velocity and pressure profiles at a particular X1 station are not similar, and the difference increases as X1/d approaches the intersection. However, the difference is more obvious in pressure profiles. The dissimilarity of the transverse velocity and pressure profiles, at a particular X1 station, are believed to be due to the stagnation pressure, backflow and confined space between the jets. After X1/d=6.36, the pressure at the edge of the jet, in +Z1 direction acquires positive value, and as X1/d increases the positive pressure moves to the interior of the jet.

Fig. 4.17 shows the transverse velocity profiles plotted in a non-dimensional form. To non-dimensionalize the velocity profiles, a separate length scale was obtained for +Z1 and -Z1 sides of the profile. The velocity profiles, at

different X1 stations, when plotted in a non-dimensional form are similar for X1/d up to 8.02 and can be described by

$$\frac{u}{u_m} = \exp(-0.693\eta_{Z1}^2) \qquad [4.1]$$

where $\eta_{Z1} = \frac{Z1}{b_{Z1}}$, b_{Z1} is the value of +Z1 or -Z1 where $u = \frac{u_m}{2}$, u_m being the centreline or maximum velocity.

Fig. 4.18 shows the variation of the velocity in the vertical direction at different X1 stations. Velocity profiles at a particular station seem to be similar, and this holds for the vertical pressure profiles too(Fig. 4.19 - 4.22 for different X1 stations). The vertical velocity profiles at different X1 stations are replotted in a non-dimensional form in Fig. 4.23, and found to be similar for X1/d up to 8.02, and can be described by

$$\frac{u}{u_m} = \exp(-0.693\eta_{Y1}^2) \qquad [4.2]$$

where η_{Y1} $\frac{Y1}{b_{Y1}}$, and b_{Y1} is the value Y where $u = \frac{u_m}{2}$.

Fig. 4.24 shows the growth rates in a jet, both in vertical and transverse directions. An individual growth rate of the jet in +Z1 and -Z1 direction is shown in Fig. 4.24. The growth rate in the +Z1 direction is less than that in -Z1 direction and this difference increases as X1/d approaches the intersection point. It seems that in the initial part of the jet, the growth in vertical direction is

equal to that in -Z1 direction; however, near the intersection point, the growth in the vertical direction is more than that in the -Z1 direction. This could also explain the non-similarity of the transverse and vertical profiles after X1/d=8.02.

Fig. 4.25 and 4.26 show respectively the centreline velocity and pressure profiles along X1. As found by Sami et. al.(1966), this study shows that the pressure in early part of the potential core is positive. The pressure, because of stagnation point, goes to positive near the intersection region.

Fig. 4.27 and 4.28 show respectively the variation of the velocity in the transverse and vertical directions at different X stations. Fig. 4.27 shows that initially the velocity(u), for X/d up to 9.96, along the transverse axis decreases, whereas Fig. 4.28 shows that the velocity(u), for X/d up to 9.96, along the vertical axis increases. Fig. 4.29 and 4.30 show the velocity profiles, in transverse and vertical directions at different X stations, in non-dimensional form. The velocity profiles in the transverse direction are similar and agree well with the equation

$$\frac{u}{u_m} = \exp(-0.693\eta_z^2) \qquad [4.3]$$

where $\eta_z = \frac{Y}{b_z}$, and b_z is the value Z where $u = \frac{u_m}{2}$.

The non-dimensional vertical velocity profiles, shown in Fig.4.30, are found to be similar up to η_Y=1.2, and are described by the equation

$$\frac{u}{u_m} = \exp(-0.693\eta_Y^2) \qquad [4.4]$$

where $\eta_Y = \frac{Y}{b_Y}$, and b_Y is the value Y where $u = \frac{u_m}{2}$.

The growth rates in transverse and vertical directions are shown in Fig. 4.31. In the initial part of the resultant jet, up to X/d of about 18, the vertical growth rate is much higher than the transverse growth rate. However, at a later stage the two growth rates are approximately the same. The initial higher growth rate in vertical direction as well as the reduced transverse growth of the resultant jet are believed to be due to the flow diverging in vertical direction and converging in the transverse direction.

In Fig. 4.30, for $\eta_Y > 1.2$ the vertical velocity profiles are not similar, however, they show a regular trend of moving away from Eq. 4.4 and after X/d=10.78 the profiles start moving towards it(and can be explained on the basis of explanation given above).

The pressure profiles in transverse and vertical direction, at different X stations, are shown in Fig. 4.32 and 4.33 respectively. The pressure profiles in vertical direction show a low pressure zone on either side of the centre, and this is believed to be due to the diverging flow

in the vertical direction. The low pressure zones merge together, after X/d=11.57, with a minimum pressure at the centre. The pressure profiles in transverse direction show a minimum pressure at the centre.

A centreline velocity and pressure profiles in a non-dimensional form, along X direction, are shown in Fig. 4.34 and 4.35 respectively. The velocity at the stagnation point is zero and it increases to a maximum value and after that the velocity decay follows three different patterns. In the first part, the decay rate is very steep, after which it follows a decay pattern of circular turbulent jet and finally the decay rate is somewhere between those of the circular and plane turbulent jets. The maximum velocity occurs after the geometric intersection, and is due to the flow curving around the stagnation point.

As shown in Fig. 4.35, the maximum or stagnation pressure occurs before the geometric intersection, a phenomena similar to that found in oblique impingement of plane or circular turbulent jet on smooth solid boundaries (Beltaos, 1974). However, soon after the stagnation point, the pressure goes to negative, a phenomena different from oblique impingement of circular turbulent jet, in which case the pressure remains positive (Beltaos, 1974).

4.2.2 Experiment 2

This experiment was also carried out in detail. The main purpose of this experiment was to study the characteristics of intersecting jets for another angle of intersection. The details of the experiment are given in table 4.1.

Fig. 4.36 through 4.43 show the pseudo-nondimensional transverse velocity profiles at different X1 stations, while the pseudo-nondimensional transverse pressure profiles, at the same stations, are shown in Fig. 4.44 through 4.51. It appears that after X1/d=1.99, the transverse velocity profiles at a particular station are not similar. After X1/d=9.08, the pressure at the edge of the jet, in +Z1 direction goes to positive, and as X1/d increases the positive pressure moves toward the interior of the jet.

Fig. 4.52 shows the transverse velocity profiles, at different X1 stations, plotted in a non-dimensional form. The profiles are found to be similar and can be approximated by the equation given below

$$\frac{u}{u_m} = \exp(-0.693\eta_{Z1}^2) \qquad [4.5]$$

Fig 4.53 shows the variation of velocity in the vertical direction for different X1 stations and the velocity profiles, at a particular station, are similar. The vertical

pressure profiles are shown in Fig. 4.54. The non-dimensional vertical velocity profiles are shown in Fig. 4.55, and are compared with the equation given by

$$\frac{u}{u_m} = \exp(-0.693\eta_{Y1}^2) \qquad [4.6]$$

For $\eta_{Y1} > 1.1$ the velocity profiles do not agree with Eq. 4.6, and the profiles are not similar, and can be explained on the basis of sudden increase in growth rate in vertical direction near the intersection. Fig. 4.56 shows the growth rate in the transverse, +Z1 and -Z1, and vertical directions. In this case the difference between the two growth rates in transverse direction is very small until it reaches very near to the intersection, where the difference starts increasing. Further, the higher vertical growth starts earlier and is believed to be due to the high stagnation pressure.

Fig. 4.57 and 4.58 show, respectively, the centreline velocity and pressure profiles in X direction. The results show the same tendencies as discussed in experiment 1.

Fig. 4.59 shows the variation of velocity in transverse direction at different X stations, and is replotted in non dimensional form in Fig. 4.60. The non dimensional velocity profiles are similar and can be approximated by

$$\frac{u}{u_m} = \exp(-0.693\eta_z^2) \qquad [4.7]$$

The variation of velocity in the vertical direction, at different X stations, is shown in Fig. 4.61. Fig 4.62 shows the same profiles plotted in a non-dimensional form. The non- dimensional velocity profiles are found similar, up to η_Y=1.2, and can be approximated by the equation given by

$$\frac{u}{u_m} = \exp(-0.693\eta_Y^2) \qquad [4.8]$$

The non-dimensional vertical velocity profiles are not similar for $\eta_Y > 1.2$ and the velocity profiles start moving towards Eq. 4.8 after X/d=11.58. The growth rates in the transverse and vertical directions are shown in Fig. 4.63. The vertical velocity profile [illegible] the growth rates follow the same tendencies as desc[illegible] for experiment 1.

The pressure profi[illegible] in transverse and vertical directions, at different X [illegible]ations, are shown in Fig. 4.64 and 4.65 respectively, and are found to show the same tendencies as in experiment 1.

The variation of centreline velocity and pressure profiles in non dimensional form are shown in Fig. 4.66 and 4.67 respectively. In this case, some measurements in the backflow region were also made.

4.2.3 Experiments 3,4 and 5

In experiment 3 and 4, only centreline velocity and pressure profiles, along X1 and X direction, were measured. The variation of centreline velocity and pressure, for experiments 3 and 4, in X1 and X directions are shown in Fig. 4.68 through 4.75. The results show the same tendencies as discussed above.

In experiment 5, centreline velocity and pressure profiles were measured in a single circular turbulent jet and these are shown in Fig. 4.76 and 4.77 respectively. In Fig. 4.76, the centreline velocity decays continuously after the potential core. In Fig. 4.77, the pressure at the centre of jet decreases from positive value to zero at X1/d of approximately 3.4, reaches a minimum value at X1/d of approximately 8 and then gradually approaches the ambient pressure.

5. GENERAL ANALYSIS

In this chapter an attempt is made to combine the results of all the five experiments, which will help in predicting some of the properties of intersecting circular turbulent jets. Dimensional considerations have been used in this analysis.

In Fig. 5.1, centreline velocity profiles, along X1, for all the experiments are plotted together. In all cases of intersecting jets(Expt. 1 to 4), the centreline velocity profiles follow, up to some distance, the velocity profile of the single jet, after which the velocity in the case of the intersecting jet is less than that of the single jet and is because of increased static pressure in the intersection region. If ξ is the distance, from the nozzle, up to which the centreline velocity profile of a intersecting jets is similar to that of the single jet, and if viscous effects are ignored(for jet Reynolds number greater than few thousand), it can be shown that

$$\frac{\xi}{H} = f(\alpha) \qquad [5.1]$$

where f shows the functional relationship. The variation of ξ/H with α is shown in Fig. 5.2. The data for normal impingement of circular turbulent jet on smooth boundaries(Beltaos, 1974), is also plotted in Fig. 5.2 and

seems to agree reasonably well with the present data. As shown in Fig. 5.2, ξ/H increases slowly with α.

Fig. 5.3 shows the centreline pressure profiles of all the five experiments. However, in this case it is difficult to locate the point where the pressure starts deviating from that of single jet, specially in case of experiments 1 and 2.

Let u_{max} be the maximum velocity along X, and X_u be the distance along X with origin at u_{max}. Let b_u be the distance along positive X_u where $u_m = u_{max}/2$, and $\eta_u = Xu/b_u$. Now, if the centreline velocity profiles in X direction are plotted, as shown in Fig. 5.4, in a non-dimensional form the profiles are similar and can be described by a single curve.

For the intersecting jets with the same nozzle diameter and velocity, u_{max} can be written as

$$u_{max} = f(\rho, M_o, H, \alpha) \qquad [5.2]$$

where ρ is the mass density of the fluid, $M_o = \rho \frac{\pi}{4} d^2 U_o^2$. Using dimensional consideration, Eq. 5.2 can be reduced to

$$\frac{u_{max}}{U_o} \left(\frac{H}{d}\right) = f(\alpha) \qquad [5.3]$$

Fig. 5.5 shows the variation of $\frac{u_{max}}{U_o} \left(\frac{H}{d}\right)$ with α, and this velocity parameter is approximately constant in the range of α tested and is approximately equal to 6.8.

If the eccentricity of maximum velocity in X direction with respect to the geometric intersection point is ζ, then it can be shown that

$$\frac{\zeta}{H} = f(\alpha) \qquad [5.4]$$

The variation of ζ/H with α is shown in Fig. 5.6, ζ/H increases linearly with α, from $\zeta/H = 0.067$ for α=30 degrees to about 0.085 for α=120 degrees.

Fig. 5.7 shows the variation of length scale(b_u) with D/H on a semilog plot, $\log(b_u/H)$ decreases linearly with D/H.

Let p_s be the maximum or stagnation pressure. Using dimensional arguments, p_s can be written as

$$\frac{p_s}{\rho U_o^2} \left(\frac{H}{d}\right)^2 = f(\alpha) \qquad [5.5]$$

The variation of $\frac{p_s}{\rho U_o^2} \left(\frac{H}{d}\right)^2$ with α is shown in Fig. 5.8. The data for oblique impingement of circular turbulent jet on smooth boundary(Beltaos, 1974) is also shown in Fig. 5.8, it seems that the difference between the two data increases with α. If S is the eccentricity of the stagnation point with respect to the geometric centre, then from dimensional considerations it can be shown that

$$\frac{S}{H} = f(\alpha) \qquad [5.6]$$

The variation of S/H with α is shown in Fig. 5.9, where S/H decreases continuously with α and approaches almost zero for α=120 degrees.

Let X_p be the distance along X with origin at stagnation point, p_m be the minimum pressure in the positive X_p direction, b_p be the distance along X_p where $p-p_m = (p_s-p_m)/2$, and let $\eta_p = X_p/b_p$. Fig. 5.10 shows the centreline pressure profiles, in X direction, plotted in a non-dimensional form. The profiles are similar except for α = 30 degrees, which shows significant deviation after η_p of about 5. However, from Fig. 5.10, p_m, for experiments 1 to 4, occurs at η_p of approximately 5. To predict p_m, the variation of p_m/p_s with α is shown in Fig. 5.11. Fig. 5.12 shows the variation of b_p/H with D/H on a semilog plot, $\log(b_p/H)$ decreases linearly with D/H.

6. SUMMARY AND RECOMMENDATIONS

6.1 Summary of the results

In case of intersecting circular turbulent jets, having same nozzle diameter and velocity, two distinct regions can be identified. In the region before the intersection, which is distinguished by co-ordinate system of X1,Y1 and Z1, the jets maintain their individual characteristics. The velocity profiles in transverse(Z1) direction at a particular X1 station are not similar; the velocity in +Z1 direction being less and is believed to be due to confined space between the jets, backflow and the existence of the stagnation point. By determining an individual length scale for each side, the velocity profiles can be plotted in a non-dimensional form and were found to be Gaussian, except very near to the intersection region. The difference between the growth of +Z1 and -Z1 side is very small and can be neglected, except very near the intersection region where the difference starts to increase. The vertical velocity profiles at any particular X1 station were found to be similar and when plotted in a non-dimensional form, the profiles were essentially Gaussian.

Initially the growth rate in vertical direction is same as in -Z1 direction, however, near the intersection, the growth rate in the vertical direction is higher and is believed to be due to the diverging flow in the vertical plane.

Along X1, initially the centreline velocity is equal to the centreline velocity of the single circular jet, however, after a distance ξ, from the nozzle, the centreline velocity is less than that of a single jet. The variation of ξ with α is shown. It is difficult to find such a unique point for centreline pressure profiles in X1 direction.

In the region after intersection, identified by X,Y,Z co-ordinate system, the velocity profiles in transverse(Z) direction were found to be Gaussian, while the profiles in vertical(Y) direction, for η_Y up to 1.2, were found similar and can be described by the error function. The vertical velocity profiles, for $\eta_Y > 1.2$, are not similar, and this is believed to be due to diverging flow in the vertical plane.

Initially the growth rate in the vertical direction is very large, while in the transverse direction, the growth rate is negative, and is due to diverging flow in the vertical direction and converging flow in the transverse direction. However, at a later stage the two growth rates are approximately the same.

Along X direction, the maximum velocity occurs after the geometric intersection point, while the stagnation pressure occurs before the geometric intersection. The variation of the eccentricity of stagnation and maximum velocity, with respect to geometric intersection, with the angle of intersection(α) has been found. The eccentricity of maximum velocity varies almost linearly with α.

The centreline velocity profiles along X direction, for experiment 1 to 4, when plotted in a non-dimensional form were found to be similar. The centreline pressure profiles, along X direction, were also found to be similar, except for α= 30 degrees, in which case the profile starts to deviate after the point of minimum pressure. The minimum pressure for all the angles of intersection was found to occur at η_p of about 5.

A functional relationship based on dimensional analysis has been developed for the stagnation pressure and maximum velocity.

The length scales for centreline velocity and pressure profiles, when plotted on a semilog plot were found to vary linearly with the function of angle of intersection.

6.2 Recommendation for further research

The first obvious recommendation would be to perform some more experiments, to cover the whole range of angles from 0 to 180 degrees. It would be interesting to find the effects of varying the velocity at the nozzles on the properties of the resulting jet. Some detailed measurements of the turbulence would be helpful in developing a better understanding of the phenomenon.

When two circular turbulent jet, having same nozzle diameter and velocity, intersect, two main features have been observed, firstly, backflow and secondly, the resulting jet

behaves more like a three dimensional jet. The vector addition of velocity or momentum flux densities would be valid because backflow cannot be predicted by these methods. Also the superposition of u^2, which works well for the parallel circular and plane turbulent jets would not be valid in case of intersecting circular turbulent jets. To develop any kind of linear equation for intersecting circular turbulent jets the pressure term in the jet momentum equations should not be ignored. To develop any kind of numerical model the above factors should be considered.

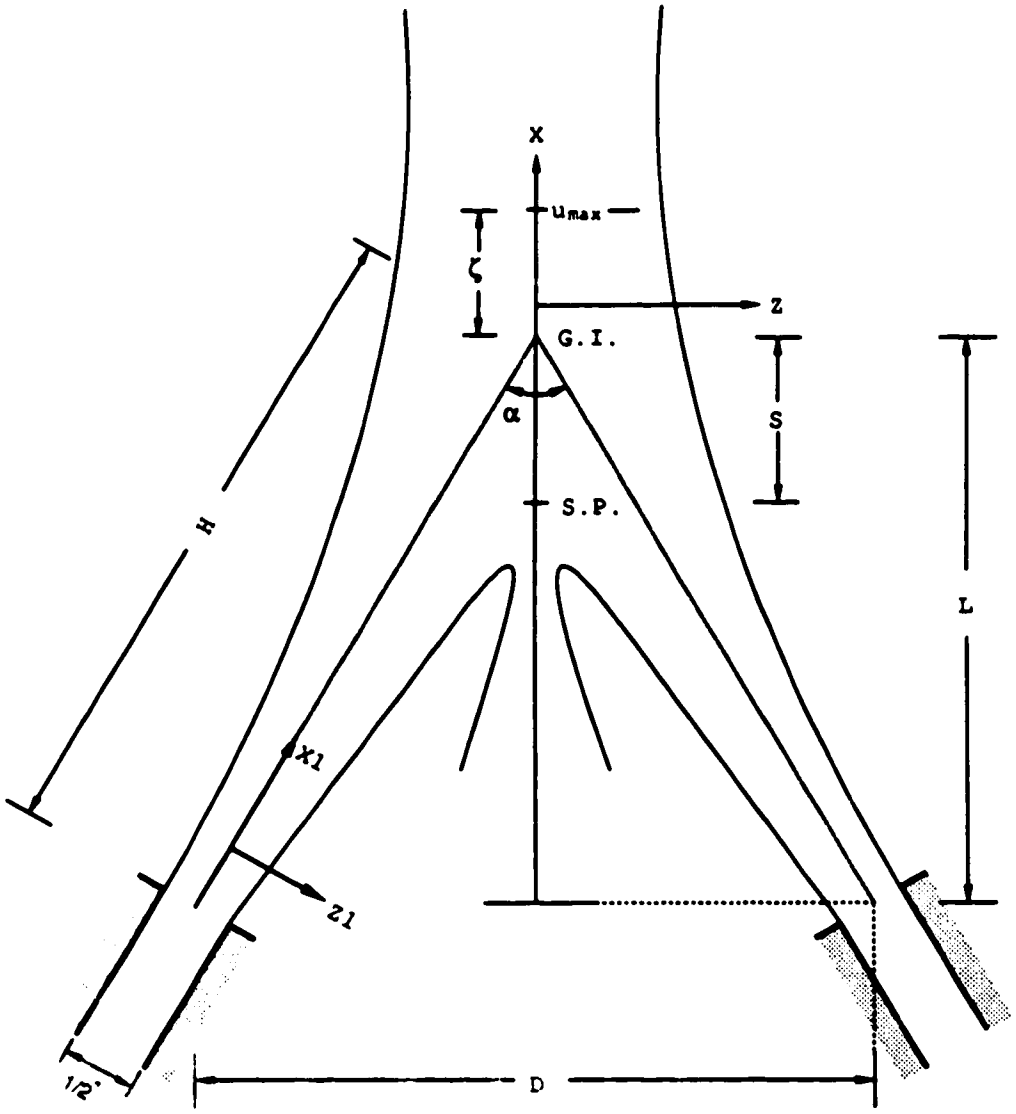

S.P. marks the location of stagnation pressure

G.I. Geometric intersection

Fig. 1.1. Definition sketch of circular turbulent intersecting jets

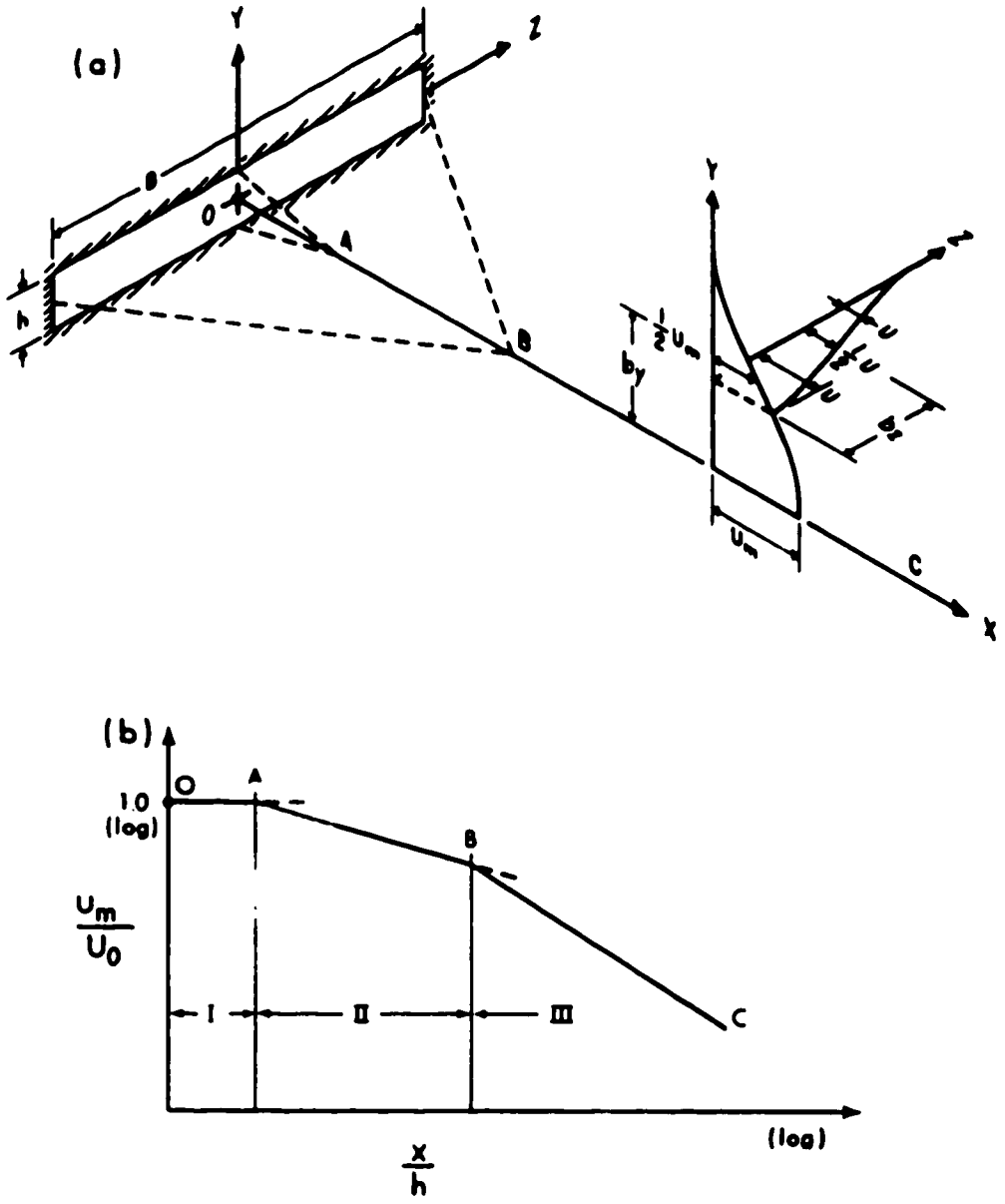

Fig. 2.1. Definition sketch for a three dimensional free jet, after Rajaratnam(1976)

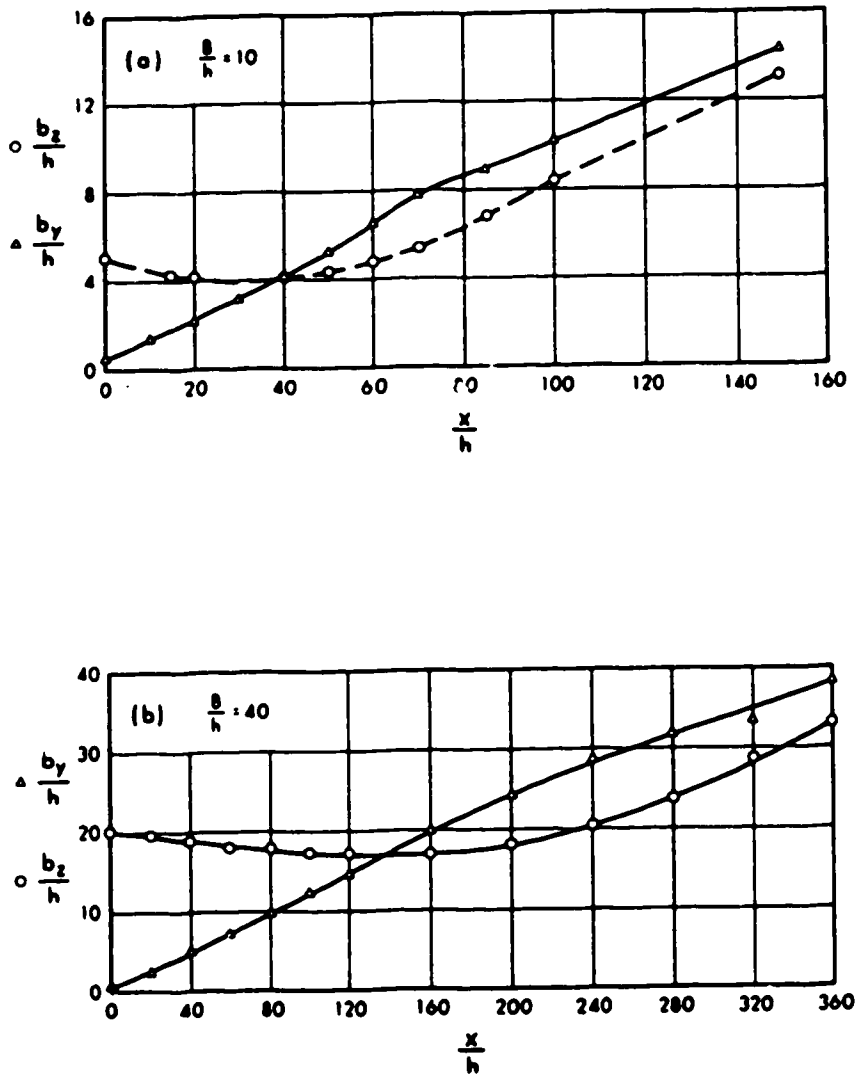

Fig. 2.2. Length scales for rectangular jets, after Rajaratnam(1976)

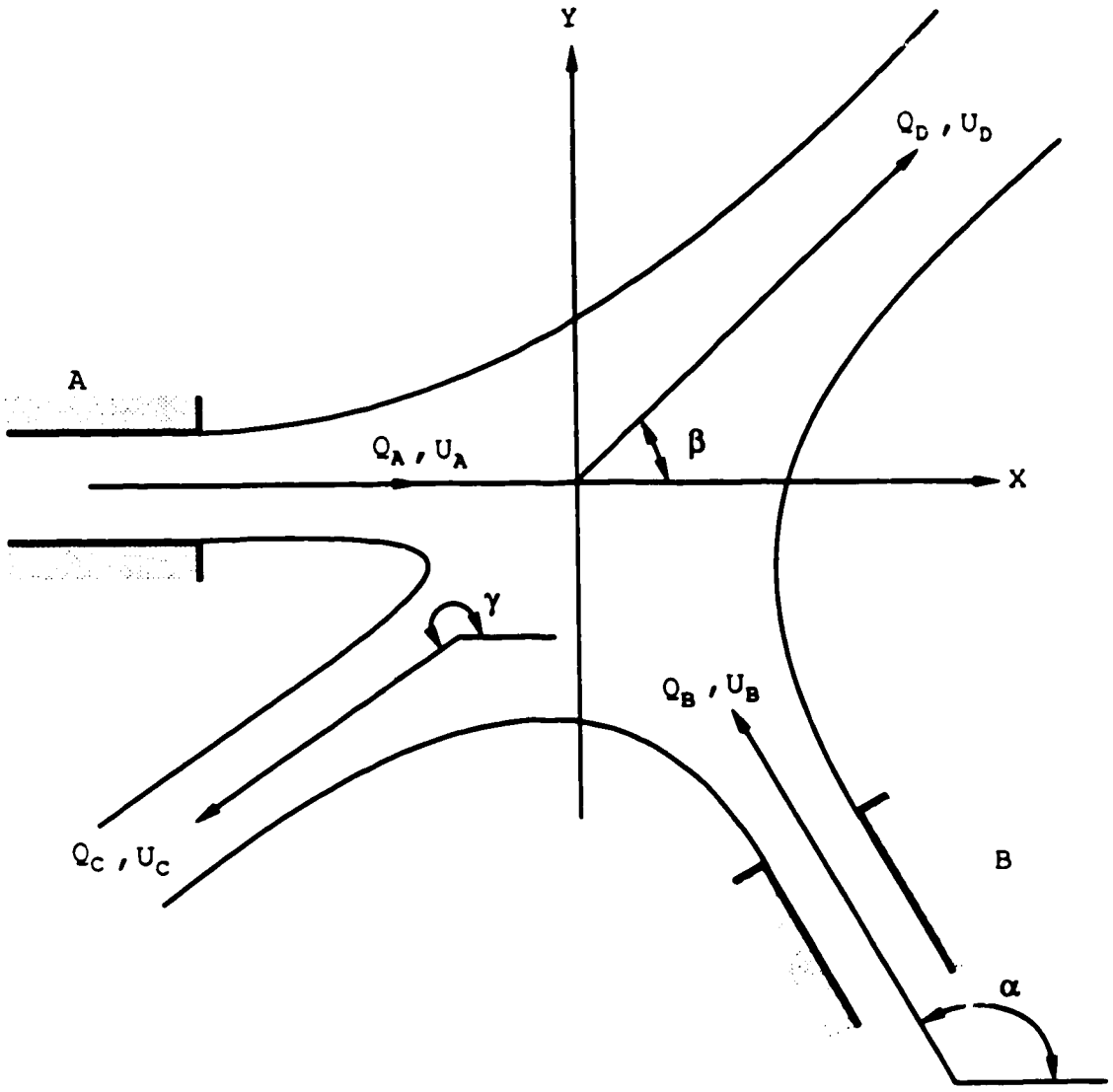

Fig. 2.3. Schematic of intersecting jets

Adapted from Maxwell et. al. (1979)

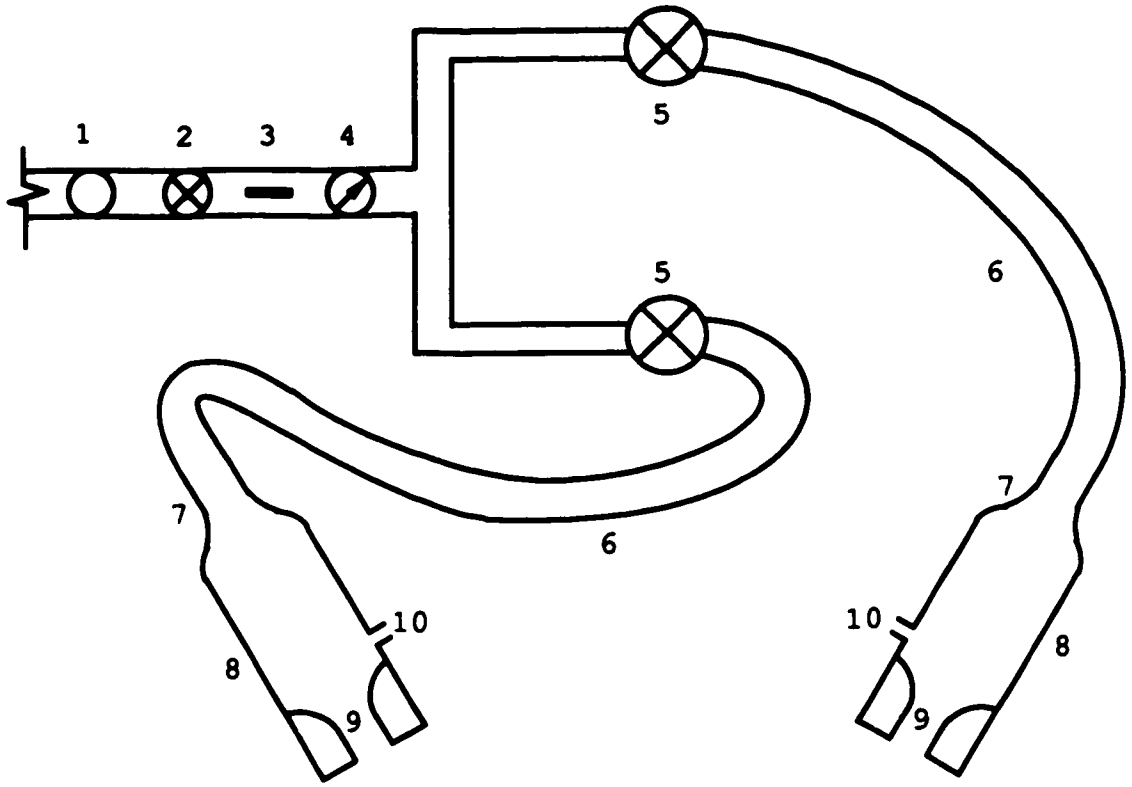

1. Moisture trap
2. Main pressure regulating valve
3. Heating element
4. Pressure gauge
5. Pressure regulating valve
6. 19 mm internal diameter tygon tubing
7. Expansion joint connecting 19 mm internal diameter copper pipe to 38 mm internal diameter copper pipe
8. 380 mm long, 38 mm internal diameter copper tube
9. 25.4 mm long, 12.7 mm internal diameter nozzle
10. 3 mm taps connected to vertical differential water manometer by means of tygon tubing

Fig. 3.1. Schematic diagram of experimental set up

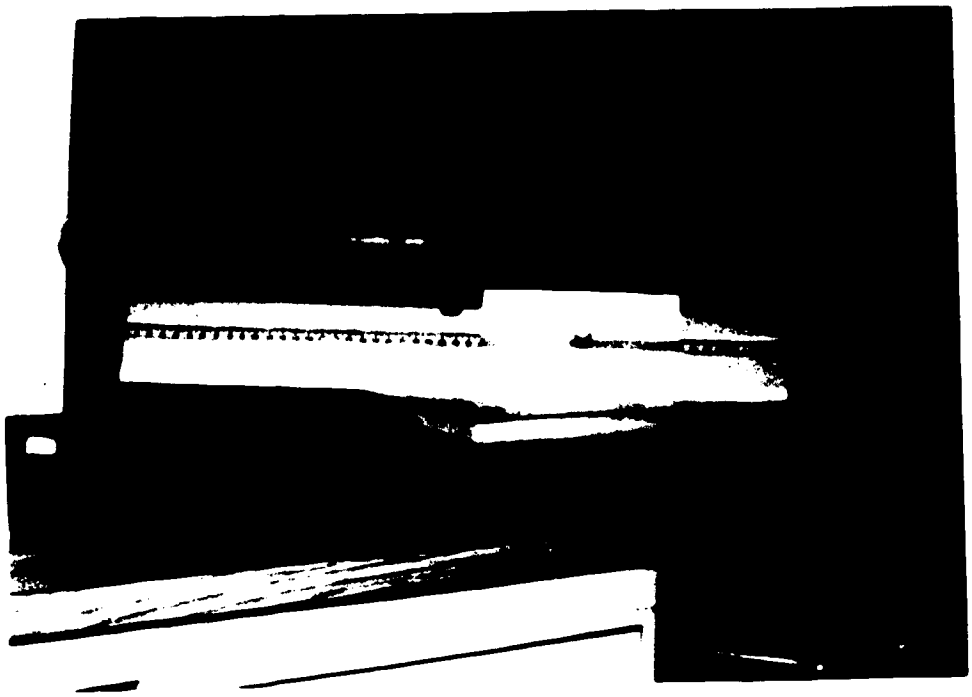

Plate 1. Universal work bench with copper pipe fixed at the top

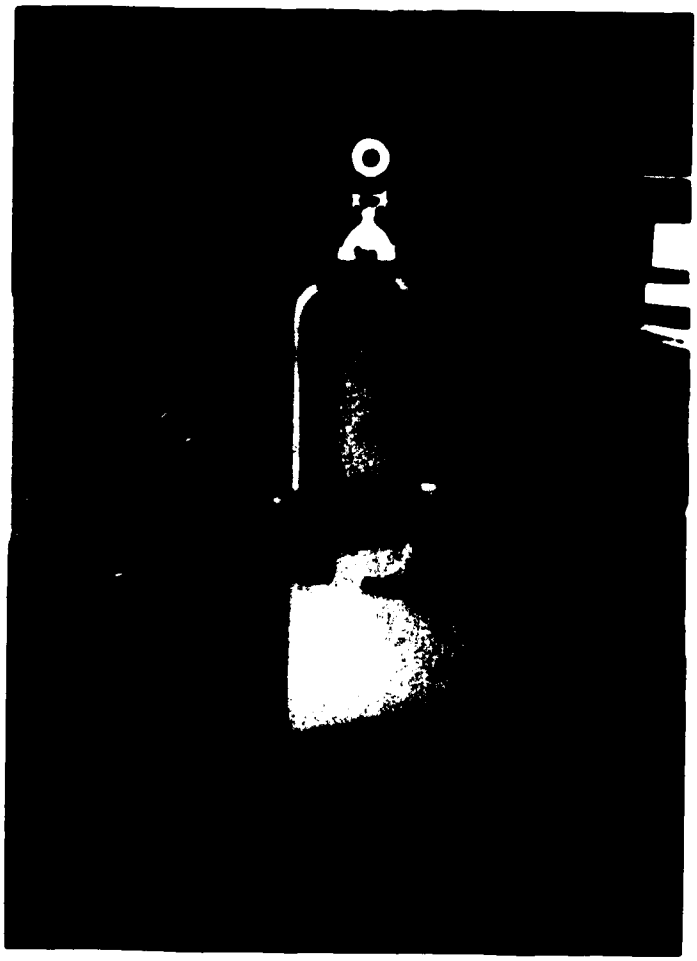

Plate 2. Three dimensional traverse

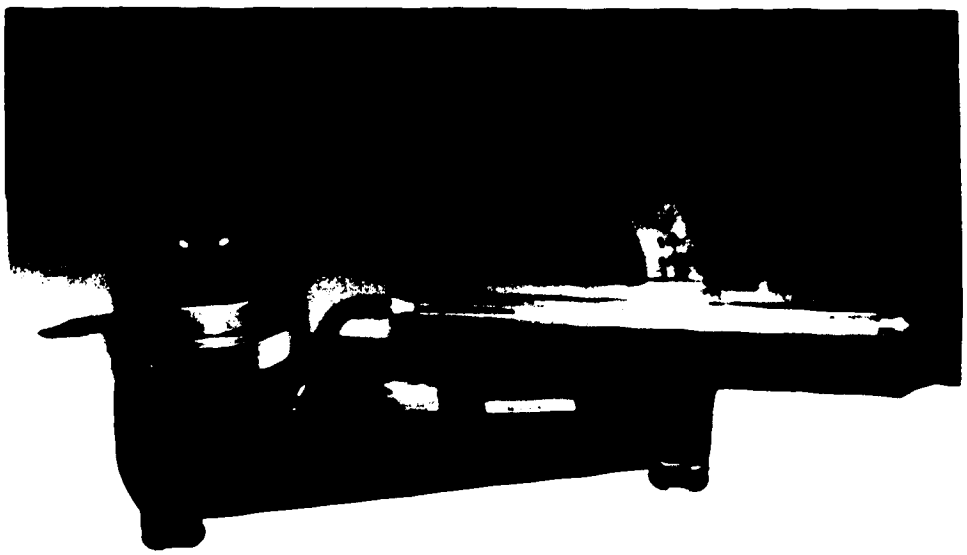

Plate 3. Micromanometer

Plate 4. General view of the experimental set up

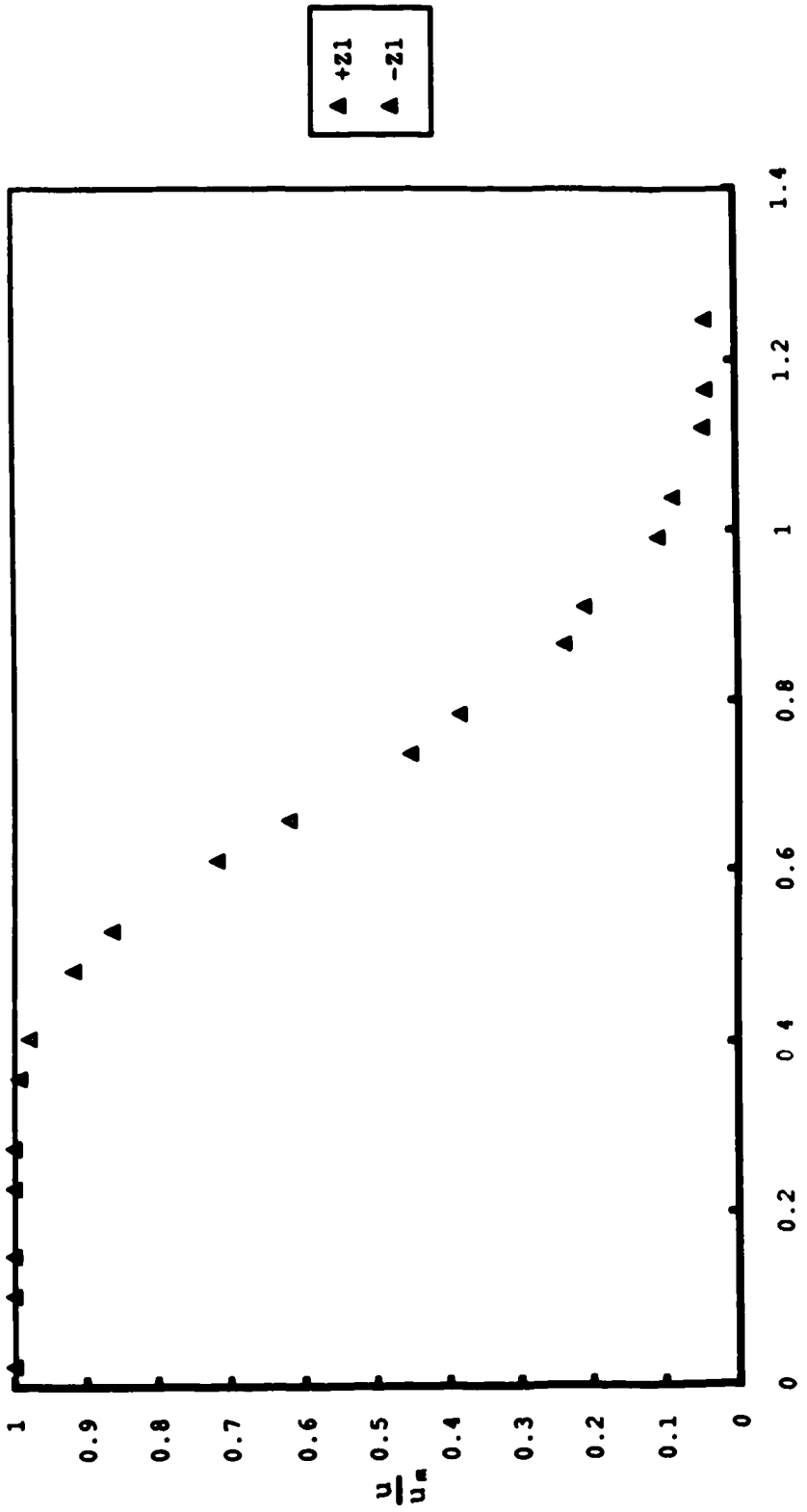

Fig. 4.1. Transverse velocity profile
Expt. 1, X1/d = 2.03

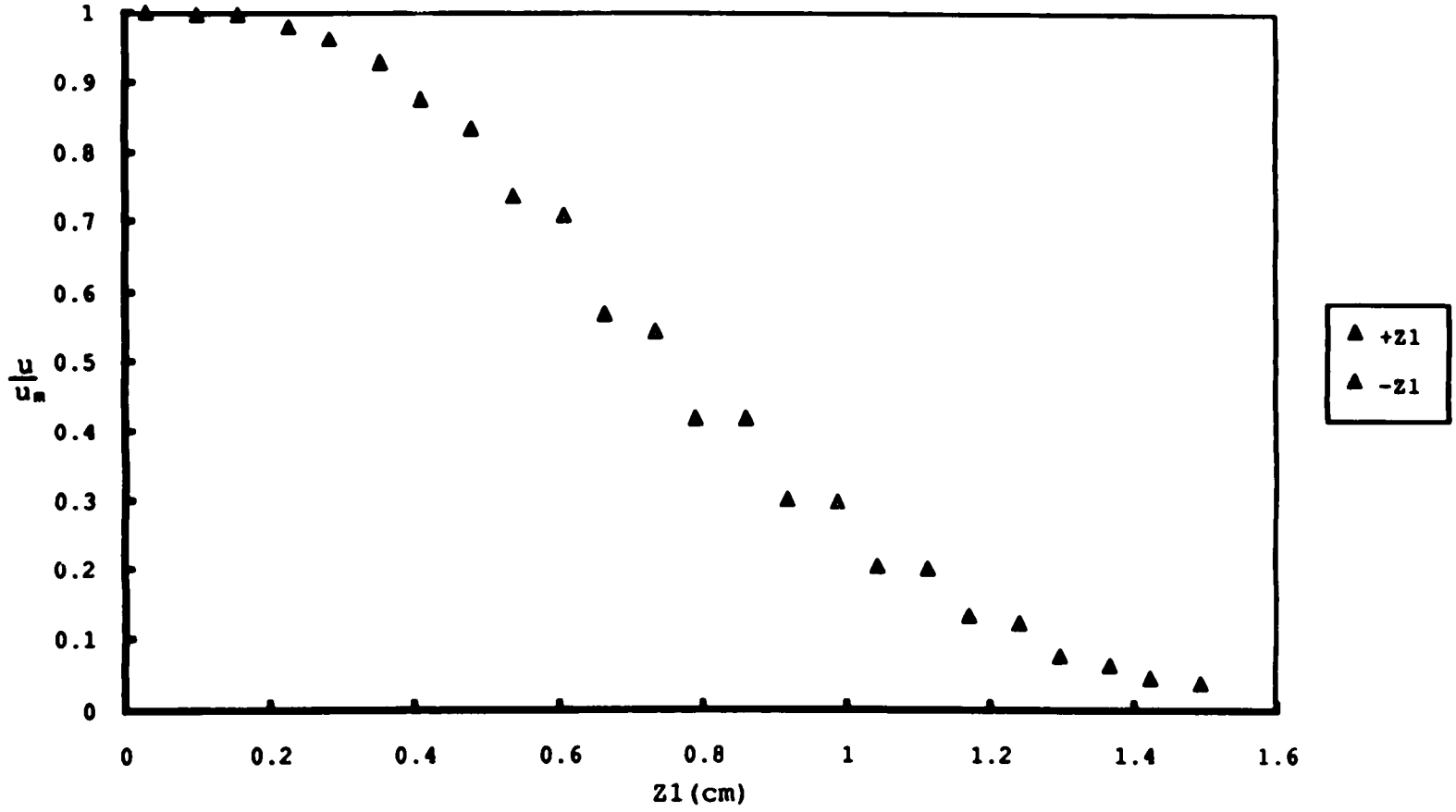

Fig. 4.2. Transverse velocity profile
Expt. 1, X1/d = 3.76

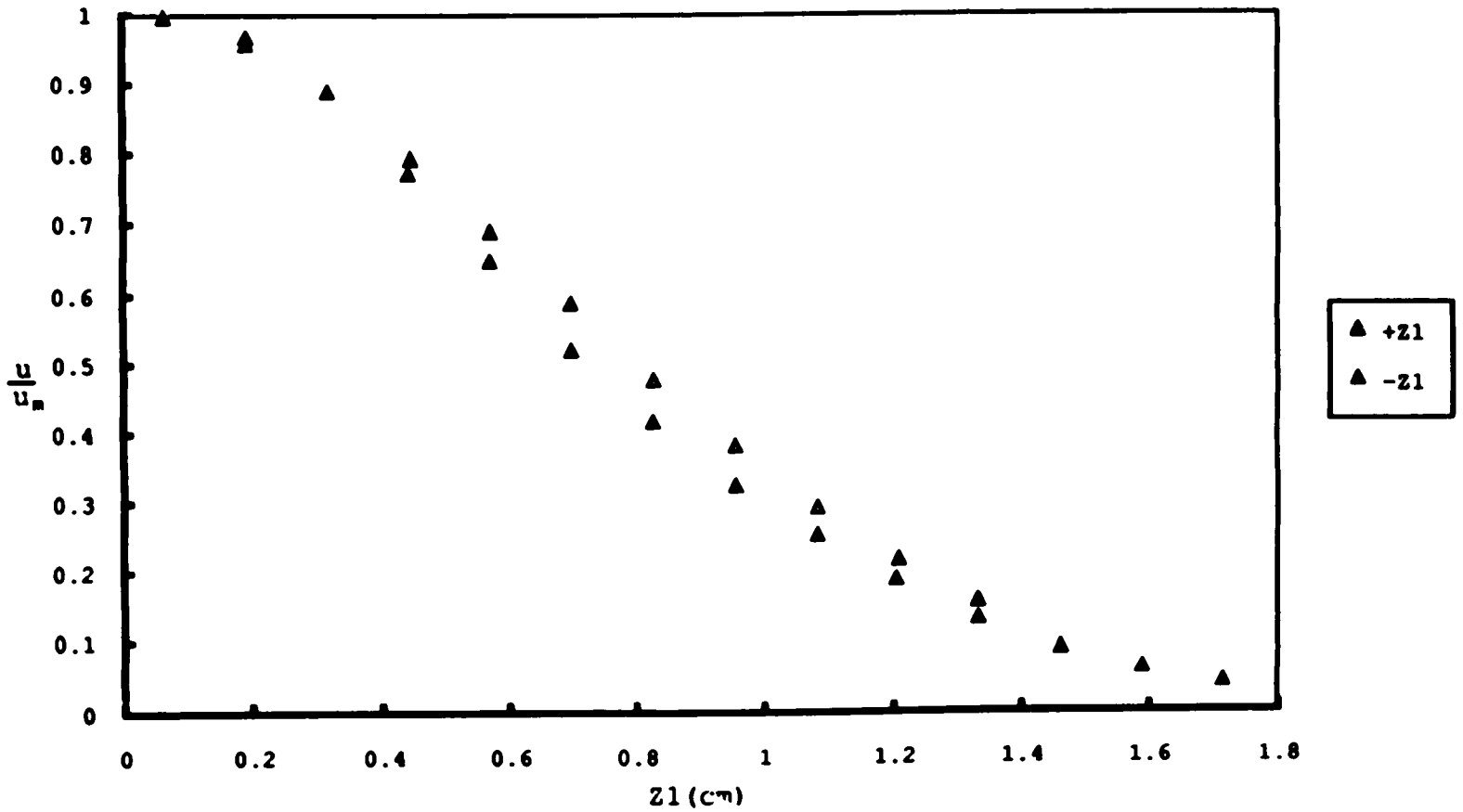

Fig. 4.3. Transverse velocity profile
Expt. 1, X1/d = 5.18

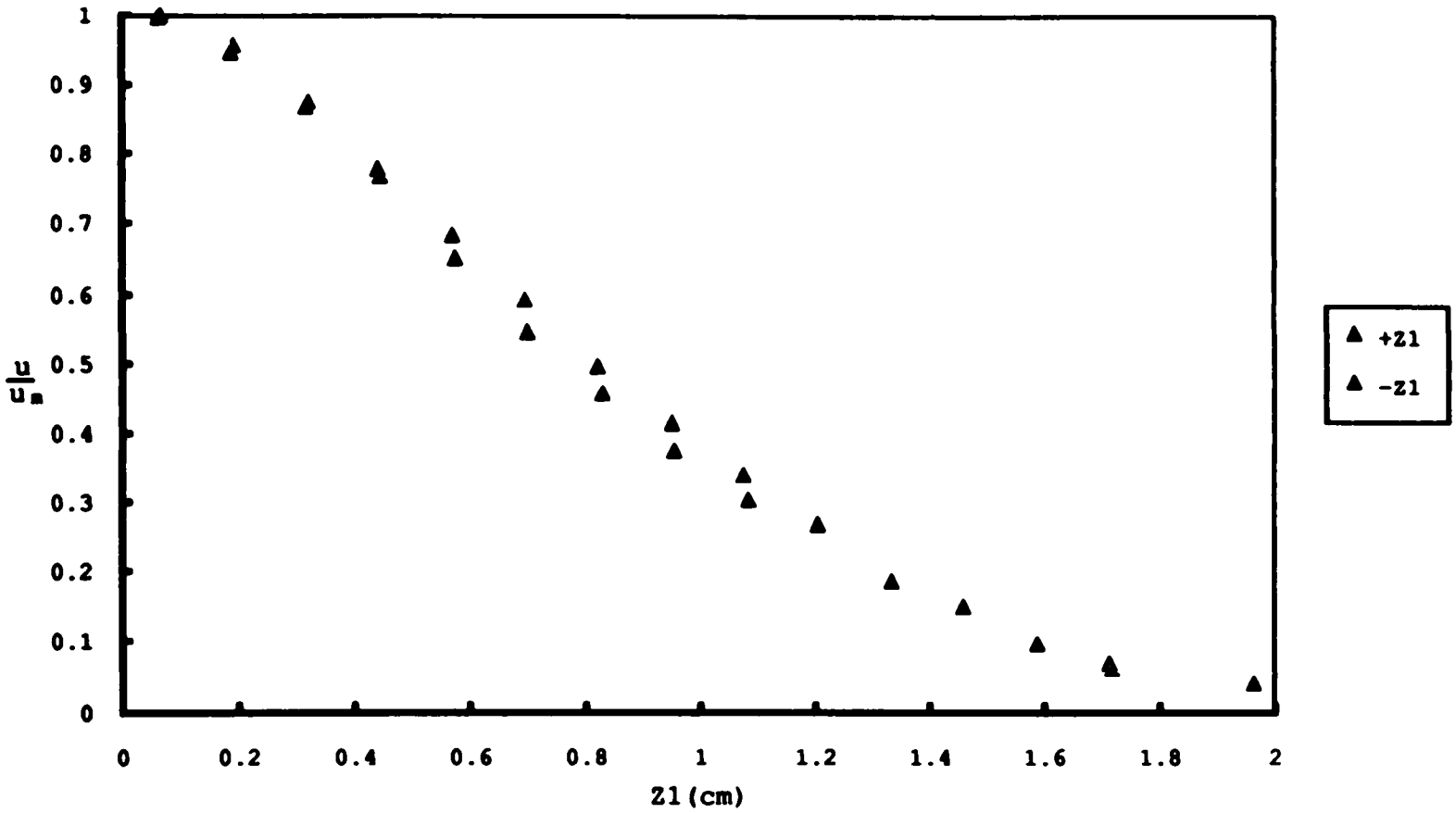

Fig. 4.4. Transverse velocity profile
Expt. 1, X1/d = 6.36

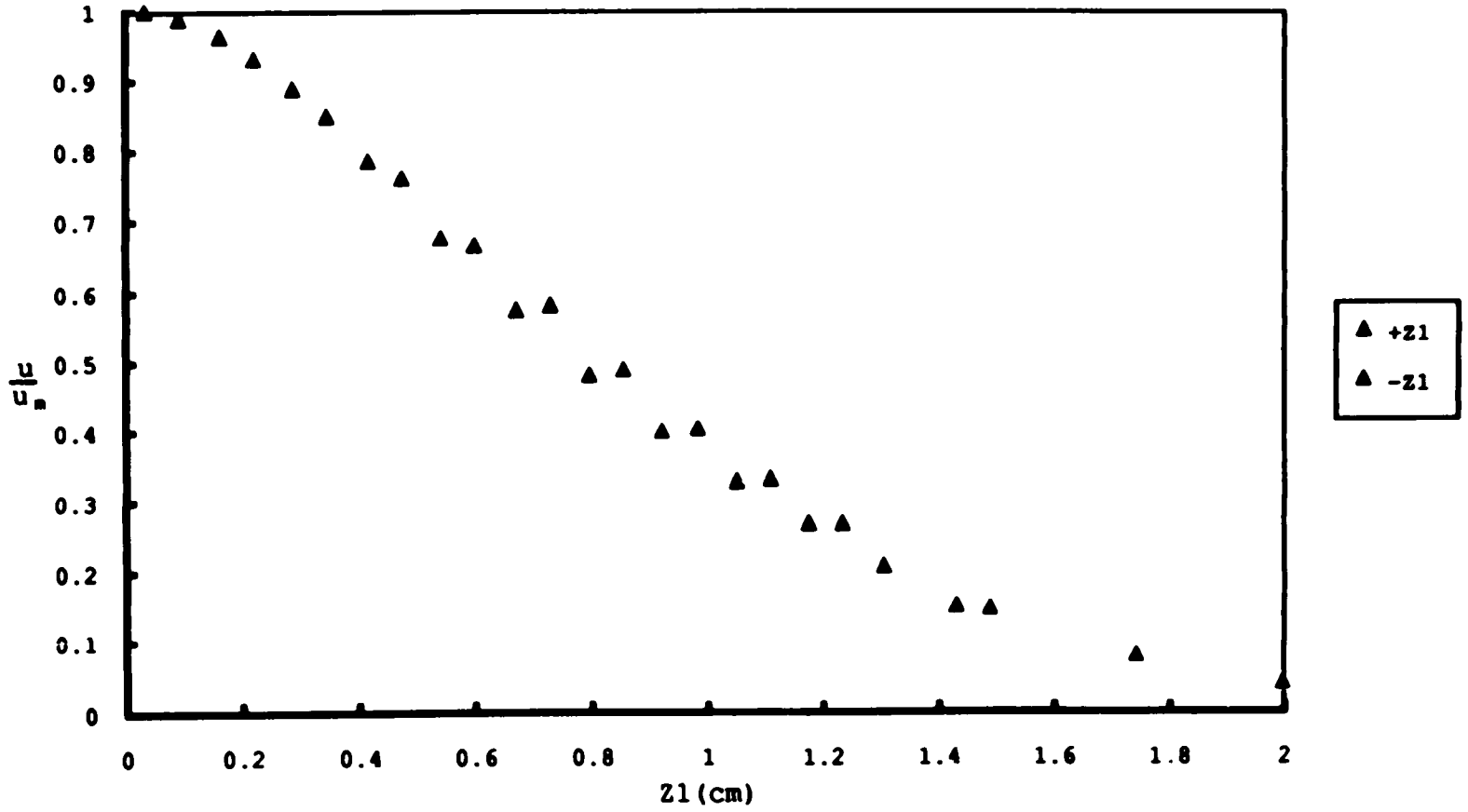

Fig. 4.5. Transverse velocity profile
Expt. 1, X1/d = 6.76

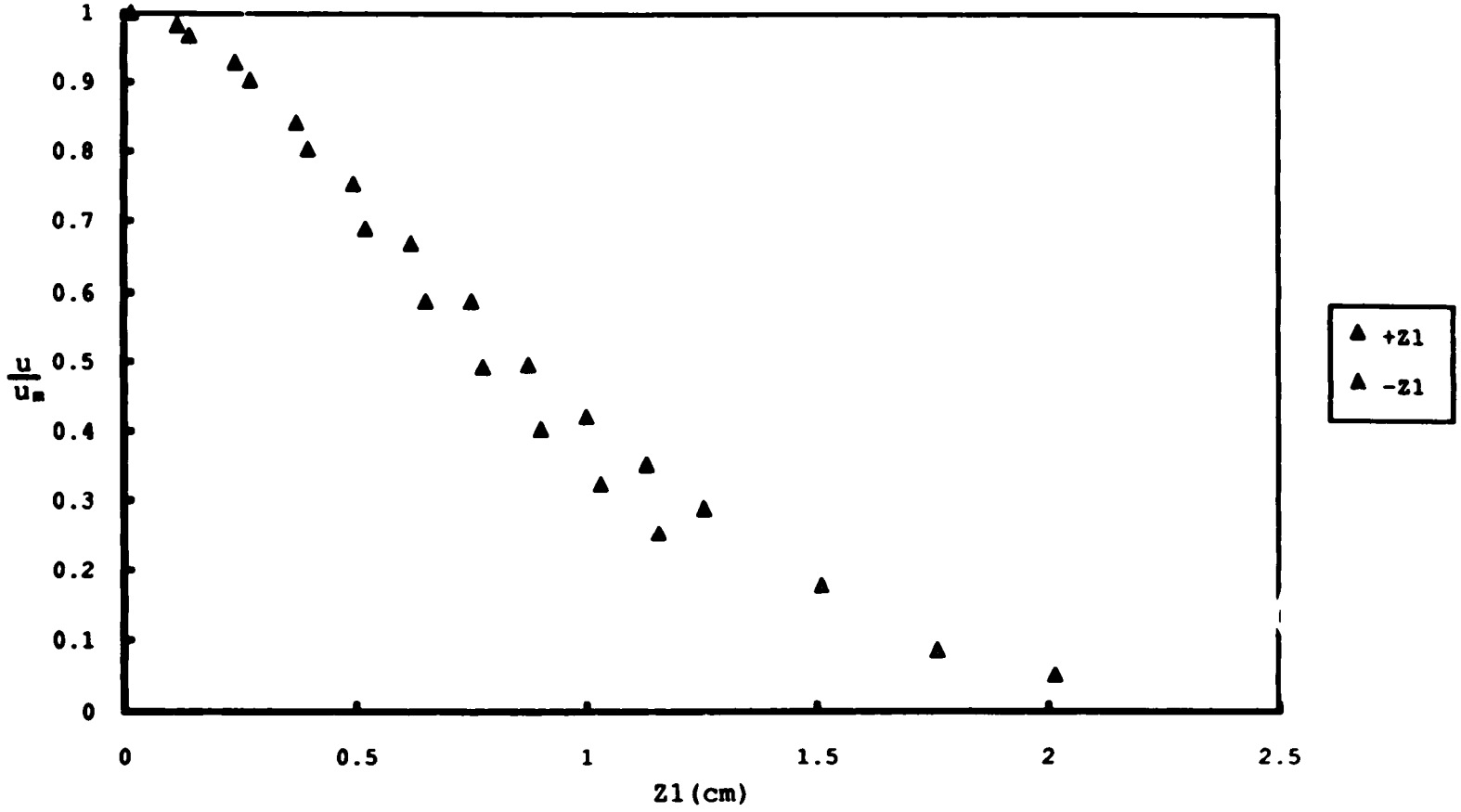

Fig. 4.6. Transverse velocity profile
Expt. 1, X1/d = 7.39

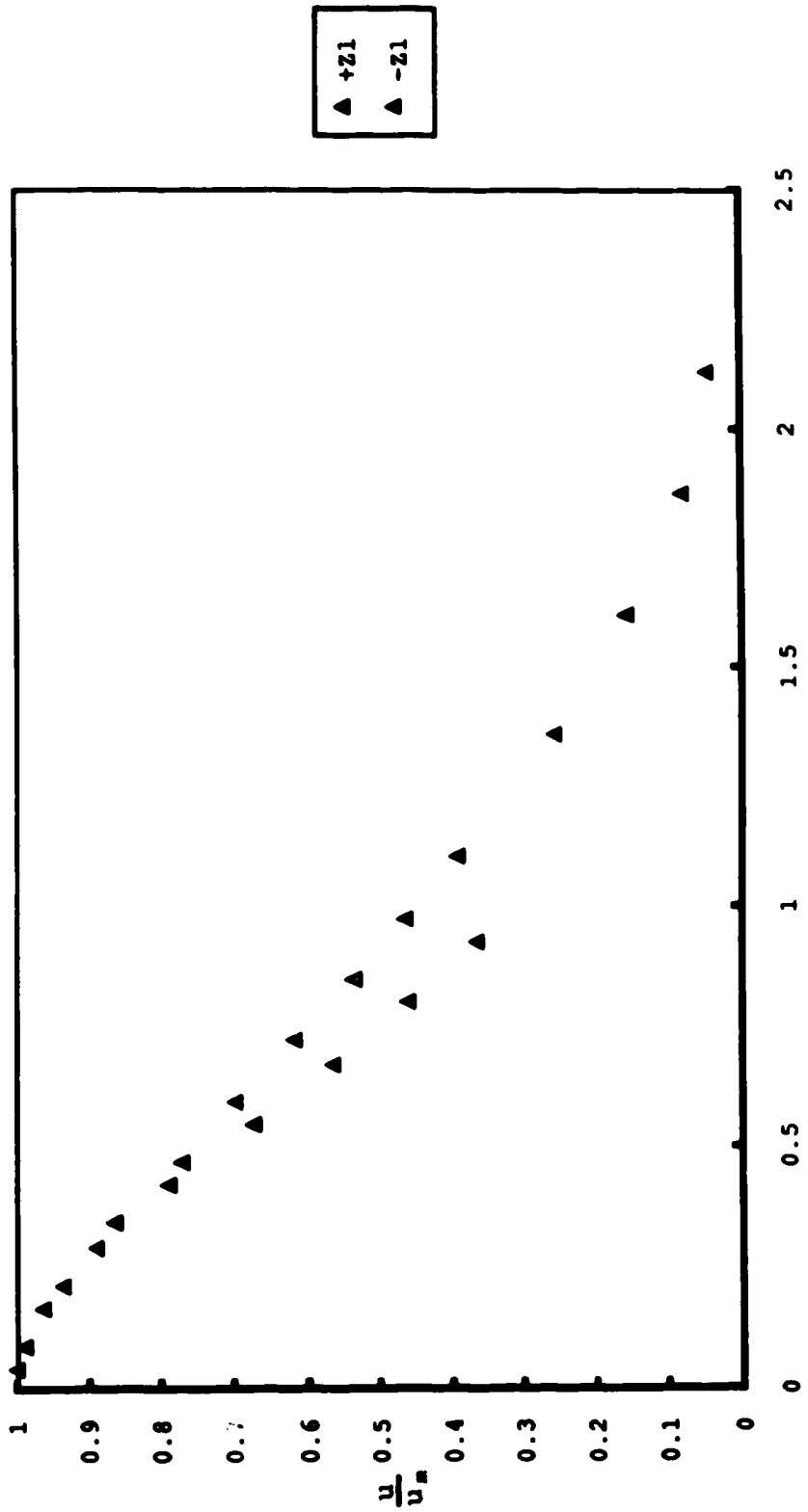

Fig. 4.7. Transverse velocity profile
Expt. 1, X1/d = 8.02

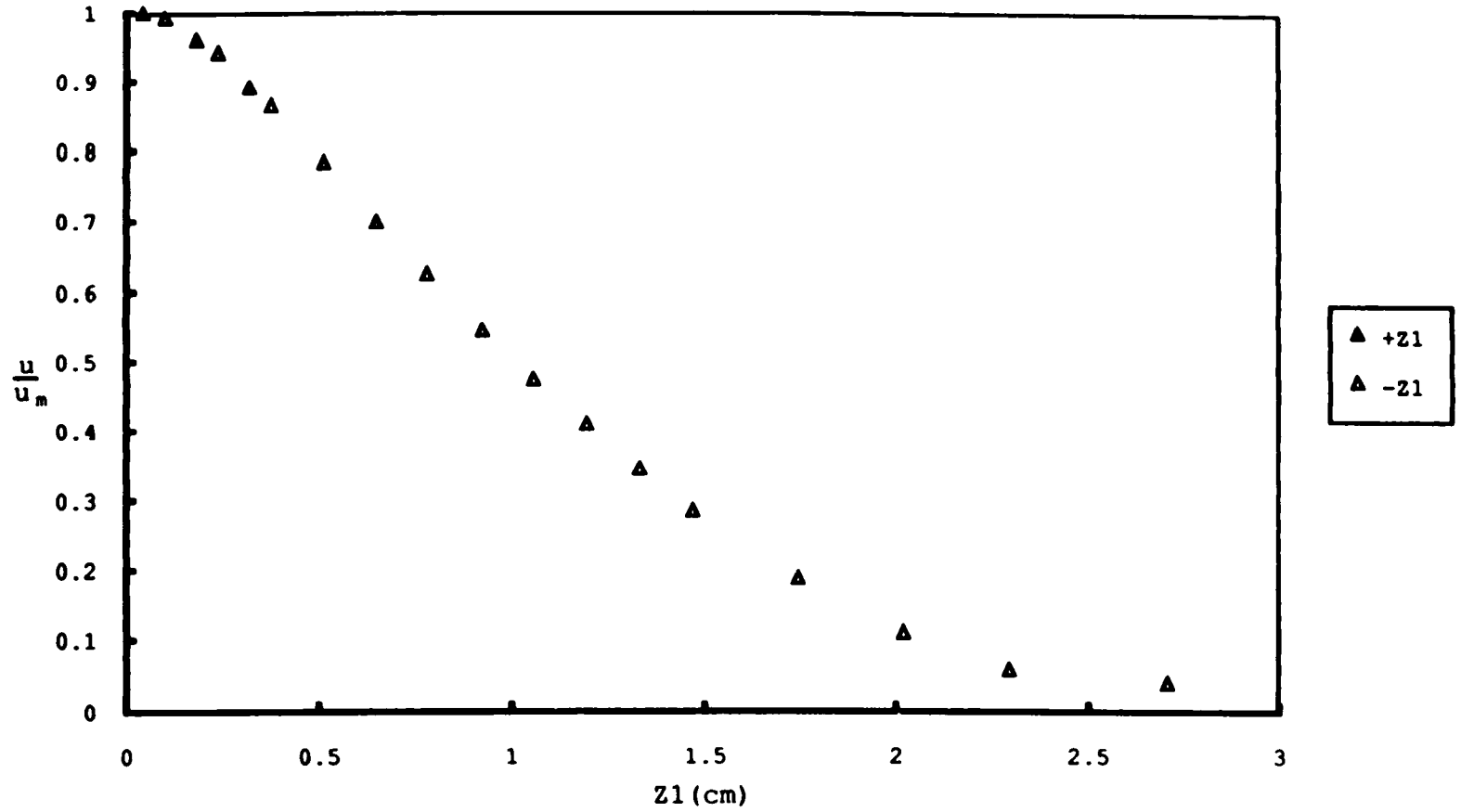

Fig. 4.8. Transverse velocity profile
Expt. 1, X1/d = 8.65

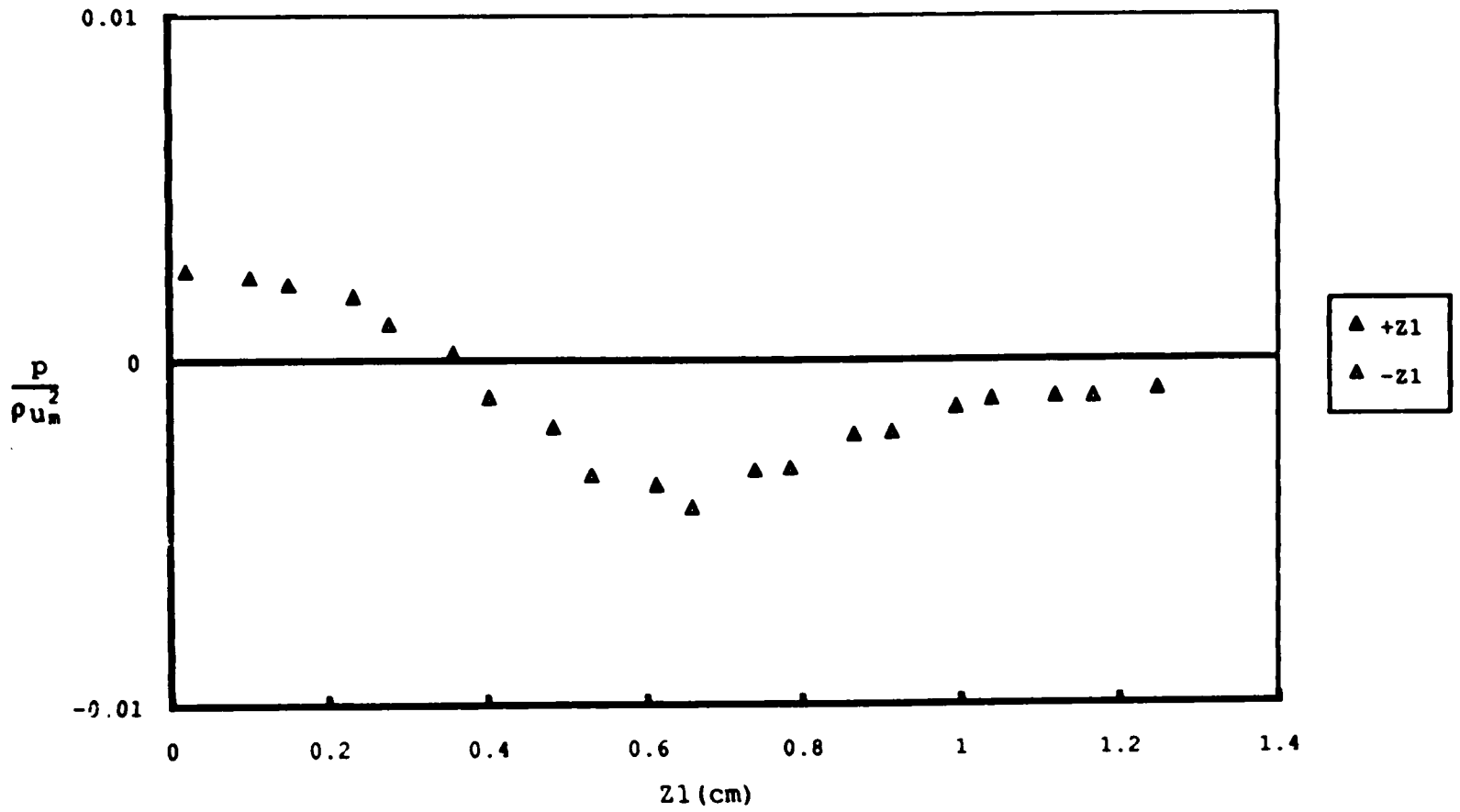

Fig. 4 9. Transverse pressure profile
Expt. 1, X1/d=2.03

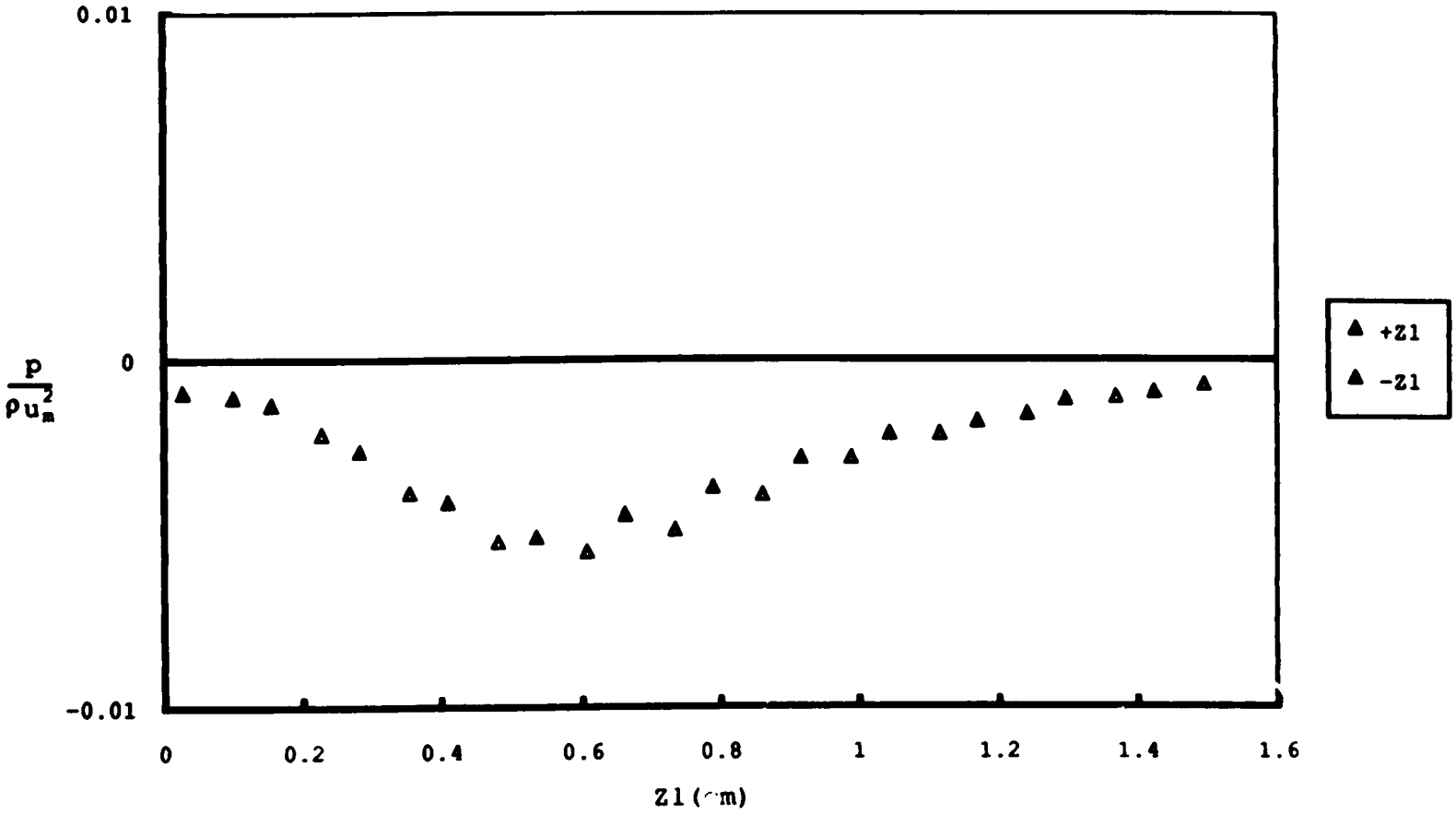

Fig. 4.10. Transverse pressure profile
Expt. 1, X1/d=3.76

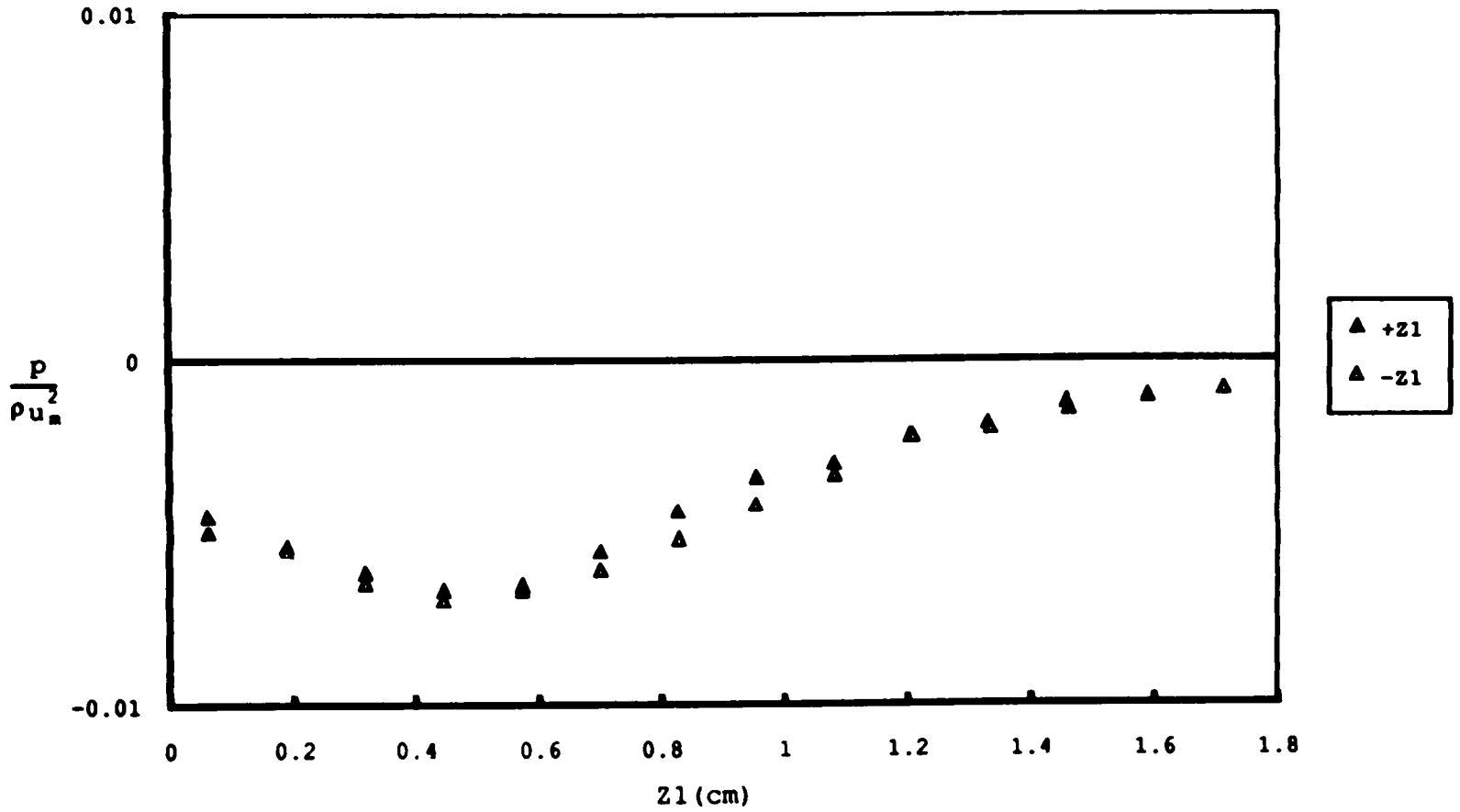

Fig. 4.11. Transverse pressure profile
Exp. 1, X1/d=5.18

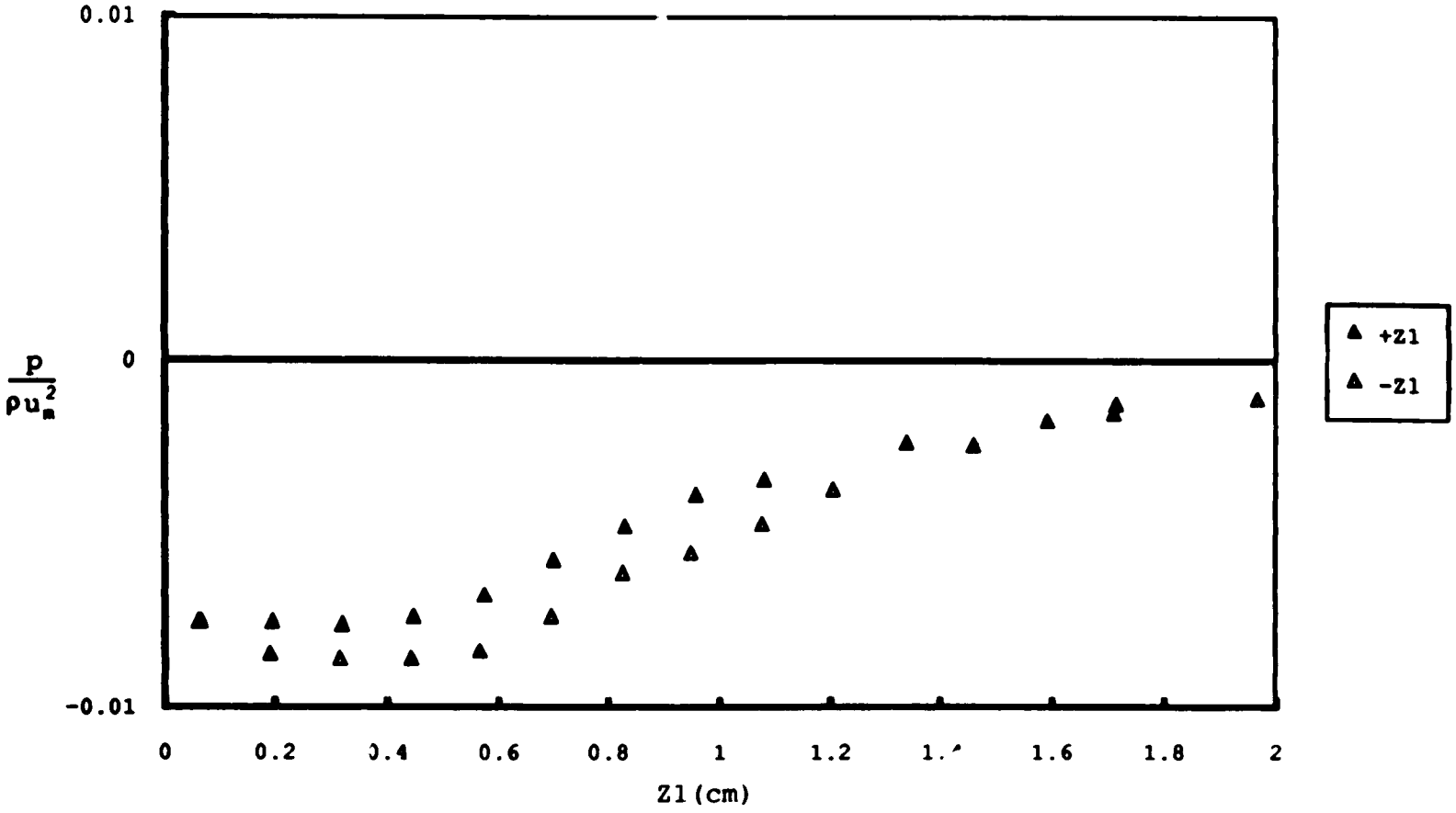

Fig. 4.12. Transverse pressure profile
Expt. 1, X1/d=6.36

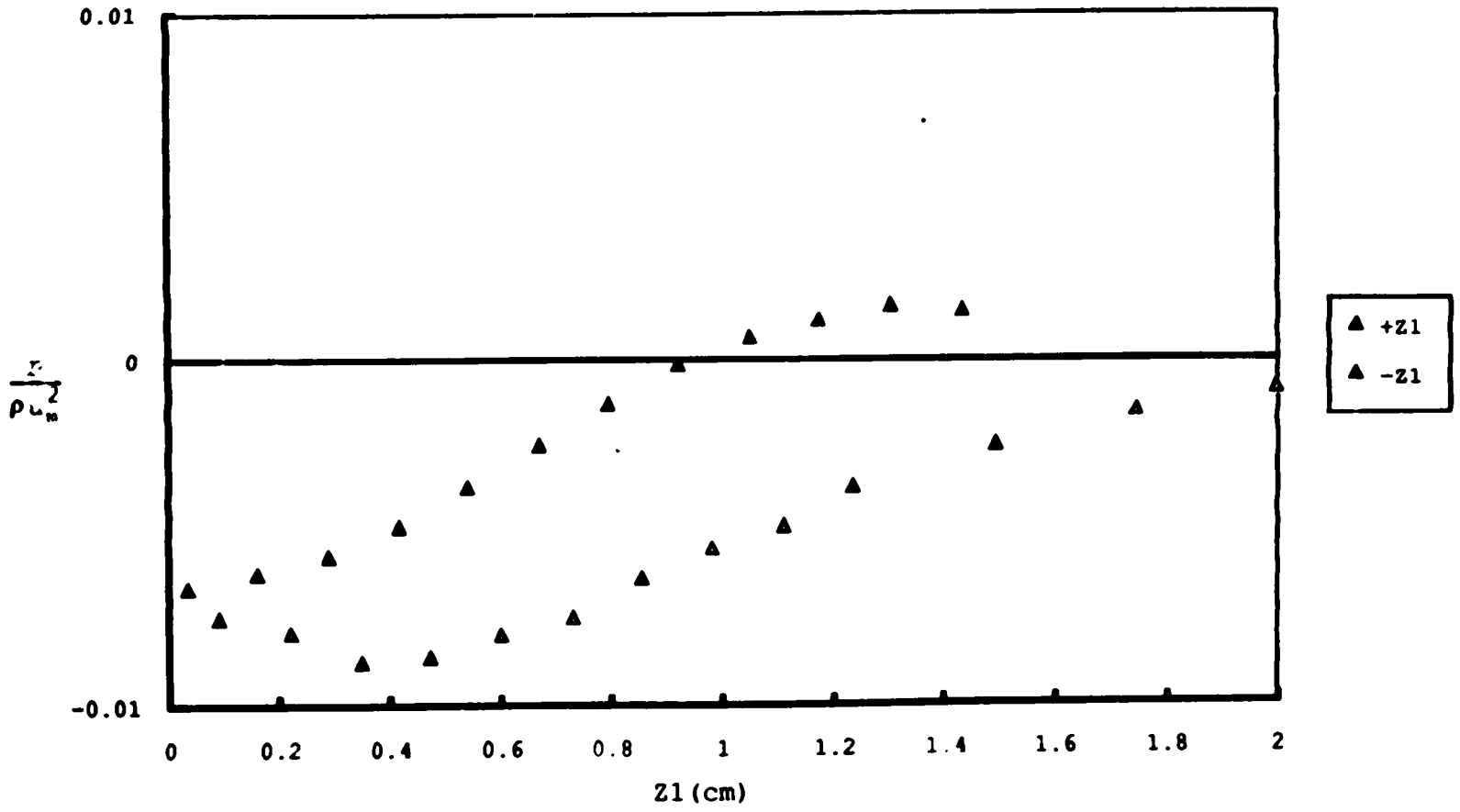

Fig. 4.13. Transverse pressure profile
Expt. 1, X1/d=6.76

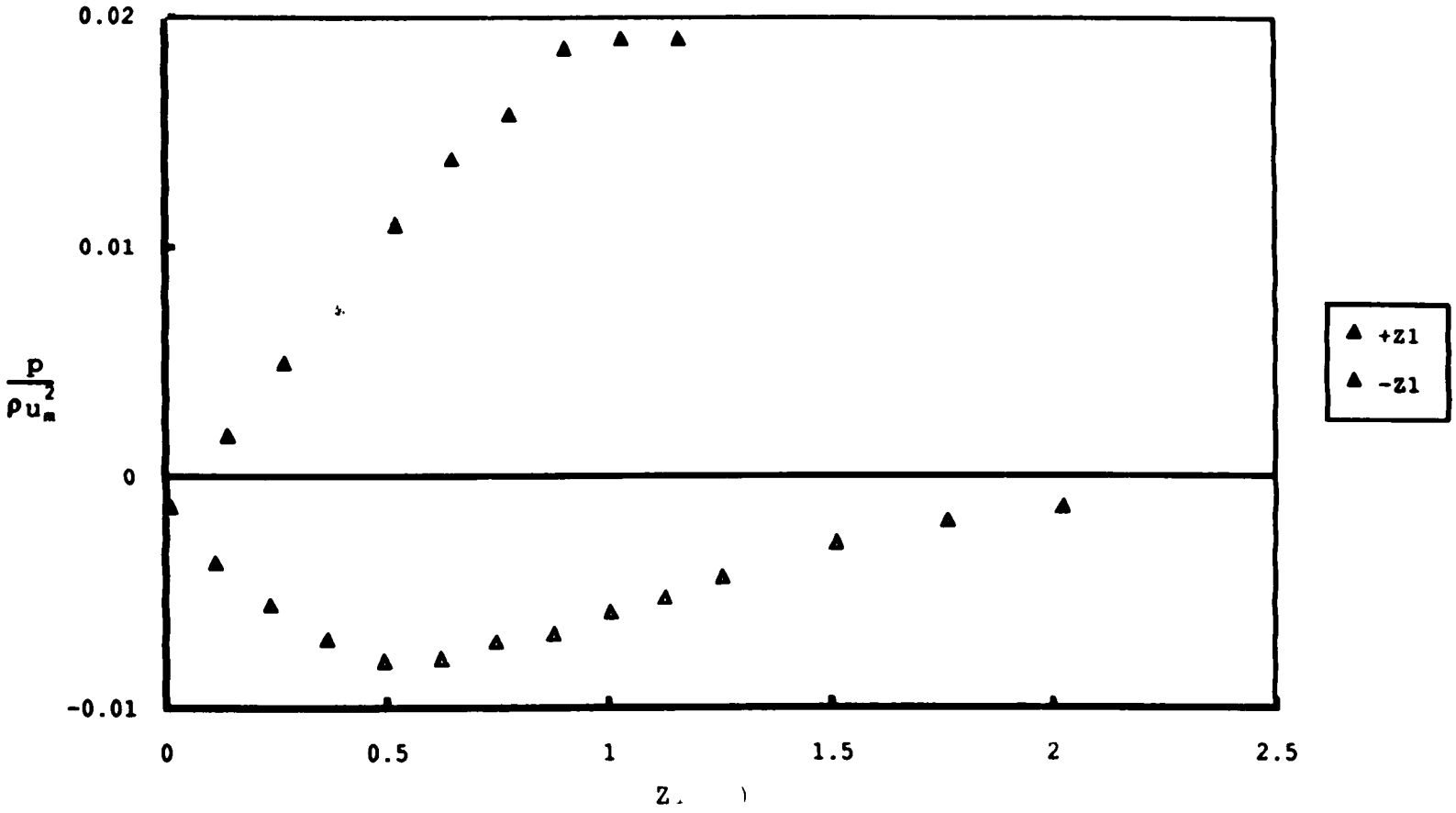

Fig. 4.14. Transverse pressure profile
Expt. 1, X1/d=7.39

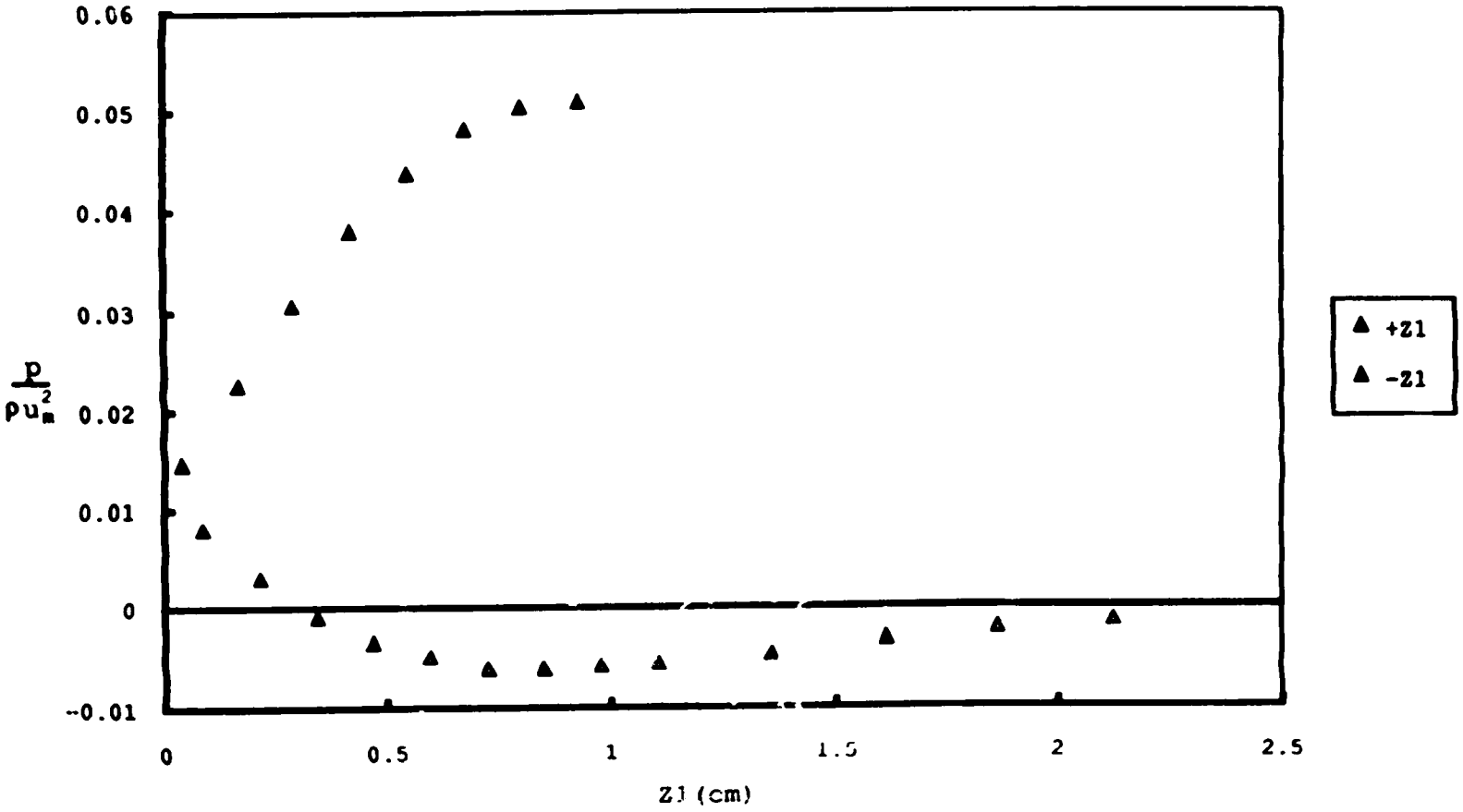

Fig. 4.15. Transverse pressure profile
Expt. 1, X1/d=8.02

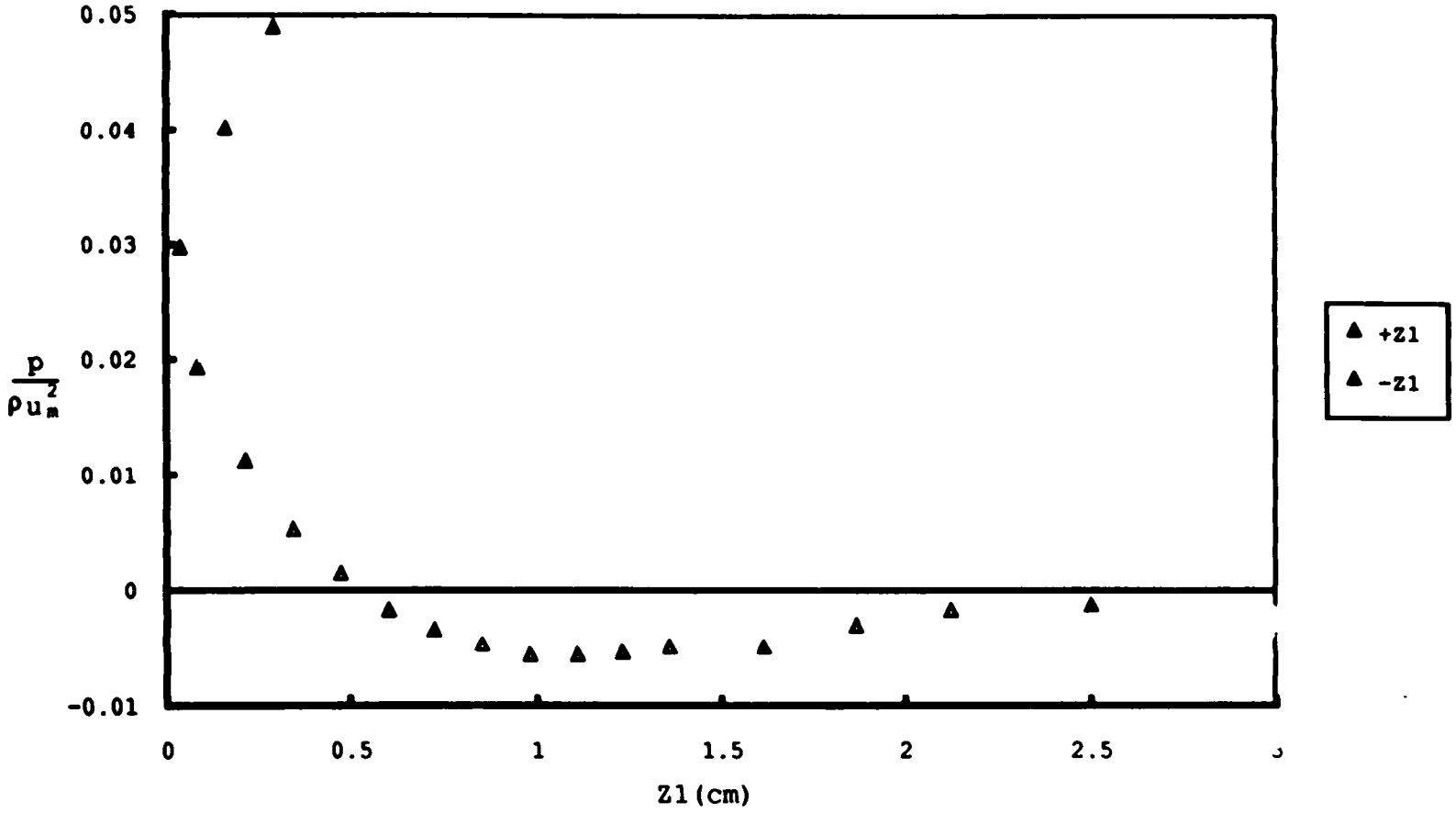

Fig. 4.16. Transverse pressure profile
Expt. 1, X1/d=8.65

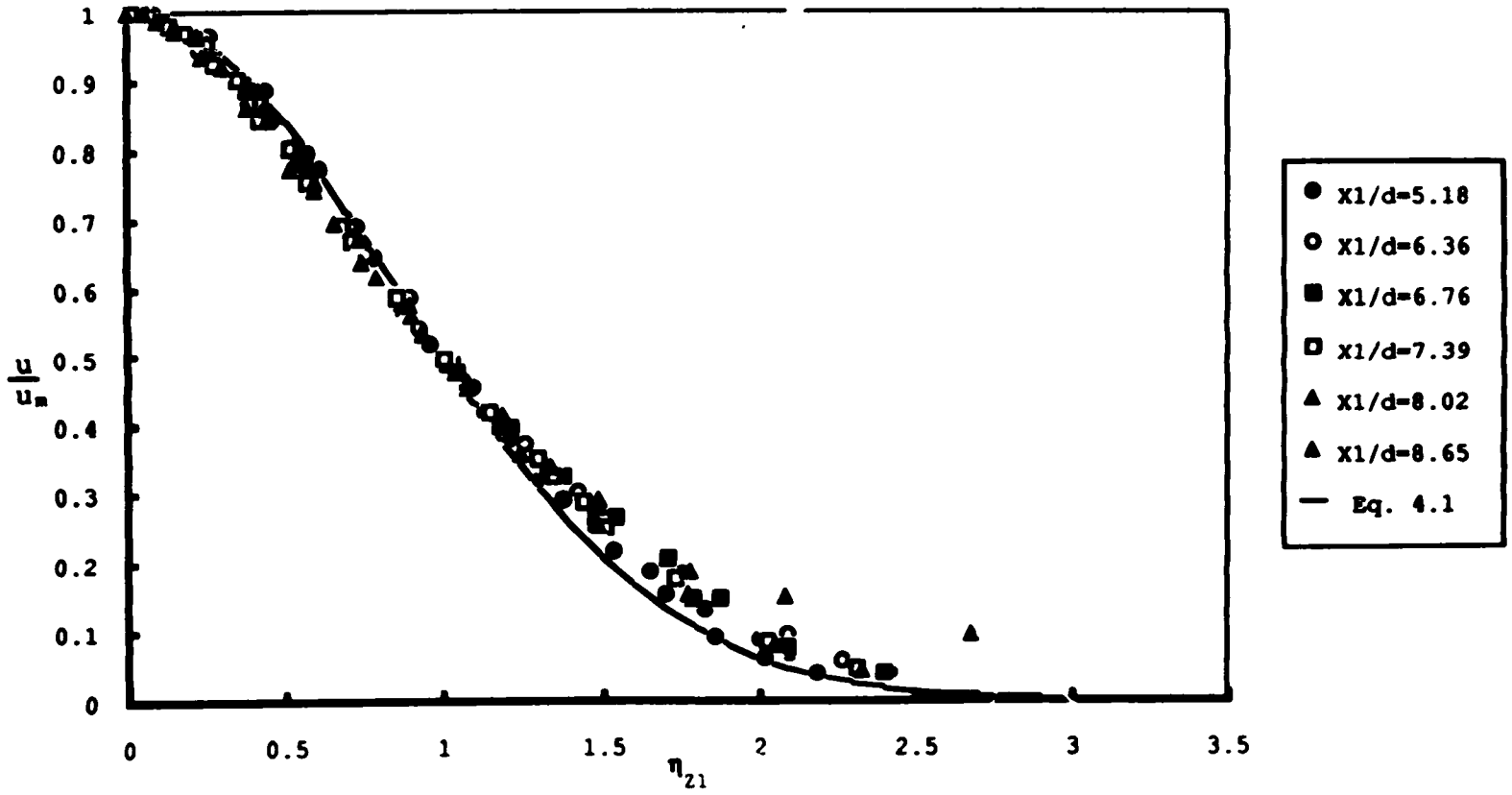

Fig. 4.17. Non dimensional transverse velocity profiles, Expt. 1

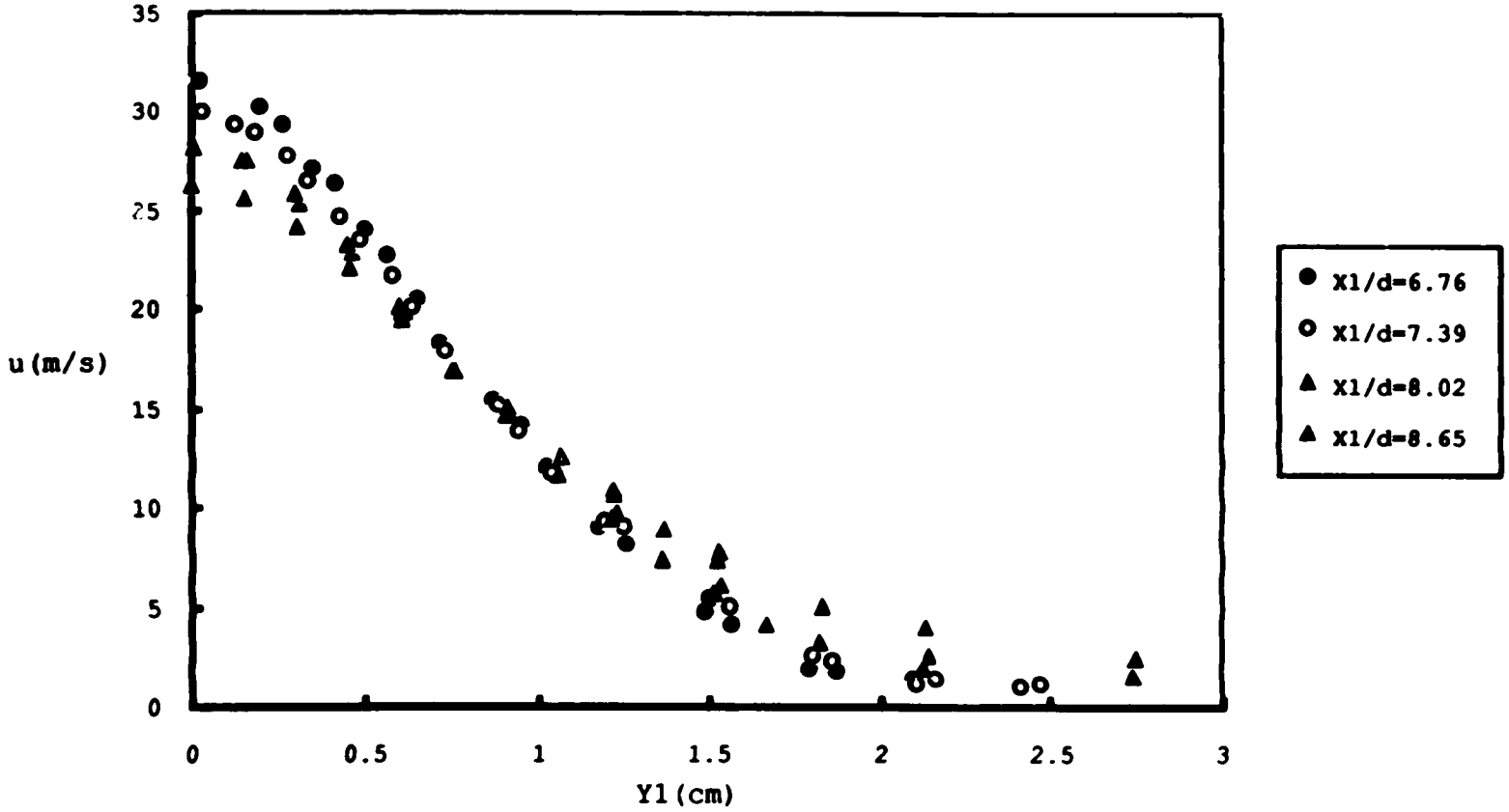

Fig. 4.18. Vertical velocity profiles
Expt. 1

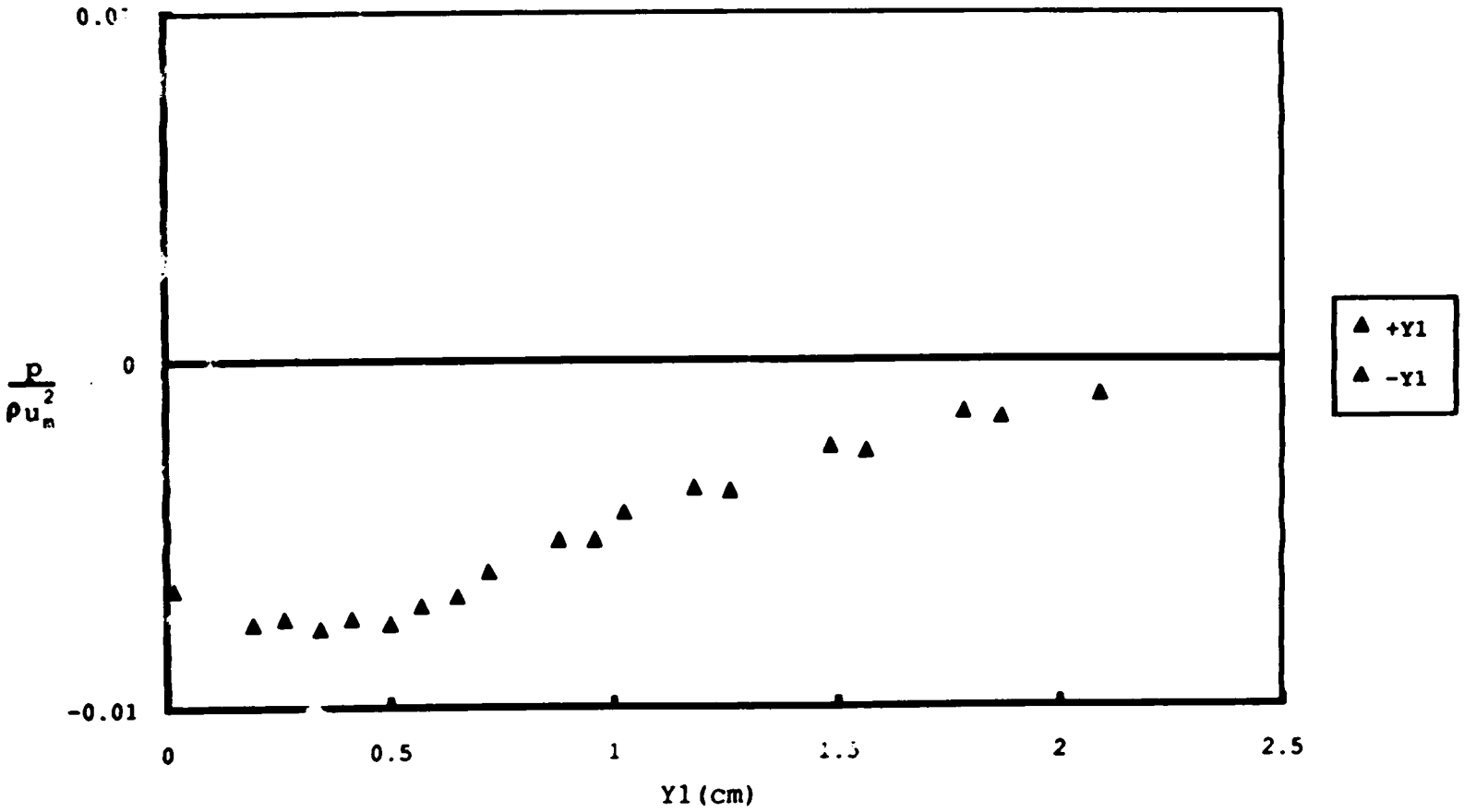

Fig. 4.19. Vertical pressure profile
Expt. 1, X1/d=6.76

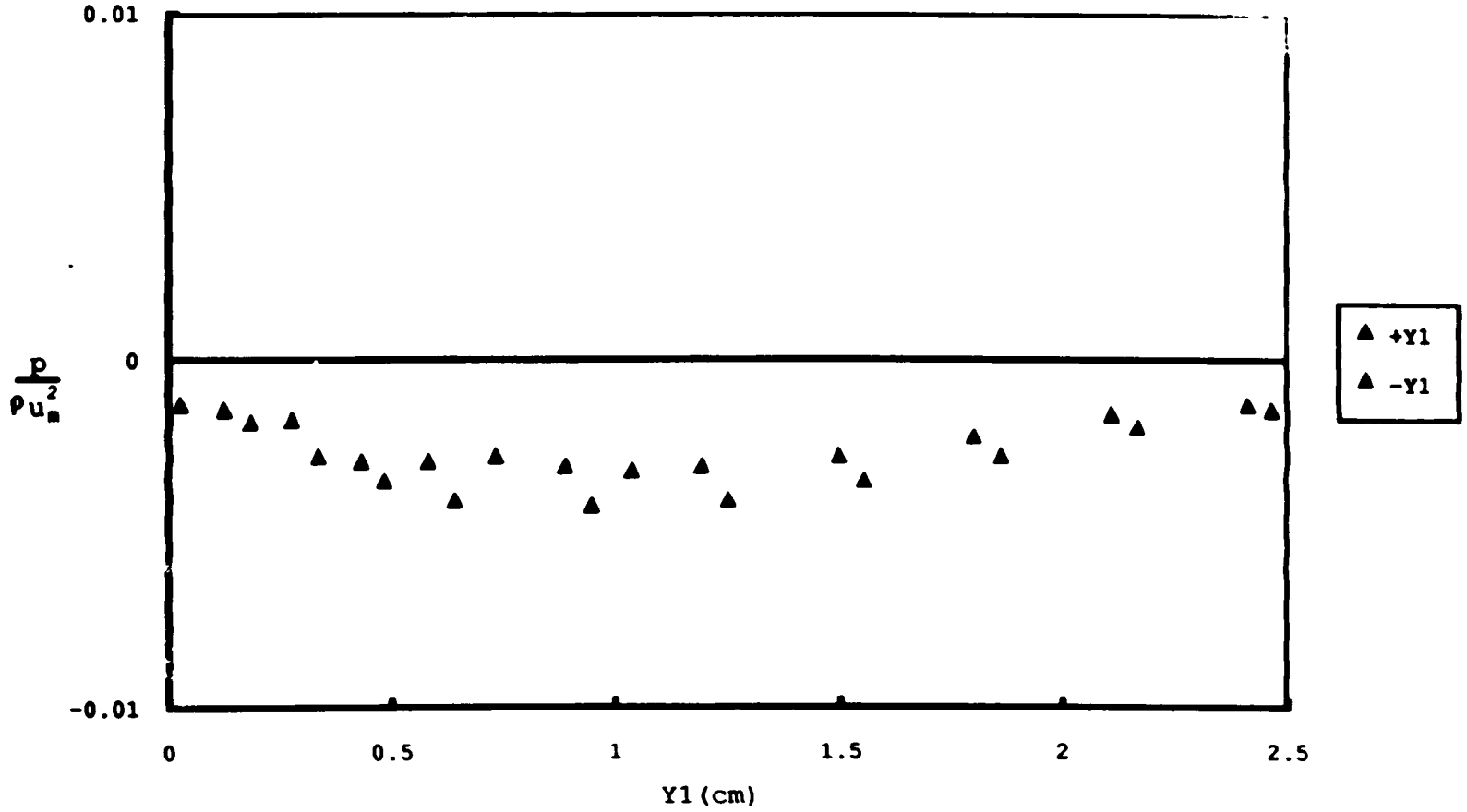

Fig. 4.20. Vertical pressure profile
Expt. 1, X1/d=7.39

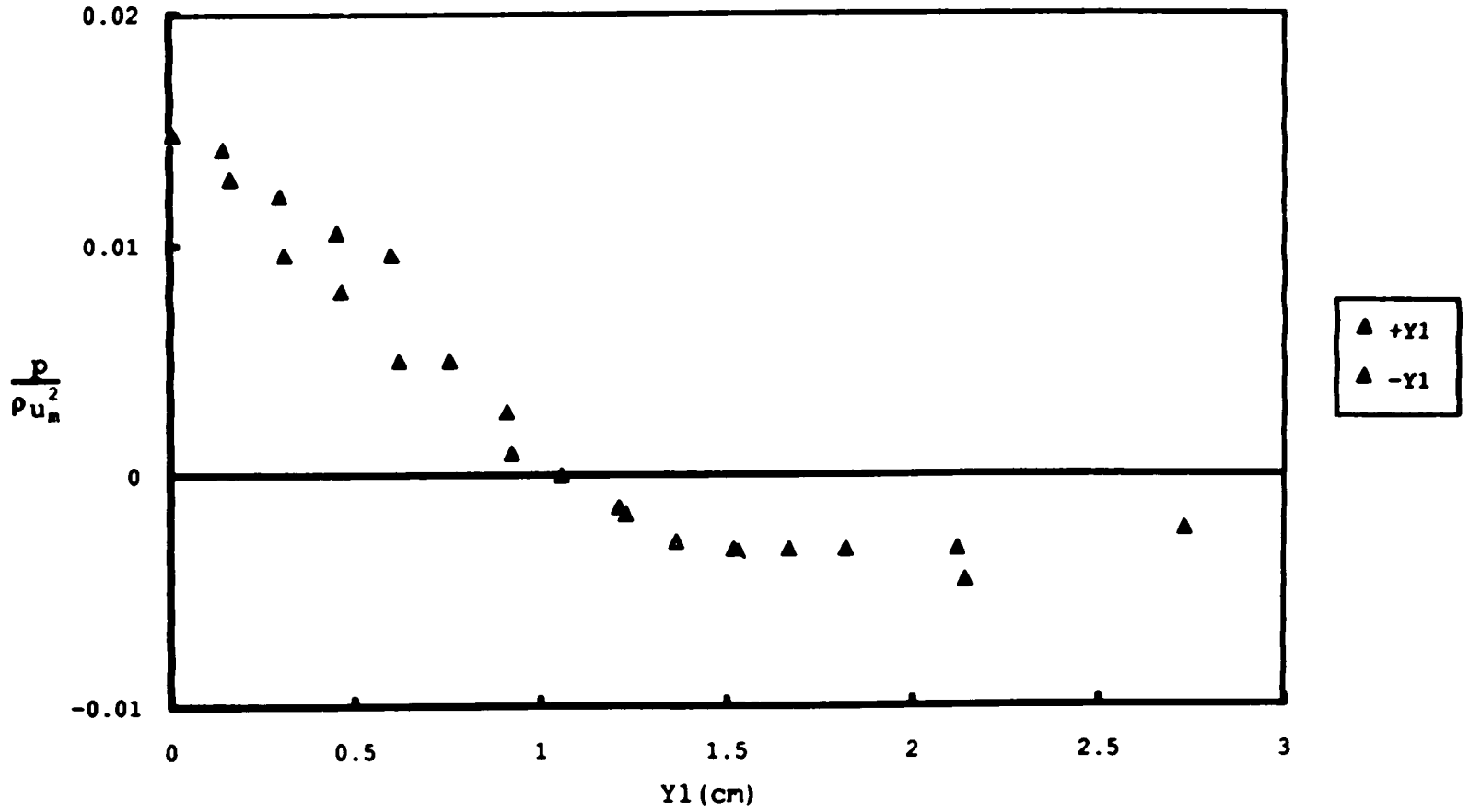

Fig. 4.21. Vertical pressure profile
Expt. 1, X1/d=8.02

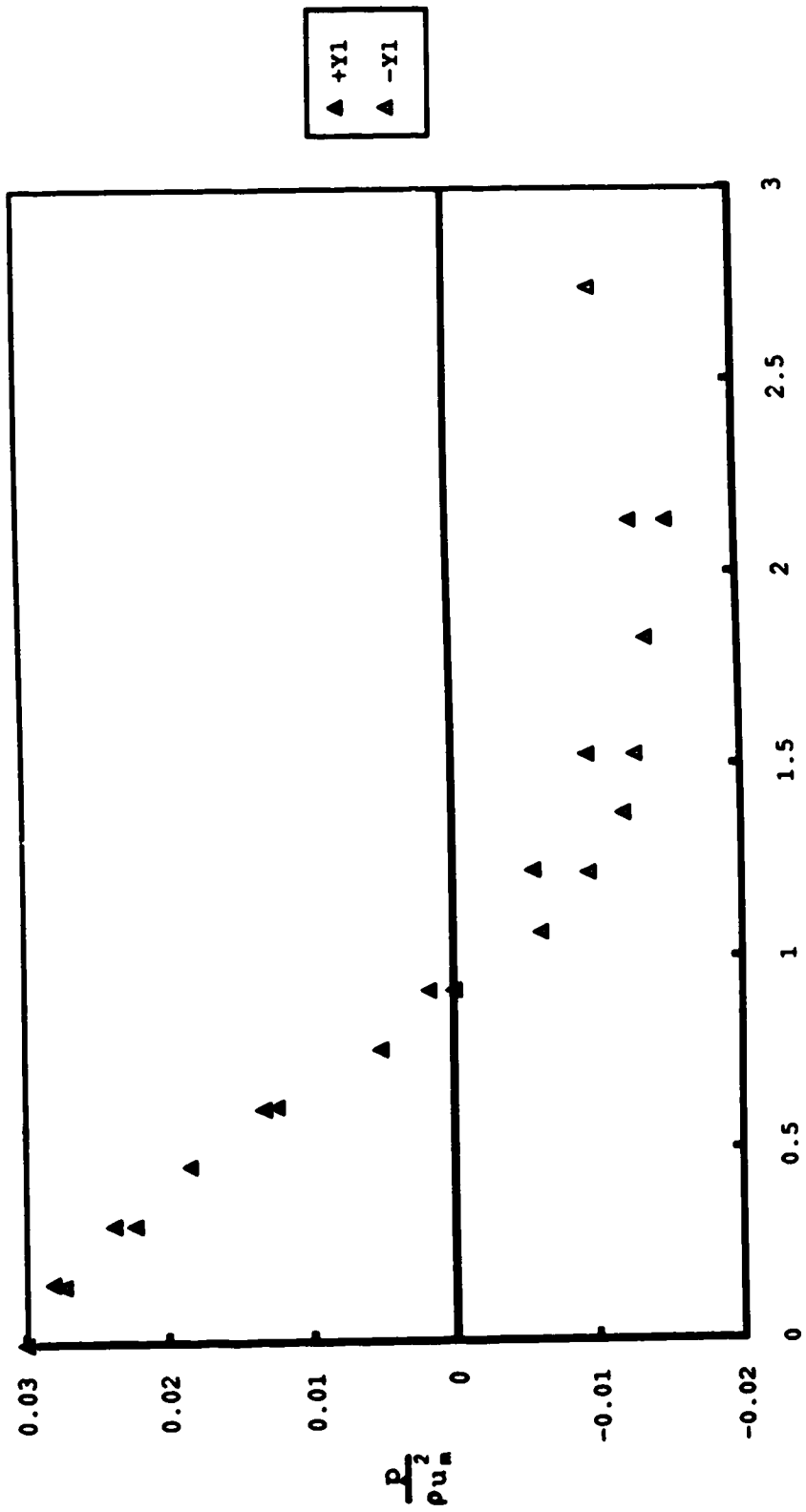

Fig. 4.22. Vertical pressure profile
Expt. 1, X1/d=8.65

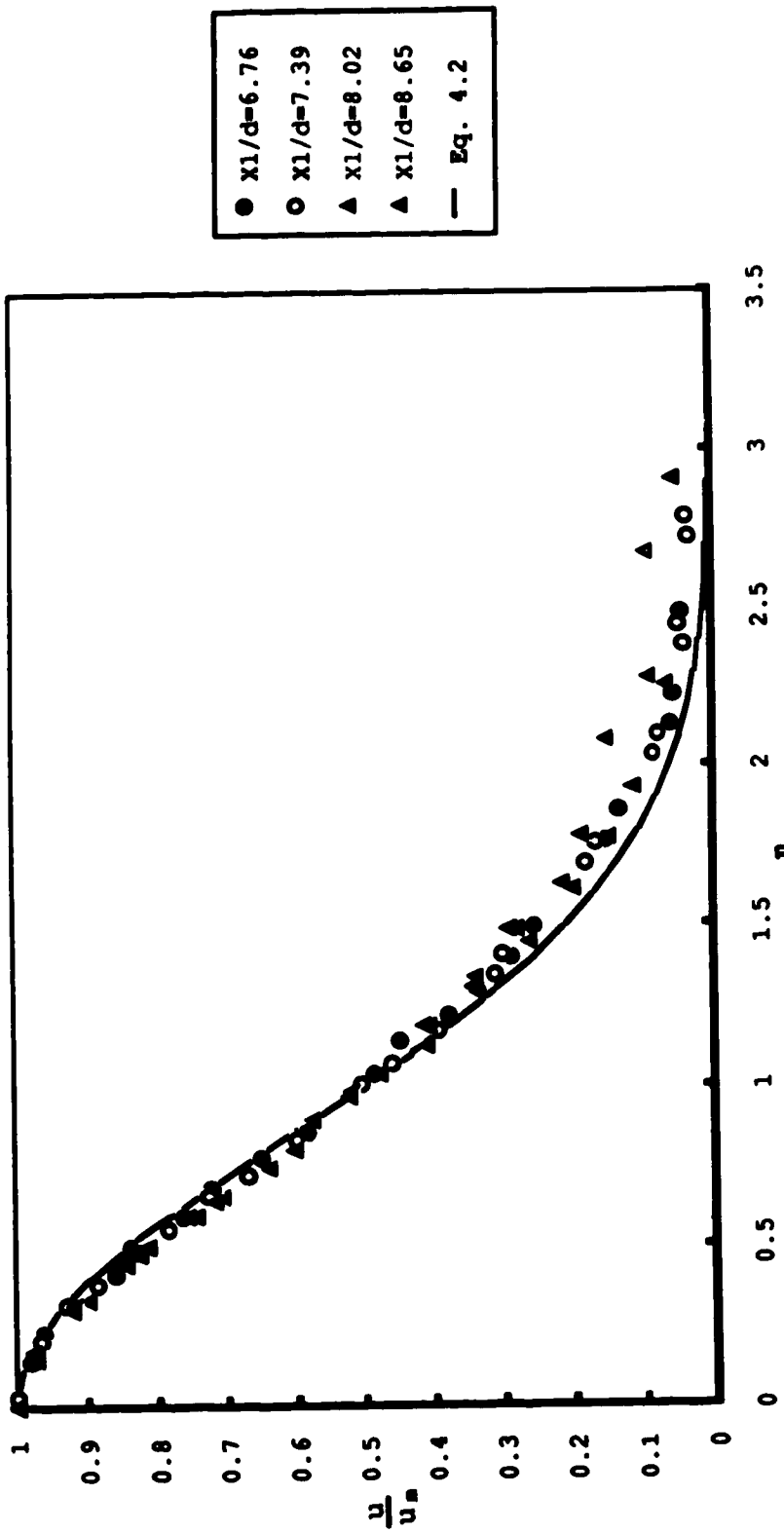

Fig. 4.23. Non dimensional vertical velocity profiles, Expt. 1

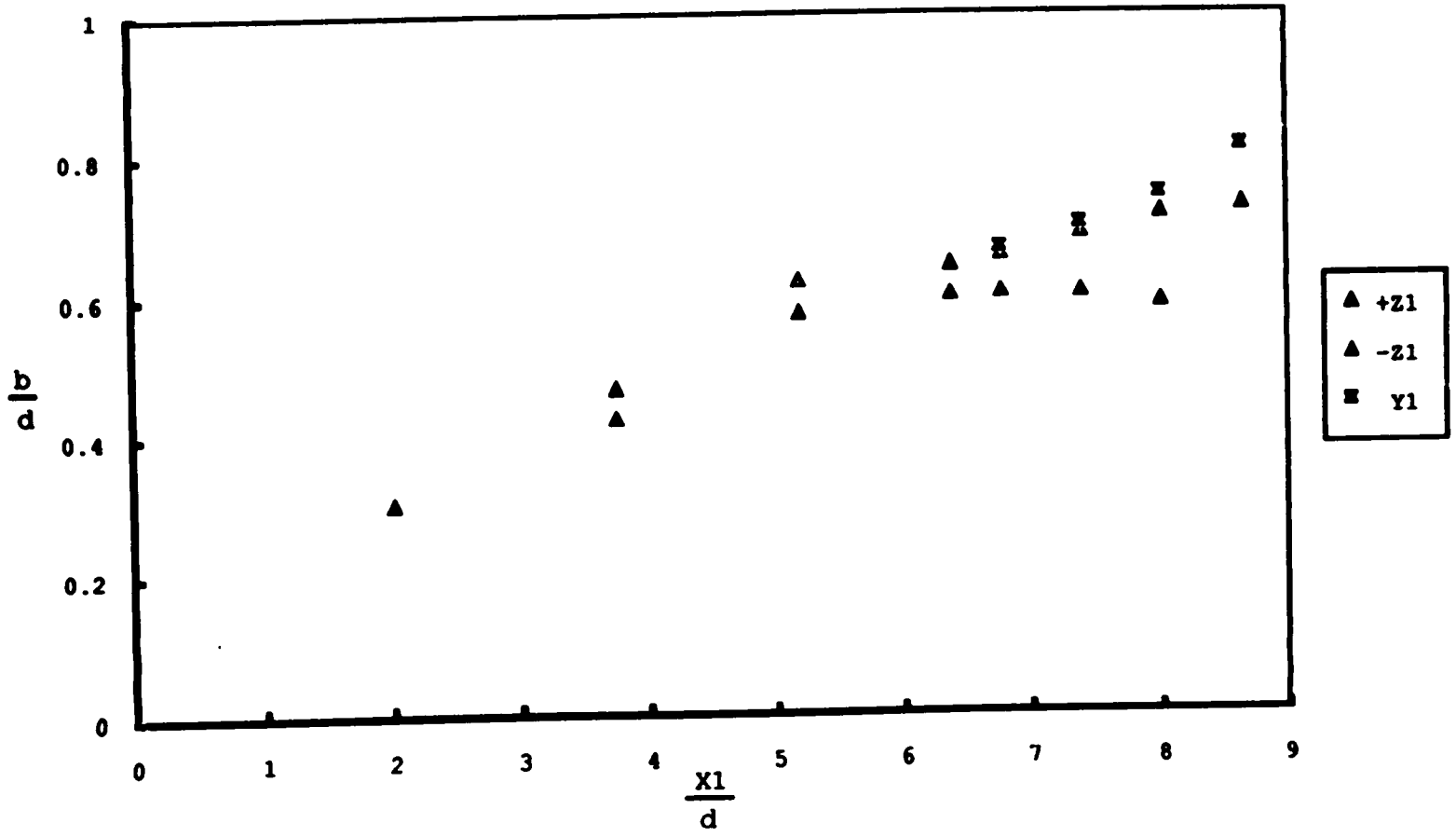

Fig. 4.24. Growth rates
Expt. 1

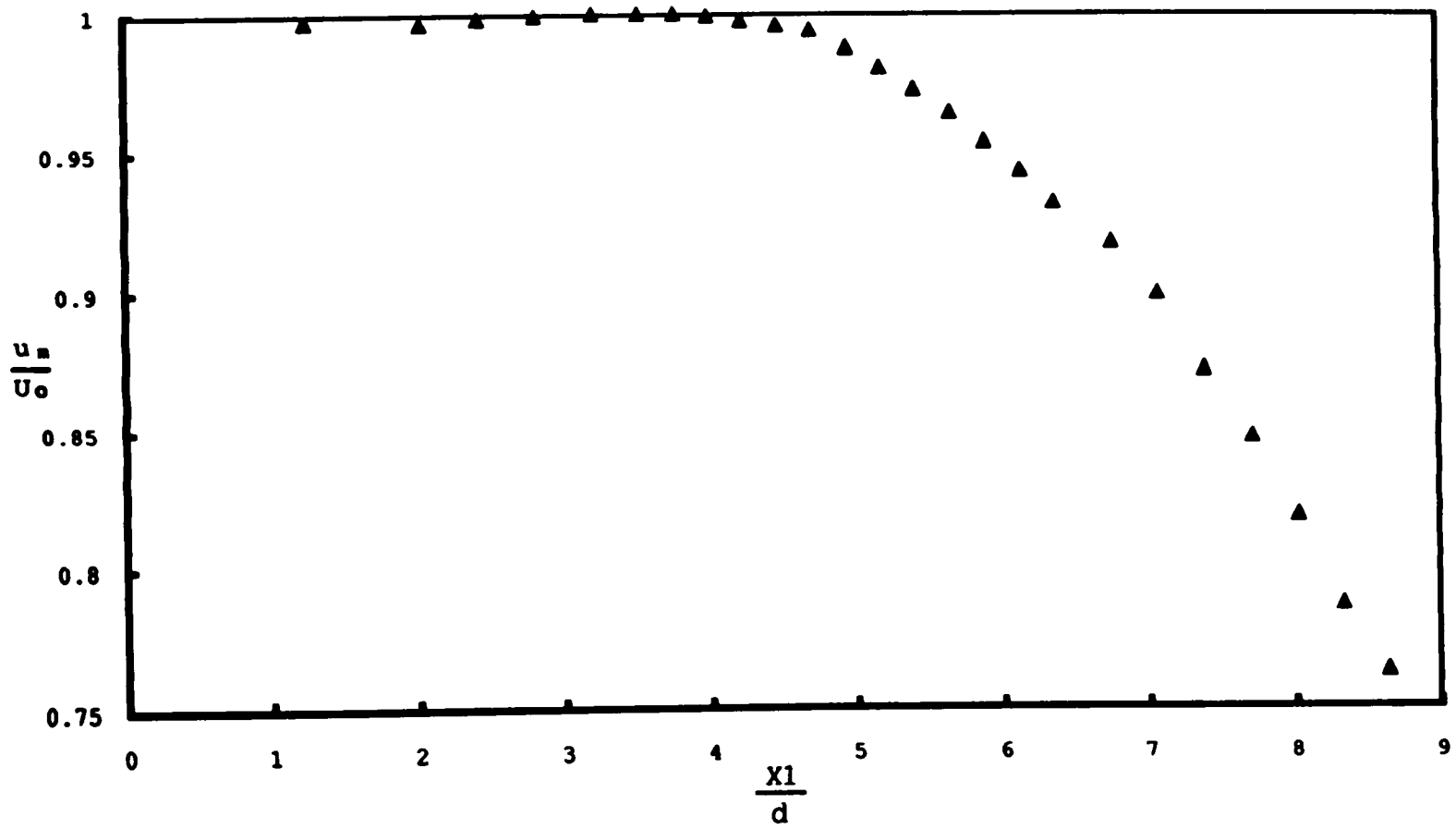

Fig. 4.25. Centreline velocity profile
Expt. 1

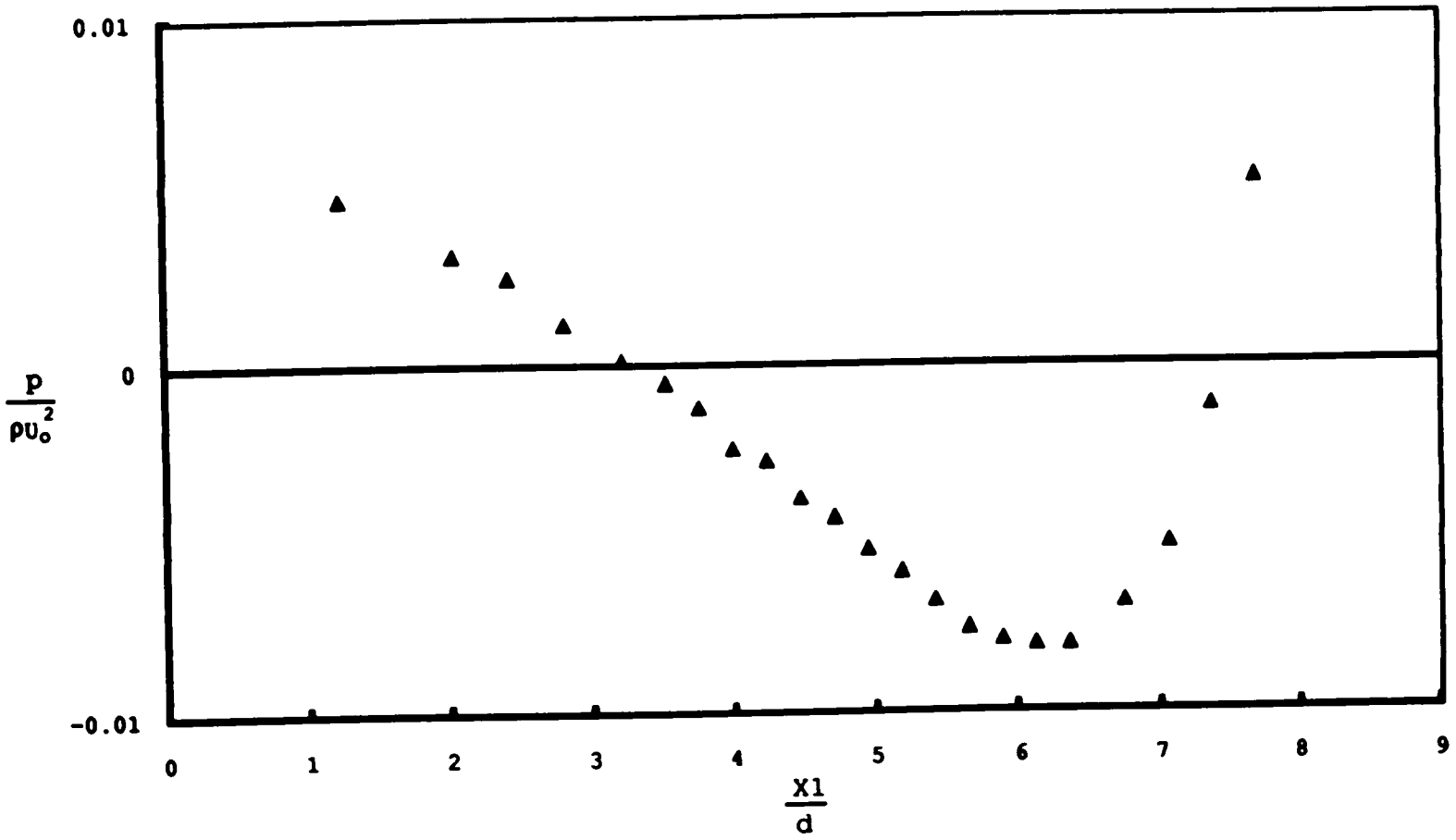

Fig. 4.26. Centreline pressure profile
Expt. 1

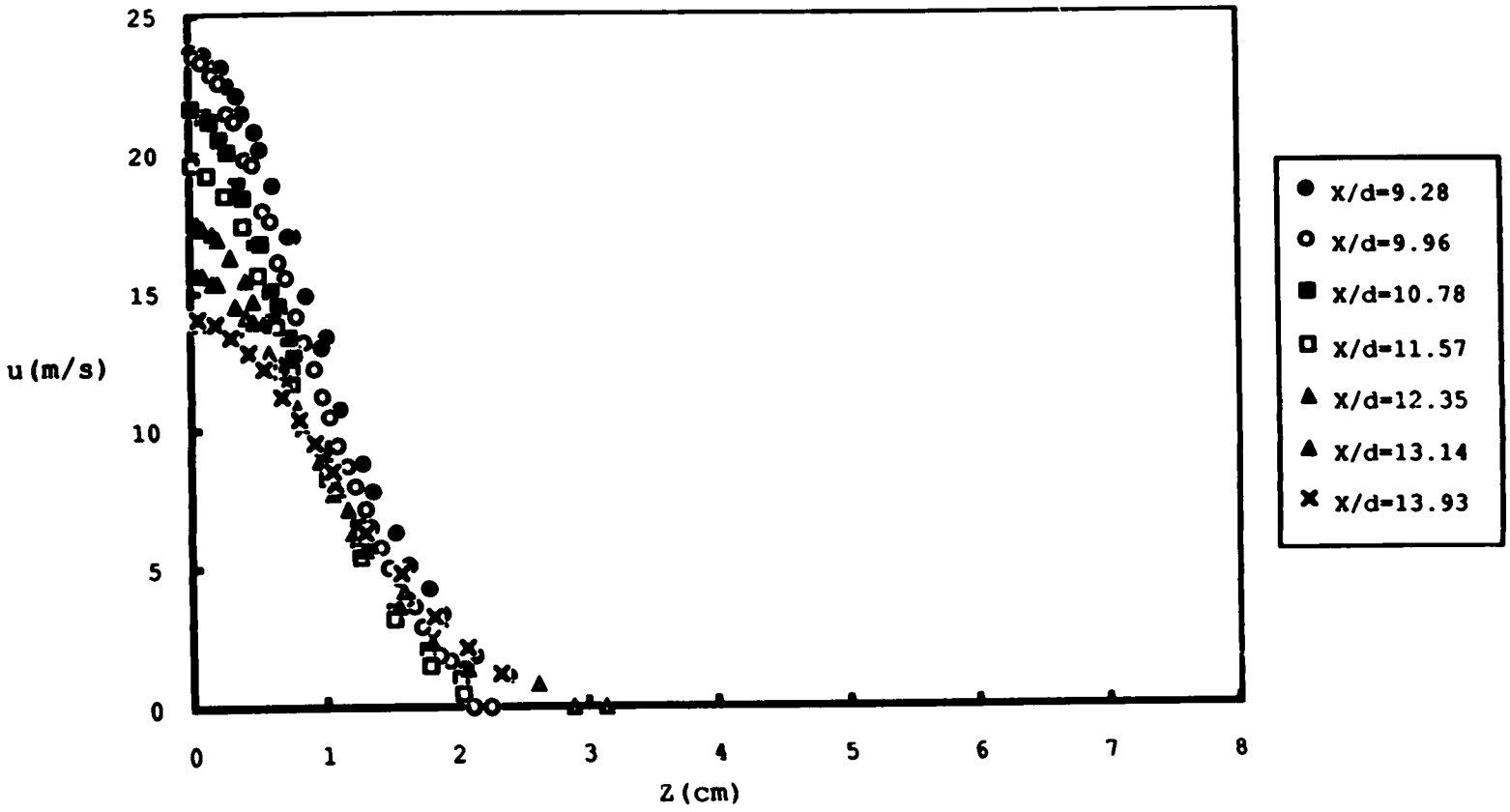

Fig. 4.27a. Transverse velocity profiles
Expt. 1

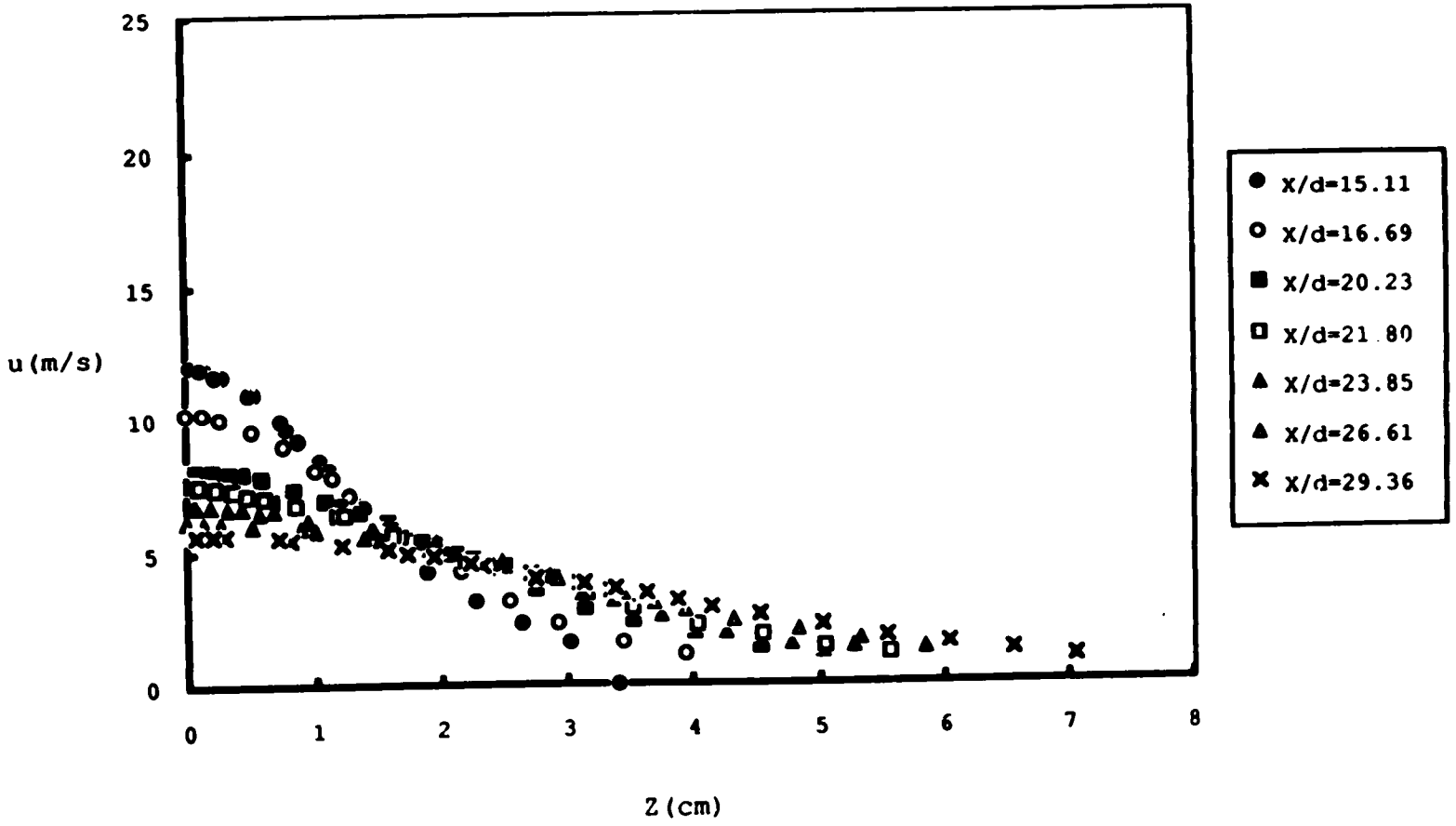

Fig. 4.27b. Transverse velocity profiles
Expt. 1

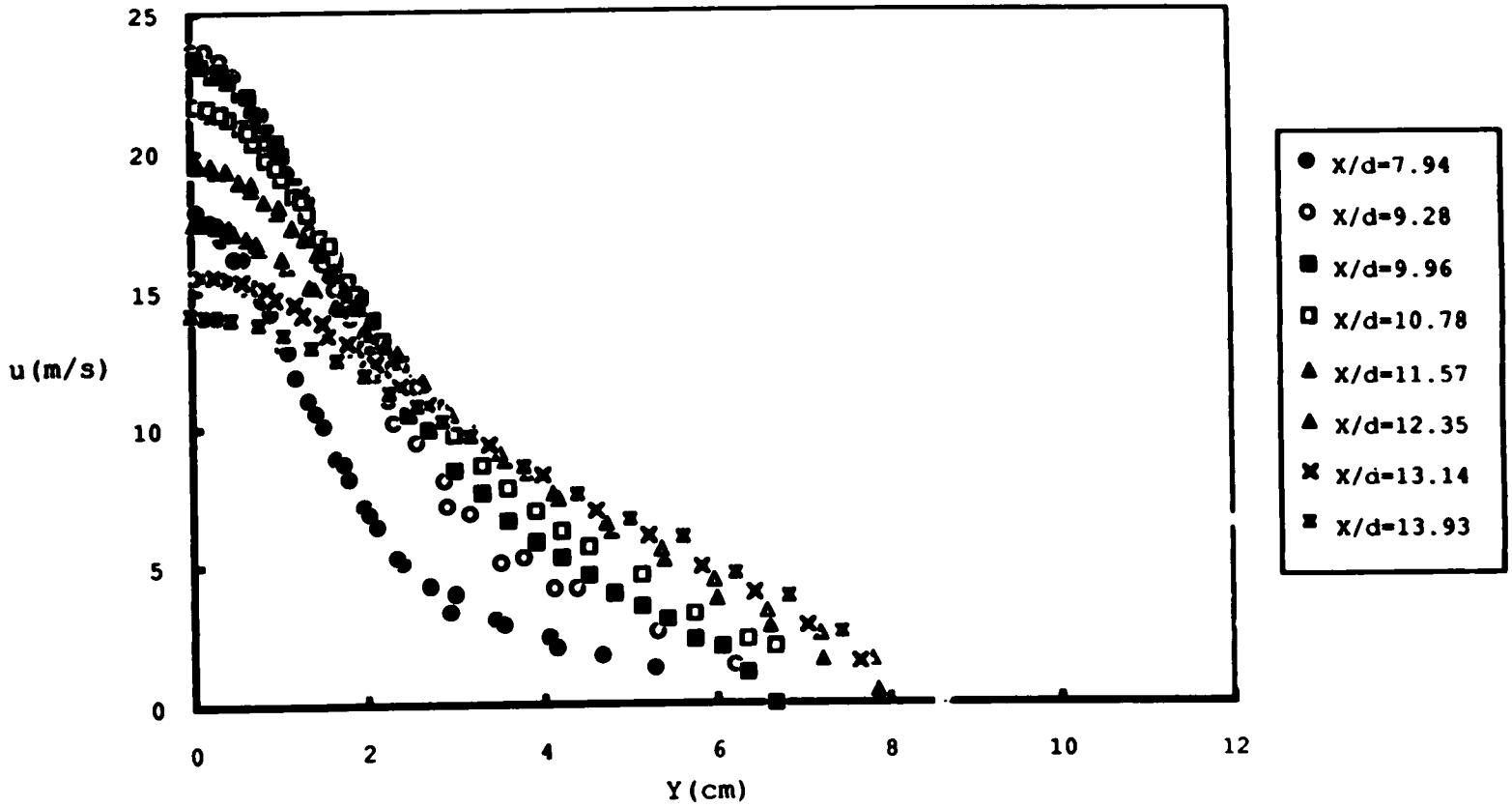

Fig. 4.28a. Vertical velocity profiles
Expt. 1

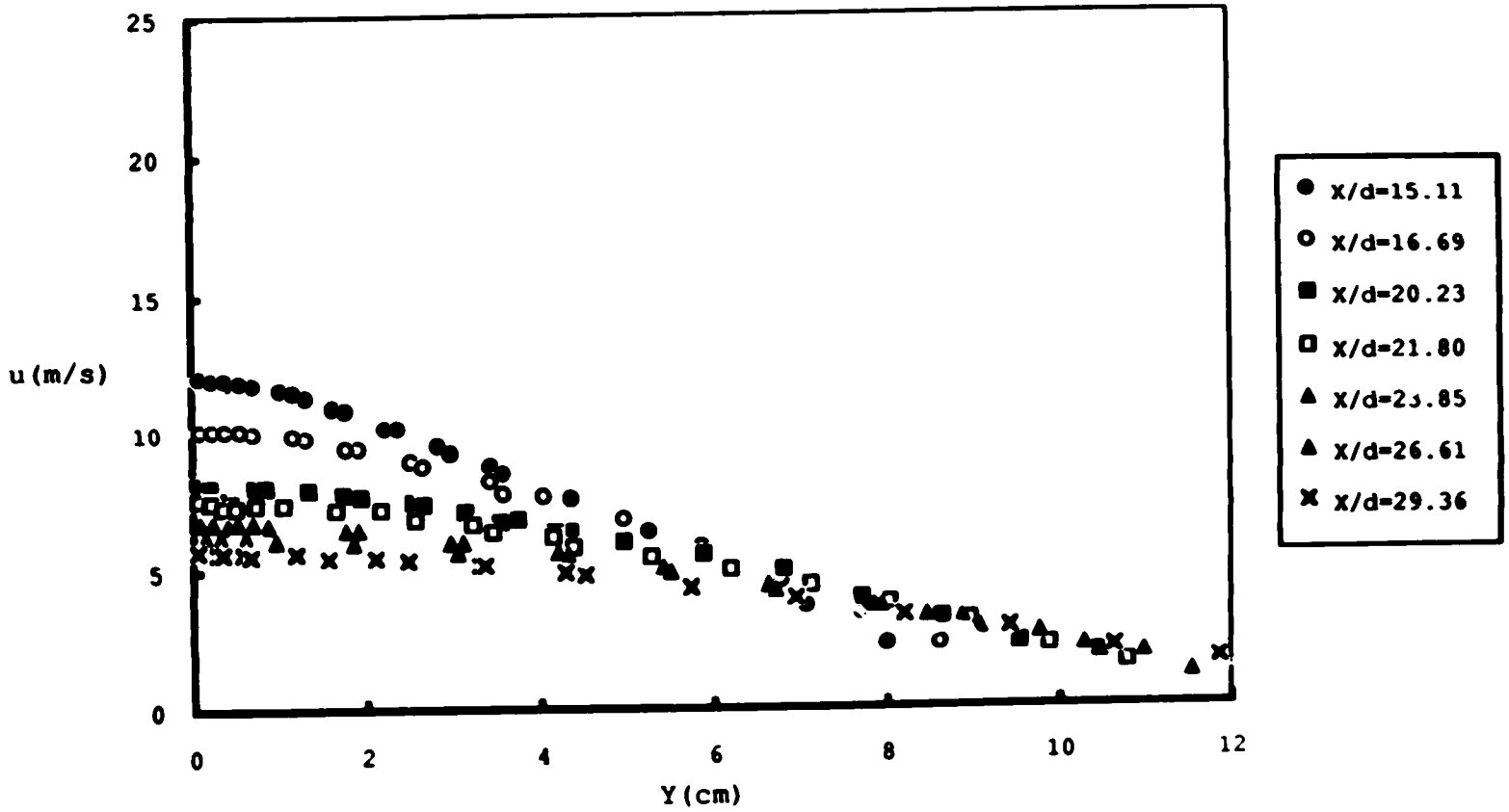

Fig. 4.28b. Vertical velocity profiles
Expt. 1

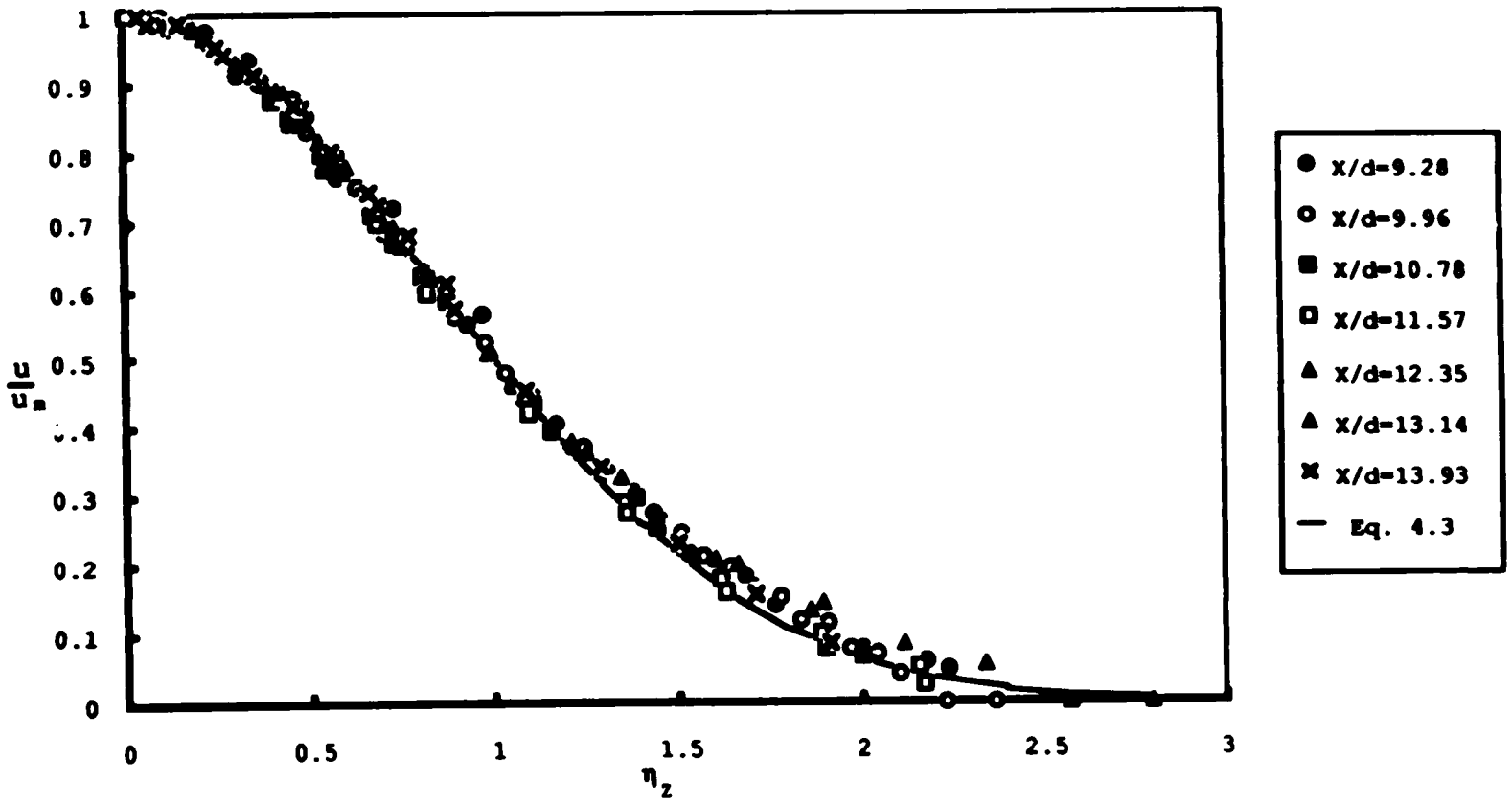

Fig. 4.29a. Non dimensional transverse velocity profiles, Expt. 1

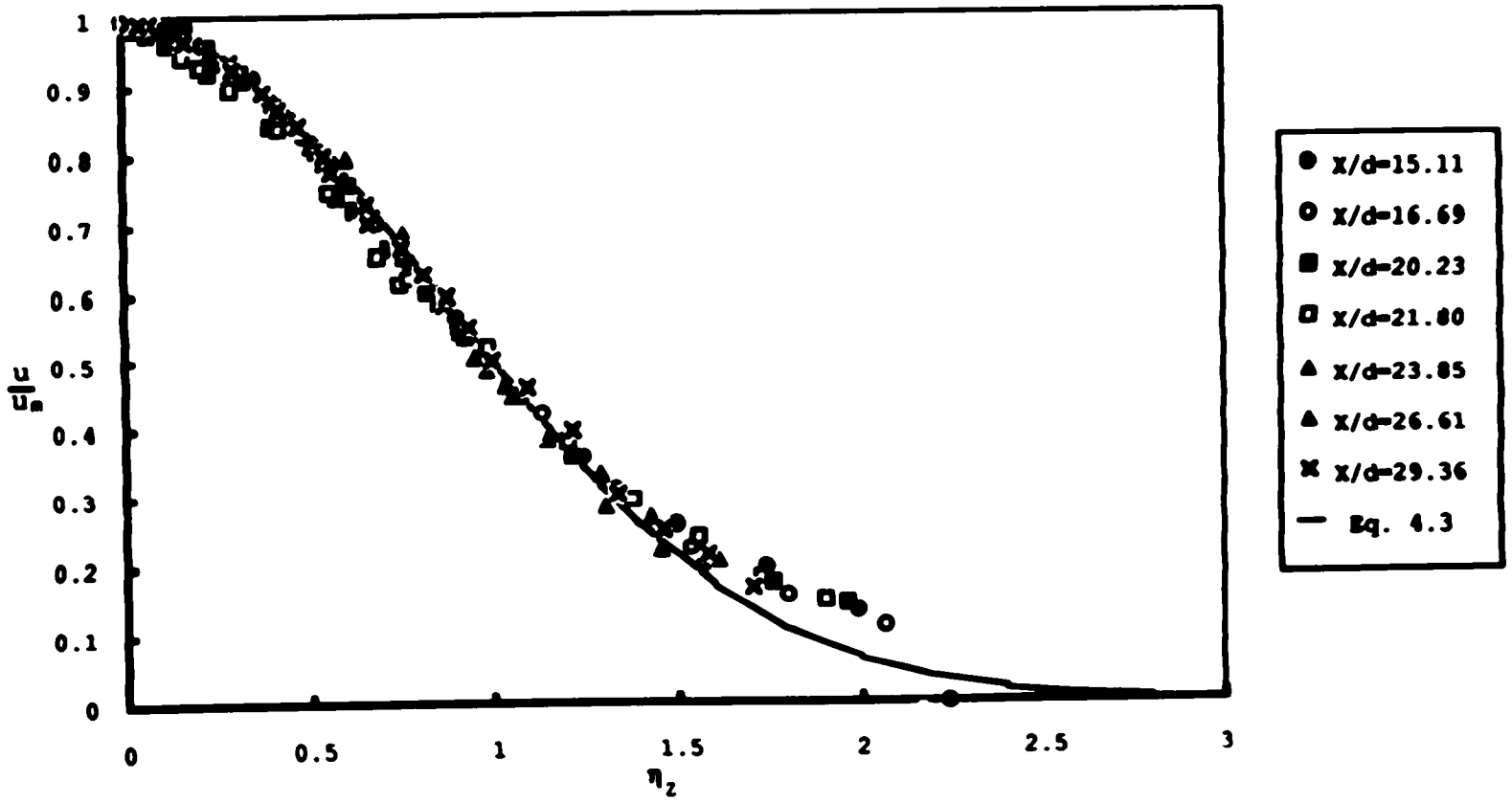

Fig. 4.29b. Non dimensional transverse velocity profiles, Expt. 1

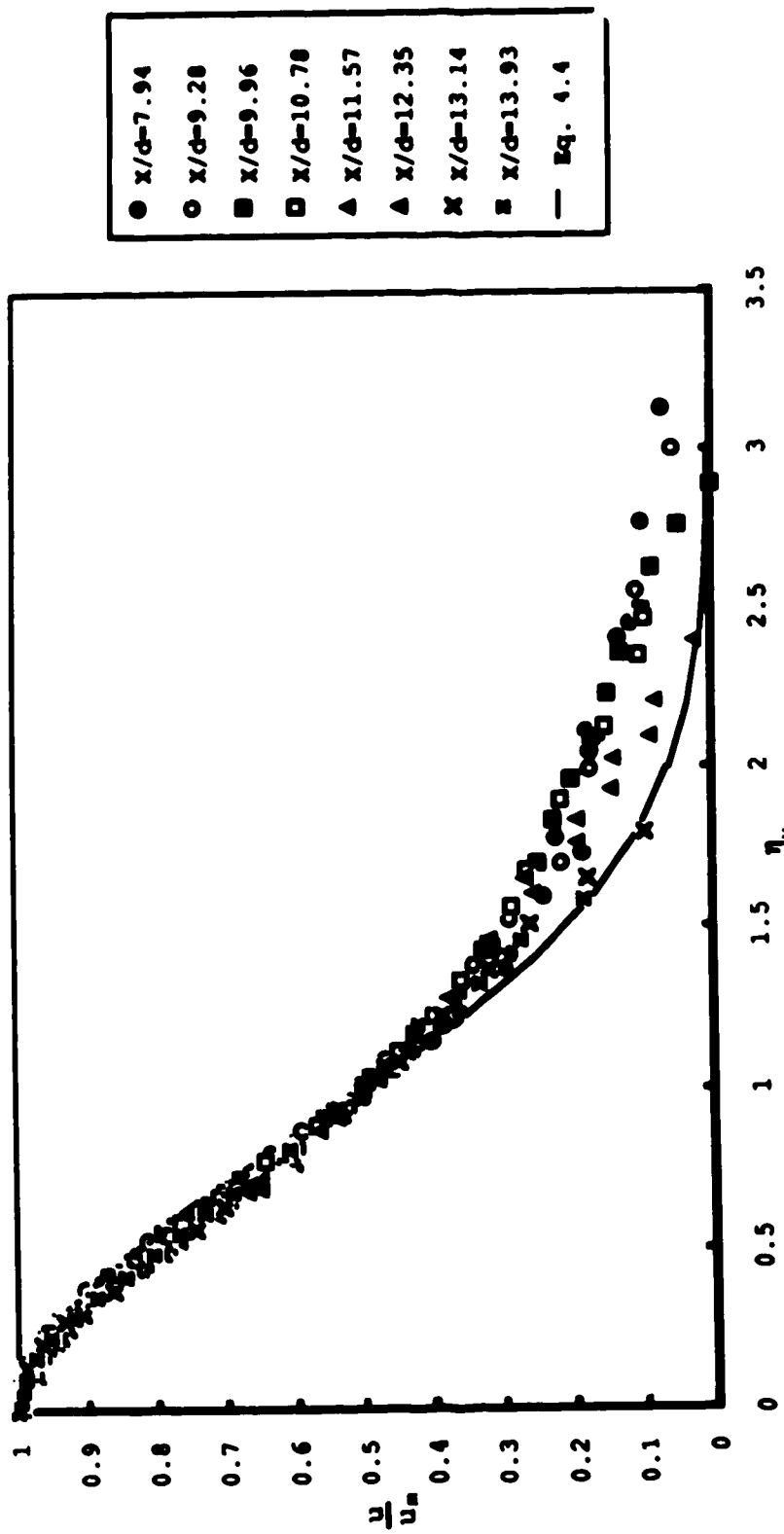

Fig. 4.30a. Non dimensional vertical velocity profiles, Expt. 1

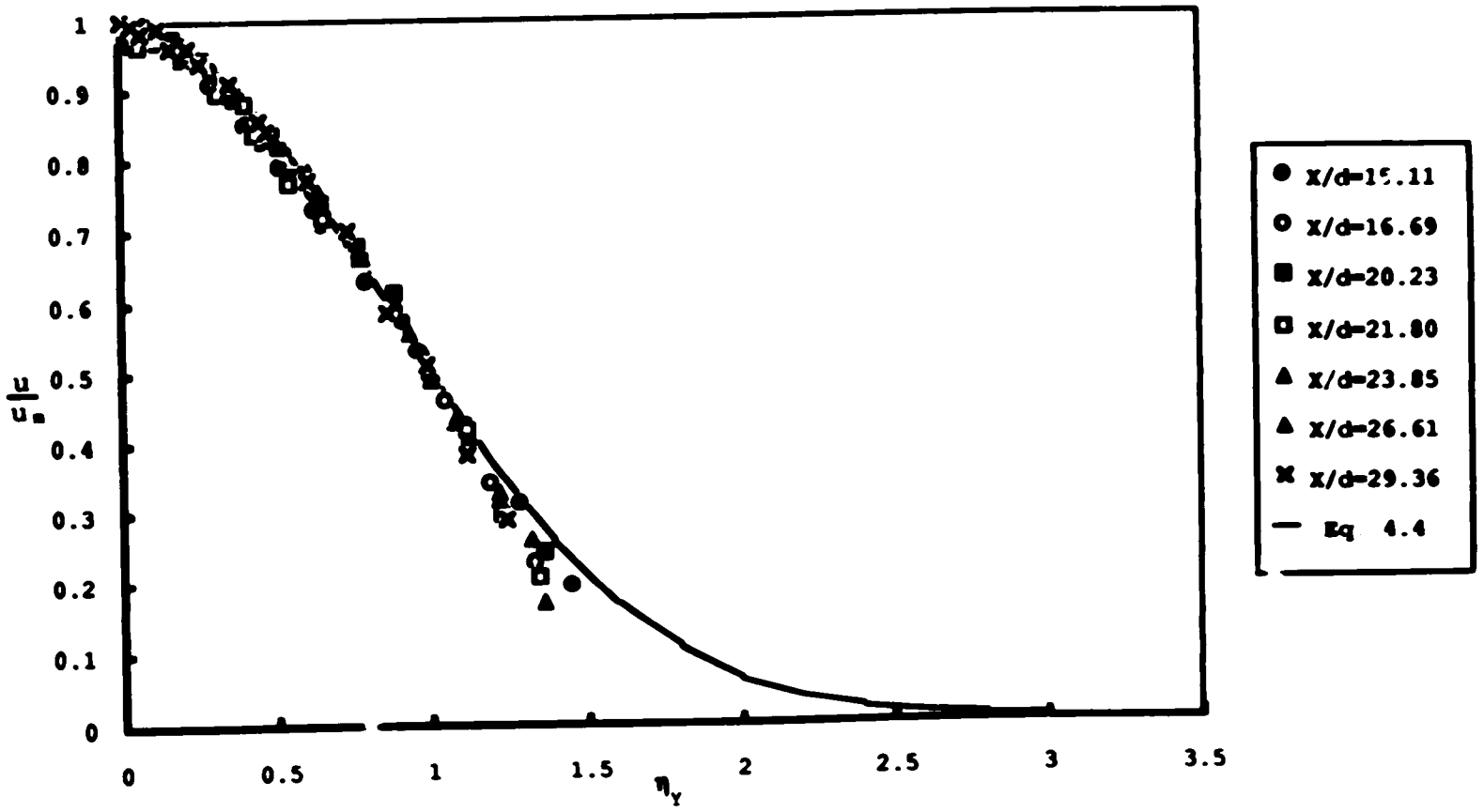

Fig. 4.30b. Non dimensional vertical velocity profiles, Expt. 1

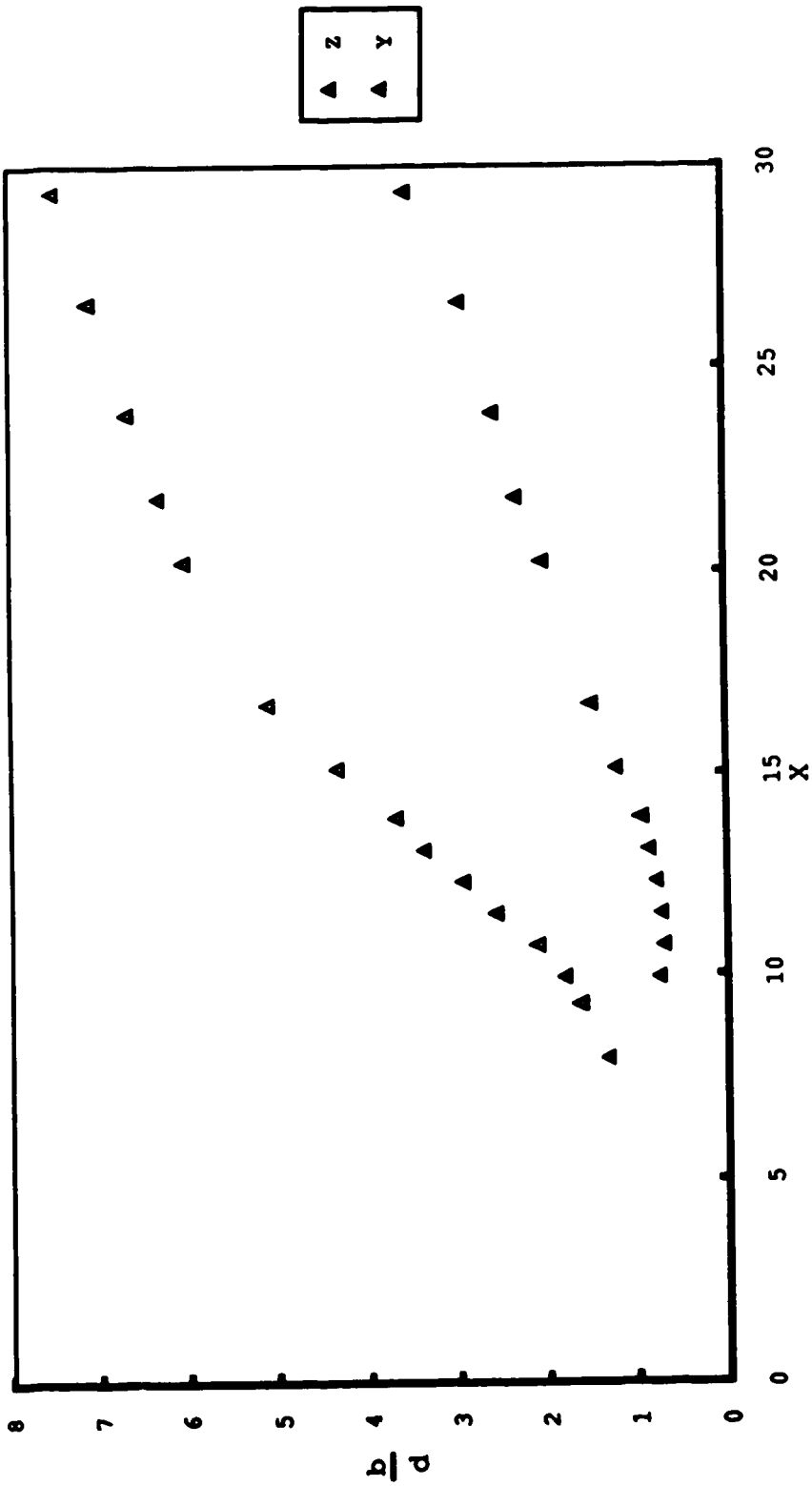

Fig. 4.31. Growth rates
Expt. 1

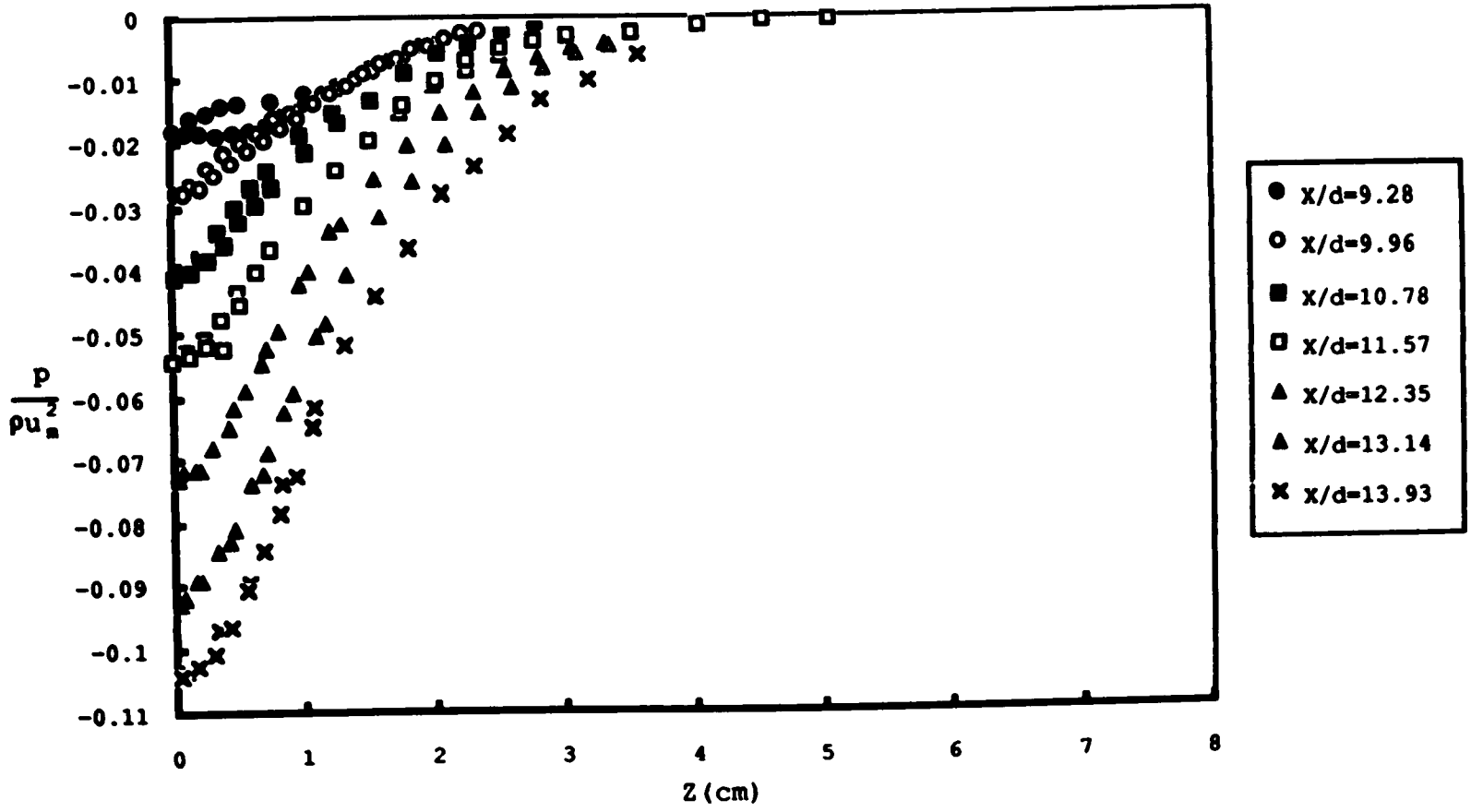

Fig. 4.32a. Transverse pressure profiles
Expt. 1

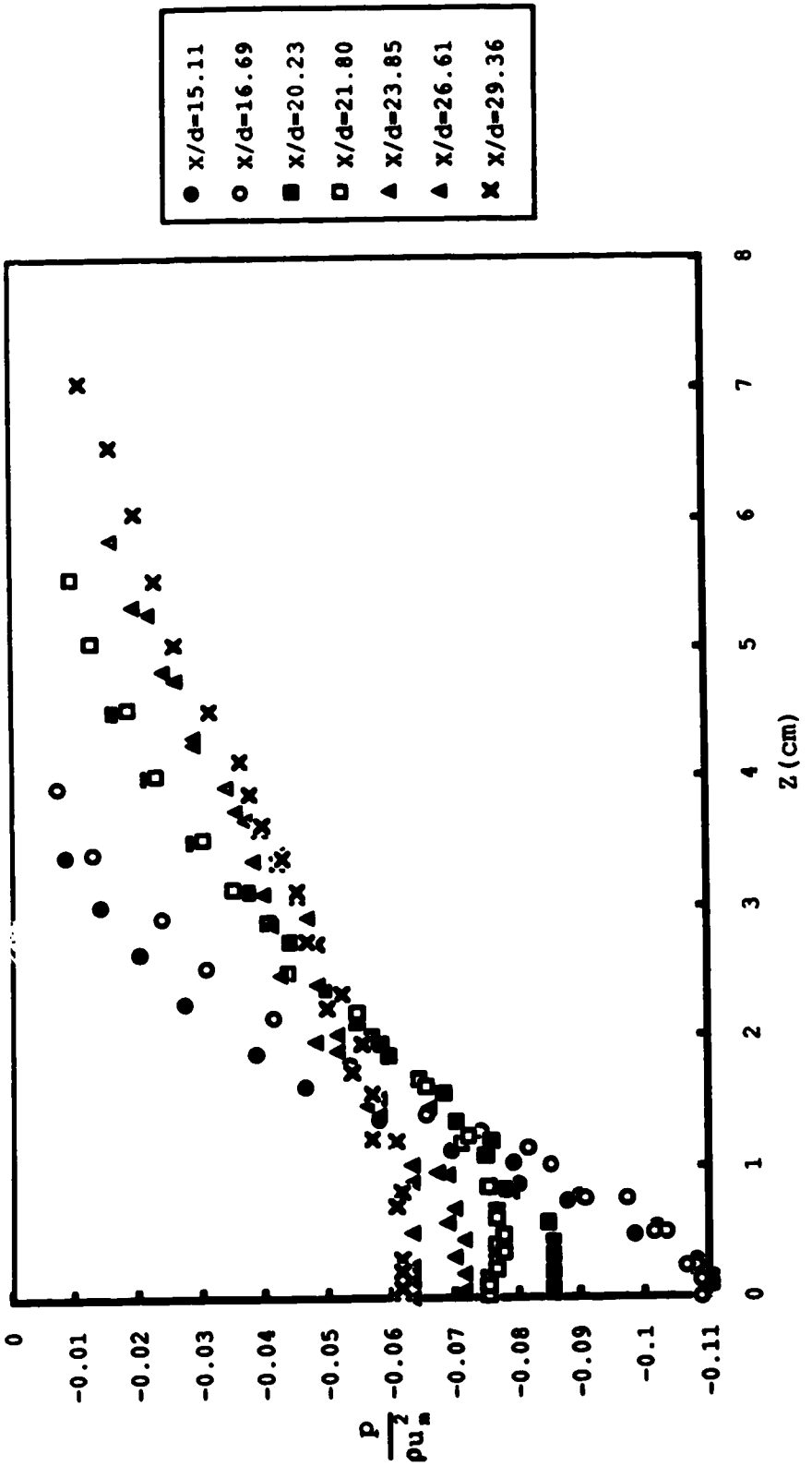

Fig. 4.32b. Transverse pressure profiles
Expt. 1

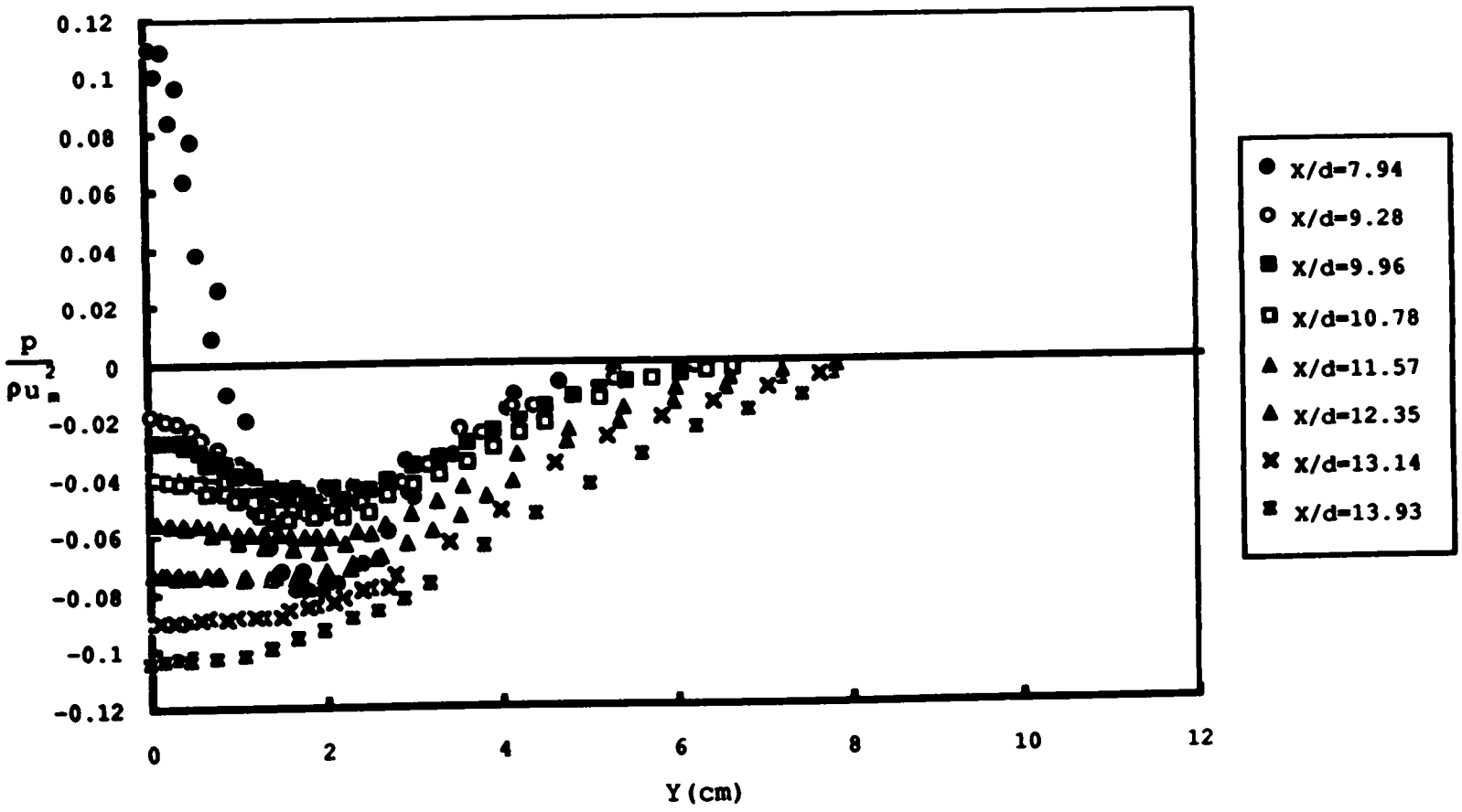

Fig. 4.33a. Vertical pressure profiles
Expt. 1

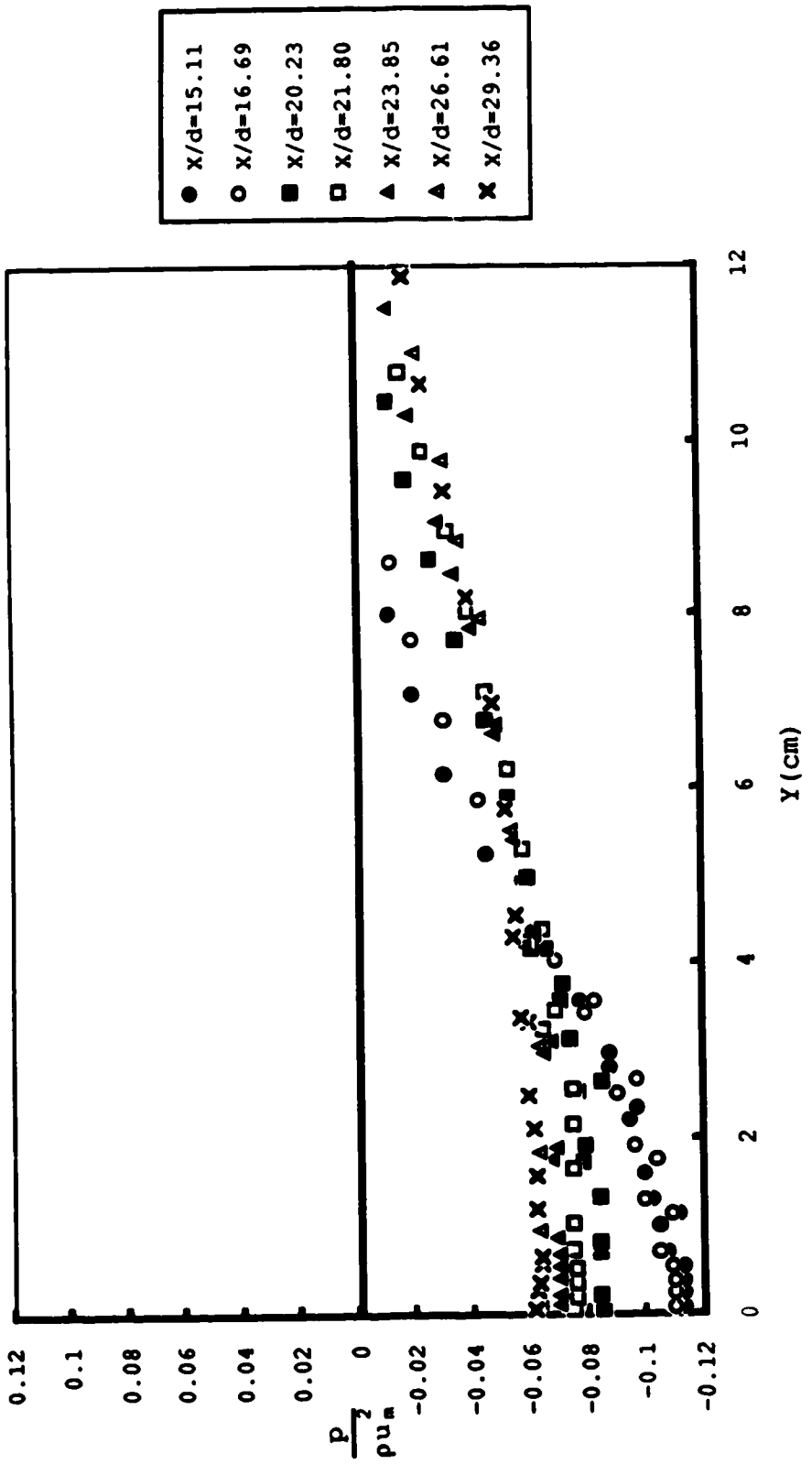

Fig. 4.33b. Vertical pressure profiles
Expt. 1

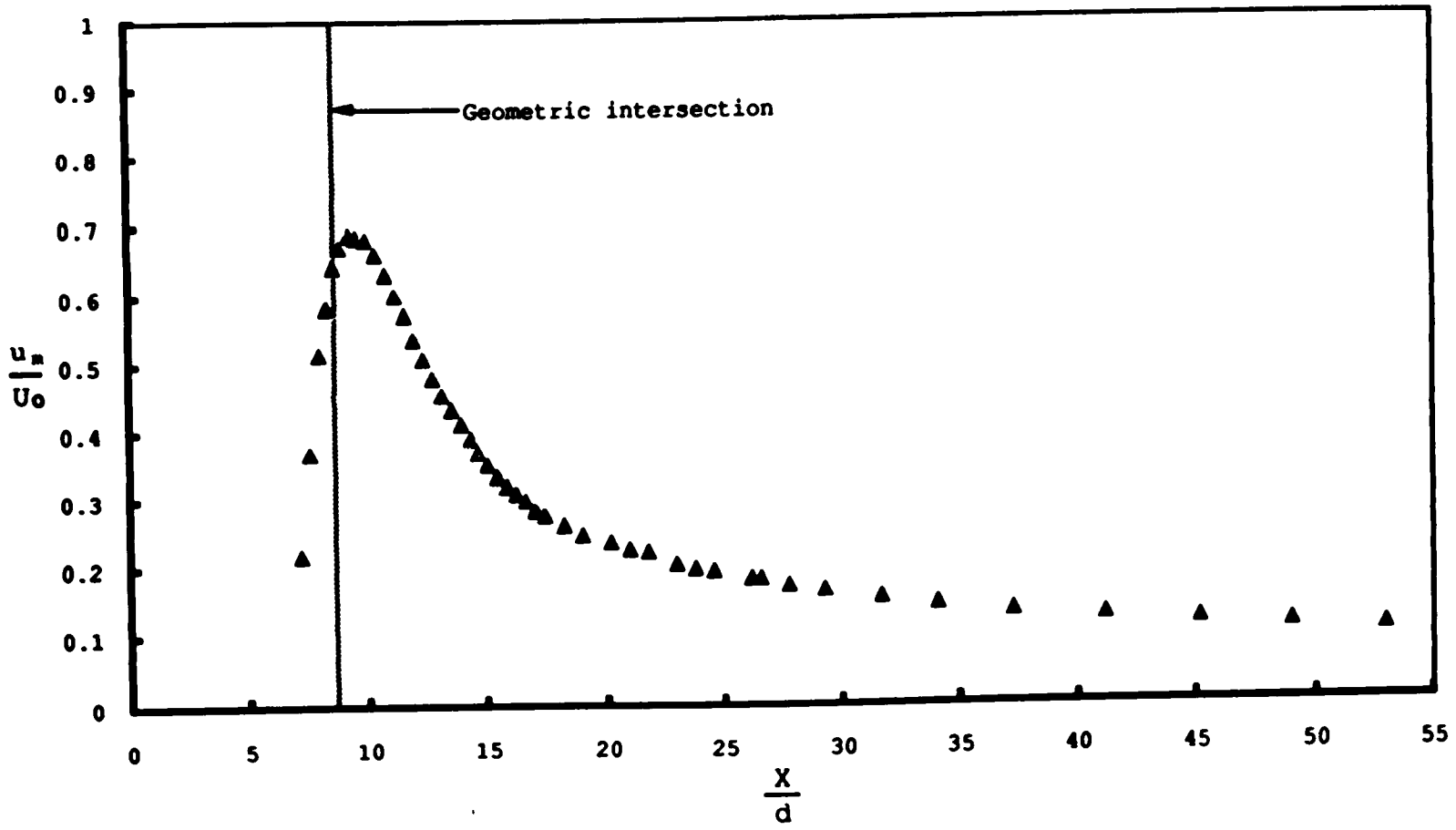

Fig. 4.34. Centreline velocity profile
Expt. 1

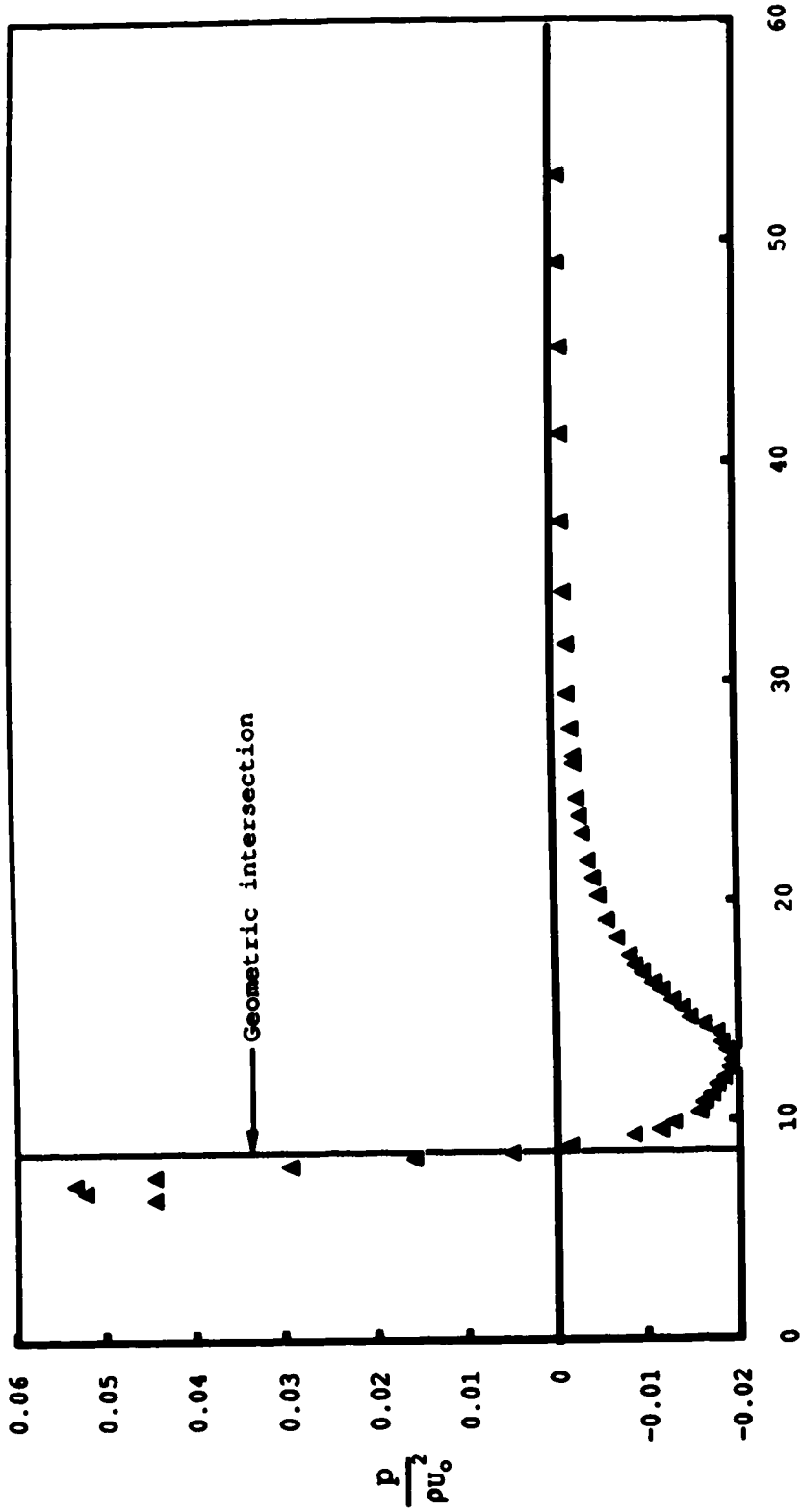

Fig. 4.35. Centreline pressure profile
Expt. 1

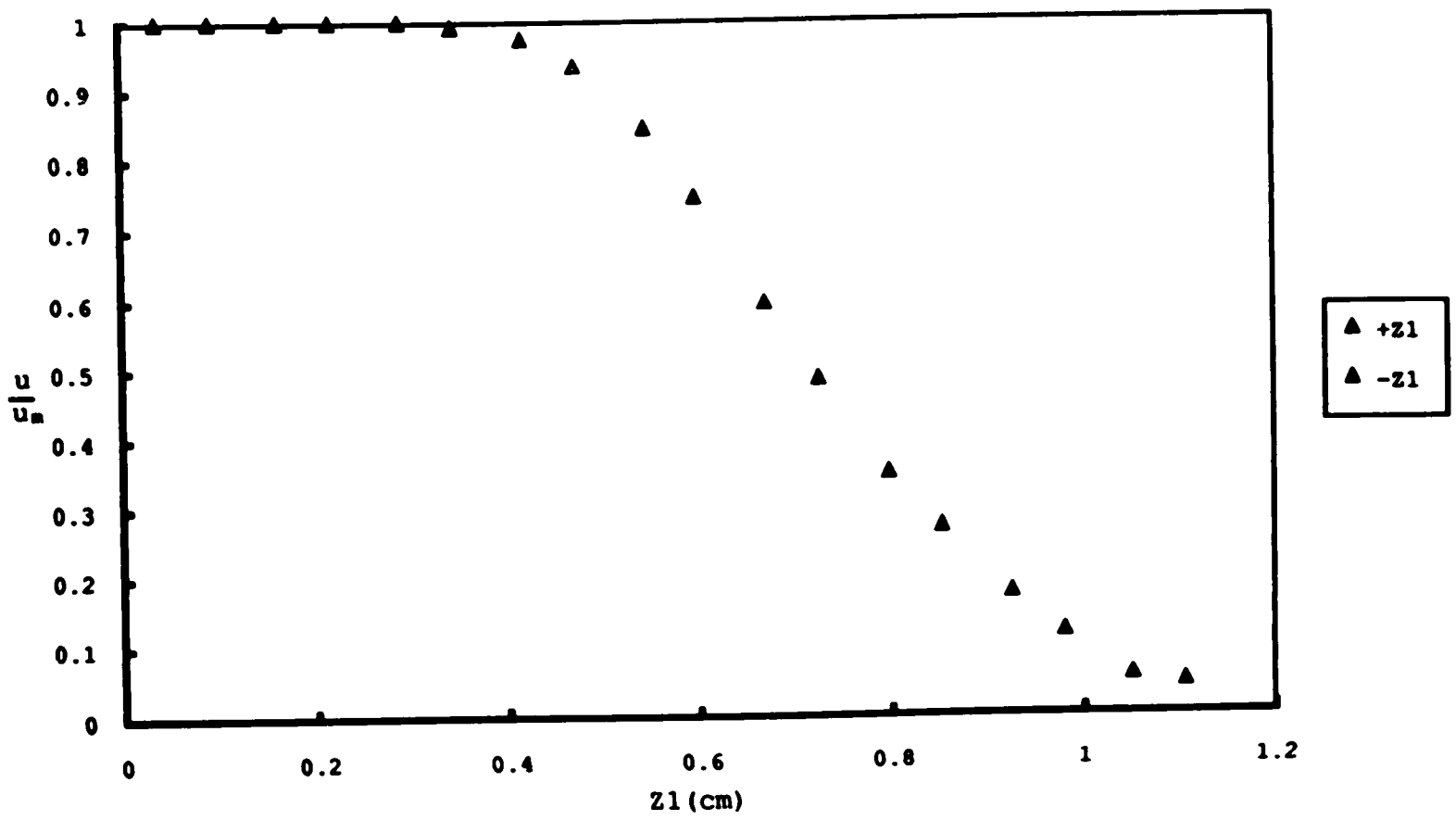

Fig. 4.36. Transverse velocity profile
Expt. 2, X1/d = 1.99

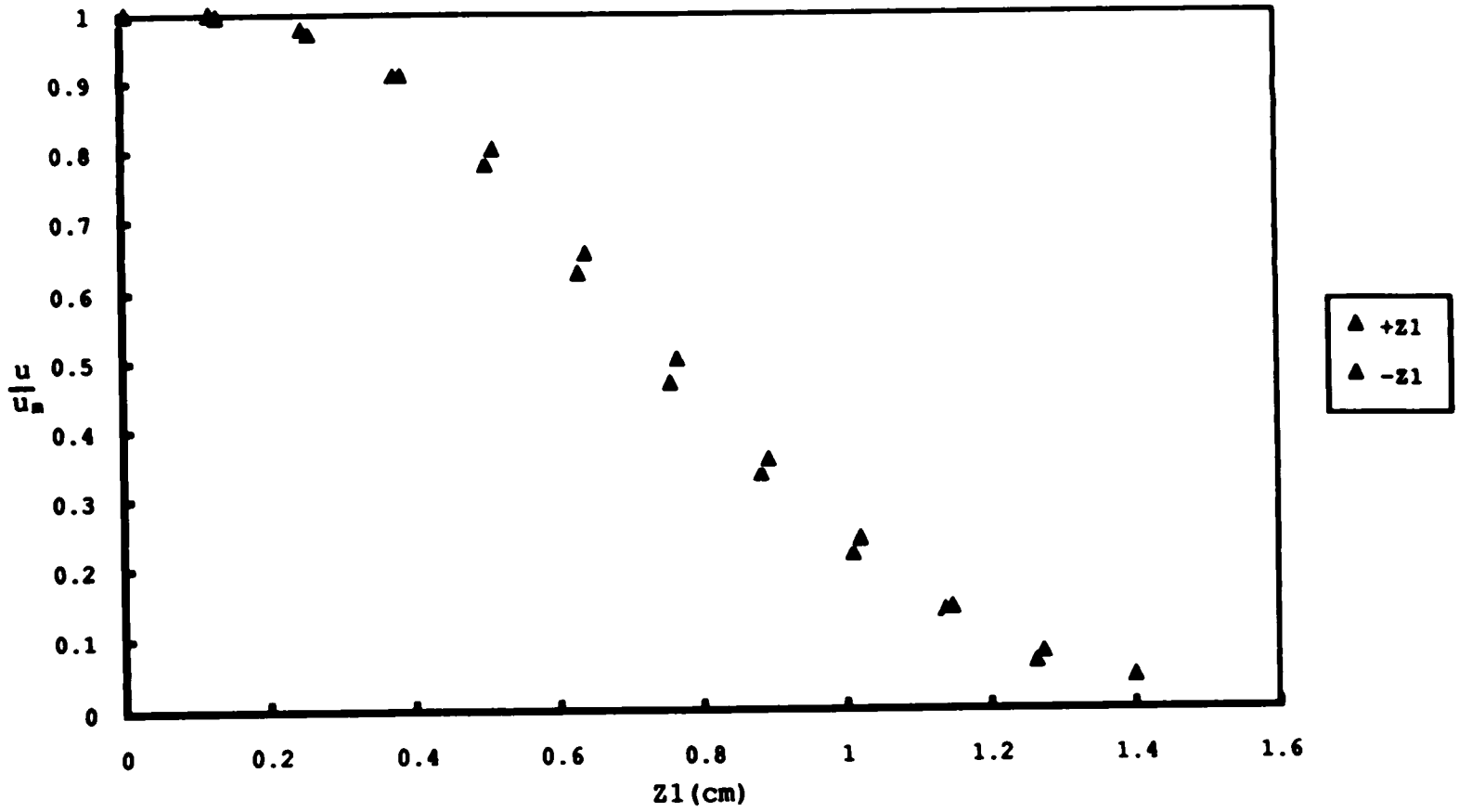

Fig. 4.37. Transverse velocity profile
Expt. 2, X1/d = 3.72

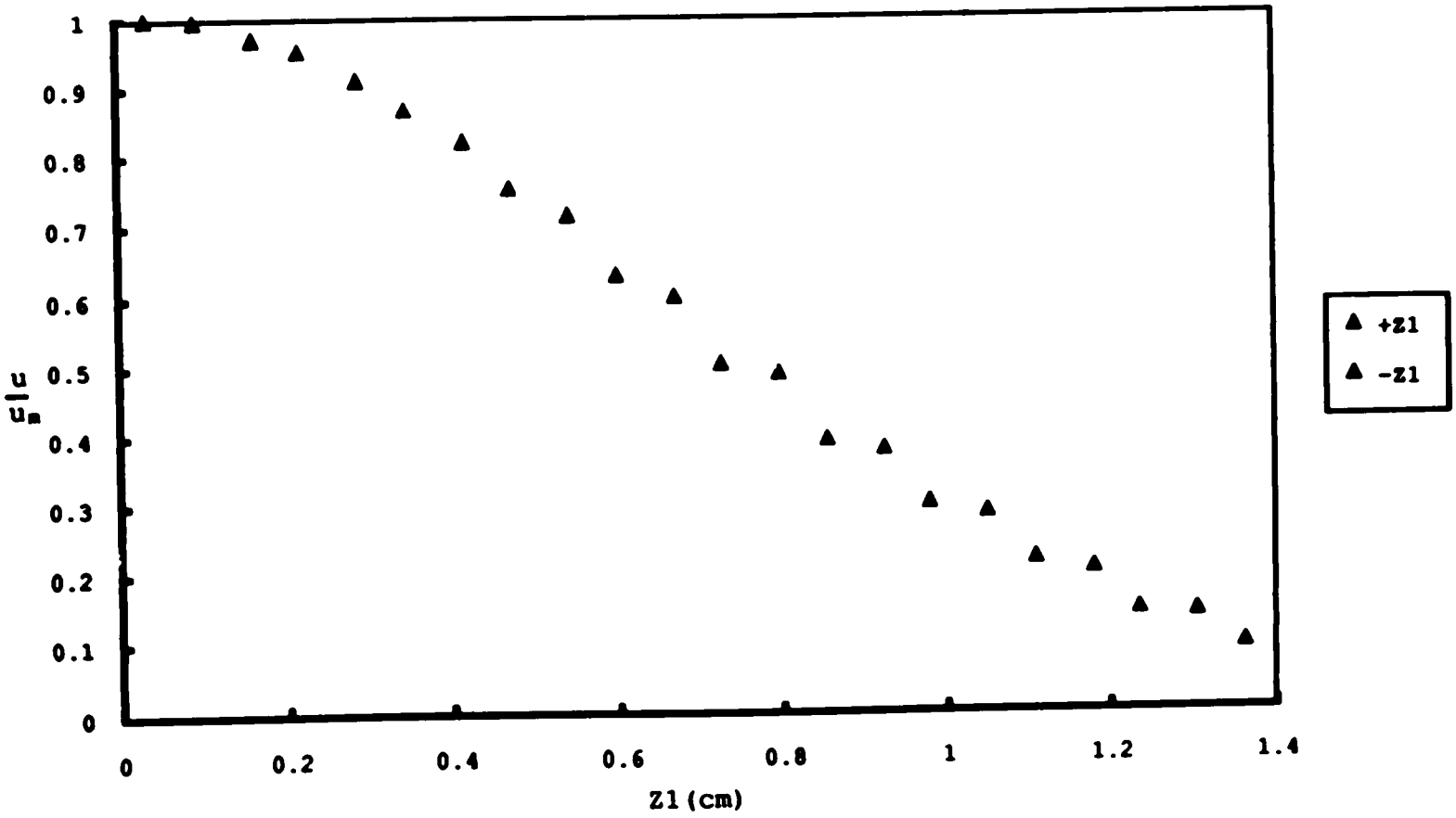

Fig. 4.38. Transverse velocity profile
Expt. 2, X1/d = 5.14

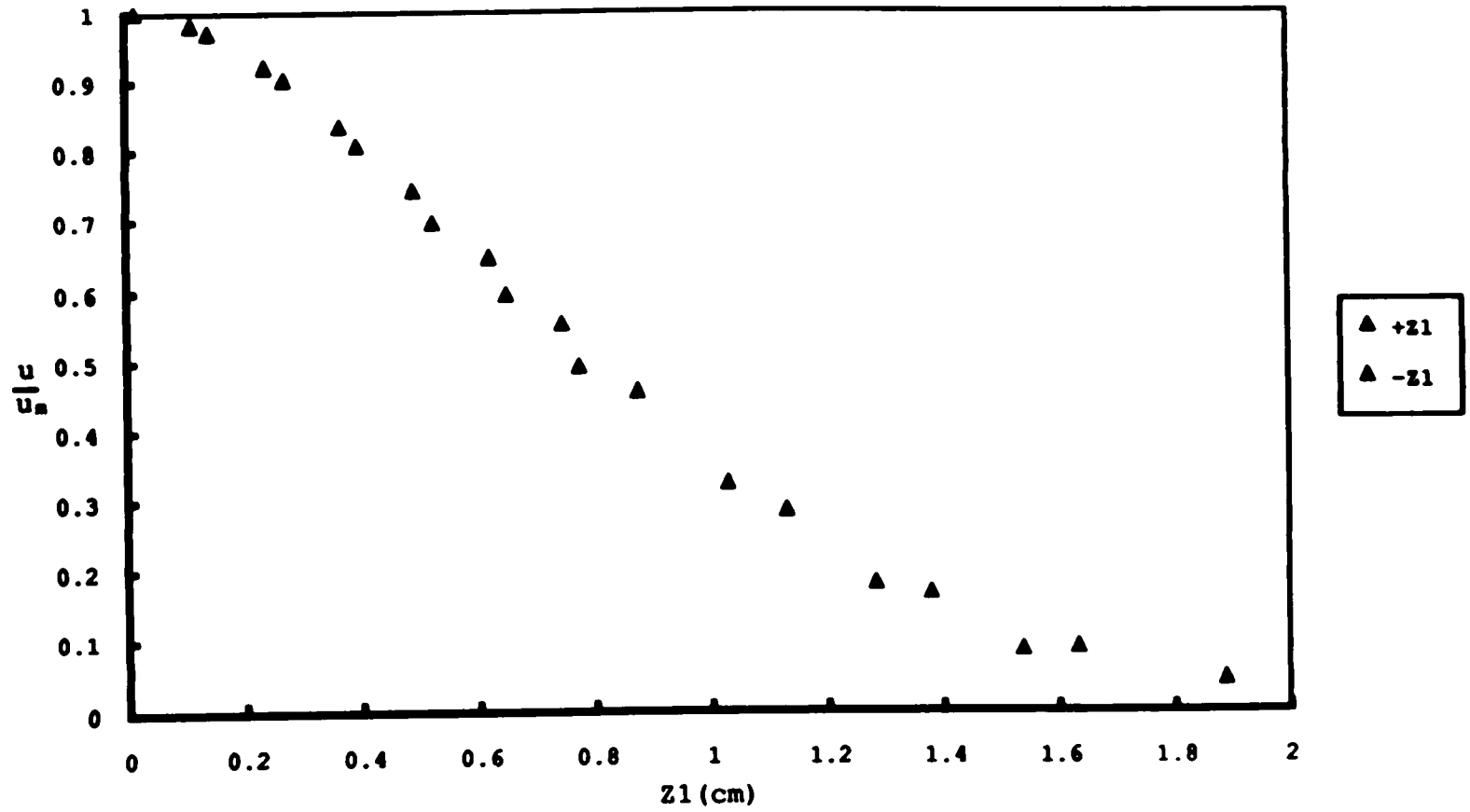

Fig. 4.39. Transverse velocity profile
Expt. 2, X1/d = 6.72

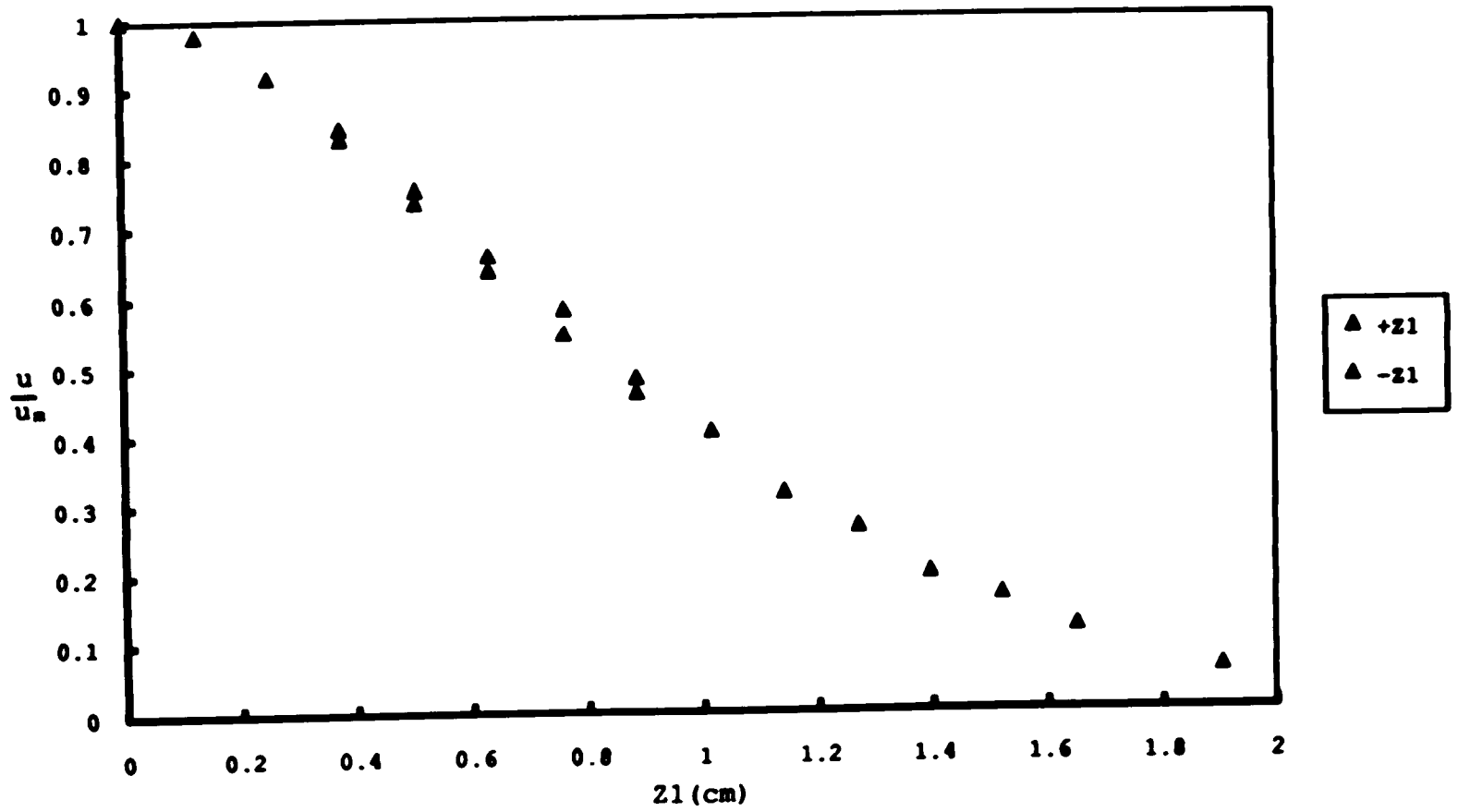

Fig. 4.40. Transverse velocity profile
Expt. 2, X1/d = 7.90

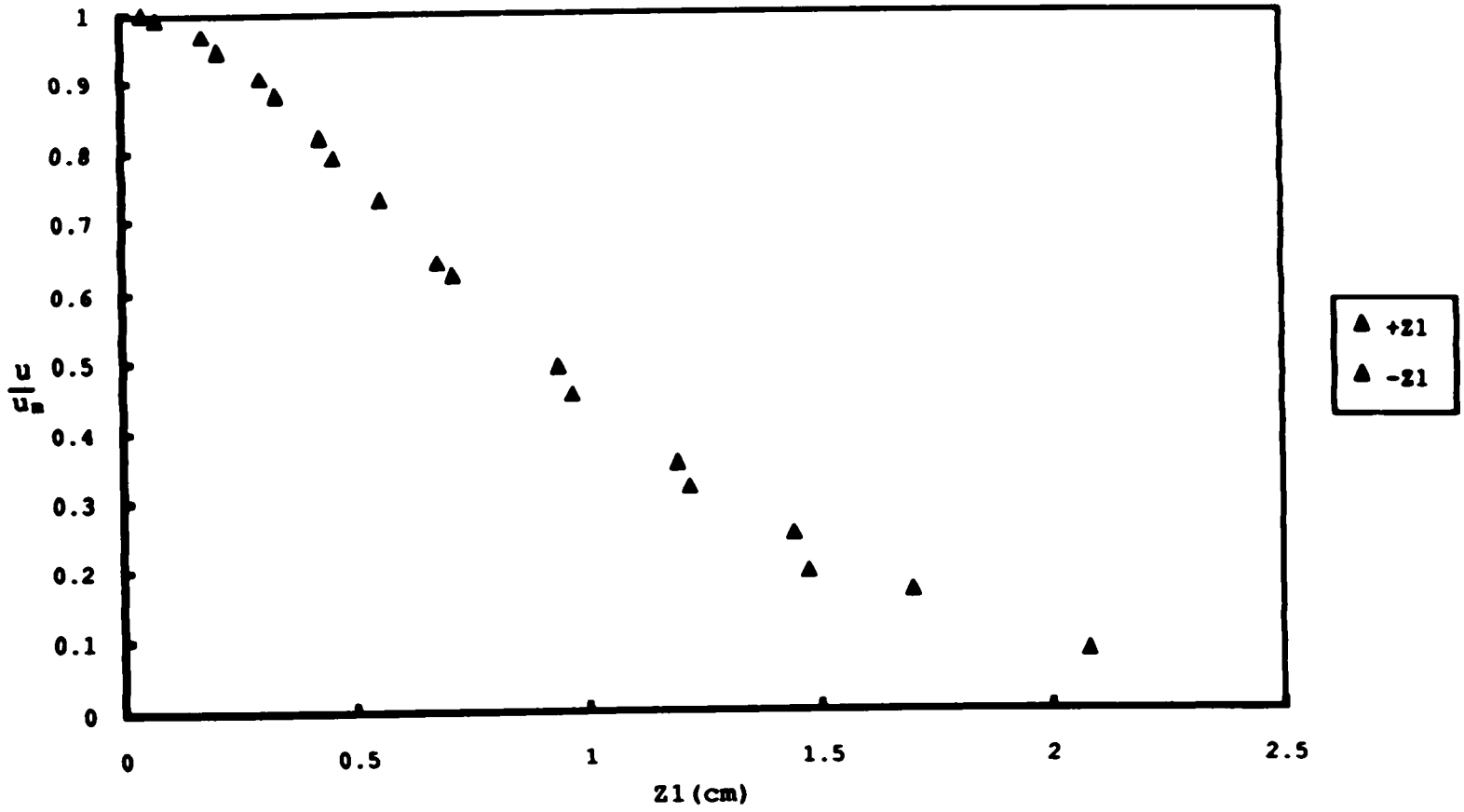

Fig. 4.41. Transverse velocity profile
Expt. 2, X1/d = 9.08

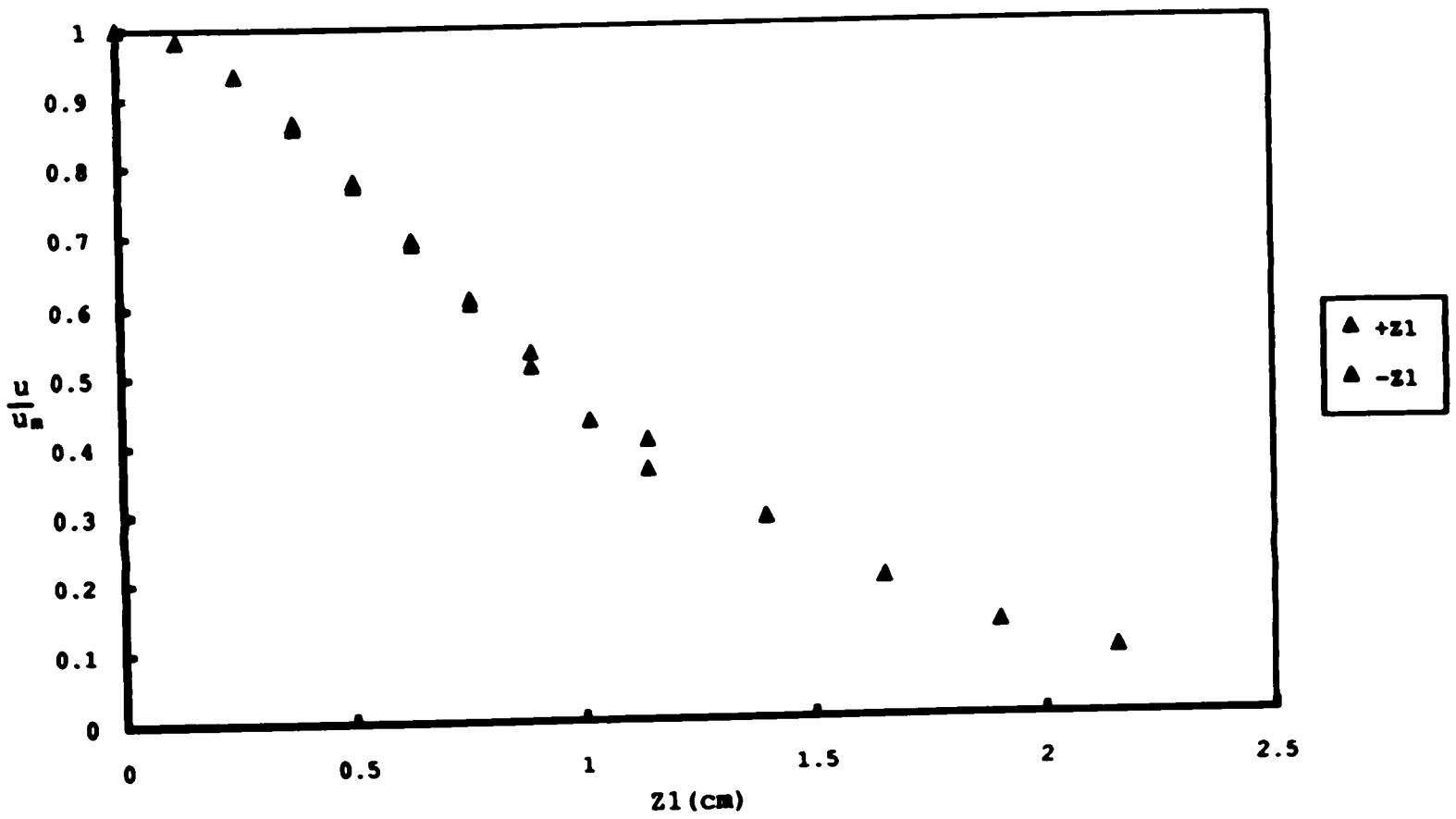

Fig. 4.42. Transverse velocity profile
Expt. 2, X1/d = 9.63

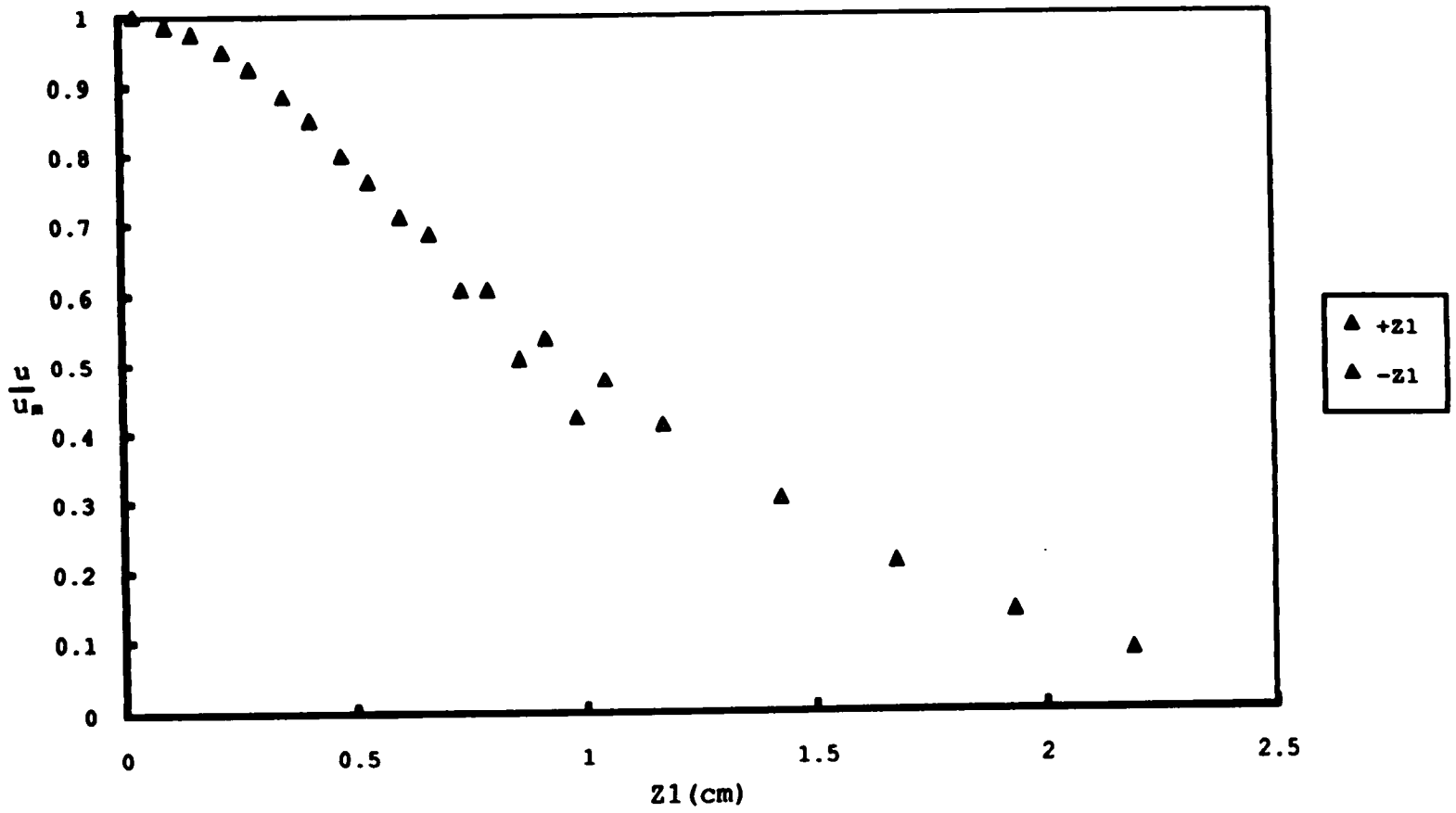

Fig. 4.43. Transverse velocity profile
Expt. 2, X1/d = 10.26

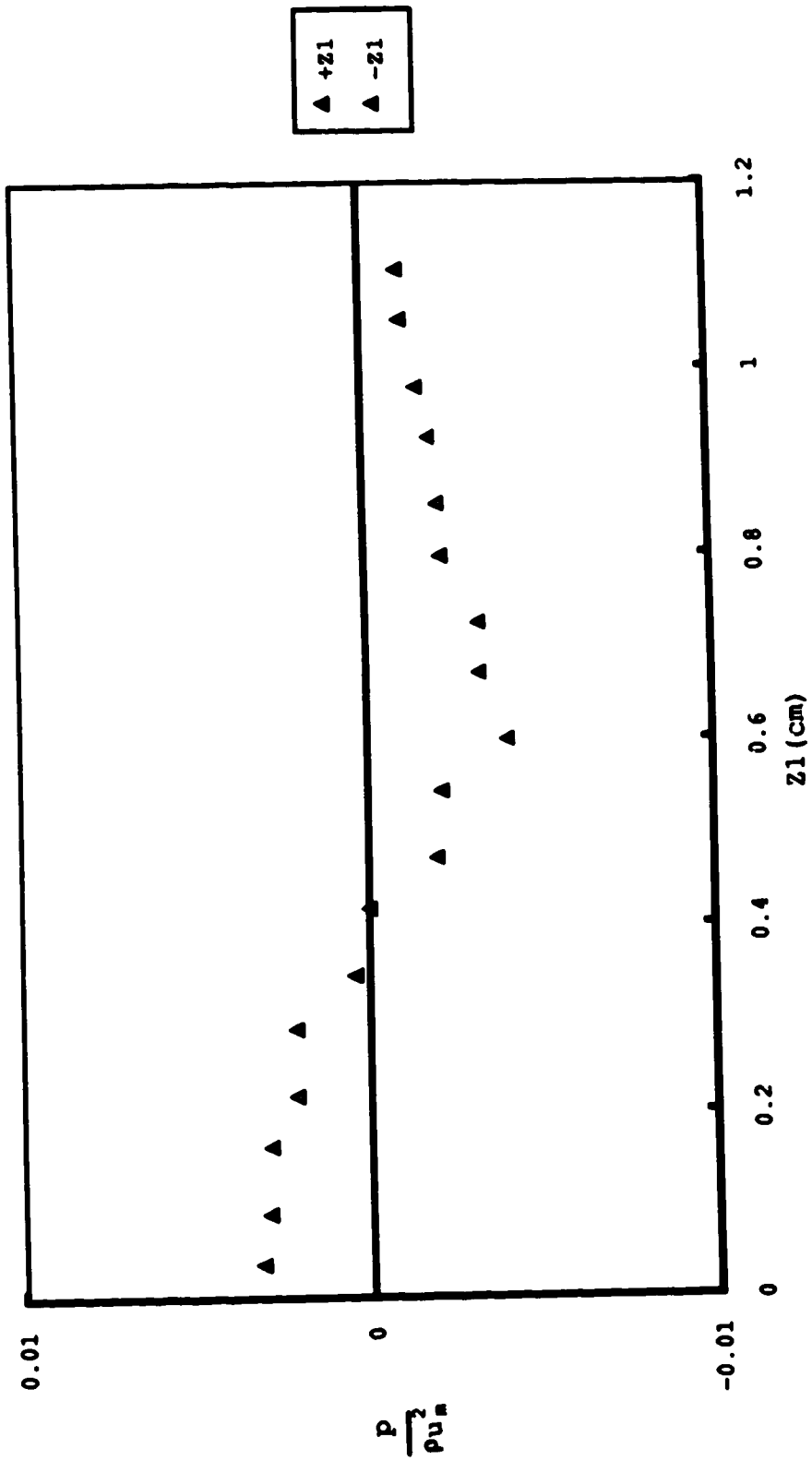

Fig. 4.44. Transverse pressure profile
Expt. 2, X1/d=1.99

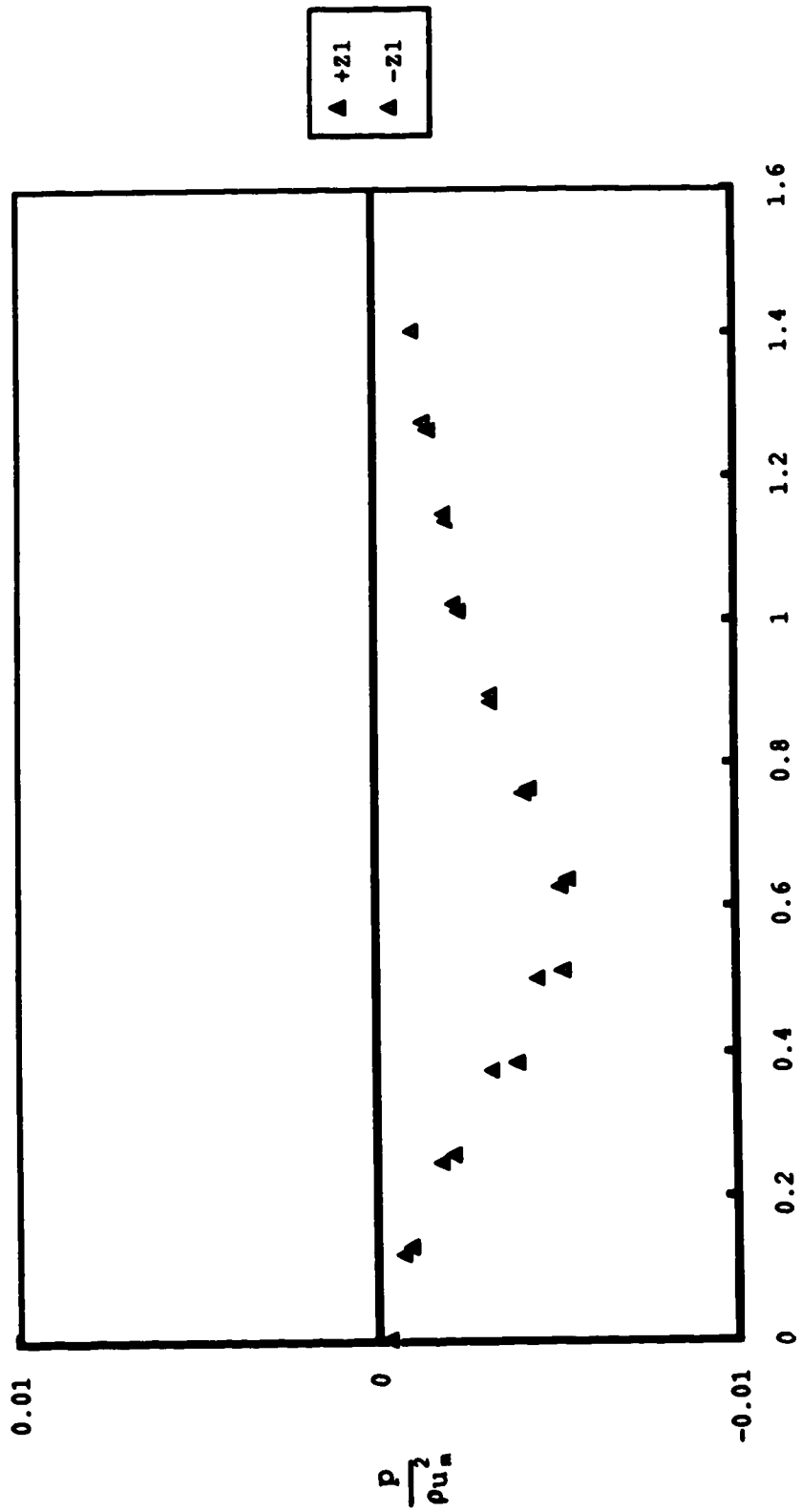

Fig. 4.45. Transverse pressure profile
Expt. 2, X1/d=3.72

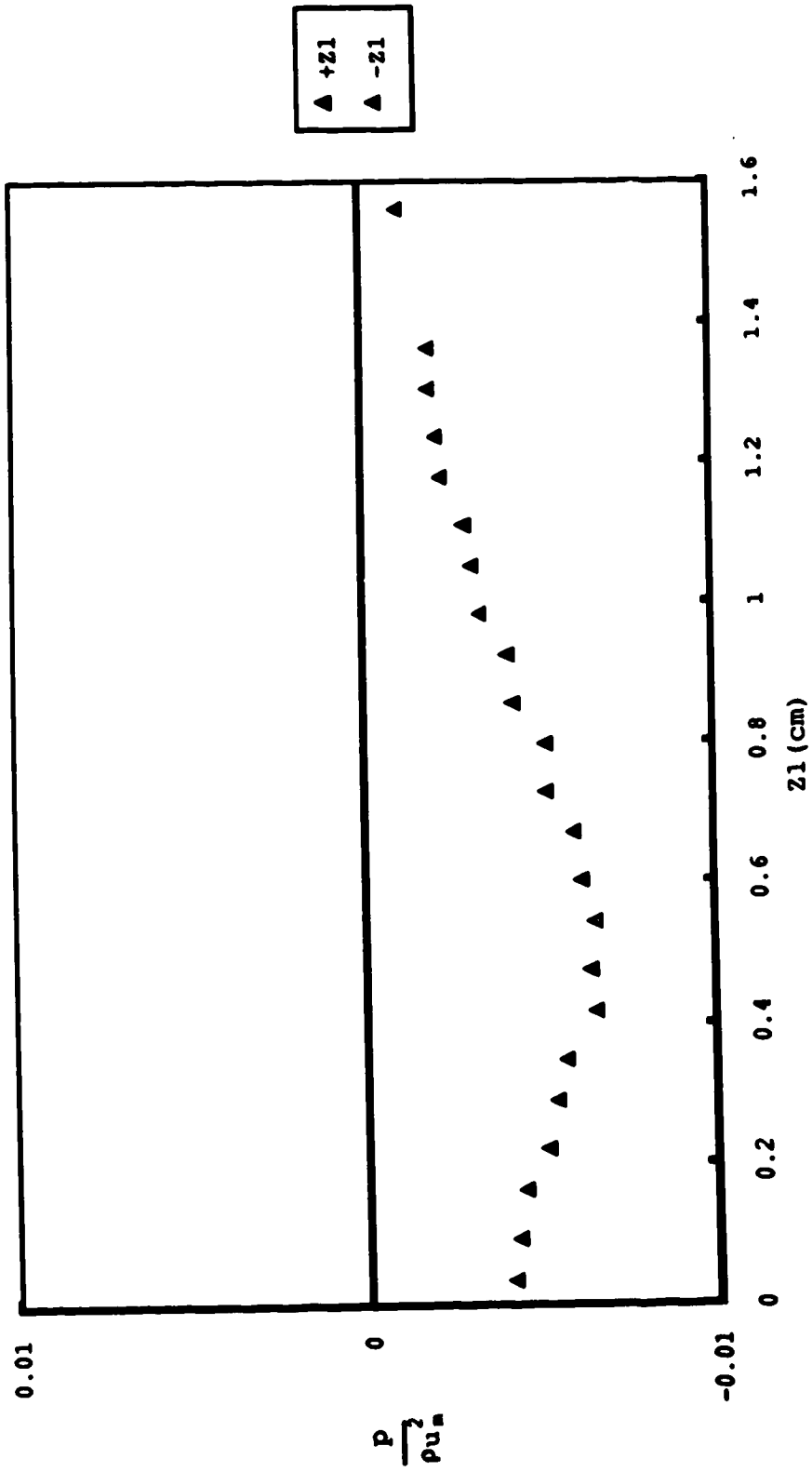

Fig. 4.46. Transverse pressure profile
Expt. 2, X1/d=5.14

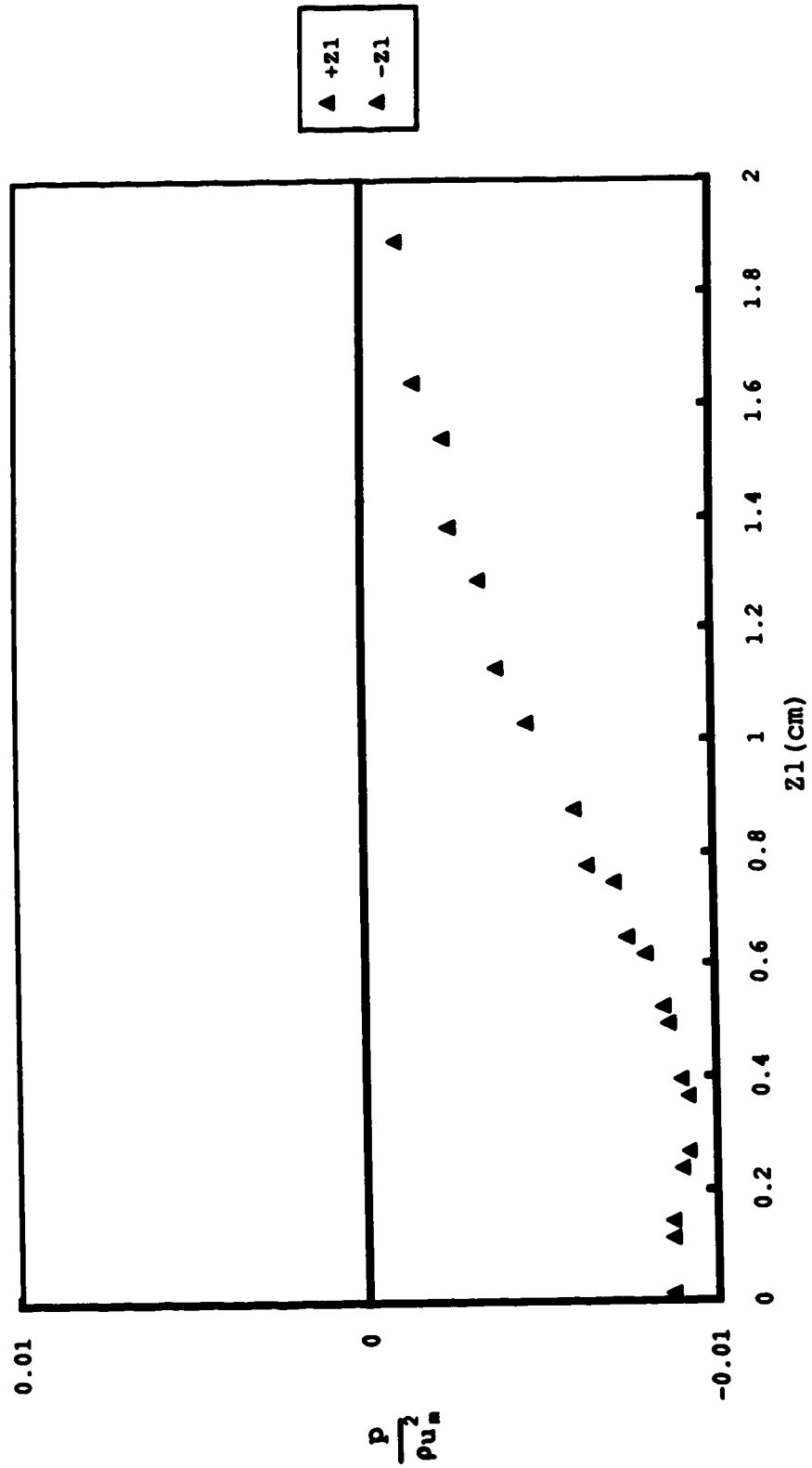

Fig. 4.47. Transverse pressure profile
Expt. 2, X1/d=6.72

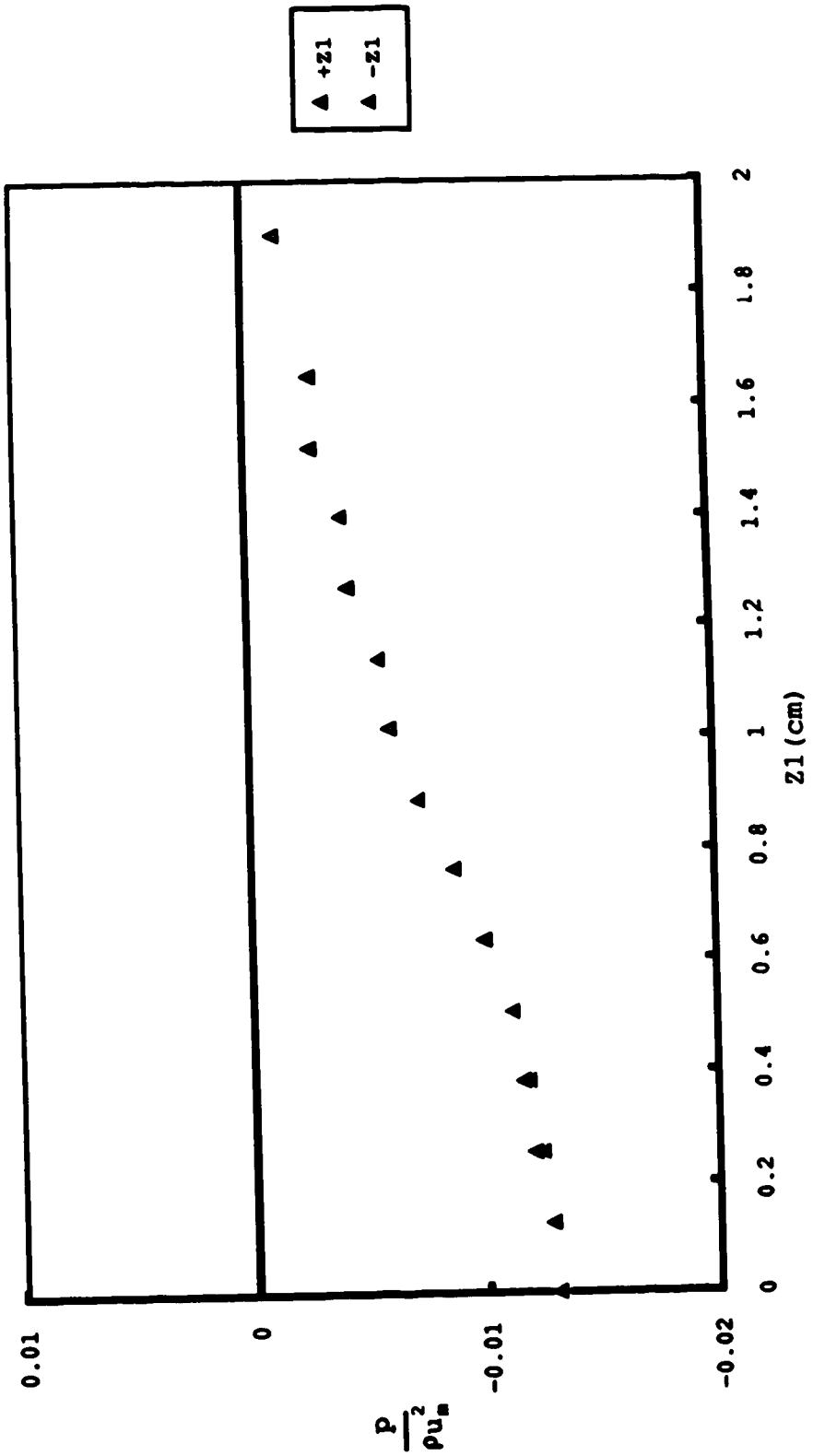

Fig. 4.48. Transverse pressure profile
Expt. 2, X1/d=7.90

Fig. 4.49. Transverse pressure profile
Expt. 2, X1/d=9.08

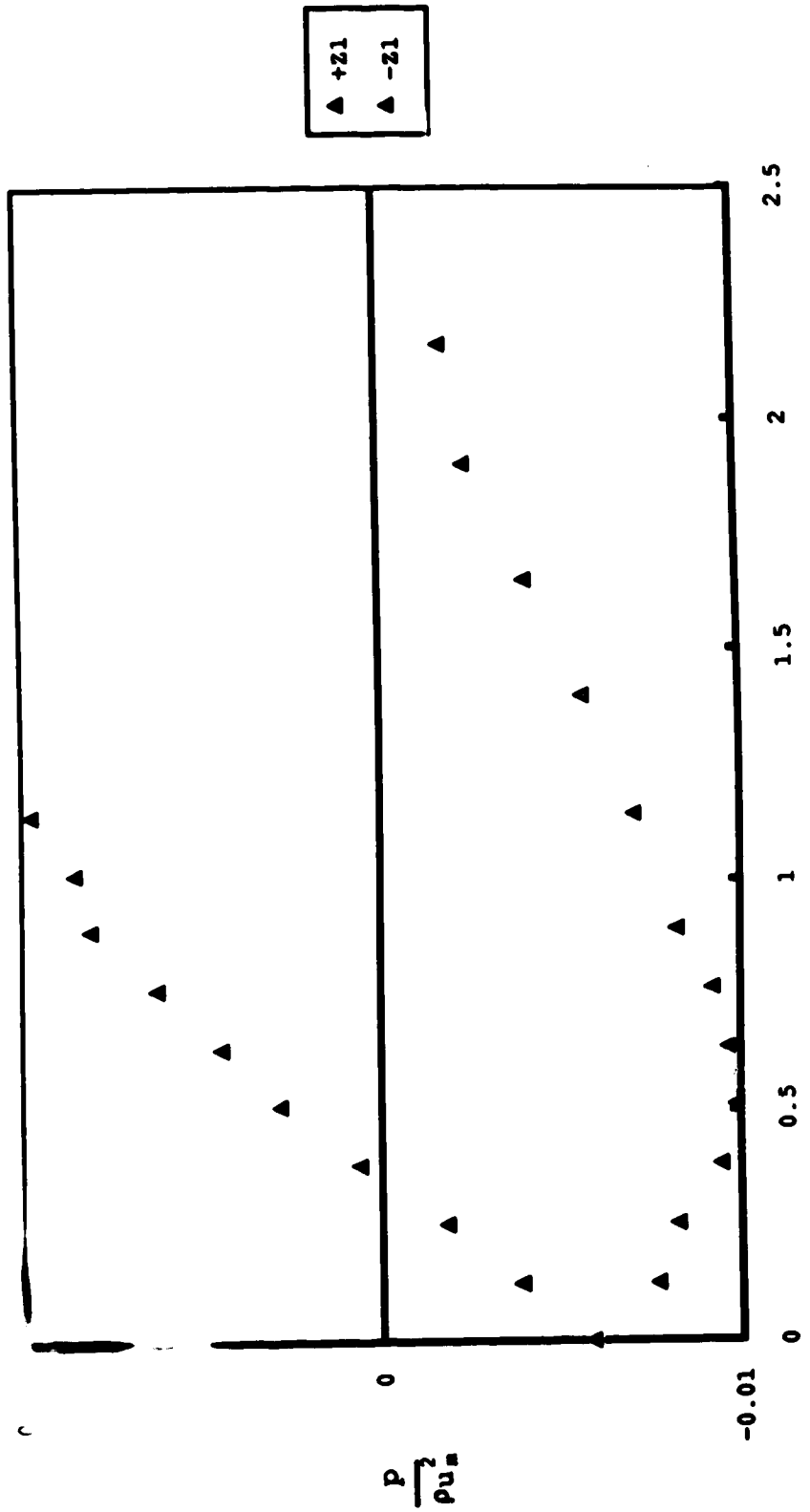

Fig. 4.50. Transverse pressure profile
Expt. 2, X1/d=9.63

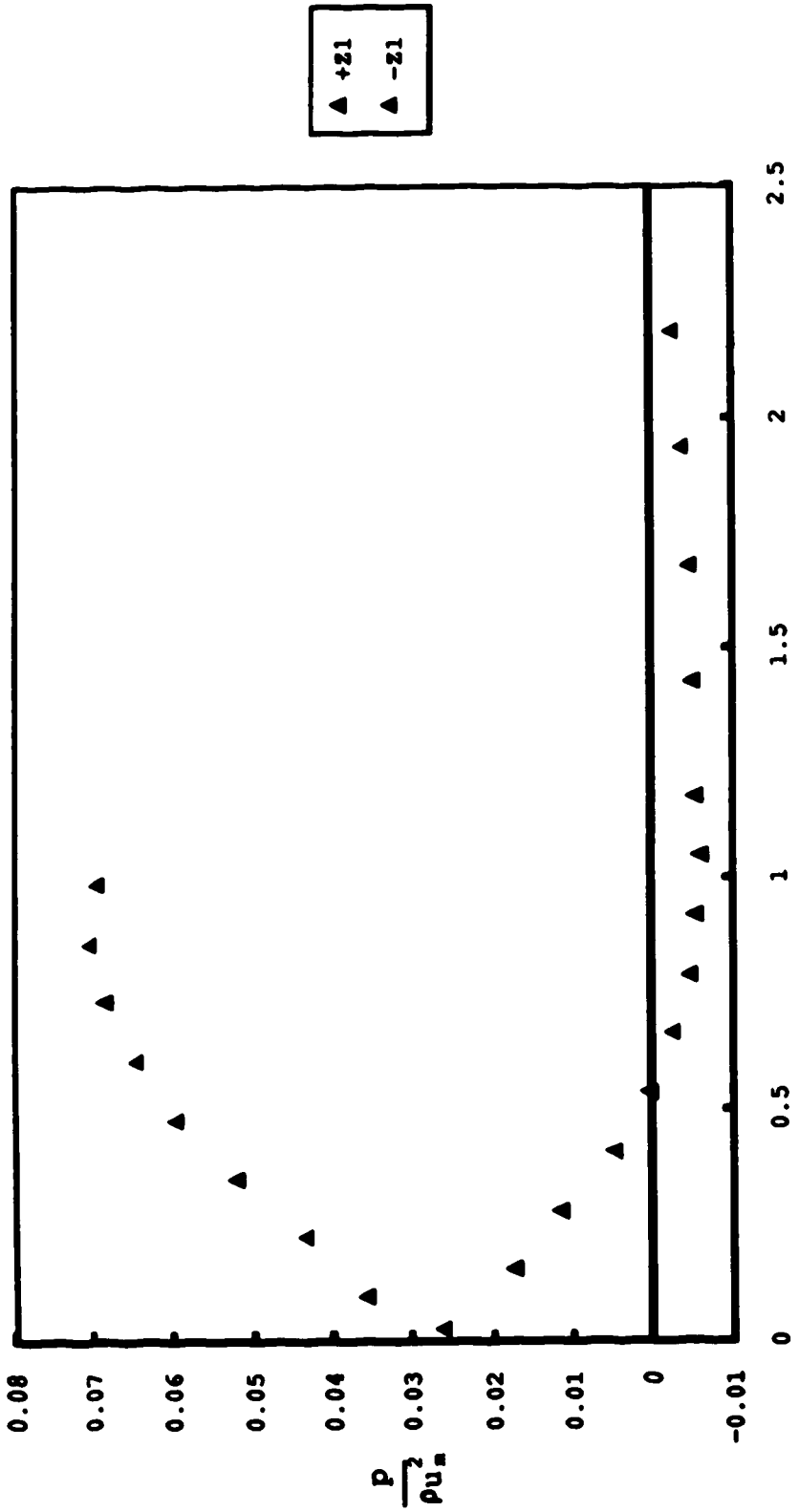

Fig. 4.51. Transverse pressure profile
Expt. 2, X1/d=10.26

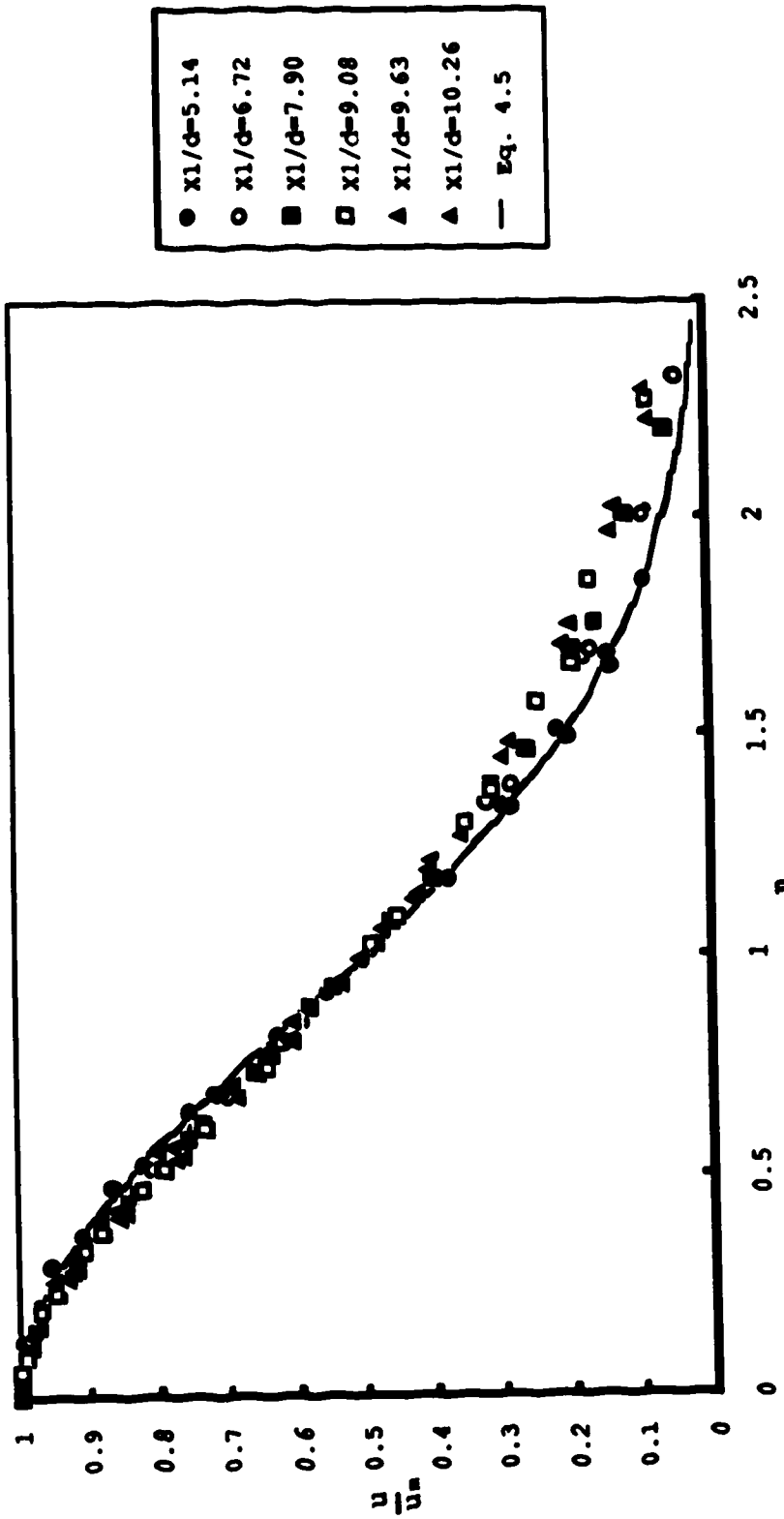

Fig. 4.52. Non dimensional transverse velocity profiles, Expt. 2

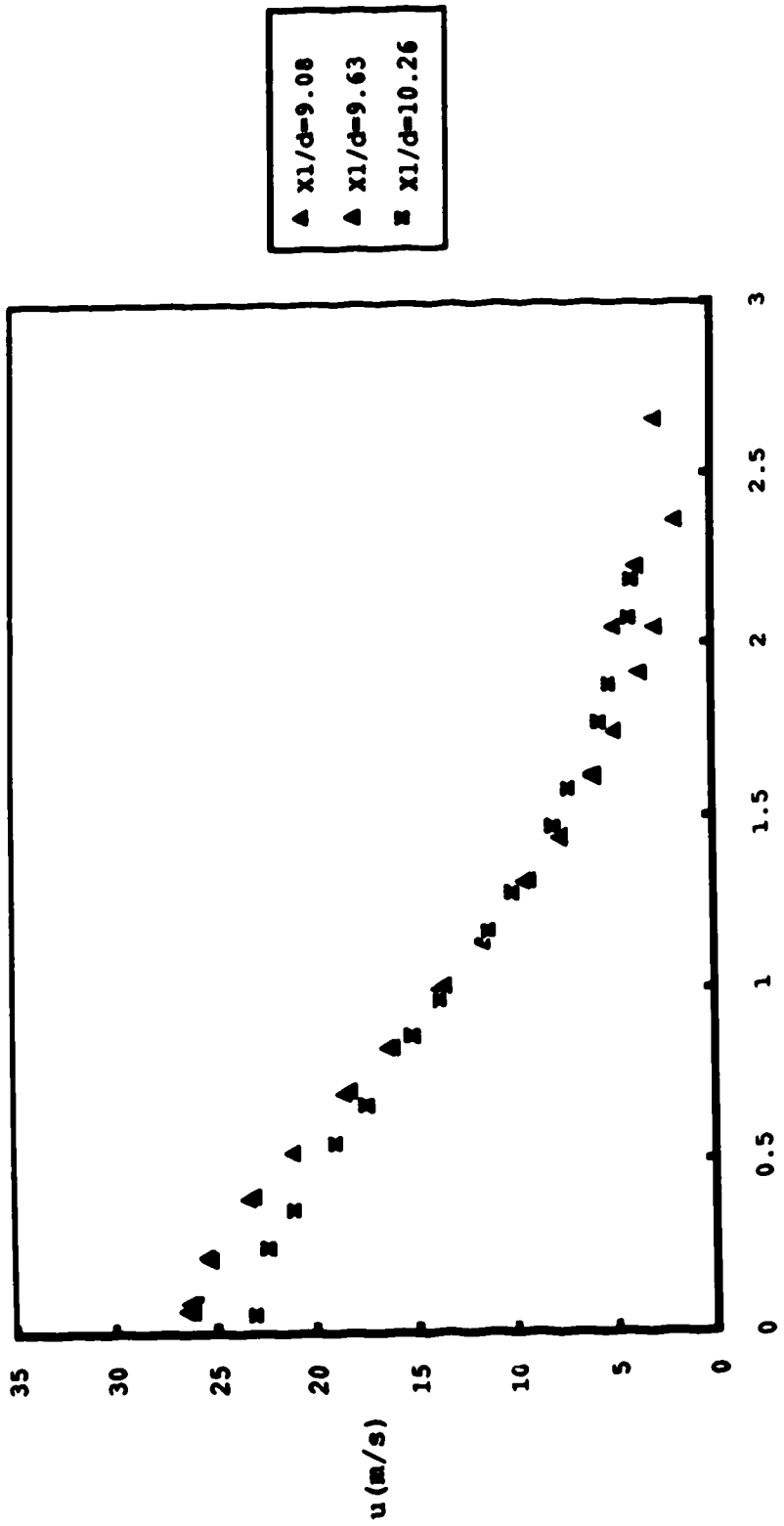

Fig. 4.53. Vertical velocity profiles
Expt. 2

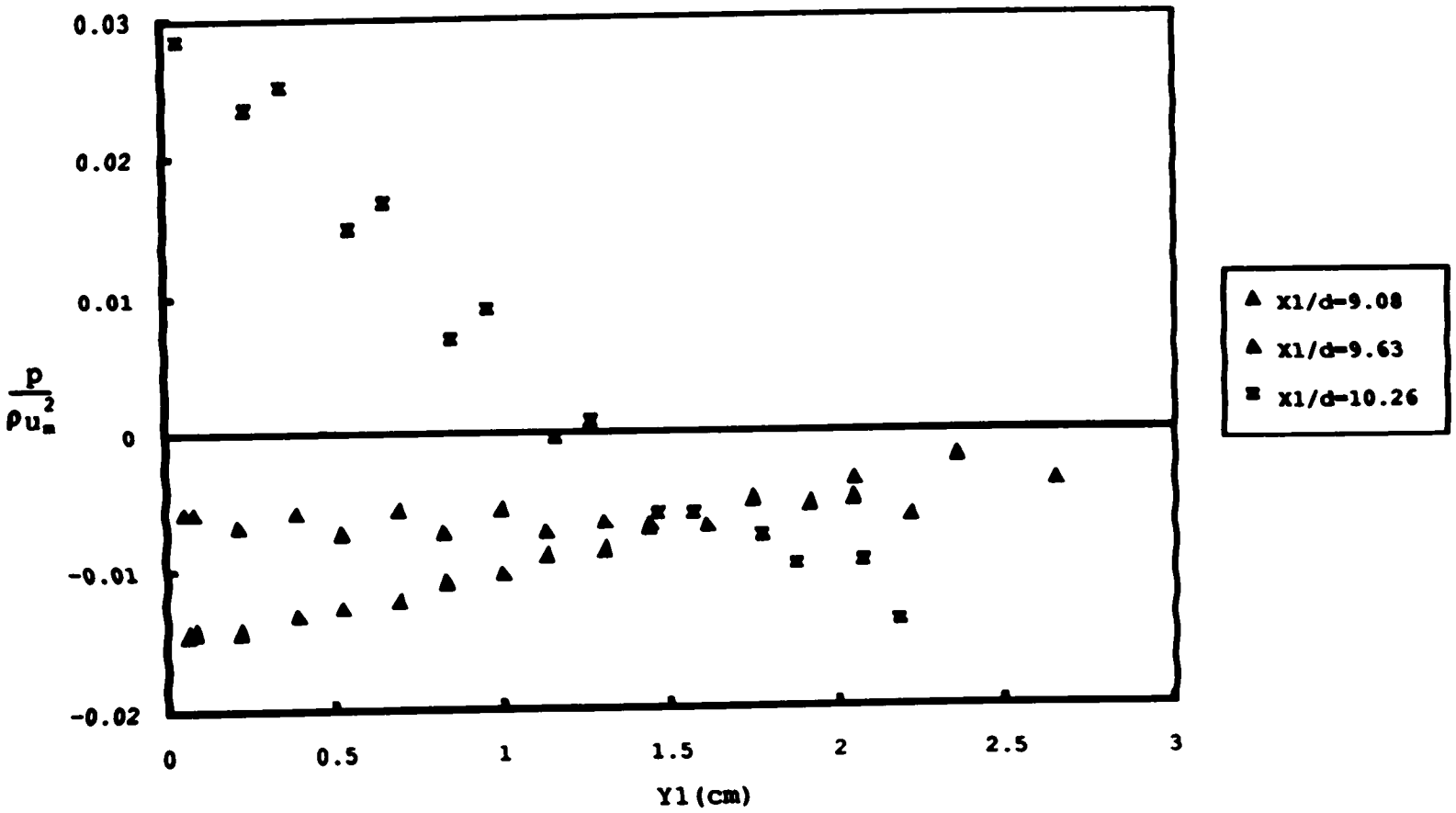

Fig. 4.54. Vertical pressure profiles
Expt. 2,

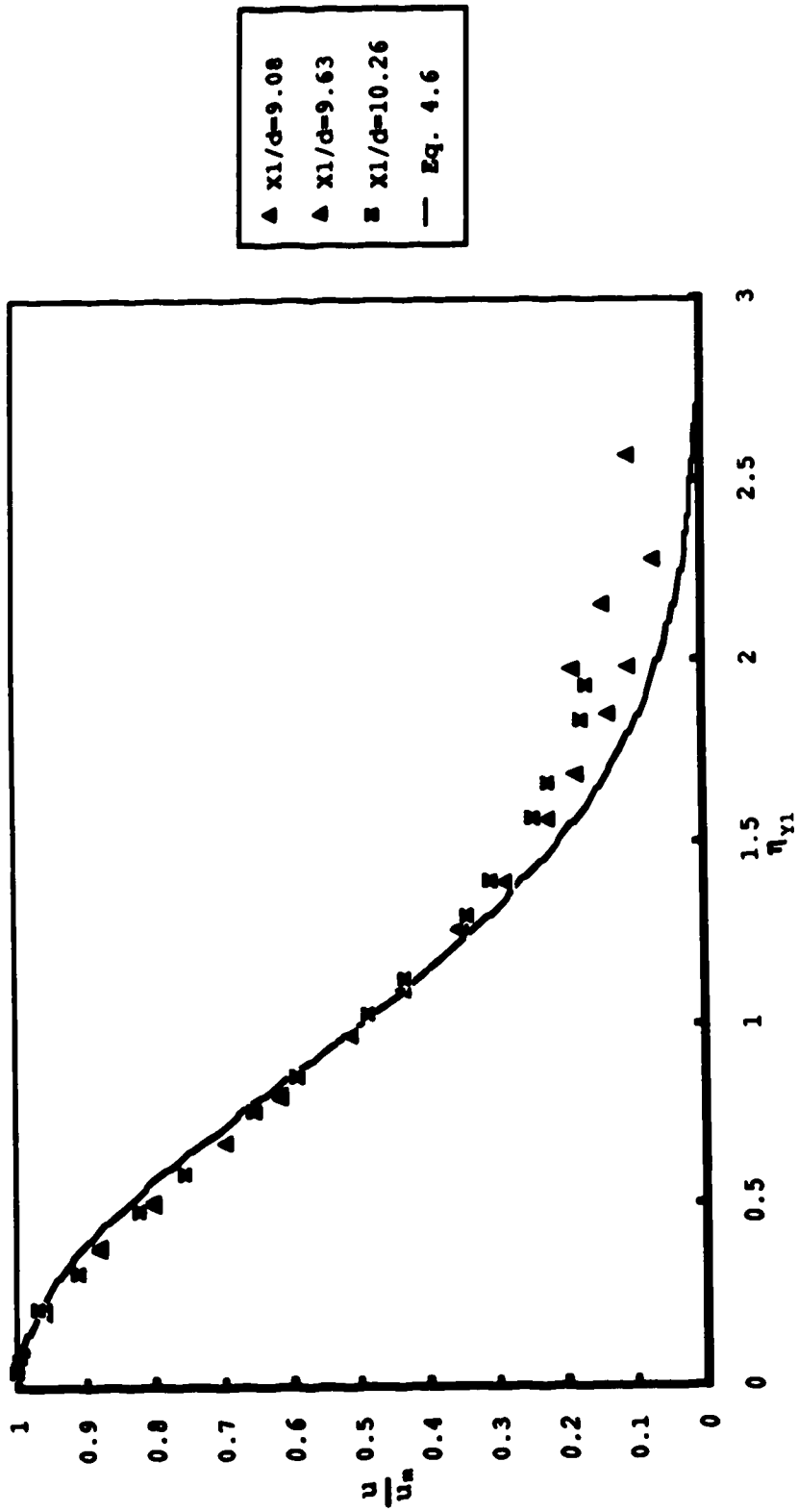

Fig. 4.55. Non dimensional vertical velocity profiles, Expt. 2

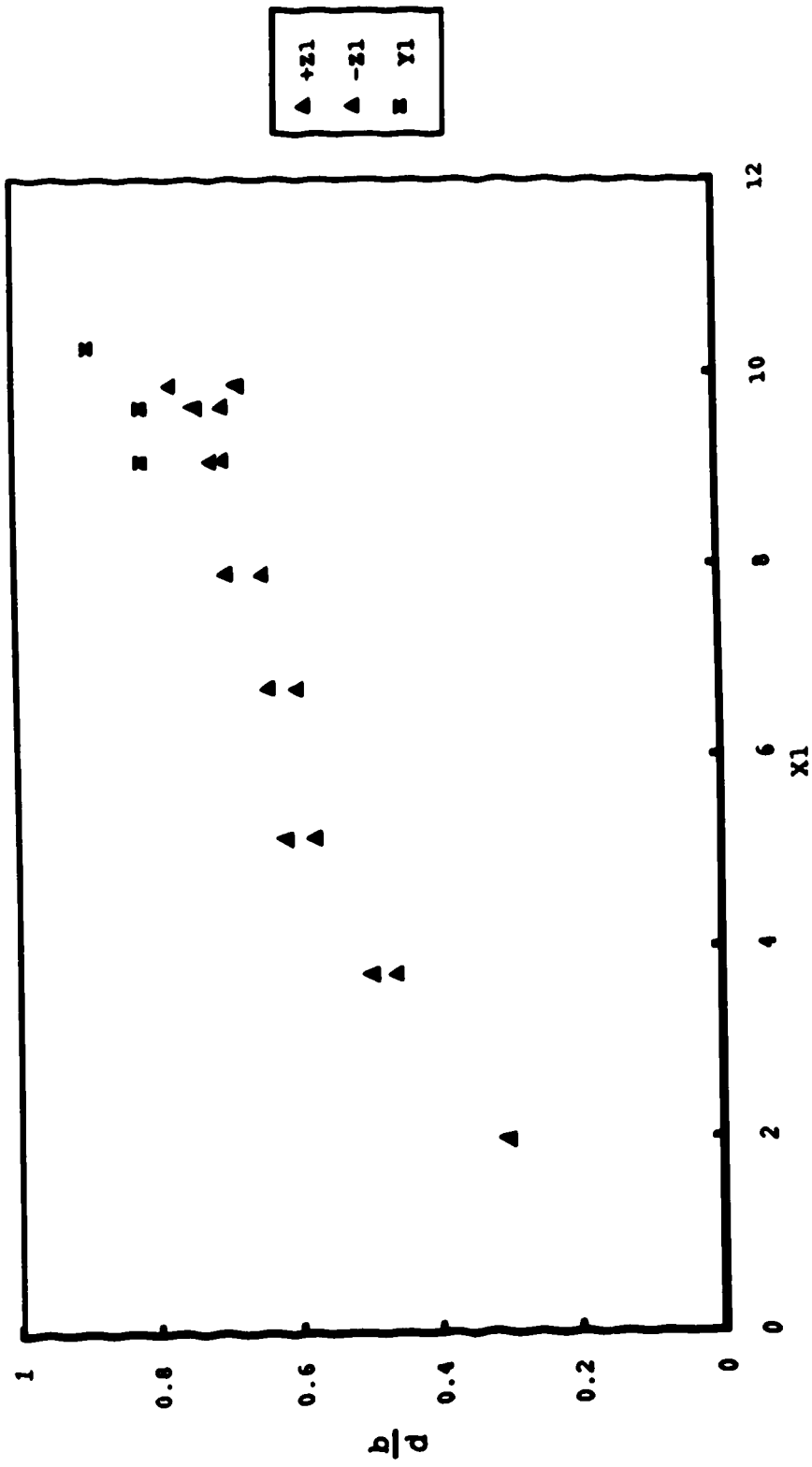

Fig. 4.56. Growth rates
Expt. 2

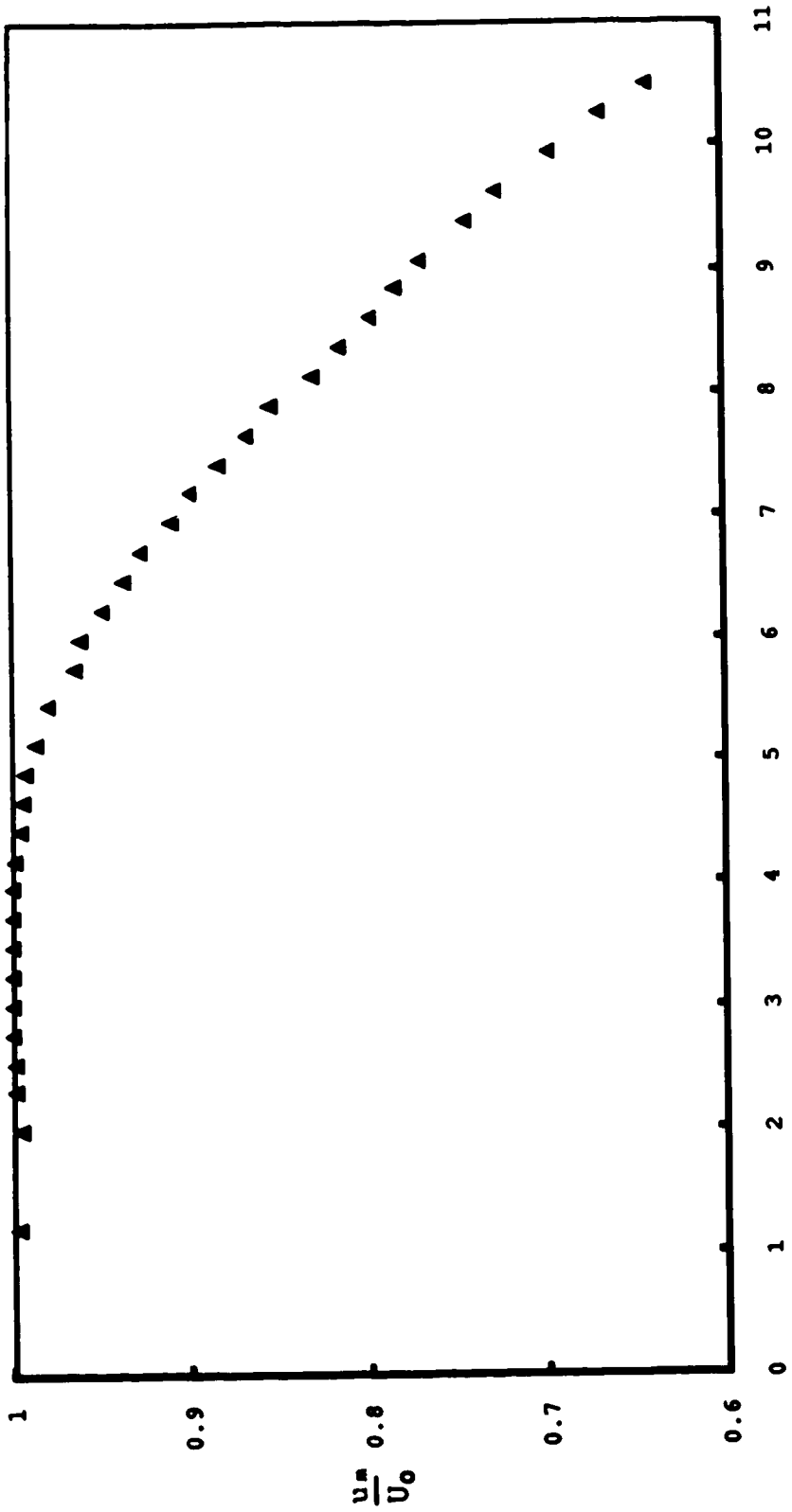

Fig. 4.57. Centreline velocity profile
Expt. 2

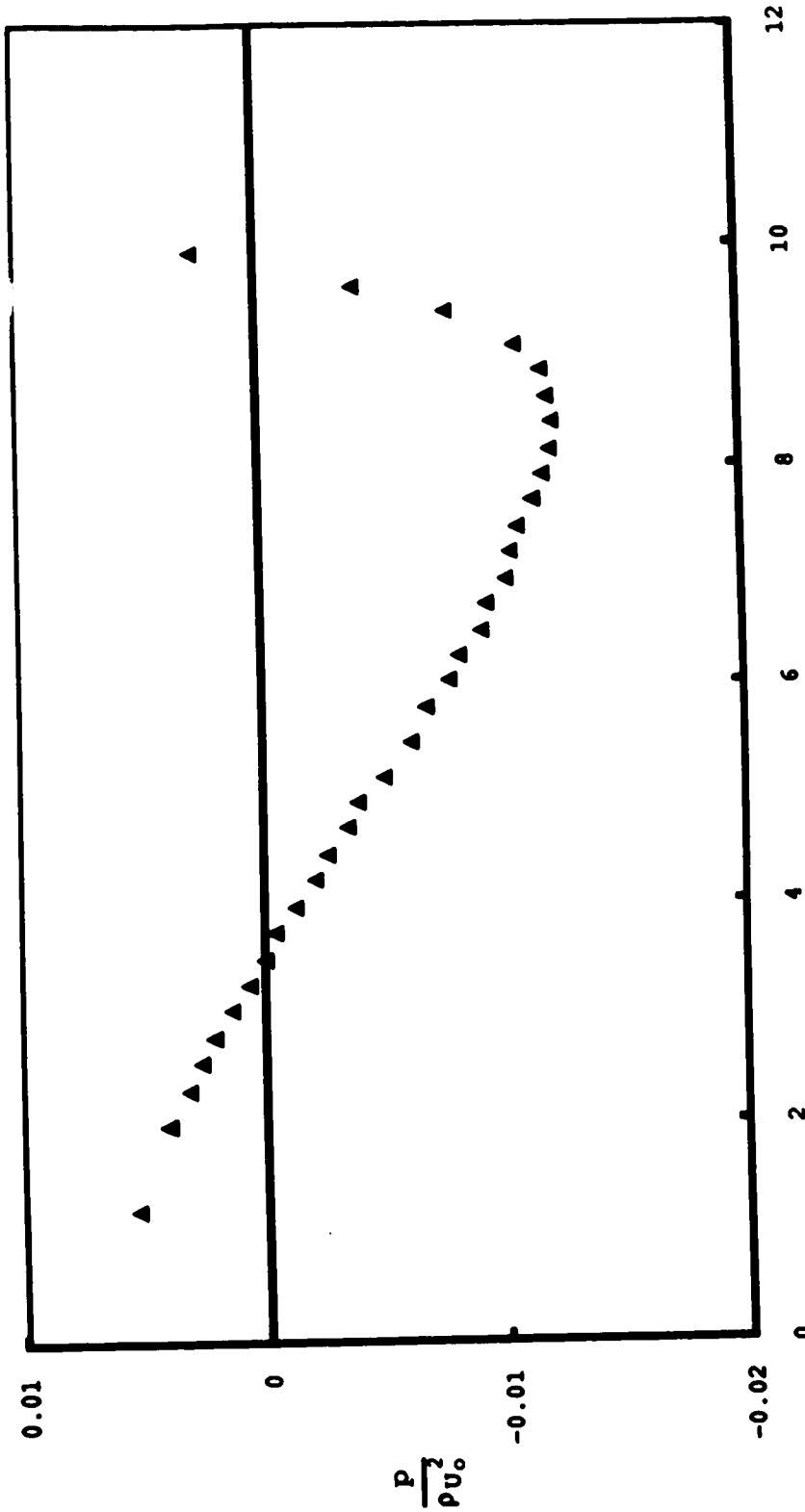

Fig. 4.58. Centreline pressure profile Expt. 2

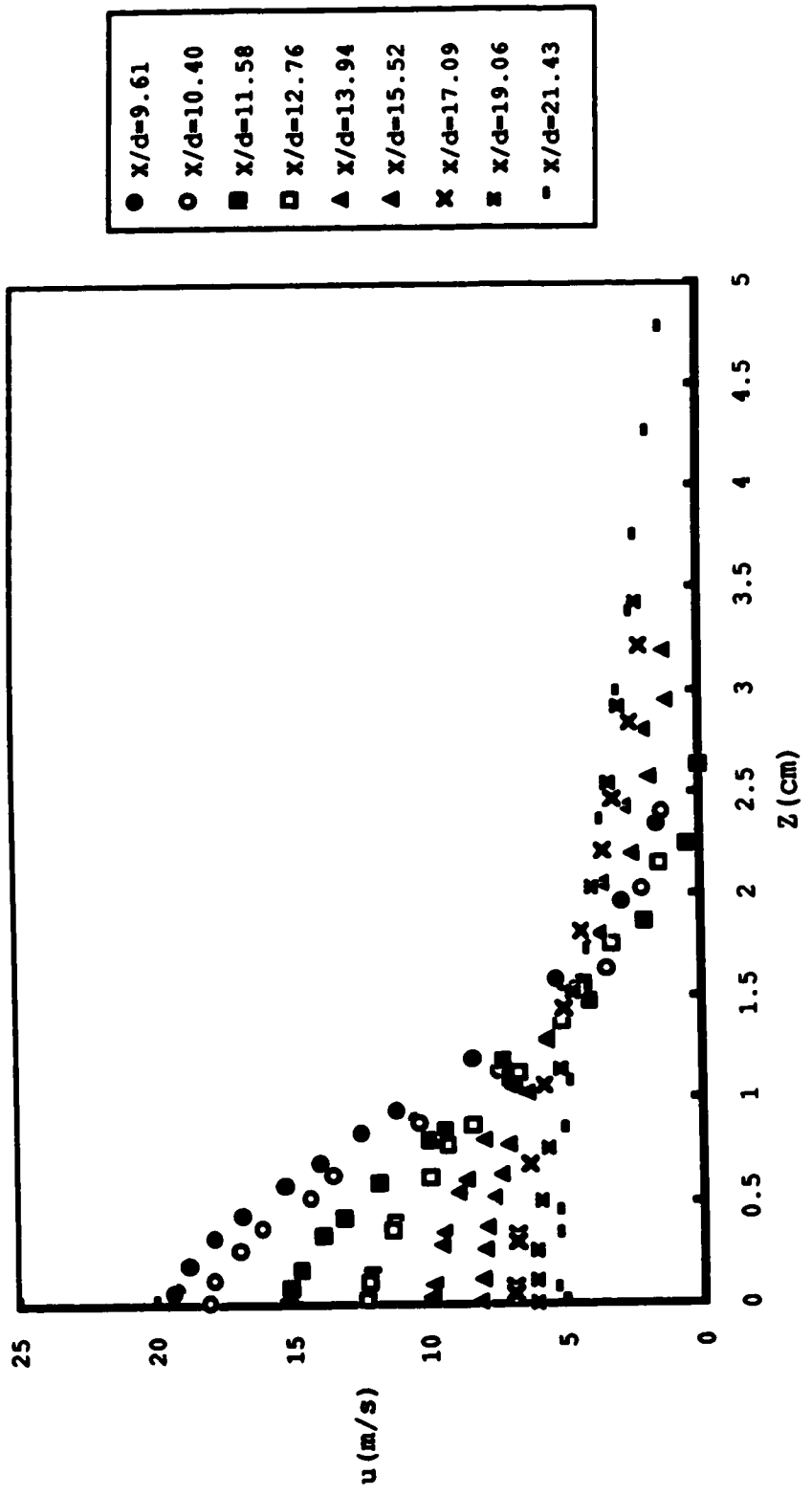

Fig. 4.59. Transverse velocity profiles
Expt. 2

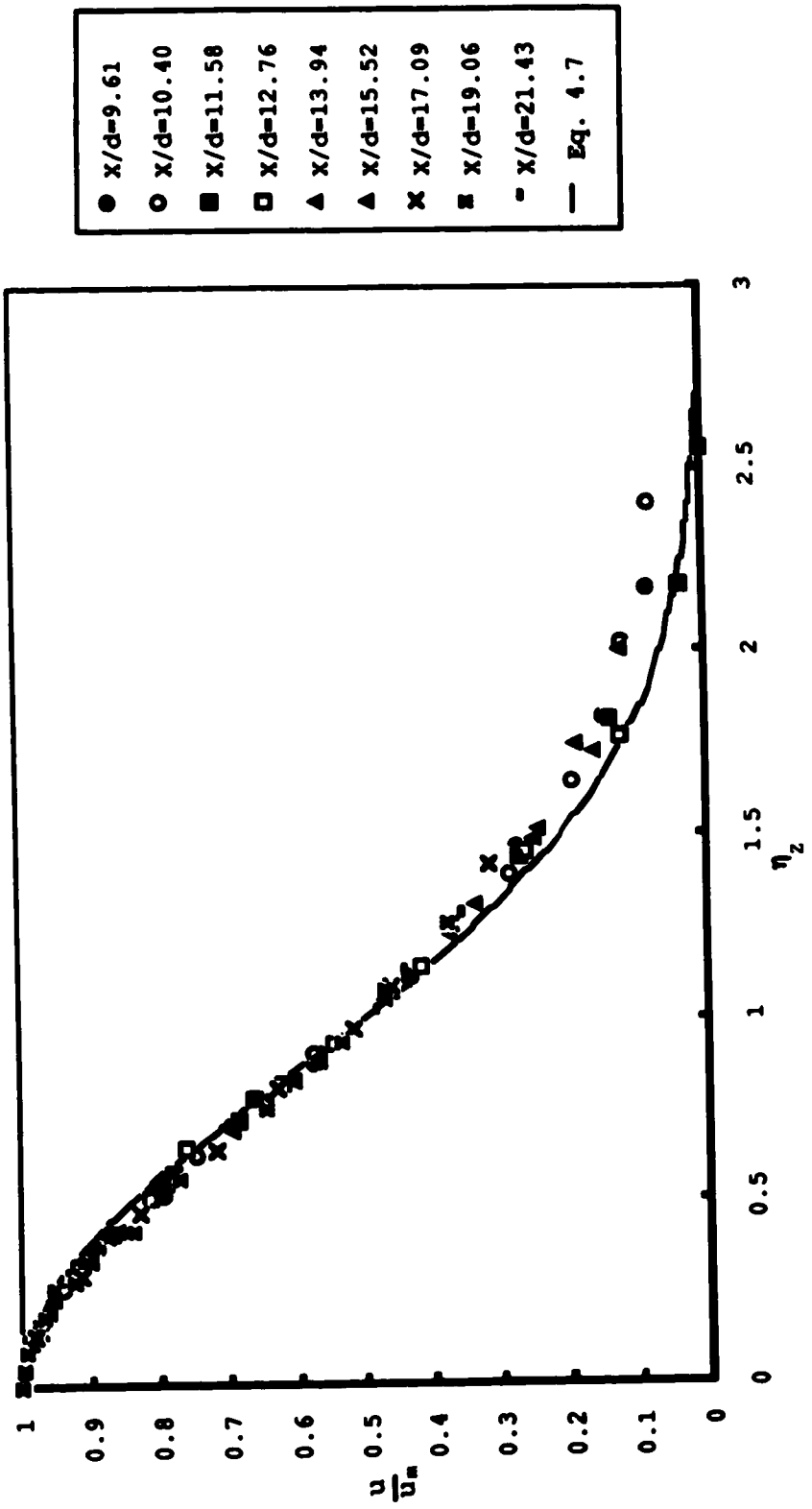

Fig. 4.60. Non dimensional transverse velocity profiles, Expt. 2

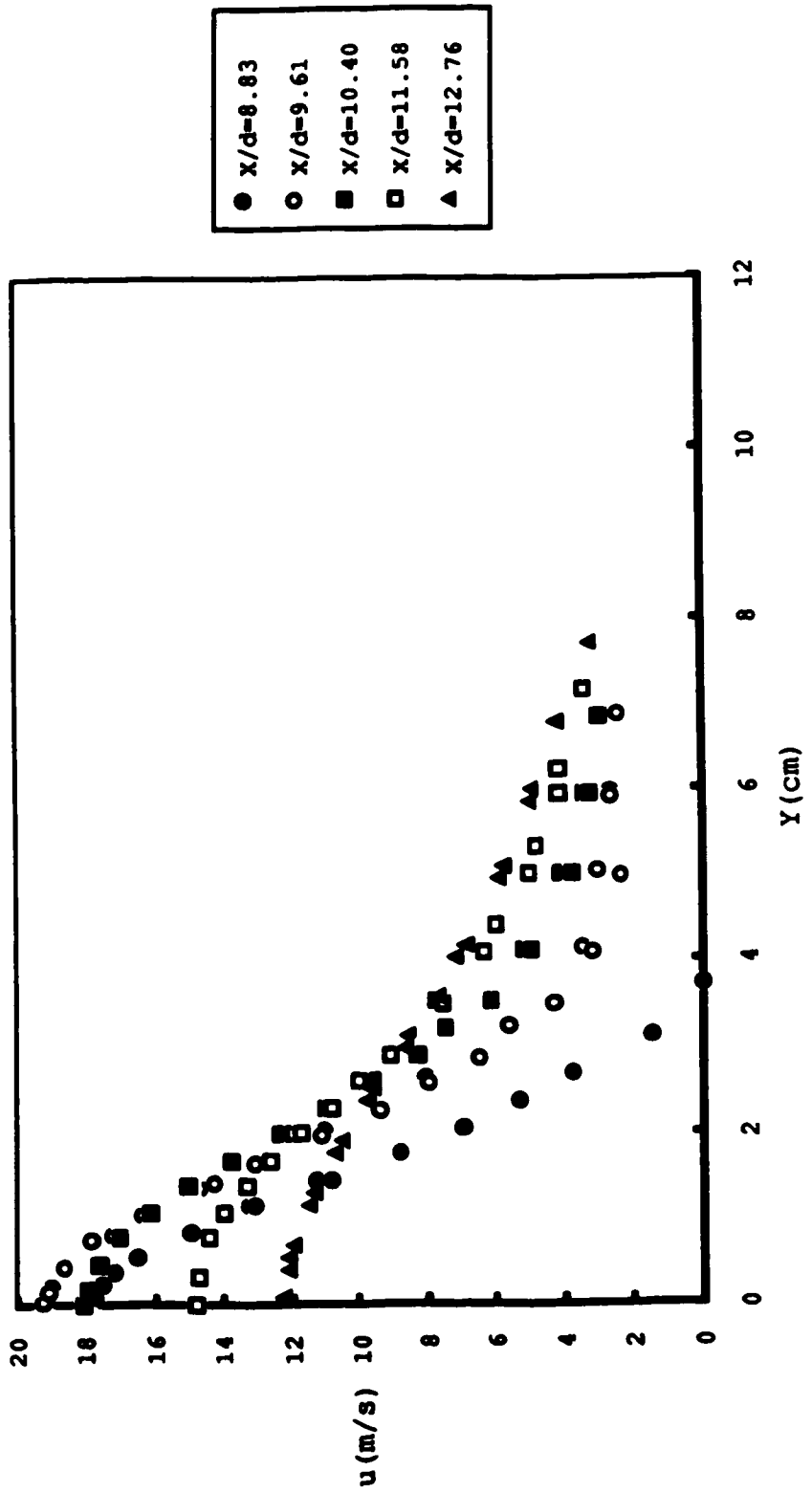

Fig. 4.61a. Vertical velocity profiles
Expt. 2

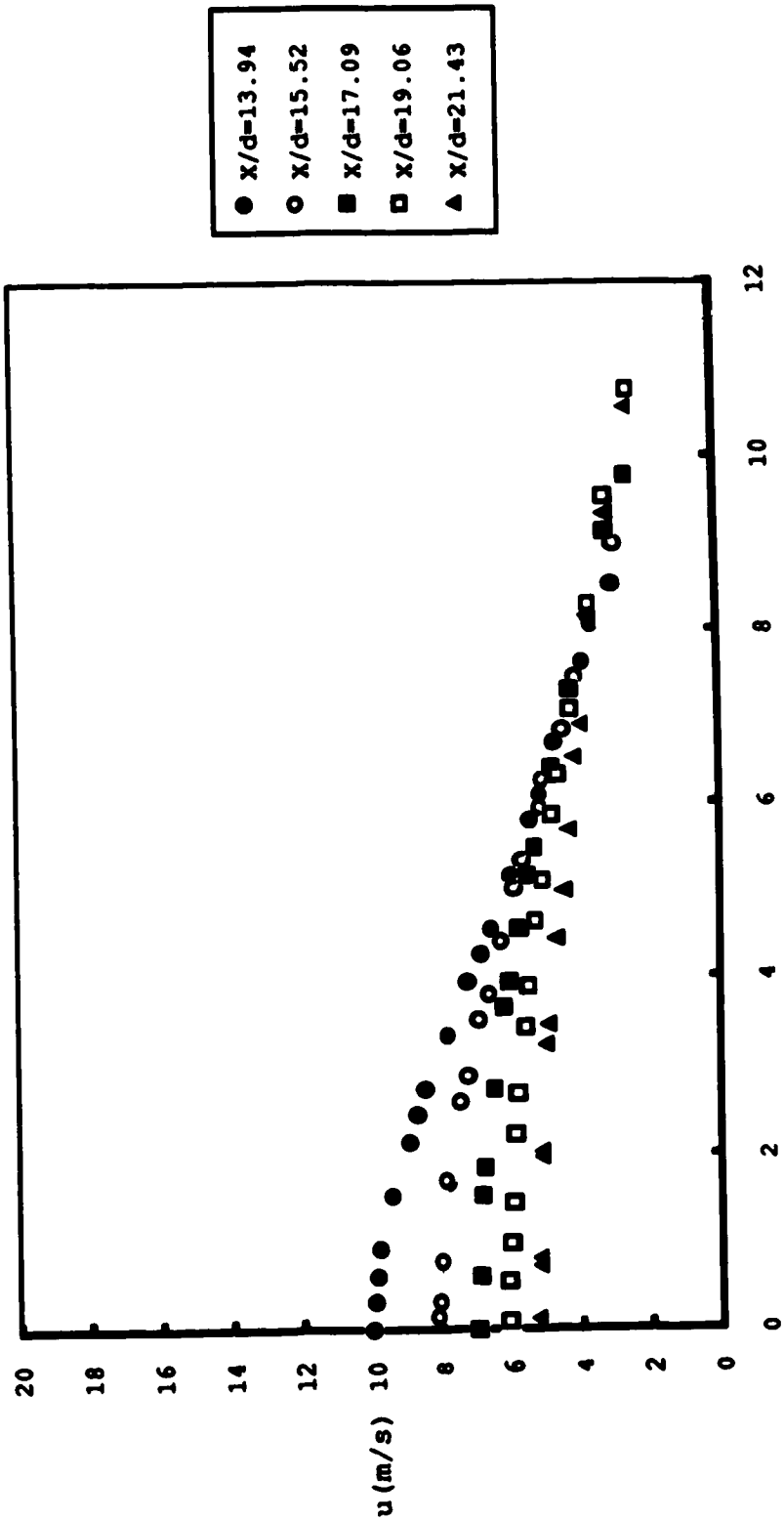

Fig. 4.61b. Vertical velocity profiles
Expt. 2

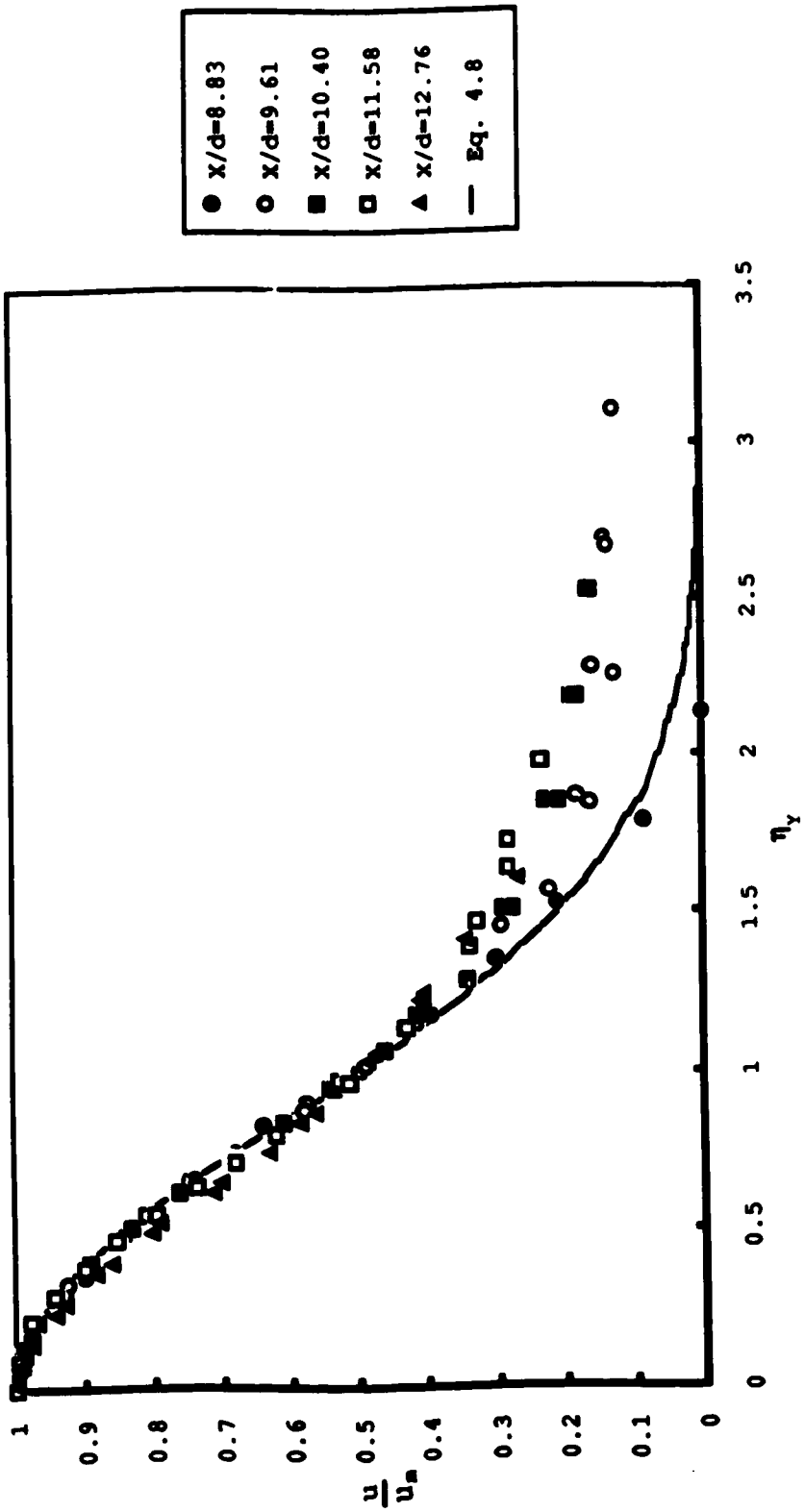

Fig. 4.62a. Non dimensional vertical velocity profiles, Expt. 2

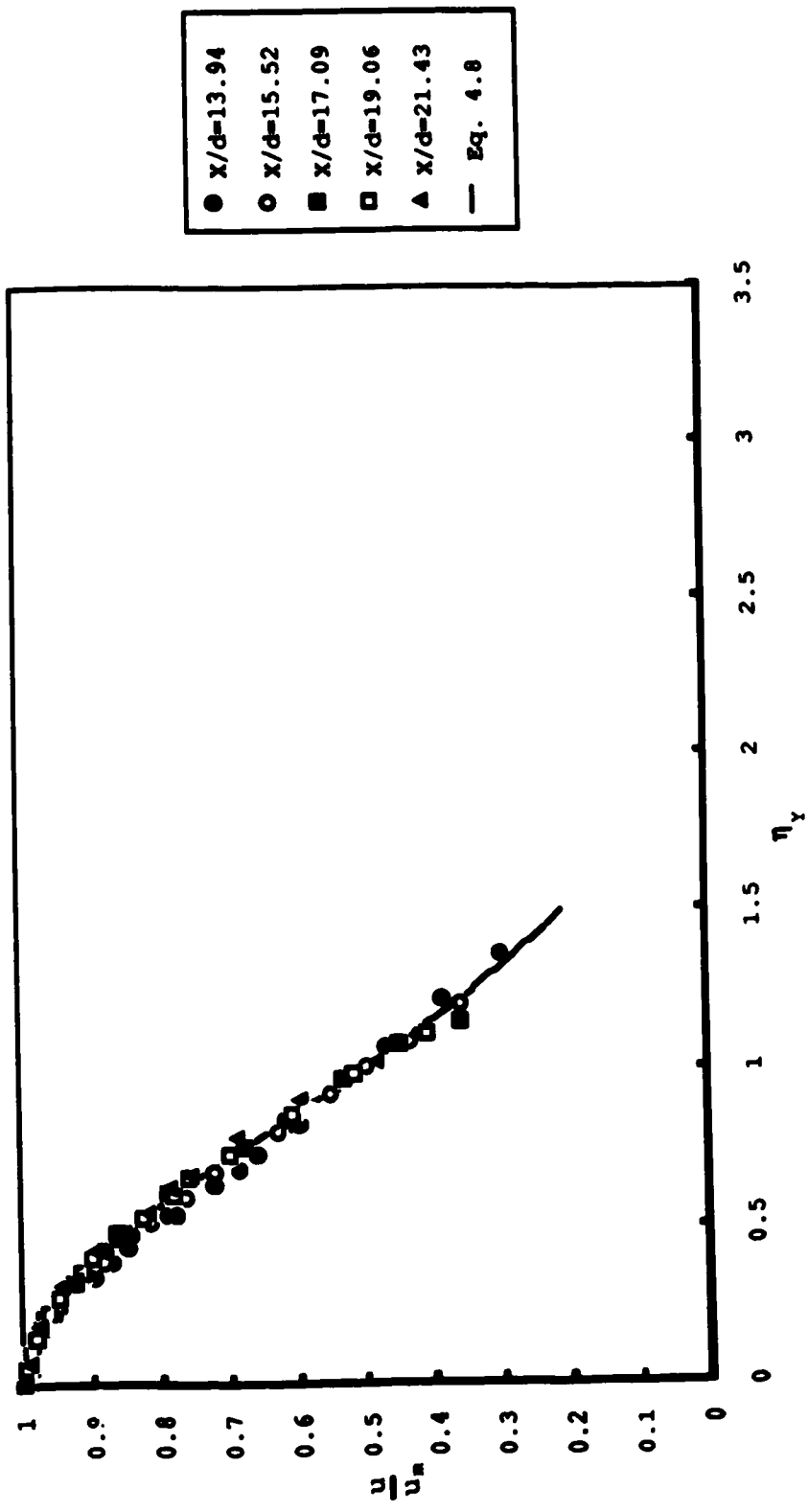

Fig. 4.62b. Non dimensional vertical velocity profiles, Expt. 2

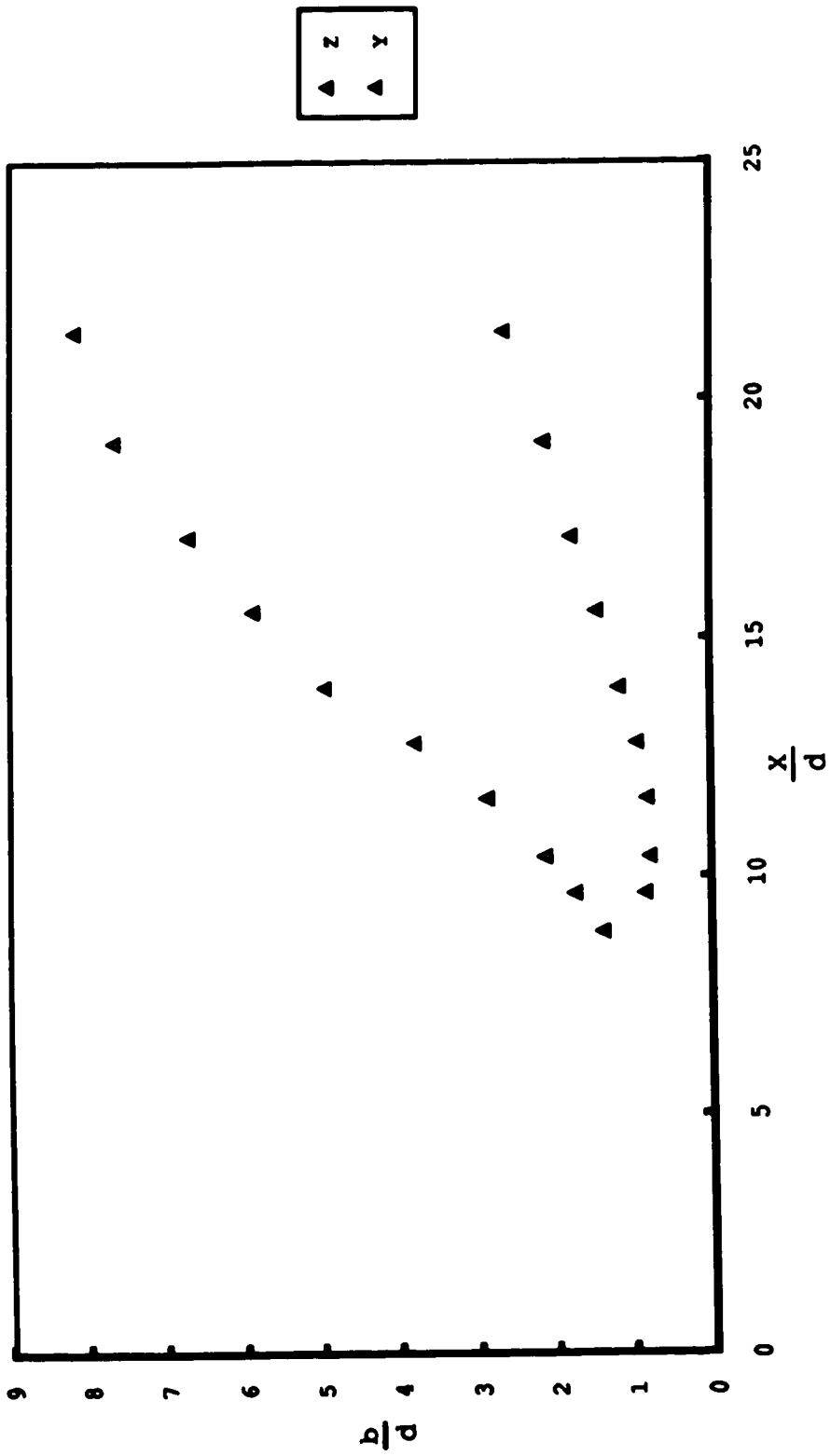

Fig. 4.63. Growth rates
Expt. 2

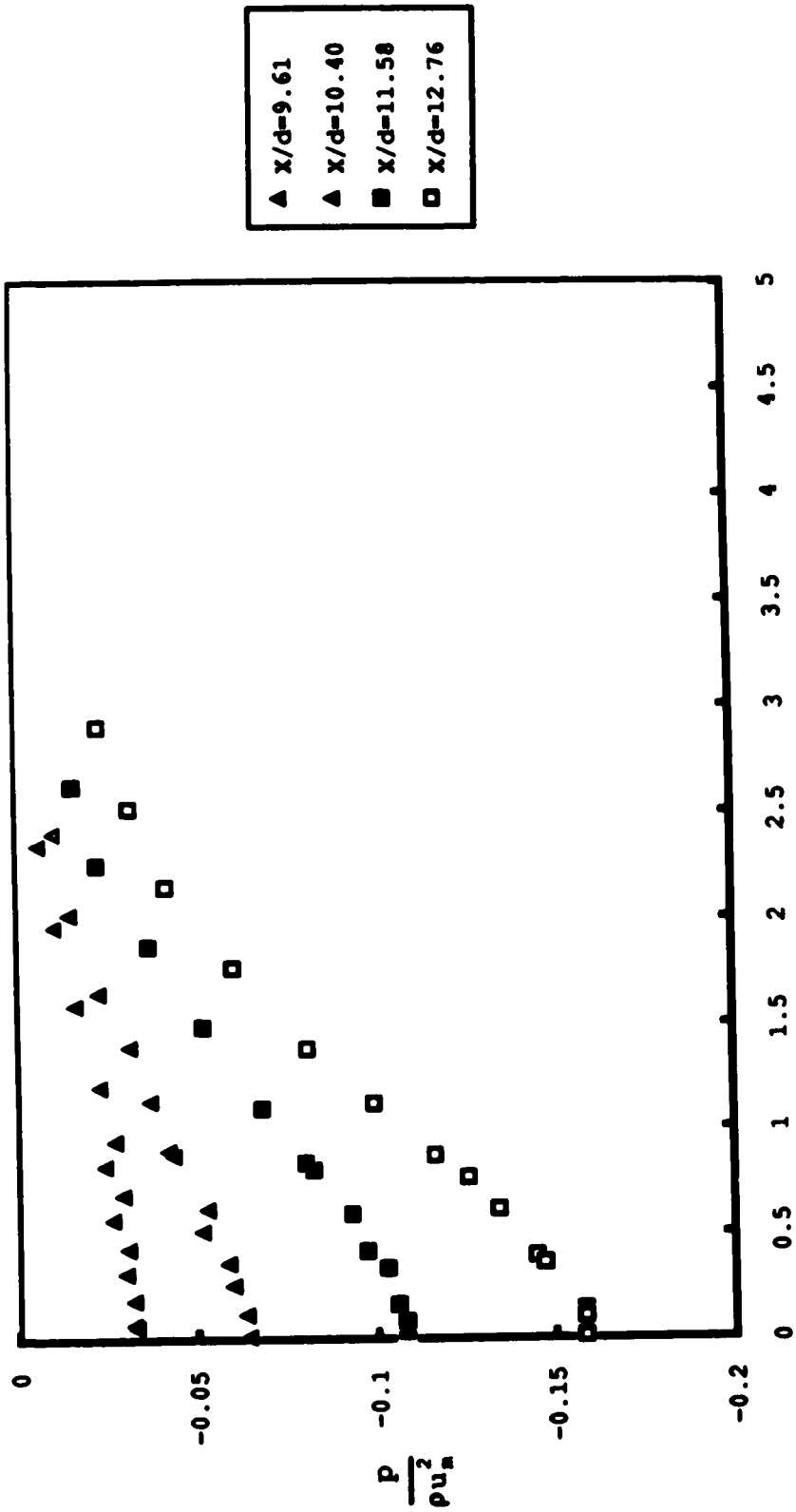

Fig. 4.64a. Transverse pressure profiles
Expt. 2

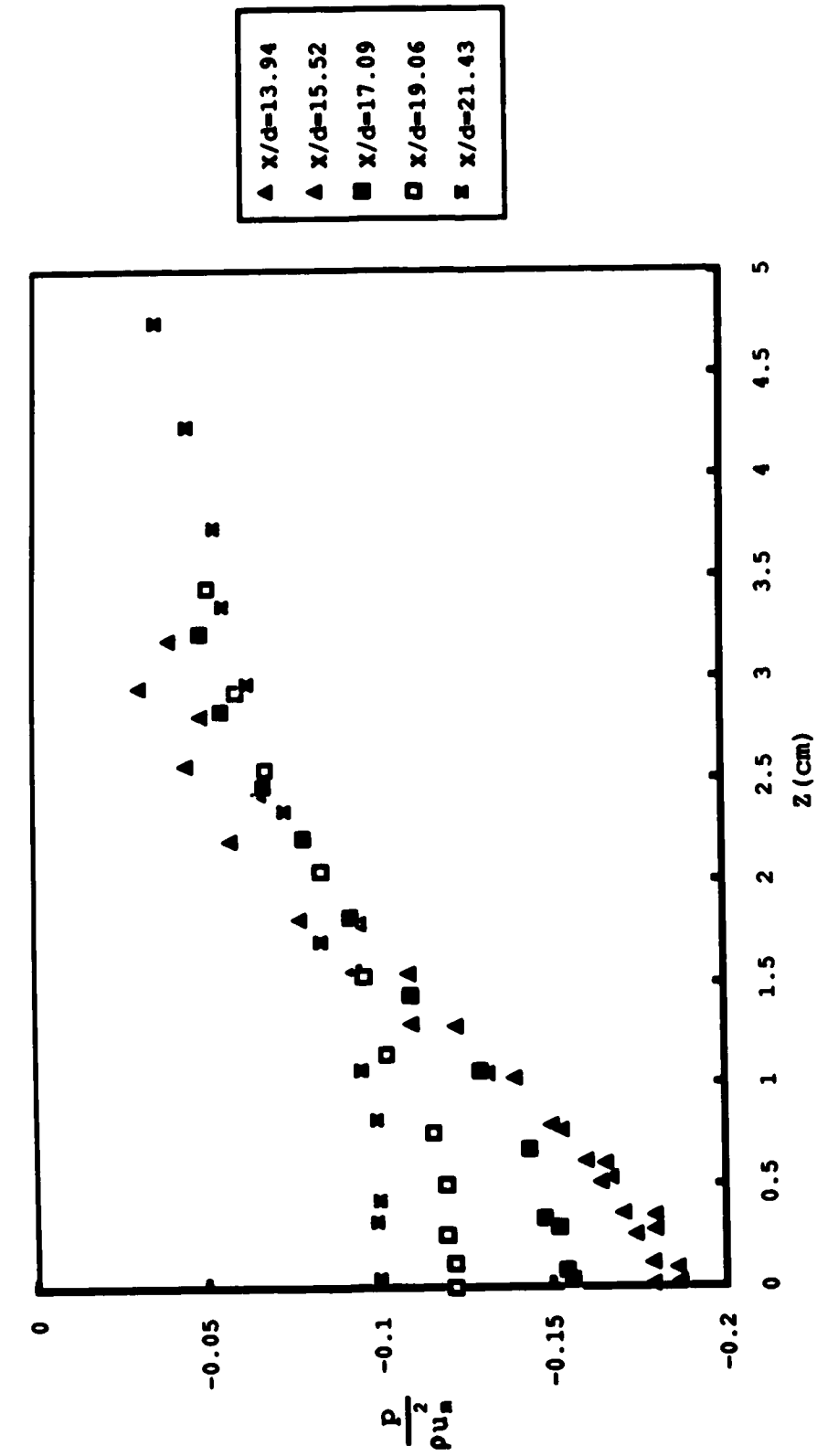

Fig. 4.64b. Transverse pressure profiles
Expt. 2

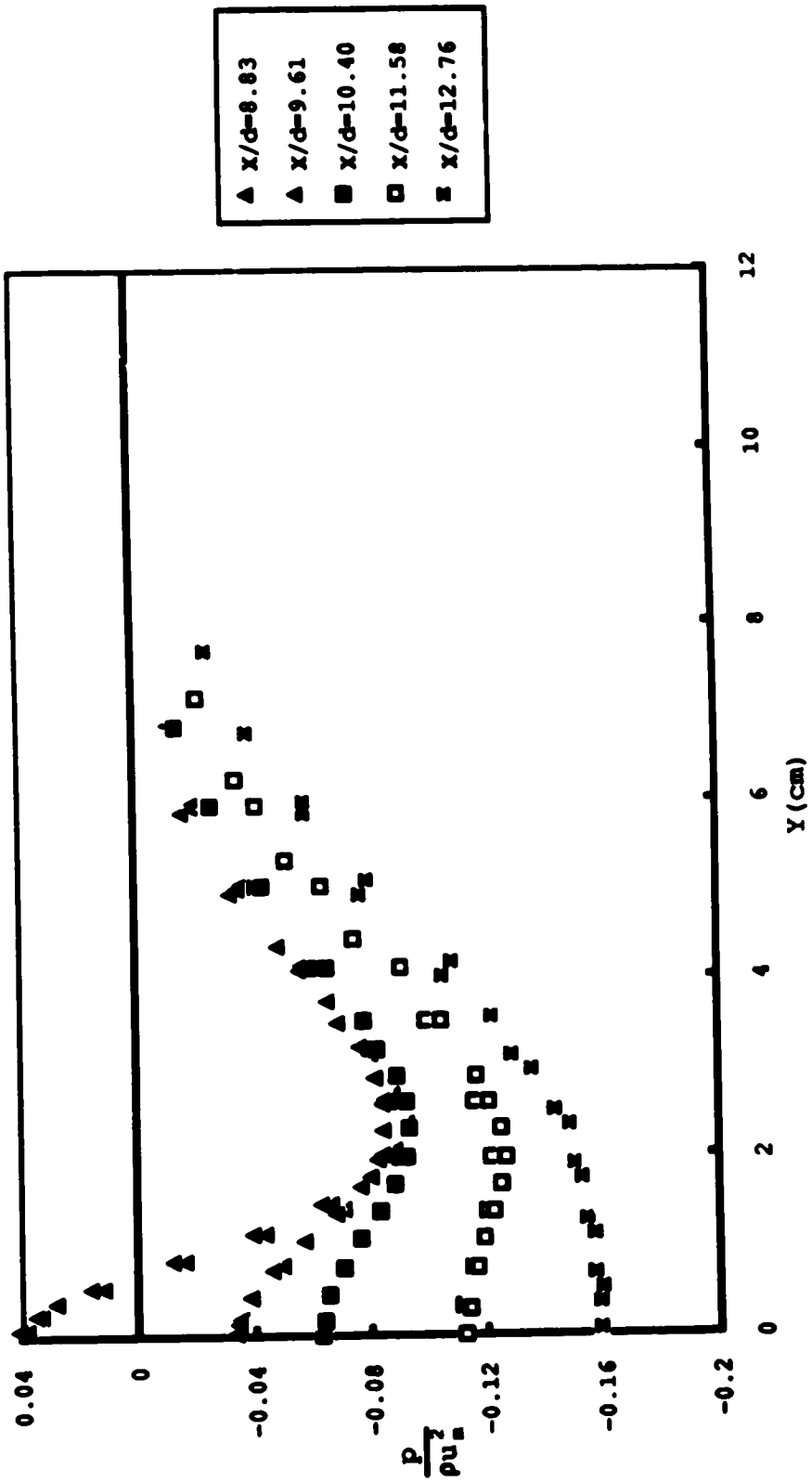

Fig. 4.65a. Vertical pressure profiles
Expt. 2

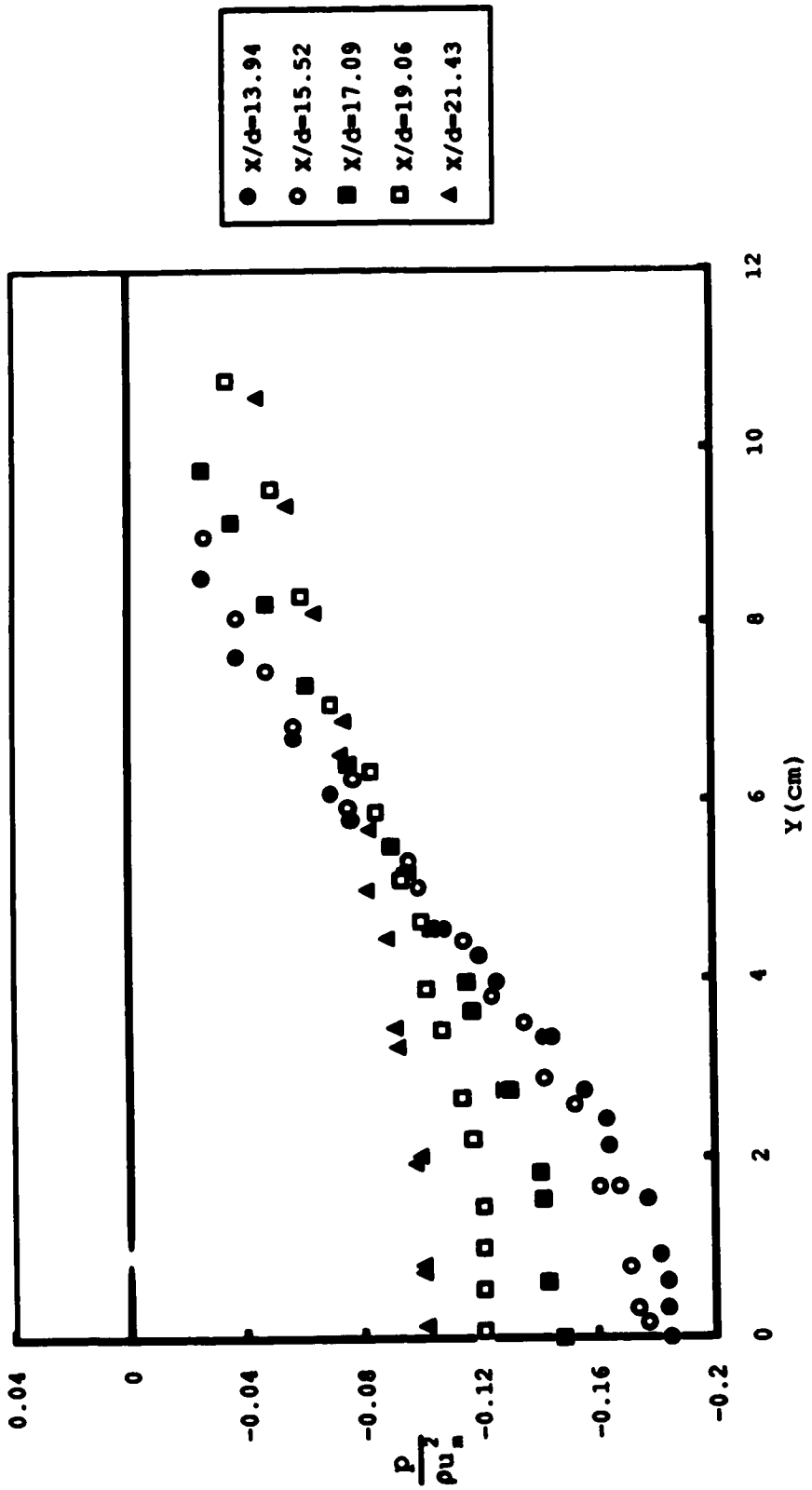

Fig. 4.65b. Vertical pressure profiles
Expt. 2

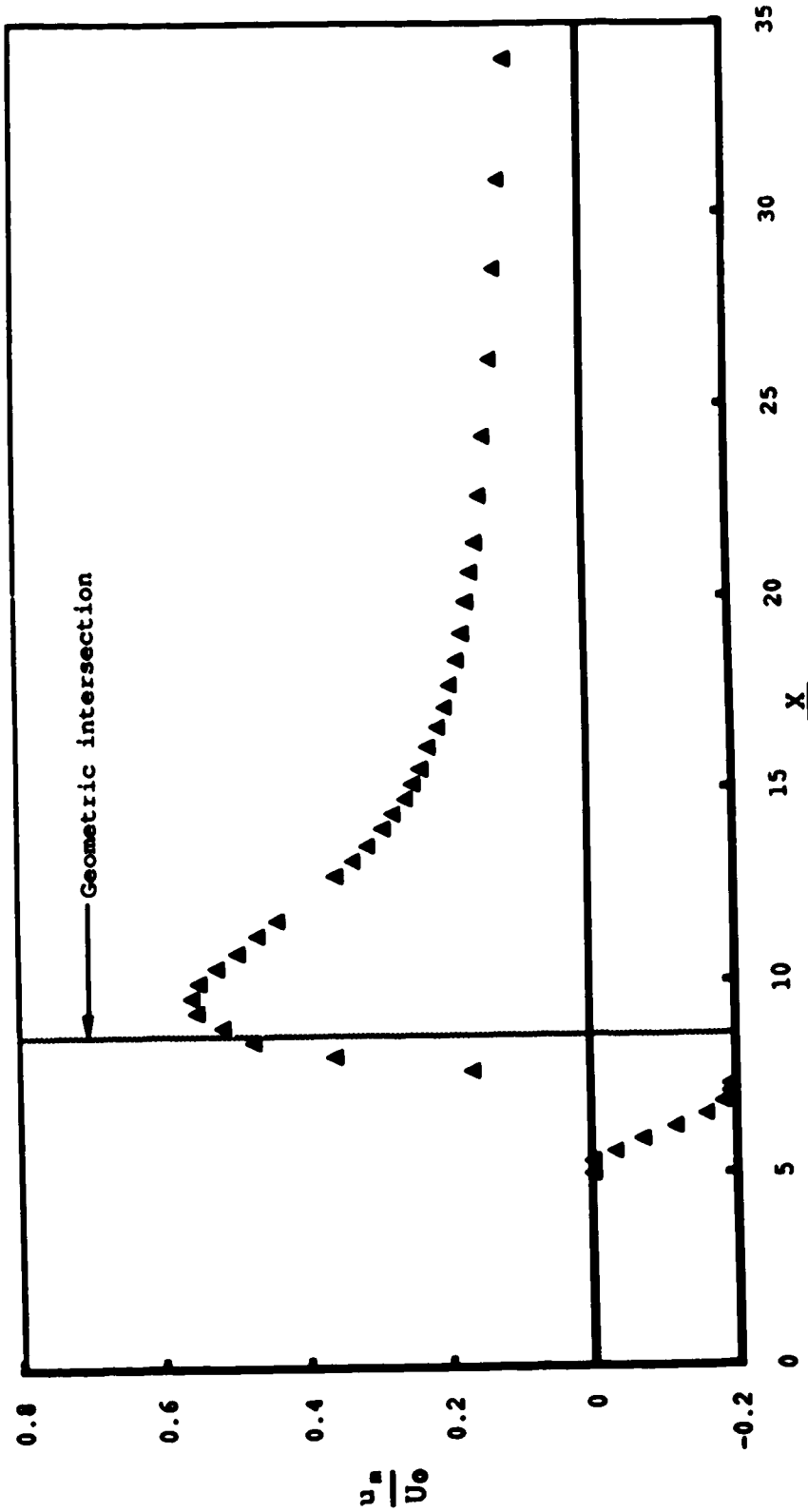

Fig. 4.66. Centreline velocity profile
Expt. 2

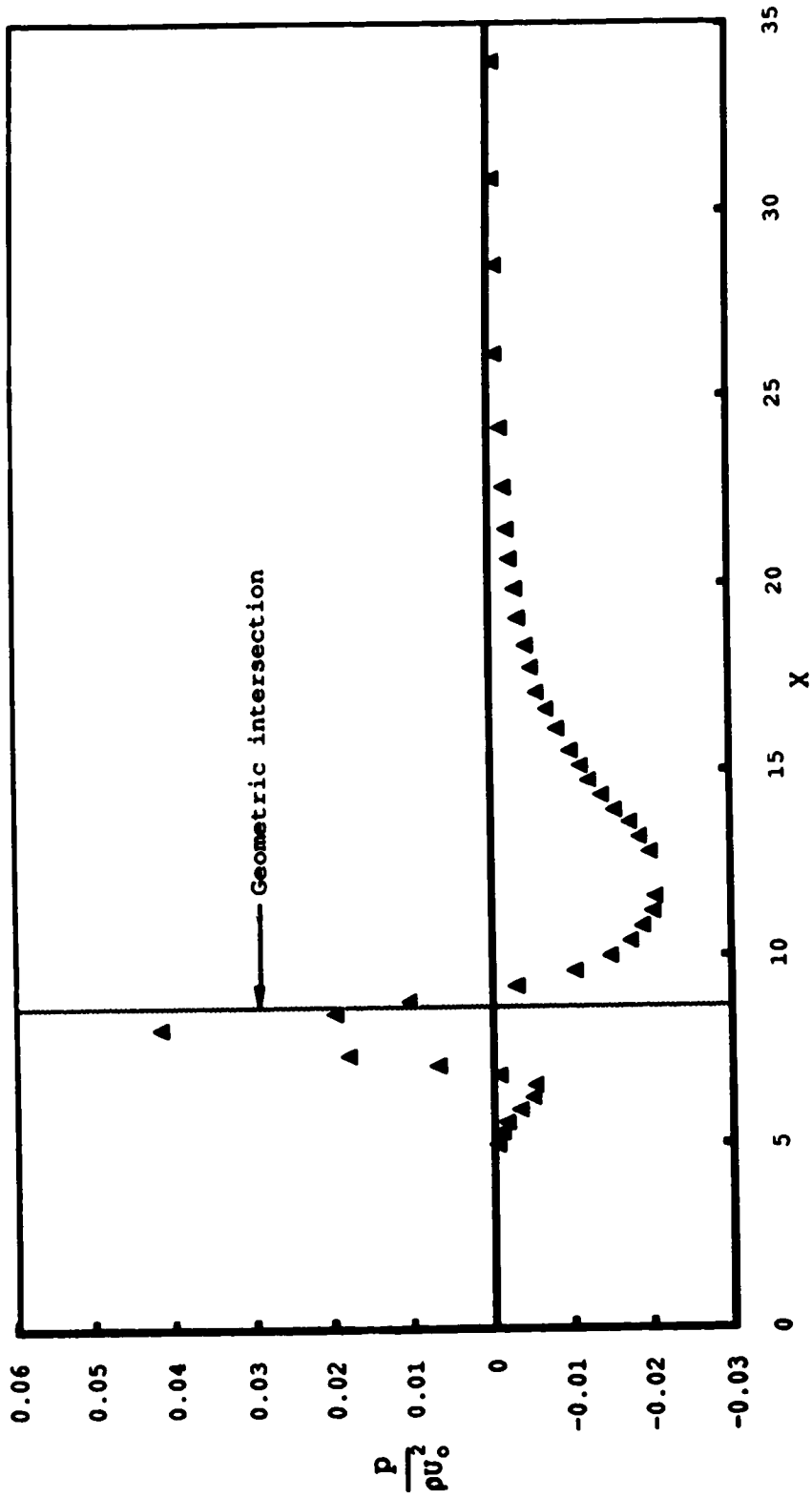

Fig. 4.67. Centreline pressure profile
Expt. 2

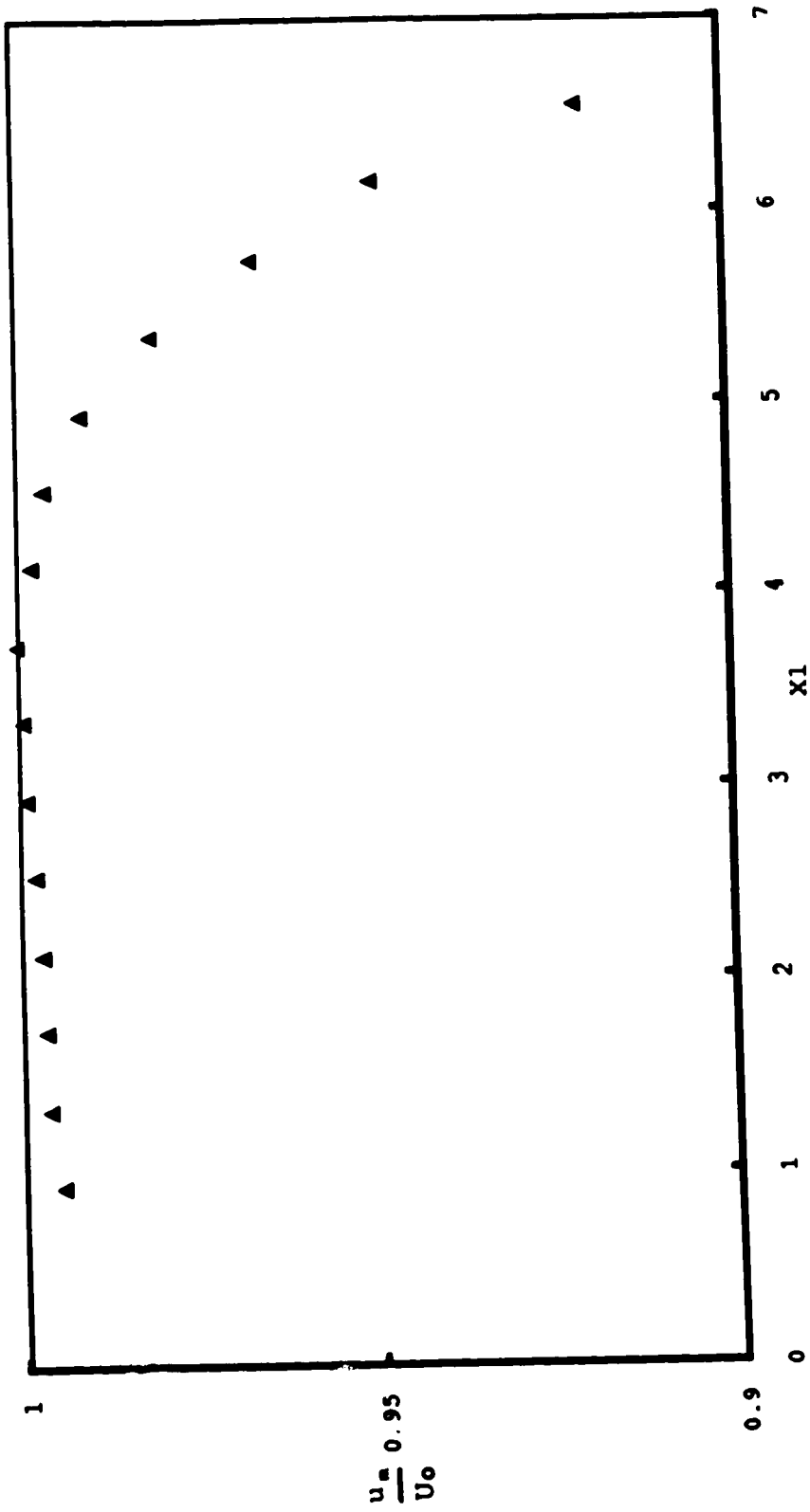

Fig. 4.68. Centreline velocity profile
Expt. 3

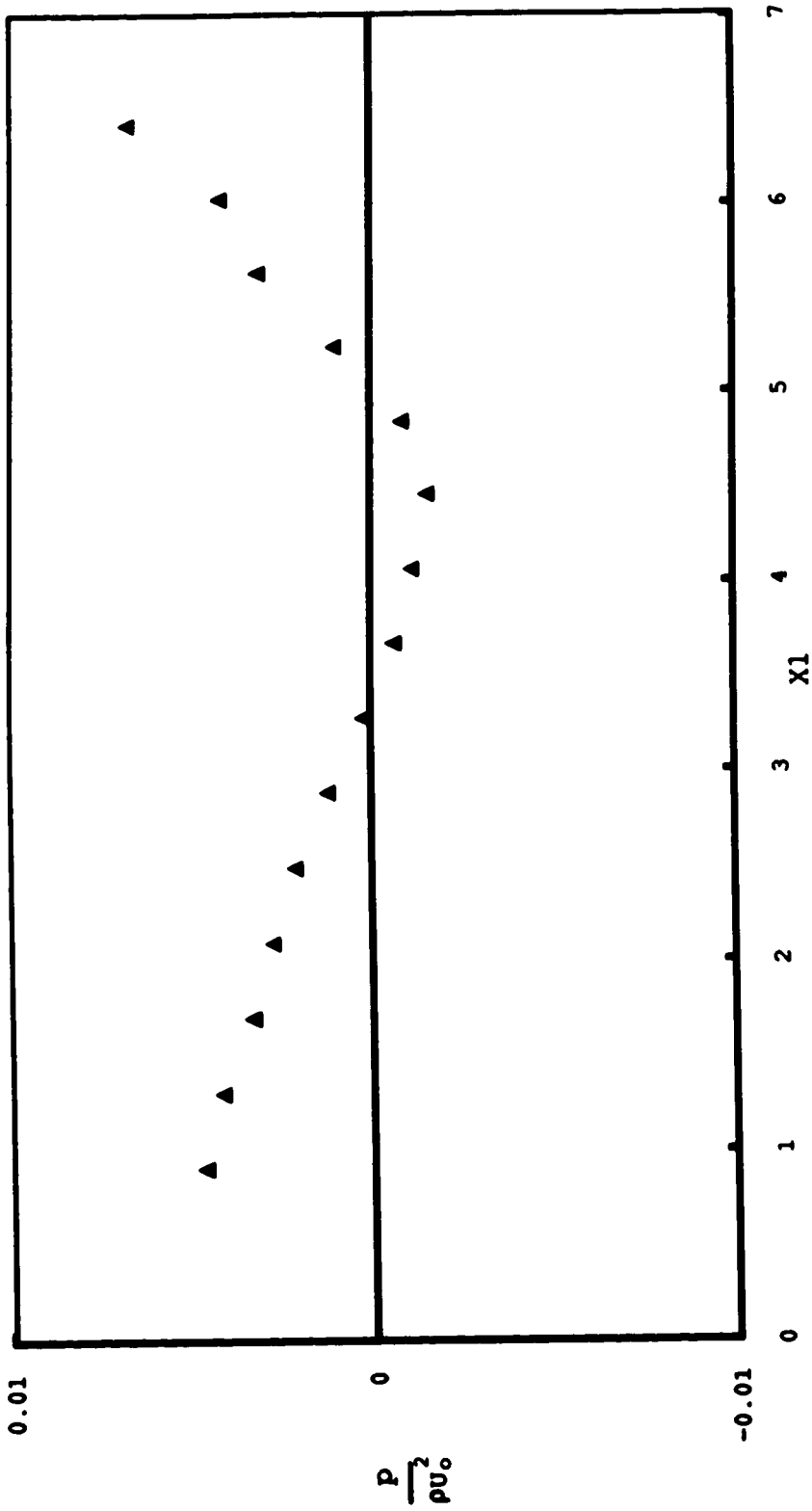

Fig. 4.69. Centreline pressure profile
Expt. 3

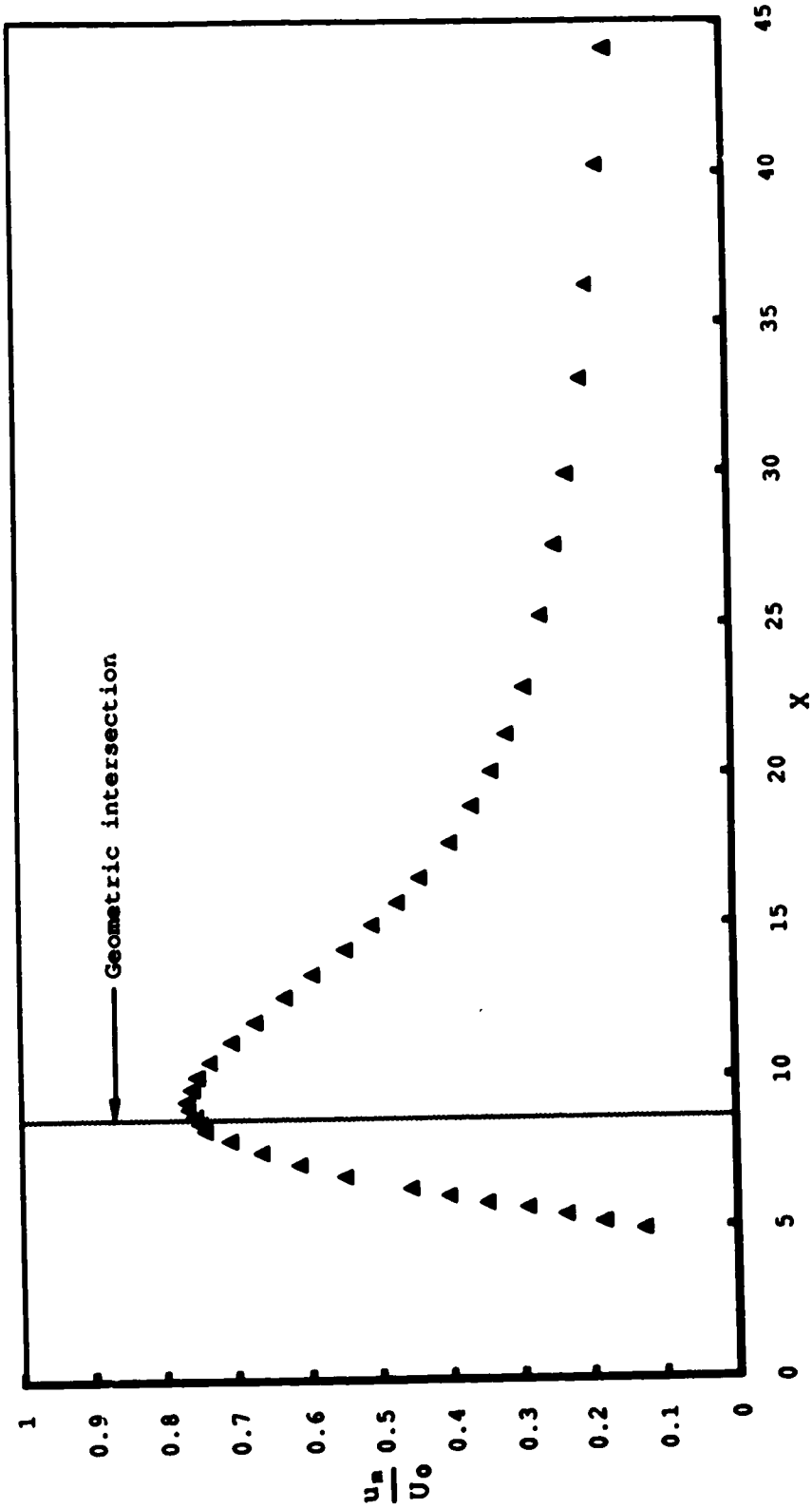

Fig. 4.70. Centreline velocity profile
Expt. 3

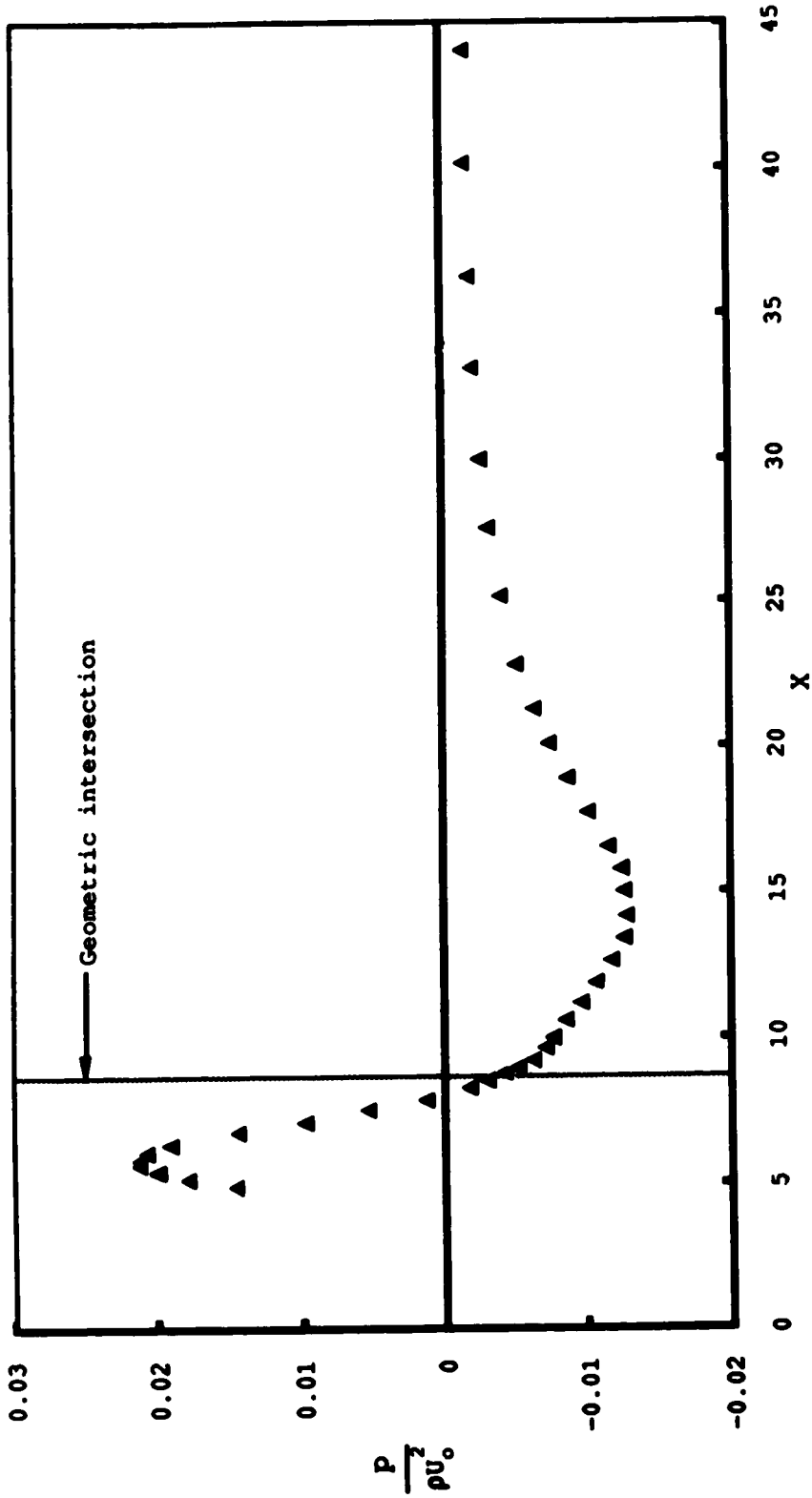

Fig. 4.71. Centreline pressure profile
Expt. 3

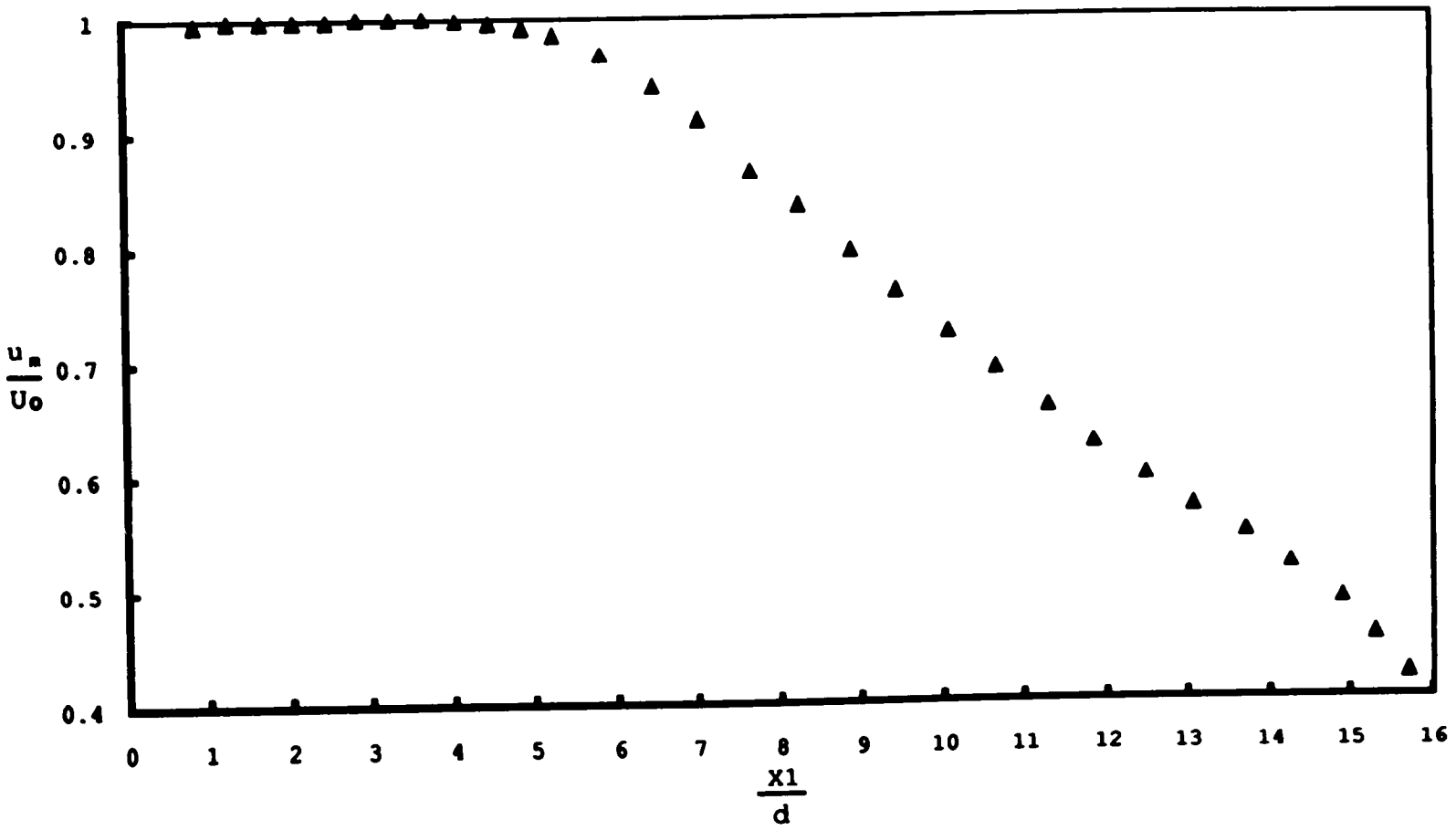

Fig. 4.72. Centreline velocity profile
Expt. 4

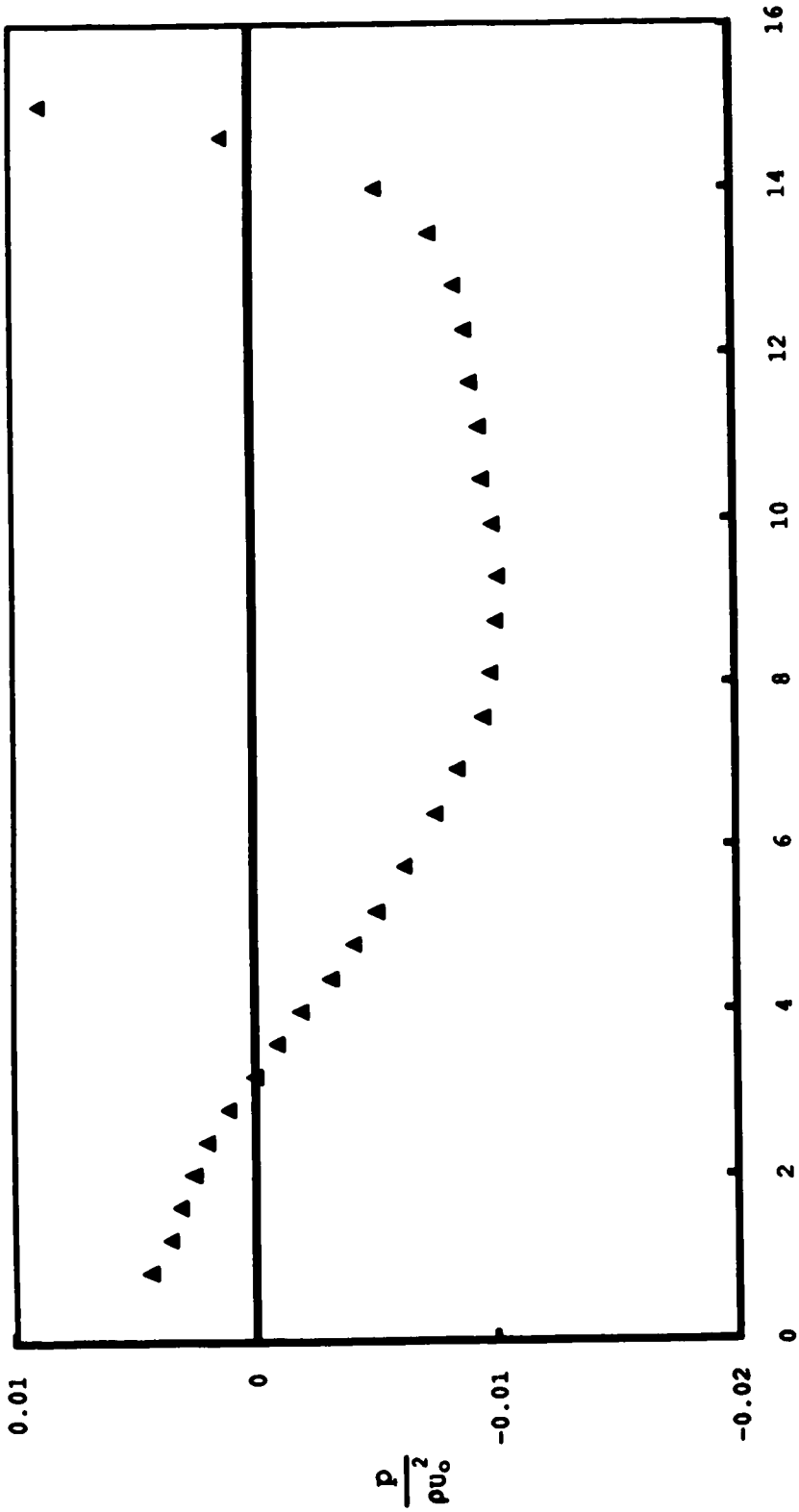

Fig. 4.73. Centreline pressure profile
Expt. 4

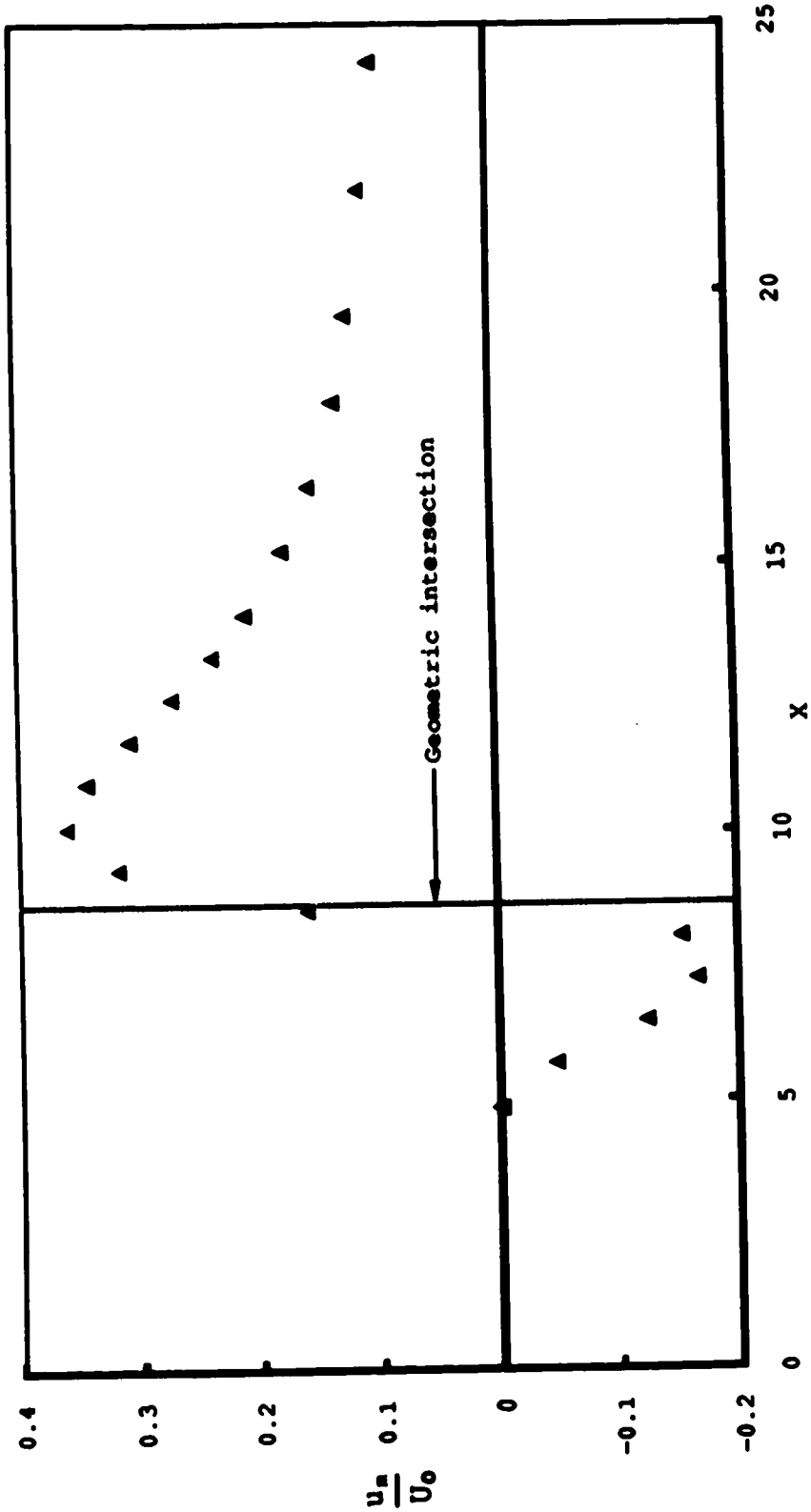

Fig. 4.74. Centreline velocity profile
Expt. 4

Fig. 4.75. Centreline pressure profile
Expt. 4

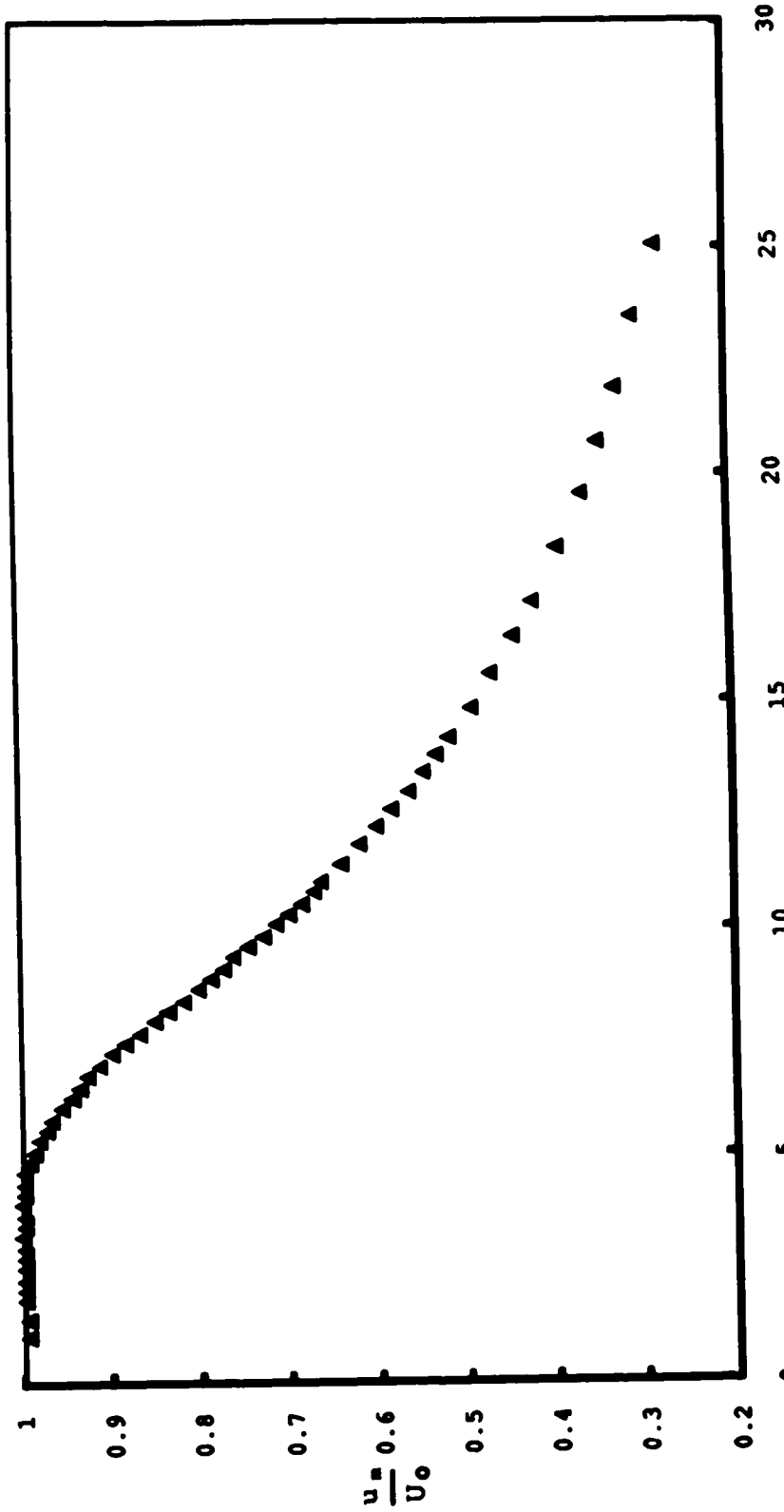

Fig. 4.76. Centreline velocity profile
Expt. 5

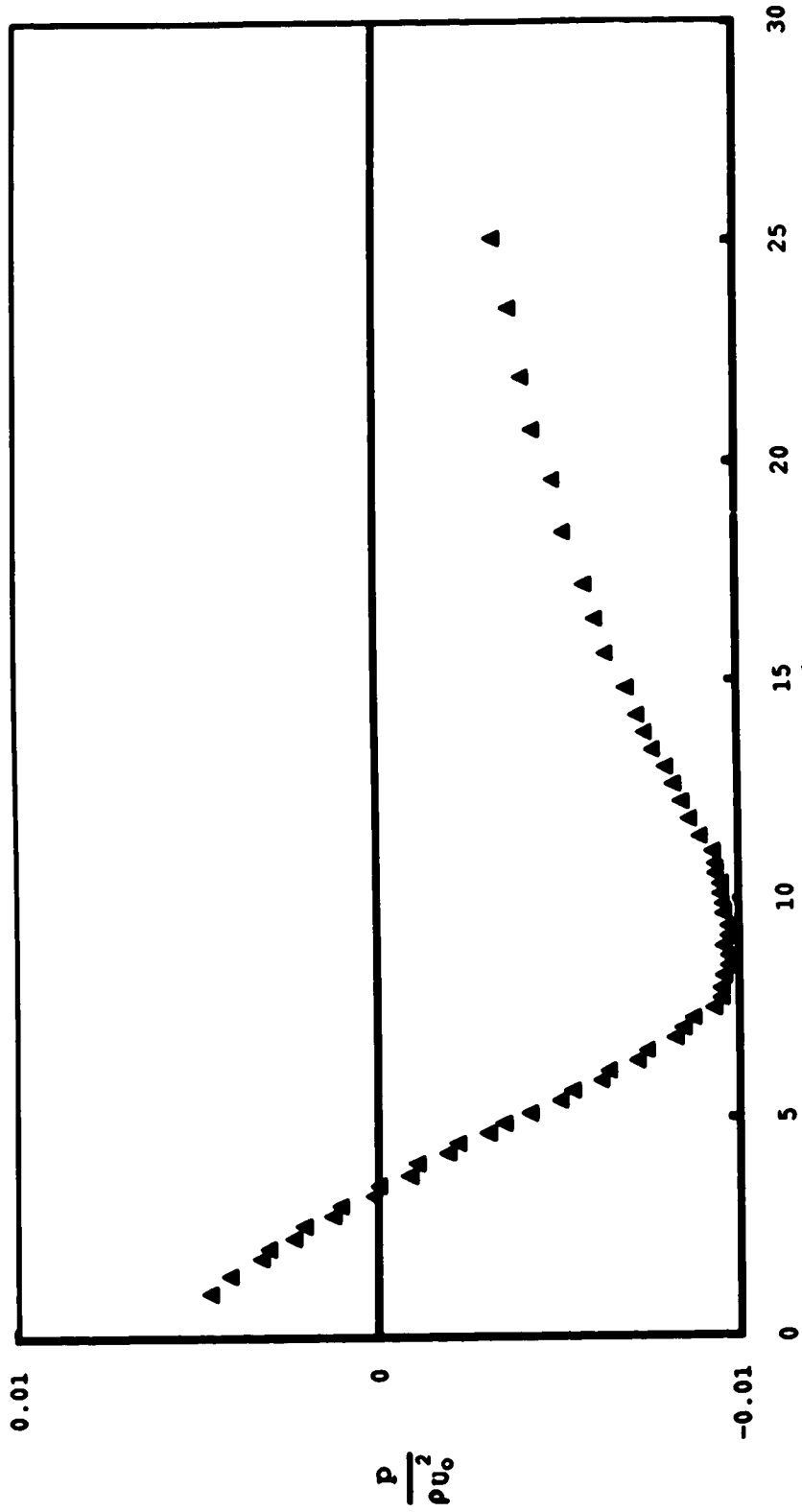

Fig. 4.77. Centreline pressure profile
Expt. 5

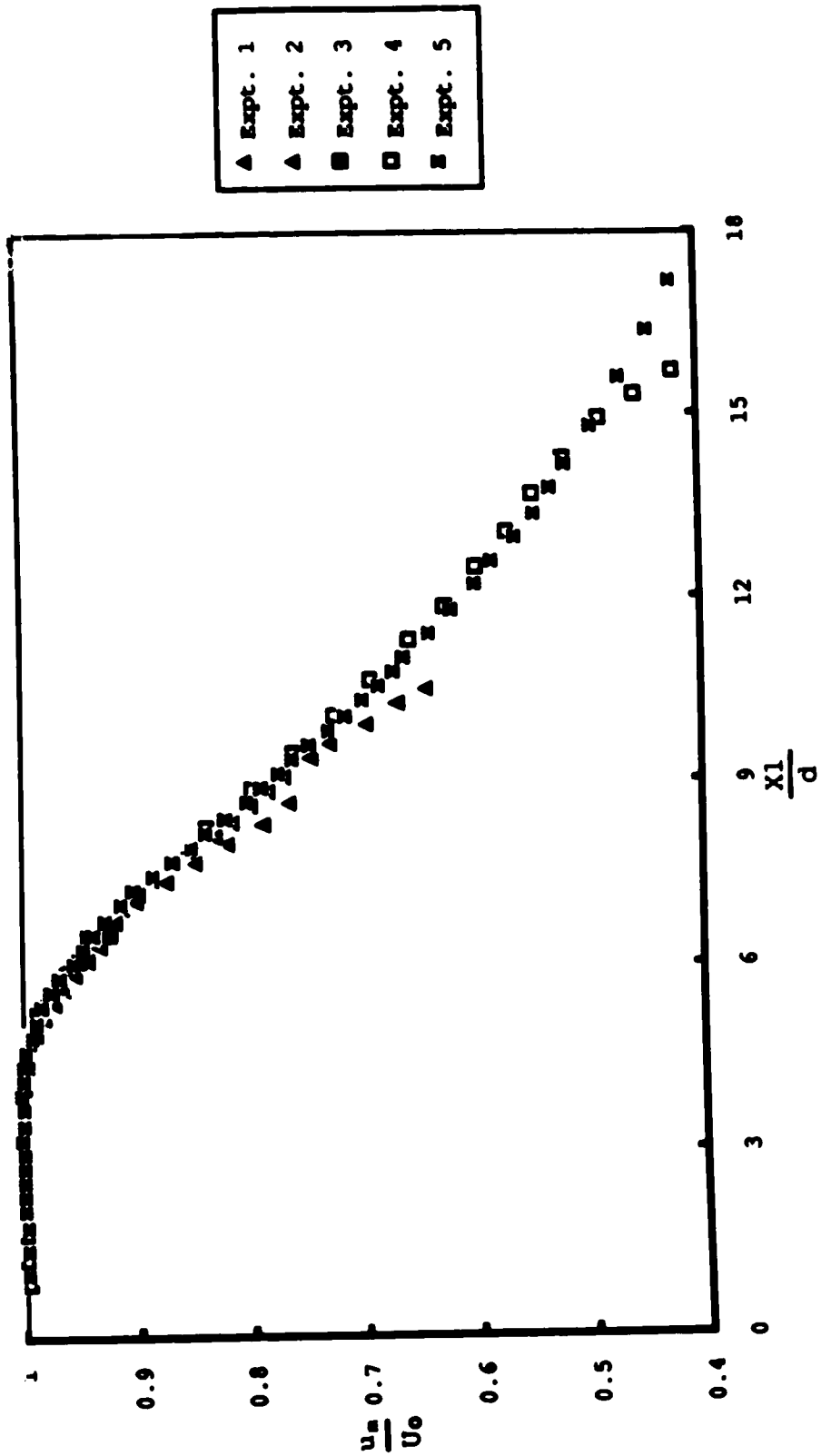

Fig. 5.1. Centreline velocity profile along X1 direction

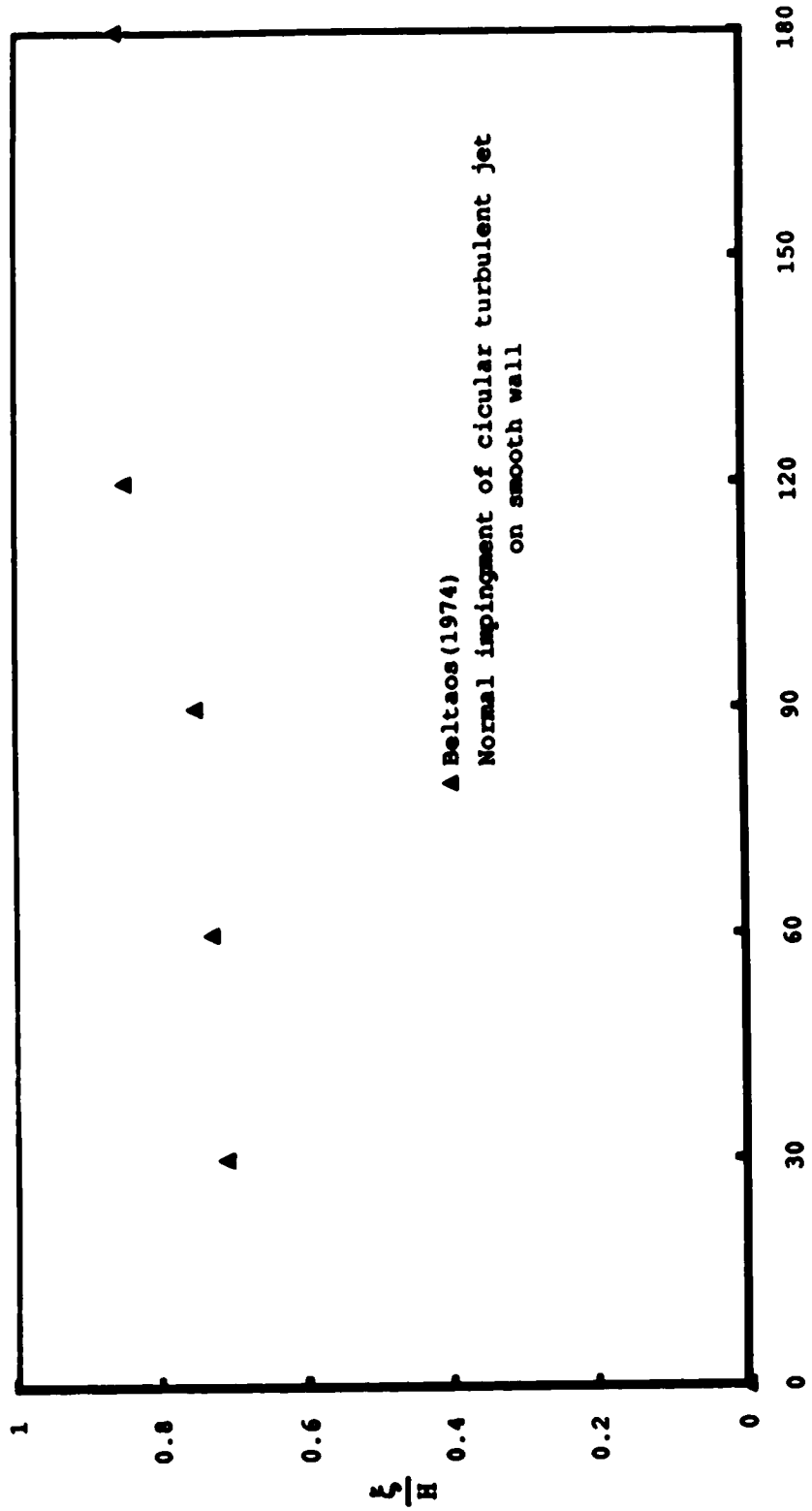

Fig. 5.2. Variation of ξ/H with α

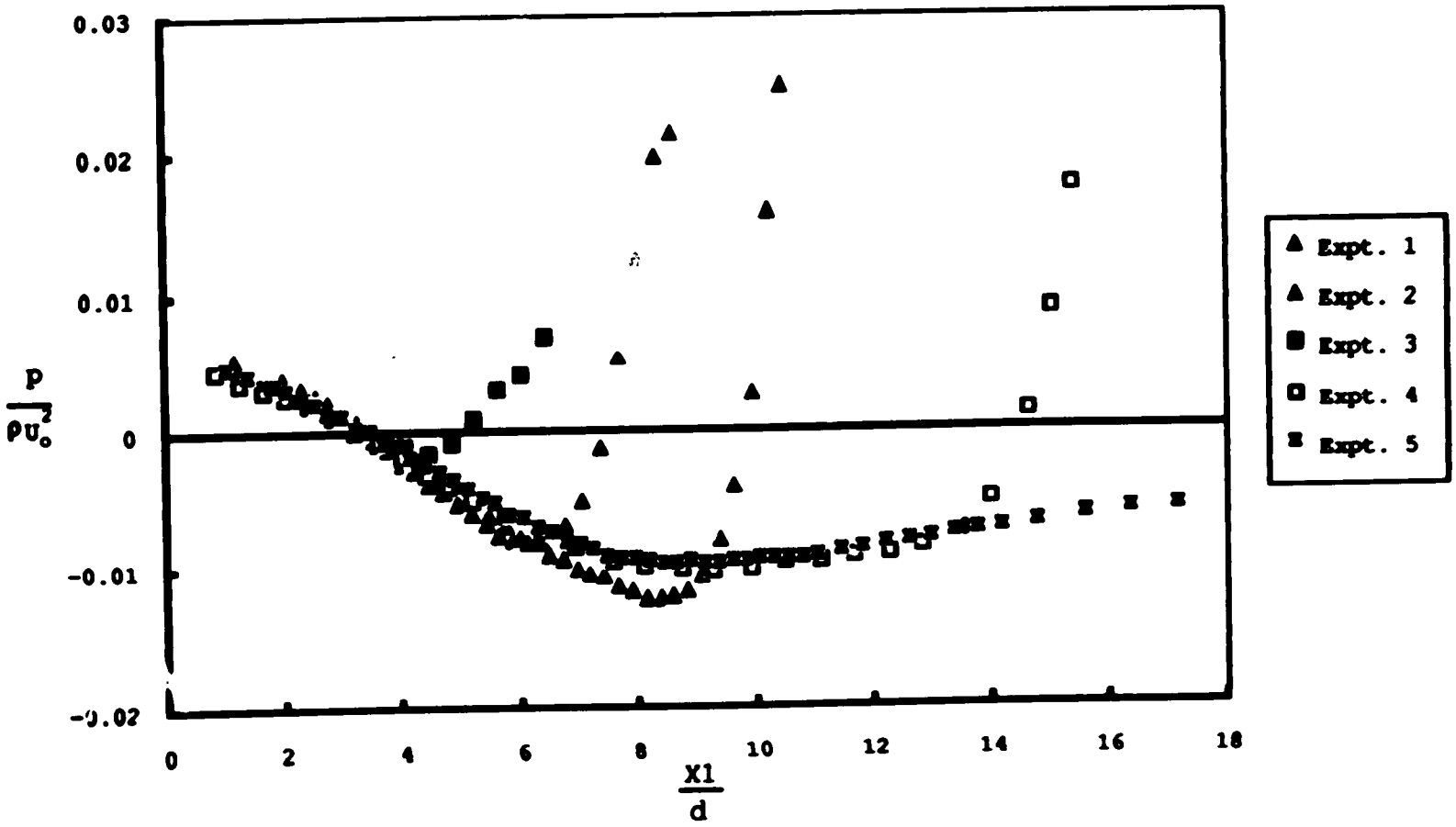

Fig. 5.3. Centreline pressure profile along X1 direction

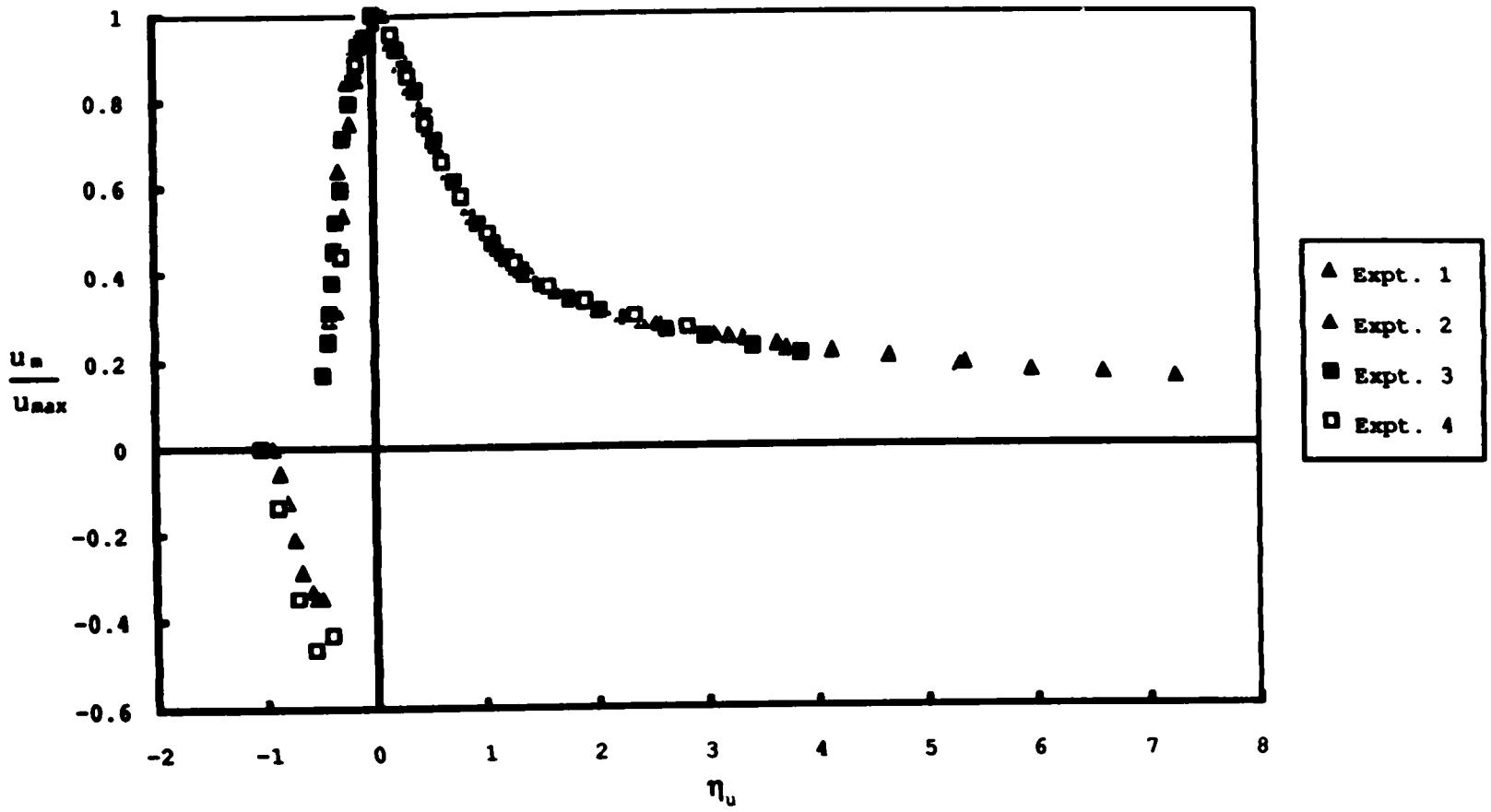

Fig. 5.4. Centreline velocity profiles along X direction

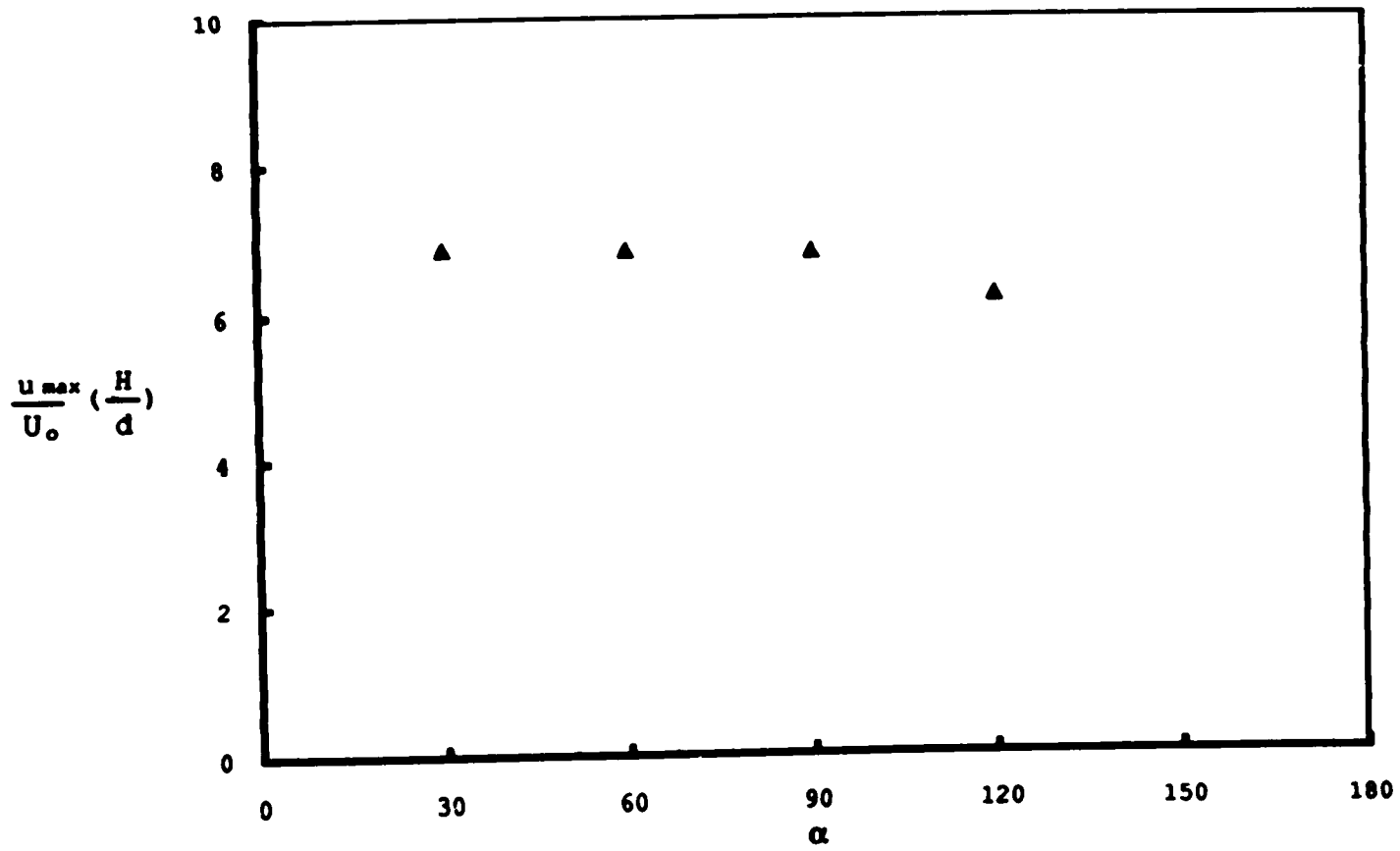

Fig. 5.5. Variation of u_{max} with α

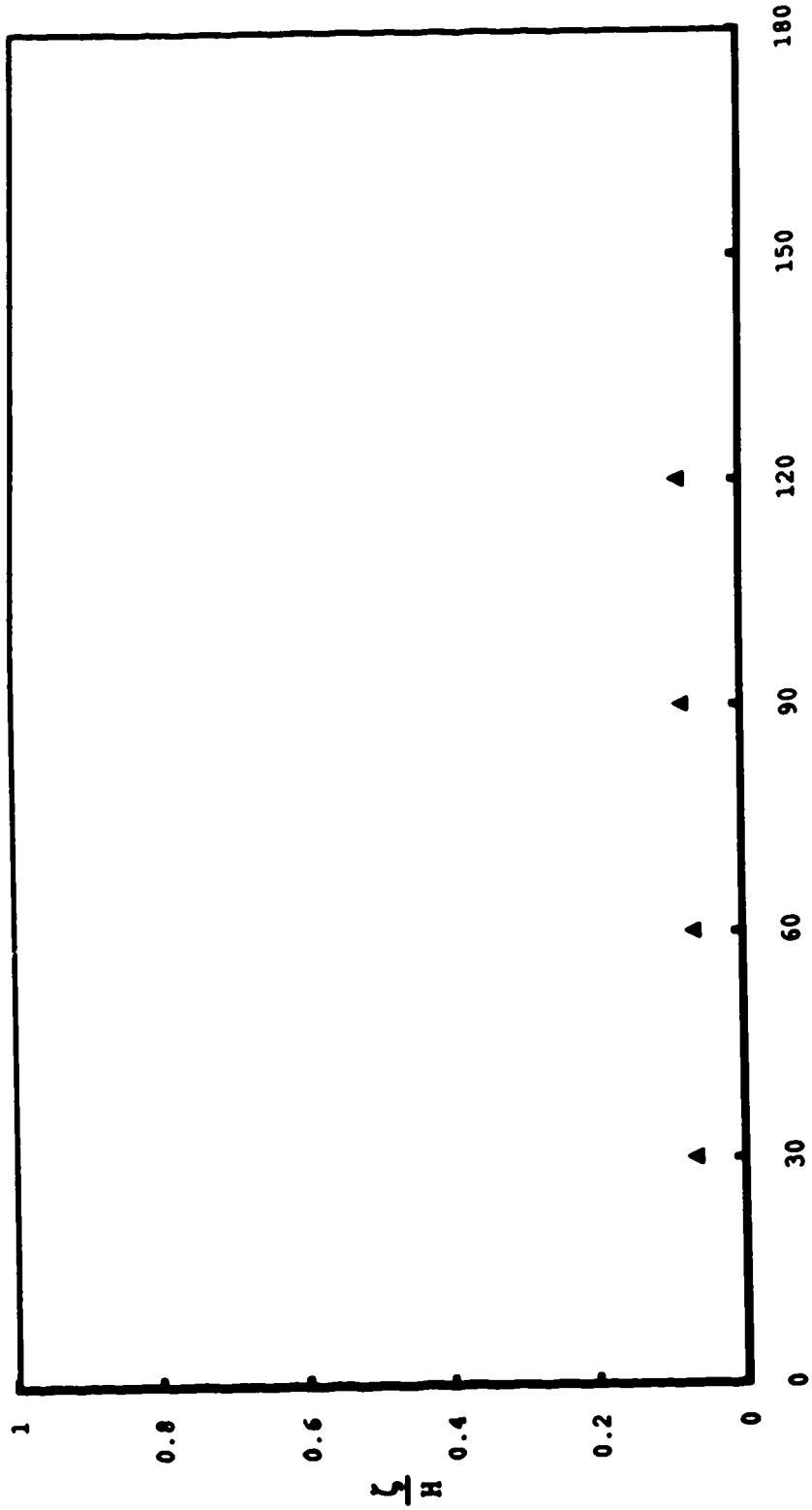

Fig. 5.6. Variation of ζ/H With α

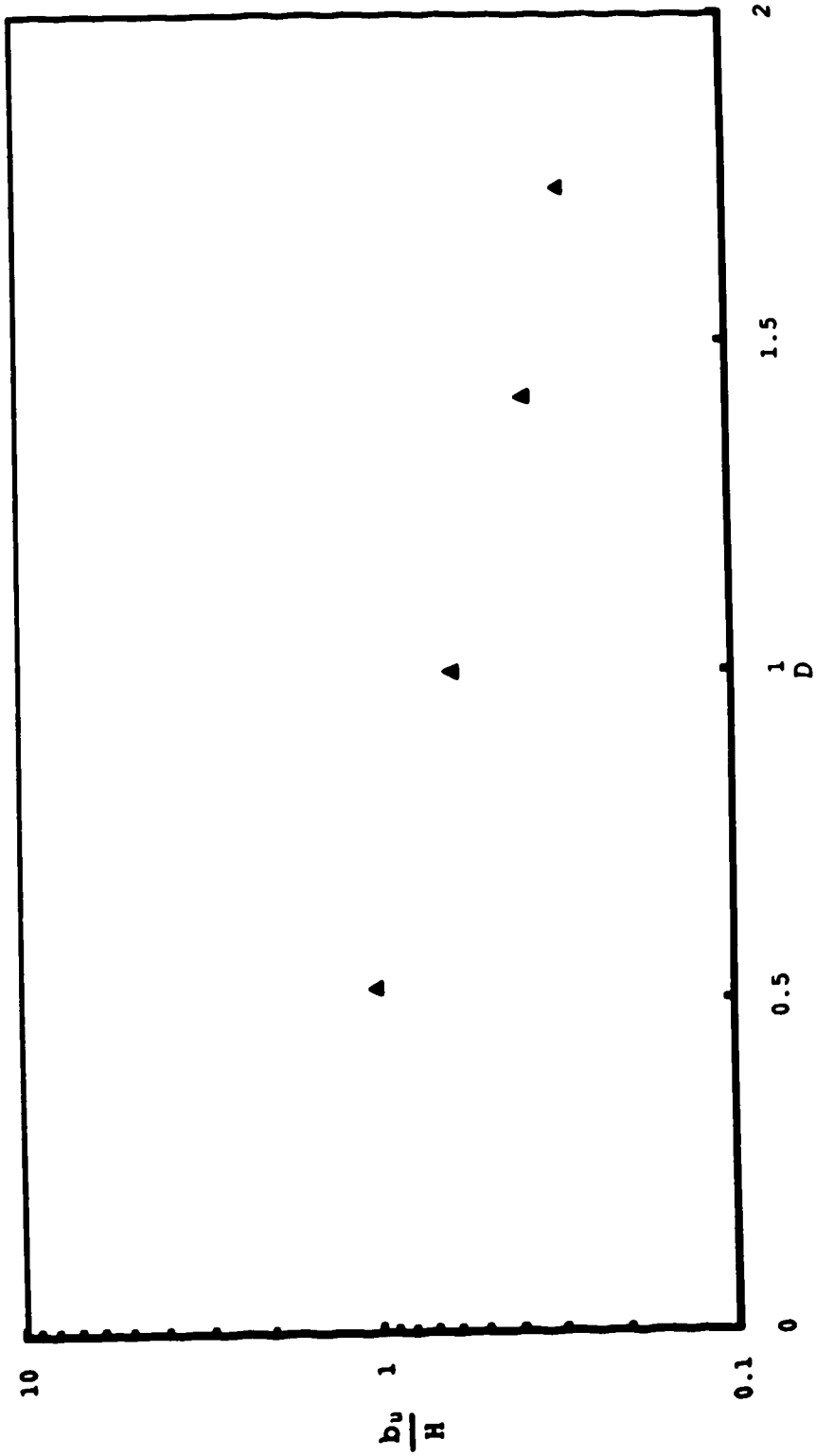

Fig. 5.7. Variation of b_u/H with D/H

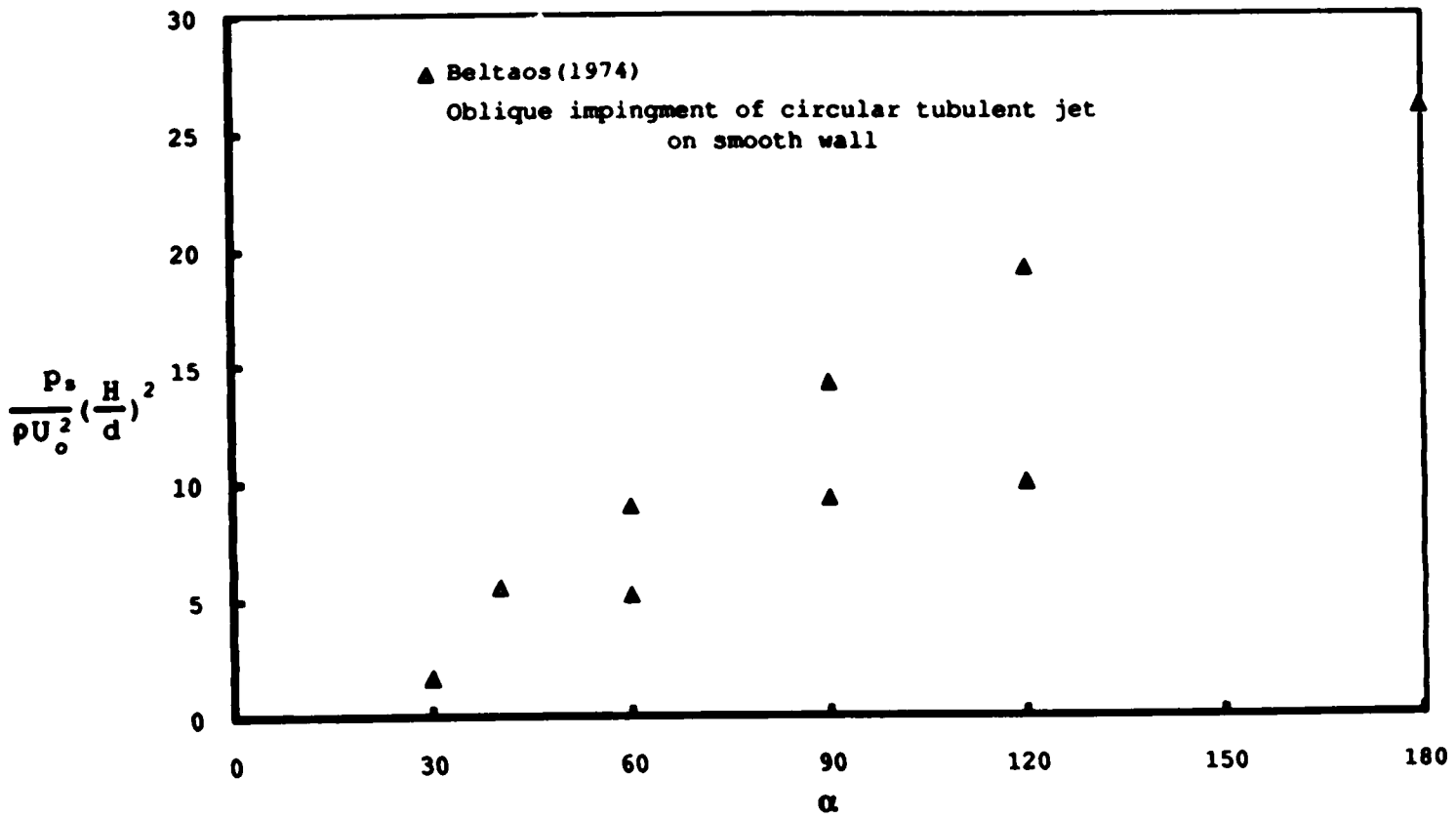

Fig. 5.8. Variation of dimensionless Stagnation pressure

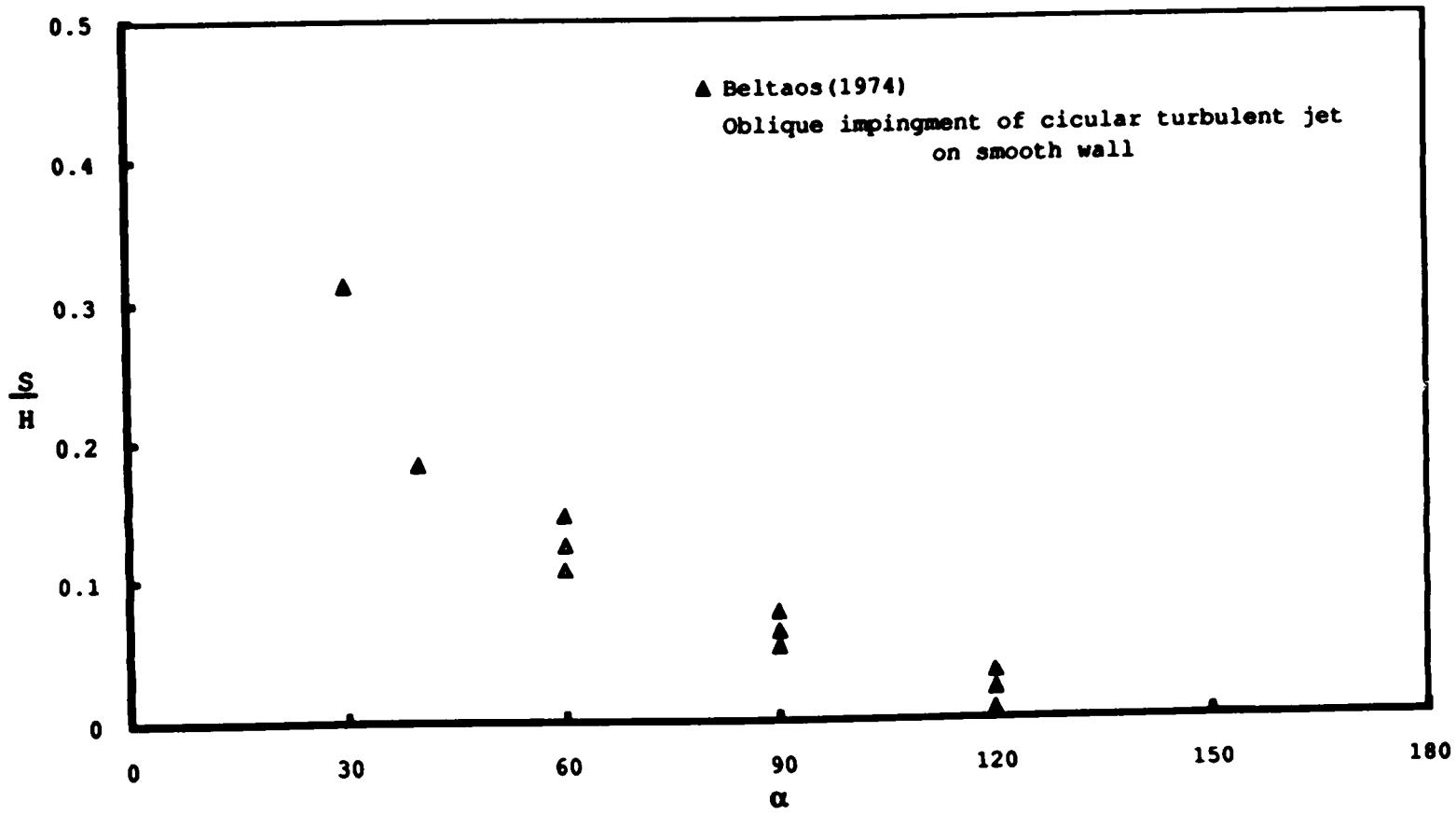

Fig. 5.9. Variation of S/H with α

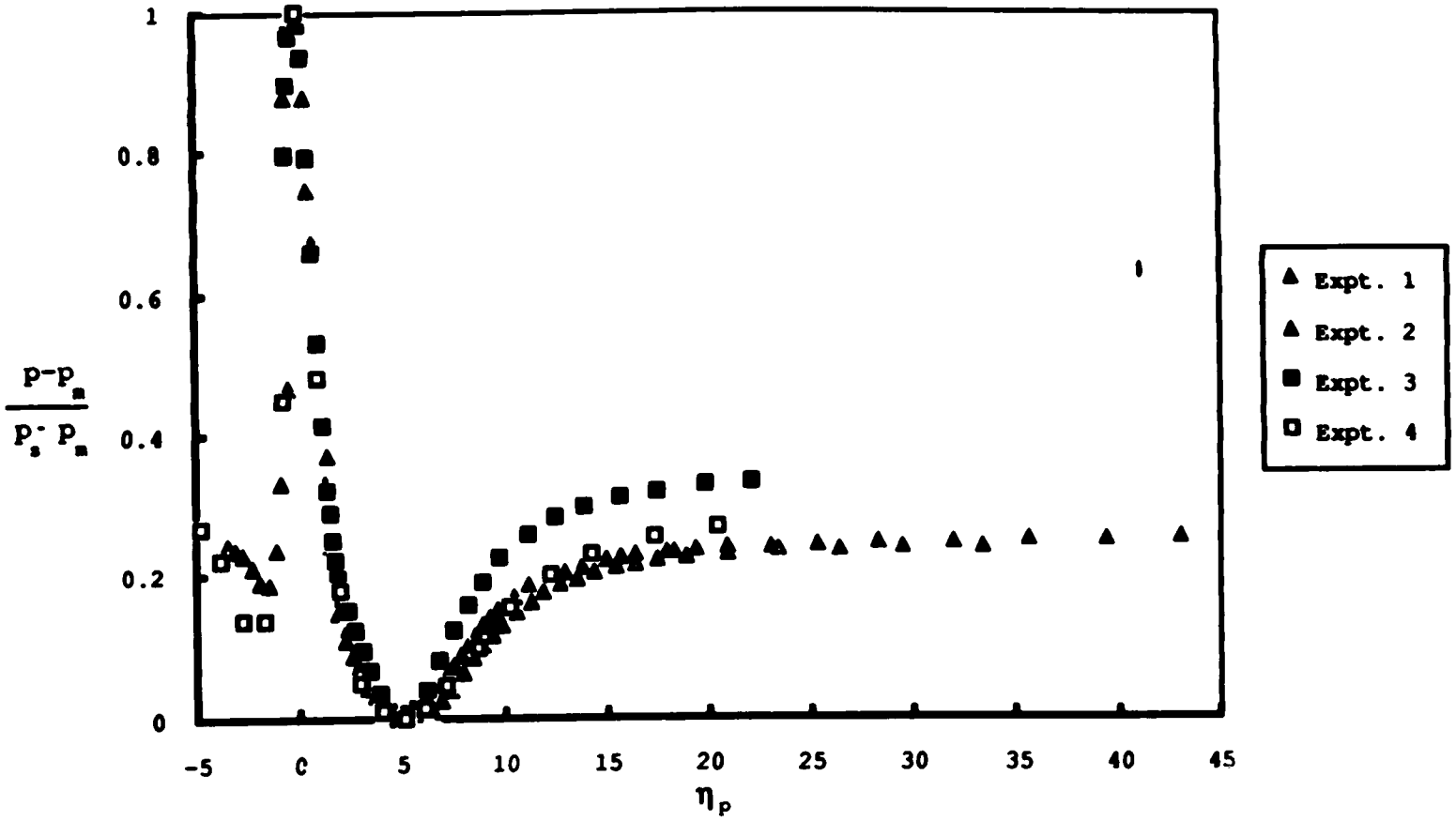

Fig. 5.10. Centreline pressure profiles along X direction

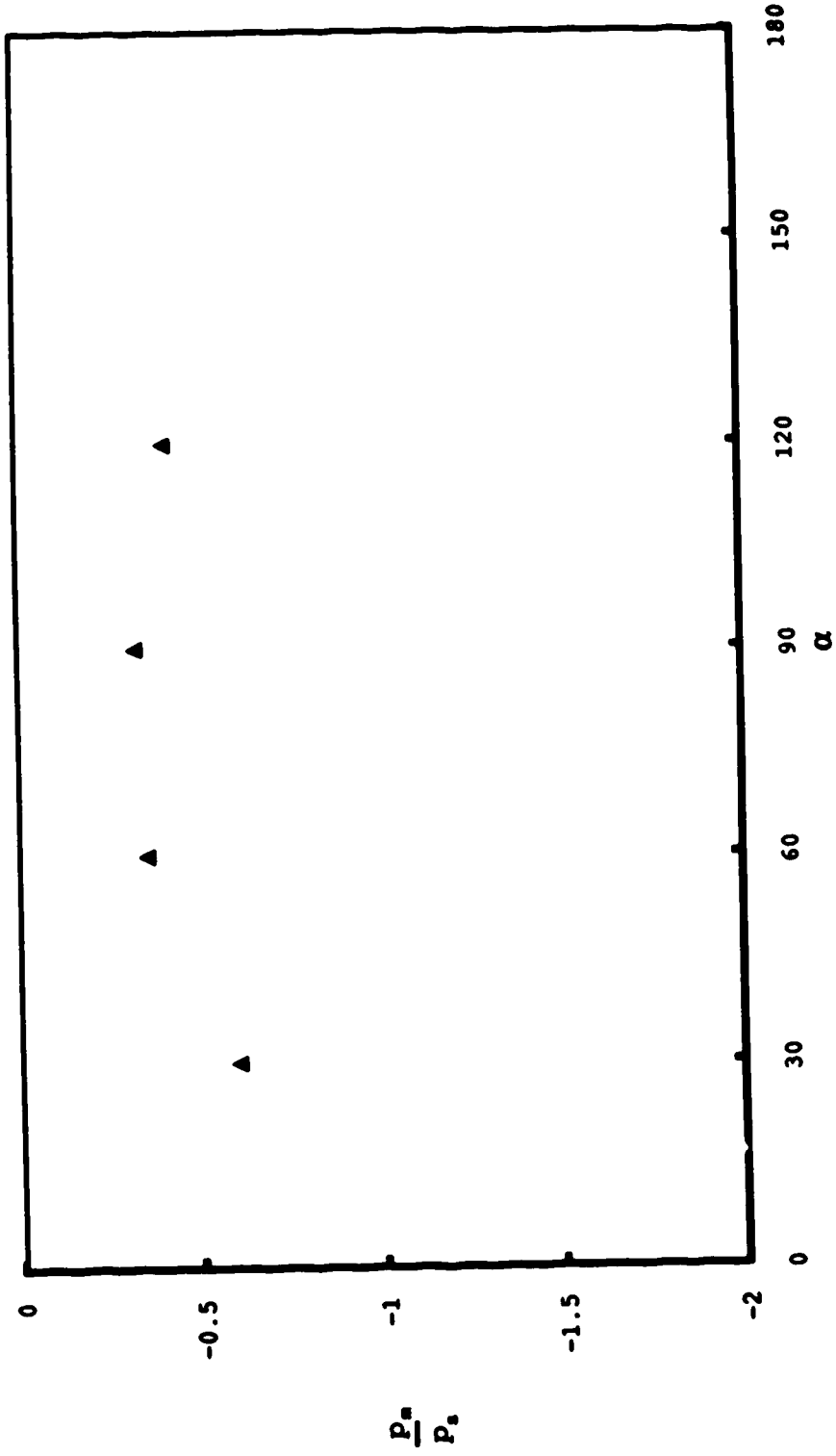

Fig. 5.11. Variation of P_a/P_s with α

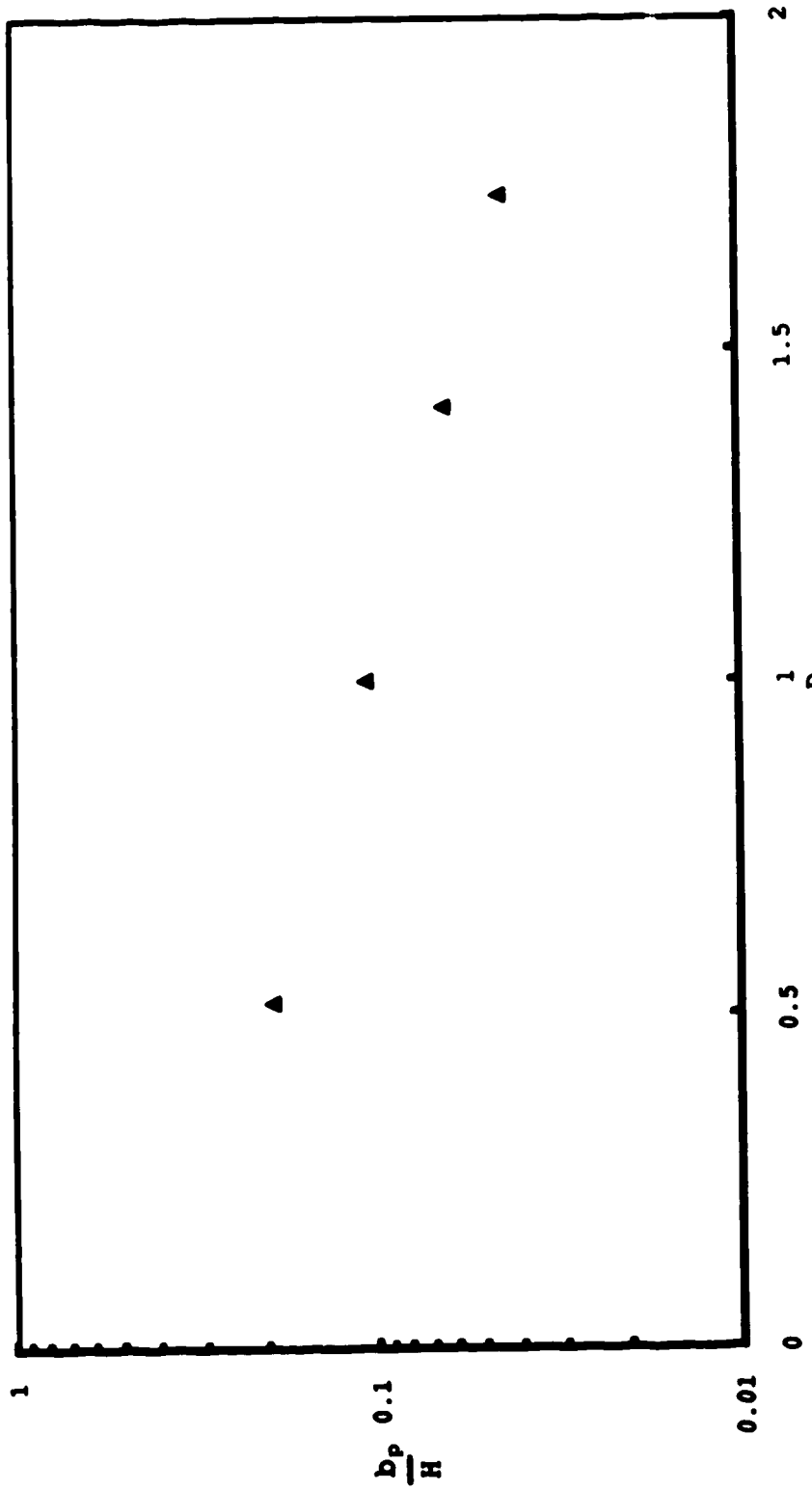

Fig. 5.12. Variation of b_p/H with D/H

References

1. Abromovich G. N., The Theory of Turbulent Jets, The M.I.T. Press, Cambridge, Massachussetts, 1963.

2. Beltaos, S., Normal Impingement of Plane Turbulent Jets on Smooth Wall, M.Sc. Thesis, Department of Civil Engineering, The University of Alberta, Edmonton, Canada, 1972.

3. Beltaos, S., Turbulent Impinging Jets, Ph.D. Thesis, Department of Civil Engineering, The University of Alberta, Edmonton, Canada, 1974.

4. Beltaos, S. and Rajaratnam, N., Impinging Circular Turbulent Jets, Journal of The Hydraulic Division, ASCE, Vol. 100, No. Hy10, October, 1974, PP. 1313-1328.

5. Chue, S. H., Pressure Probes for Fluid Measurements, Prog. Aerospace Sci., Vol. 16, 1975, No. 2, PP. 147-223.

6. Kind. R. J. and Suthanthiran, K., The Interaction of Two Opposing Plane Turbulent Wall Jets, J. Fluid Mech., 1973, Vol. 58, Part 2, PP. 389-402.

7. Maxwell, W. H. C. and Snorrason, A., Measurements in Intersecting Submerged and Induced Jets, Technical Report, Department of Civil Engineering, The University of Illinois at Urbana-Champaign, Illinois, U.S.A., 1979.

8. Maxwell, W. H. C. and Snorrason, A., Measurements in Merging Flow, UILU-WRC-81-0155, Research Report No. 155, Department of Civil Engineering, The University of Illinois at Urbana-Champaign, Illinois, U.S.A., 1981.

9. Pani, B. and Dash, R., Three Dimensional Single and Multiple Free Jets, Journal of Hydraulic Engineering, ASCE, Vol. 109, No. 2, February, 1983, PP. 254-269.

10. Rajaratnam, N., Turbulent Jets, Elsevier Scientific Publishing Co., 1976.

11. Sami, S., Carmody, T. and Rouse, H., Jet Diffusion in the Region of Flow Establishment, J. Fluid Mech., 1967, Vol. 27, Part 2, PP. 231-252.

12. Tanaka, E., Experimental Studies on the Interference Effects of Two Axially Symmetric Jets, Proceedings of the 9th Japan National Congress for Appl. Mech., 1959.

13. Taylor, G. I., Flow Induced by Jets, J. Aerosp. Sci., Vol. 25, PP. 464-465, 1958.